Development and Characterization of Dendritic Cell-Targeted Polymers for Cancer Immunotherapy

Kefan Song

A dissertation
submitted in partial fulfillment of the
requirements for the degree of

Doctor of Philosophy

University of Washington
2025

Reading Committee:
Suzie H. Pun, Chair
Hao Yuan Kueh
Shijie Cao

Program Authorized to Offer Degree:
Bioengineering

University of Washington

Abstract

Development and Characterization of Dendritic Cell-Targeted Polymers for Cancer Immunotherapy

Kefan Song

Chair of the Supervisory Committee:

Suzie H. Pun

Department of Bioengineering

Cancer vaccines and immunomodulators such as STING agonists hold great promise as cancer therapeutics but face many delivery challenges. In this work, we used polymers to deliver peptide antigens and STING agonists to dendritic cells to enhance therapeutic outcomes while minimizing off-target toxicity. In **Chapter 1**, we discussed key aspects in designing effective peptide-based cancer vaccines. In **Chapter 2**, we developed a mannosylated polymer platform to facilitate peptide antigen delivery to the lymph nodes and dendritic cells. In **Chapter 3**, we incorporated a lytic peptide D-melittin to the cancer vaccine platform to enhance cross-presentation and activation of antigen-specific $CD8^+$ T cells. In **Chapter 4**, we report a mannosylated STING agonist drugamer platform to deliver STING agonists to dendritic cells while minimizing toxicity. In **Chapter 5**, we generated structurally different STING agonist drugamer platforms and combined with cancer vaccines to enhance antitumor immunity. In **Chapter 6**, I discussed the use of a fibronectin-binding peptide in cancer immunotherapy and proposed future directions.

Table of Contents

List of Figures

List of Tables

Acknowledgements

First and foremost, I want to thank my advisor, Suzie Pun. You've taught me so much, not just about being a good scientist, but about being a good person. Whenever I faced challenges, whether it was a failed experiment, a rejection, or self-doubt, you always knew exactly what to say to help me regain my confidence and perspective. Conversations with you always left me feeling less anxious and more motivated to move forward. You are my role model, not only for your scientific achievements but for the kind of mentor and person you are. Thank you for believing in me, for giving me space to grow, and for always being there when I needed guidance. I feel so lucky to have had you as my mentor, and the lessons I've learned from you will stay with me for the rest of my life.

To my committee members, Patrick Stayton, Hao Yuan Kueh, Shijie Cao and Drew Sellers, thank you for challenging me, encouraging me, and guiding me to become a better scientist. Your advice and feedback have been invaluable throughout this process.

To my mentors Shixian Lv, Meilyn Sylvestre and Albert Yen, thank you for bringing me to the world of immunotherapy and teaching me all the animal techniques. I've learned so much from you, not just about research, but also about being a good mentor myself. You've set an example I'll always strive to follow.

To my labmates and collaborators, Ian Cardle, Emmeline Cheng, Audrey Olshefsky, Alex Prossnitz, Meilyn Sylvestre, Shixian Lv, Lucy Yang, Albert Yen, Drew Sellers, Nataly Kacherovsky, Trey Pichon, Clinton Heinze, Ben Nguyen, Melissa Ling, Abe Wu, Kairui Jiang, Sydney Funk, Ethan Mickelson, Kelly Wang, Trevor Corrigan, Simba JoKonya, Omeed Yazdani, Arie Lin-Goldstein and Tran Luu, I feel so lucky to have been part of such a supportive

and collaborative group. Thank you, Ben Nguyen, for your collaboration and support throughout my PhD journey. You not only synthesized the polymers that made this research possible, but also stuck with me through all the ups and downs of the experiments. Thank you, Kelly Wang, Omeed Yazdani, Ben Nguyen and Tran Luu, for making long days in the lab not just bearable but often fun.

To my friends in Seattle, Zhiying Xie, Siyu Zhang, Waterlily Huang, Steven Hsu, Claire Tao, and Yilin Song, thank you for always being there for me and supporting me. Thank you for getting me out of the lab and bringing me into the mountains for hiking and snowboarding. I'm grateful for every moment we've shared.

To my partner, George Guo, you always knew how to cheer me up when I was in a bad mood, and your belief in me has helped me believe in myself. I'm incredibly lucky to have you by my side. You've been my greatest source of strength and joy, and I look forward to everything that lies ahead with you by my side.

To my parents and my grandma, thank you for supporting every decision I've made and always encouraging me to follow my passions and pursue my dreams. Thank you for your patience, your understanding and for always making me feel loved. I will forever be grateful for the foundation you've given me.

Chapter 1 : Design and Evaluation of Synthetic Delivery Formulations for Peptide-Based Cancer Vaccines[1]

Kefan Song and Suzie H. Pun

ABSTRACT

With the recent advances in neoantigen identification, peptide-based cancer vaccines offer substantial potential in the field of immunotherapy. However, rapid clearance, low immunogenicity and insufficient antigen-presenting cell (APC) uptake limit the efficacy of peptide-based cancer vaccines. This review explores the barriers hindering vaccine efficiency, highlights recent advancements in synthetic delivery systems and features strategies for the key delivery steps of lymph node drainage, APC delivery, cross-presentation strategies and adjuvant incorporation. This paper also discusses the design of preclinical studies evaluating vaccine efficiency, including vaccine administration routes and murine tumor models.

[1] Chapter reproduced from: Song, K., & Pun, S. H. (2024). Design and Evaluation of Synthetic Delivery Formulations for Peptide-Based Cancer Vaccines. *BME frontiers*, 5, 0038.

1.1 INTRODUCTION

In recent decades, cancer immunotherapy has gained significant attention as an approach that directly targets the immune system, generates less side effects, and is able to treat cancers that are not responsive to traditional treatments. Therapeutic cancer vaccines are a type of immunotherapy that activates the adaptive immune system to fight against cancer. Sipuleucel-T, the first FDA-approved therapeutic cancer vaccine, treats prostate cancer by generating activated dendritic cells (DCs) displaying tumor antigen from patient peripheral-blood mononuclear cells (PBMCs) and reinfusing the cells back to prime the T cells for an effective antitumor immune response.[1] However, this *ex vivo* process is labor-intensive, time-consuming and cost-ineffective.

An alternative vaccination approach delivers antigens to activate antigen-presenting cells (APCs) *in vivo*. Several therapeutic cancer vaccines employing this strategy are currently undergoing evaluation in clinical trials.[2–4] Cancer vaccine antigens can take various forms, including tumor cell lysates[5,6], DNA[7], RNA[8], peptides[9] and proteins[10]. With defined structures and facile chemical production, peptide-based cancer vaccines offer distinct benefits compared to other forms. Peptide antigens directly serve as T cell epitopes, requiring fewer processing steps than DNA and RNA to be presented on the surface of DCs and also exhibit favorable safety profiles compared to virus-based cancer vaccines.[11] However, the relatively low immunogenicity of peptide antigens necessitates the incorporation of adjuvants to activate the adaptive immune system.[12] Additionally, peptides face challenges related to *in vivo* instability and susceptibility to enzyme degradation, and therefore often require carriers for delivery to desired cells.

This review addresses key considerations in the design and evaluation of peptide-based cancer vaccines, including selection of tumor antigens, development of delivery platforms, integration of adjuvants, route of administration and preclinical evaluation models.

Tumor antigens are the key component of cancer vaccines and fall into two categories: tumor-associated antigens (TAAs) and tumor-specific antigens (TSAs).[13] TAAs are antigens that are overexpressed in tumor cells.[14] Human epidermal growth factor receptor 2 (HER2) is a TAA that is overexpressed in approximately 30% of human breast cancers.[15] Multiple HER2-targeted peptide vaccines have shown promising results in treating patients with breast cancer.[16] Another example of a TAA is gp100, which is enriched in melanomas.[17] Patients with metastatic melanoma who received a combination of interleukin-2 (IL-2) and gp100 peptide cancer vaccine had improved clinical responses than patients who received IL-2 alone.[18] TAAs are shared among different patients, making them suitable for developing universal, cost-effective and time-efficient treatments. However, TAAs are not uniquely expressed on tumor cells and thus are susceptible to central tolerance and dampened T cell responses.[13] In addition, cancer vaccines targeting TAAs are not completely tumor-specific and might generate toxicity in healthy tissues.

Tumor somatic mutations generate neoantigens, a subset of TSAs. Unlike TAAs, TSAs are exclusively expressed in tumor cells. They are more immunogenic and have better affinity to MHC molecules as they are not affected by central tolerance.[19] With the advancements in next-generation sequencing (NGS) and bioinformatics, neoantigens have gained increasing attention over the past years. Neoantigens can be used to create personalized cancer vaccines. Patient samples, including tumor tissue and normal tissue (PBMCs), are collected, and NGS is used to identify mutations. Algorithms and computational methods are used to predict neoepitopes for personalized vaccines.[20] Multiple peptide-based neoantigen vaccines have been tested in clinical

trials.[21–23] In a phase I/Ib glioblastoma study, neoantigen vaccines containing synthetic long peptides mixed with poly-ICLC (polyinosinic and polycytidylic acid, stabilized with poly-L-lysine and carboxymethylcellulose) generated circulating neoantigen-specific $CD4^+$ and $CD8^+$ T cells and increased tumor-infiltrating T cells in patients not receiving dexamethasone.[21] In another phase Ib clinical trial, neoantigen peptides mixed with poly-ICLC in combination with anti-PD-1 demonstrated safety and immunogenicity in advanced melanoma, non-small cell lung cancer and bladder cancer patients.[22] Neoantigen peptide vaccines also induced long-term neoantigen-specific T cells with a memory phenotype in melanoma patients.[23]

Tumor antigens are presented on tumor cell surface through major histocompatibility class I (MHC I) molecules to be recognized and eliminated by cytotoxic T cells. Many cancers have evolved to downregulate the expression of MHC I molecules to evade T cell killing.[24,25] However, recent studies have shown that T cells are still responsible for tumor killing in antigen-negative tumor cells through Fas-dependent "bystander" killing[26] and in MHC I-negative tumors through the NKG2D–NKG2DL axis.[27] In this case, tumor killing is antigen-independent, but antigen-specific T cell activation is required, demonstrating the utility of cancer vaccines in MHC I-negative tumors.

1.2 MECHANISMS AFFECTING THE EFFICIENCY OF PEPTIDE-BASED CANCER VACCINES

Antigen-presenting cells (APCs) are the primary cellular targets for cancer vaccines, playing a critical role in taking up, processing and presenting tumor antigens to naïve T cells in the lymph nodes to generate antigen-specific T cells. Activated T cells then circulate in the bloodstream to find their targets and mount an antitumoral response.

As professional APCs, dendritic cells (DCs) are target cells for antigen peptide delivery that possess a unique capability to activate naïve T cells. Dendritic cells can sense infection or endogenous danger from signals such as pathogen-associated molecular patterns (PAMPs) and damage-associated molecular patterns (DAMPs). PAMPs and DAMPs are detected by pattern recognition receptors expressed on DCs and lead to activation and maturation of the DCs.[28] Activated DCs upregulate expression of co-stimulatory molecules on their surface and also produce pro-inflammatory cytokines and chemokines.

Antigens captured by the DCs are processed for presentation to T cells by two pathways. In the first pathway, endogenous antigens present in the cytosol are degraded into peptides by the proteasome, loaded onto Major Histocompatibility Complex (MHC) Class I molecules in the endoplasmic reticulum (ER), and then transported to the DC surface to activate $CD8^+$ T cells.[29] $CD8^+$ T cells, also known as cytotoxic T cells, are directly involved in killing tumor cells. Upon antigen recognition, they release cytokines, granule-associated enzymes and death receptor-ligand engagement to eliminate cancer cells.[30] In the second pathway, exogenous antigens that are endocytosed are degraded into peptides by endosomal proteases. Vesicles containing these peptides are fused with vesicles containing MHC Class II molecules, allowing peptides from exogenous antigens to be loaded onto MHC Class II molecules. These loaded peptides are then transported to the DC surface to activate $CD4^+$ T cells.[29] $CD4^+$ T cells, also known as helper T cells, contribute to the development and maintenance of an antitumoral response.[31] In some dendritic cells, exogenous antigens can be presented on MHC Class I molecules by retrotranslocation to activate $CD8^+$ T cells, a process called cross-presentation.[32] In peptide-based cancer vaccines, most peptide antigens are exogenous antigens and activate $CD4^+$ T cells

through the MHC Class II pathway. Effective tumor cell eradication requires cross-presentation in DCs to mount strong $CD8^+$ T cell responses.

T cell priming requires three signals.[33] First, T cell receptors (TCRs) recognize the cognate antigenic peptide presented by MHC molecules on DCs. Second, co-stimulatory molecules, such as B7.1 (CD80) and B7.2 (CD86) on DCs interact with CD28 on T cells.[34] Antigen recognition without co-stimulation can result in T cell anergy.[35] Third, cytokines released by activated DCs induce T cell expansion and differentiation.[36] Peptide antigens are known to be non-immunogenic and are insufficient to stimulate DCs to express the co-stimulatory molecules required for effective T cell activation. Consequently, adjuvants, which modulate the immune response and enhance the immunogenicity of the antigen, need to be incorporated in the vaccine formulation to elicit a robust T cell response against tumor cells.

This review will discuss key aspects of designing effective peptide-based cancer vaccines, including LN trafficking, DC uptake, cross-presentation and adjuvant incorporation (**Figure 1.1**).

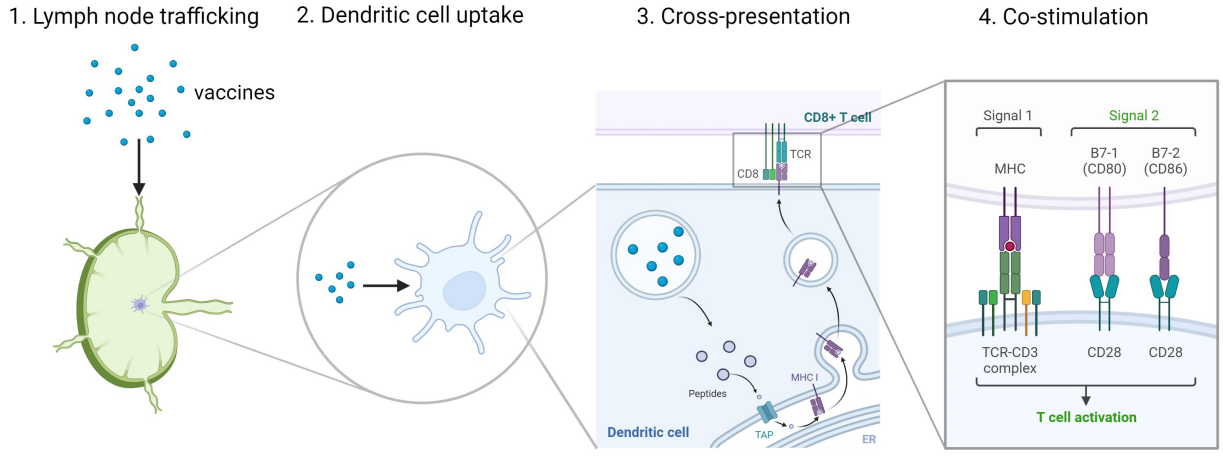

Figure 1.1 Key aspects of designing effective peptide-based cancer vaccines.

Cancer vaccines need to enter the lymph nodes, be processed by dendritic cells, access the MHC Class I pathway through cross-presentation, and induce the expression of costimulatory

molecules in antigen presenting cells for effective T cell activation. Created with BioRender.com.

1.2.1 Lymph node delivery

Vaccine formulations can be delivered to peripheral, tissue resident DCs that are then activated and transmigrate into lymphatic vessels to reach lymph nodes or drain directly into the lymph node for uptake by and activation of immature DCs residing in the lymph node.[37,38] Molecular size is one of the greatest determinants in LN delivery. When substances are administered to the interstitial space through subcutaneous, intramuscular or intradermal injection, molecules that are below 10 nm in size can access blood capillaries. Conversely, particles over 100 nm are excluded from direct diffusion into the vasculature due to the size constraints within interstitial aqueous channels.[39] Particles with hydrodynamic diameter between 10 and 100 nm are able to be transported to the lymph nodes efficiently.[40,41] Different kinds of biomaterials including polymers[42], lipid nanoparticles[43], and inorganic nanoparticles[44] with size falling within this range have been developed for LN delivery. For instance, Lynn et al. developed a peptide cancer vaccine platform with peptide-TLR7/8 conjugates that self-assemble into nanoparticles around 20 nm in size, irrespective of the peptide sequence.[45] The peptide antigen was linked to a hydrophobic block on one end to facilitate particle formulation through micellization and a charge-modifying group was incorporate on the opposite end to stabilize the nanoparticles (~20 nm in size). Synthetic long peptides in the particle form were retained longer in the draining lymph nodes and had higher DC uptake compared to the peptides in soluble form. LN-targeting nanoparticles also elicited a stronger immune response compared to nondraining 1 μm nanoparticles or soluble antigens.[46]

Particle size also affects the location of nanoparticles inside LNs and the cell types that they interact with. In one study, labeled tracers of various sizes were infused into the skin of mice. The 10 nm and 30 nm dextran tracers were found in the subcapsular sinus (SCS) at early time points, due to direct LN drainage and size exclusion barrier of the LN conduits, whereas 500 nm particles were found deeper in the LN parenchyma at later time points as they were transported by migratory cells.[47] Particles with larger sizes (200 nm) can drain into the lymph node sinus, potentially due to interstitial hydrodynamic forces after injection, where they are internalized by lymphatic sinuses (LS) – DCs, which are a subset of LN resident DCs that can generate rapid T cell responses.[48] Nanoparticles below 100 nm can get into the LN follicles, but small particles (5 – 15 nm) were cleared after 48 h, whereas large particles (50 – 100 nm) retained for over five weeks, generating more delivery to follicular dendritic cells (FDCs) and a higher humoral immune response.[49] In addition, $CD169^+$ SCS macrophages phagocytose nanoparticles above 30 nm and suppressing those macrophages allowed more 100 nm nanoparticles to accumulate in LN follicles and enhanced the humoral immunity.[50] Tumor also affects lymphatic transport of antigens. 500 nm particles were transported to the tumor-draining lymph nodes (TDLNs) to a greater extent in melanoma models compared to naïve models, probably due to tumor-induced matured APCs being more migratory. In contrast, melanoma decreased 10 nm and 30 nm dextran tracers accumulation in TDLNs compared to drainage from normal skin.[47]

Another strategy for enhancing LN delivery involves “albumin hitchhiking”. Albumin present in the interstitial fluid naturally travels to the bloodstream through the lymphatic system. Peptide-based cancer vaccines can be designed to bind to albumin and use this route to deliver antigens to the lymphatic system. Zhu et al. designed an albumin-binding vaccine by conjugating thiol-modified antigen and thiol-modified CpG to maleimide-functionalized Evans Blue derivatives,

which bind to human serum albumin. When administered subcutaneously, the vaccines bind to albumin in the interstitial space and are transported to the LNs. This approach also improves APC delivery as albumin can be internalized by APC through endocytosis. The results showed a 100-fold increase in LN delivery compared to the benchmark incomplete Freund's adjuvant (IFA).[51] Similarly, Liu et al. developed amphiphiles consisting of peptide antigen and CpG DNA linked to a lipophilic albumin-binding tail. Lipid-modified CpG showed 12-fold higher LN accumulation compared to soluble CpG over 7 days after injection. Mice immunized with antigen and albumin-binding CpG adjuvant induced 32-fold higher amounts of antigen-specific T cells compared to immunization with antigen and unmodified CpG.[52]

1.2.2 Dendritic cell-targeting strategies

Targeting ligands that bind to receptors preferentially expressed by DCs can facilitate vaccine uptake through receptor-mediated endocytosis. The mannose receptor (CD206) is a C-type lectin that is highly expressed on immature DCs.[53] Both liposomes and polymers have been functionalized with mannose to enhance peptide delivery to DCs.[54–57] For instance, Lv et al. compared polymeric micelles with same micellar core but different coronas (PEGylated, cationic or mannosylated) and demonstrated higher inguinal lymph nodes accumulation of the mannosylated micelles and 16-fold higher DC internalization than PEGylated micelles and 79-fold higher DC internalization than cationic micelles (**Figure 1.2**).[57] CD40 is a transmembrane receptor expressed on APCs. Rosalia et al. encapsulated antigens and adjuvants in poly(lactic-co-glycolic acid) (PLGA) and coated the nanoparticles with an agonistic αCD40-mAb to target DCs.[58] Similarly, Trabbic et al. coated gold nanoparticles with β-1,3-glucans (B13G) to target Dectin-1 on APCs.[59]

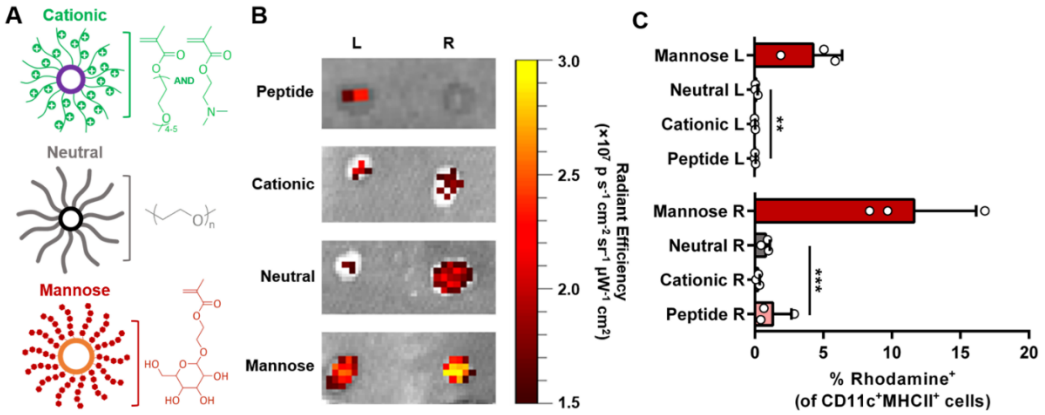

Figure 1.2 Dendritic Cell Targeting Strategies

(a) Cationic, neutral and mannose micelle structures. (b) Fluorescence imaging of right and left draining inguinal lymph nodes (48 h post-treatment). Mannosylated micelles are retained more efficiently in lymph nodes. (c) Flow cytometry analysis of lymph node-resident cells confirms that mannose-micelle formulations are internalized by $CD11c^{+}MHCII^{+}$ DCs. Data are presented as mean ± SD. N = 3 biological replicates. Statistical significance was calculated using one-way ANOVA with post-hoc Fisher's LSD test (**P ≤ 0.01, ***P ≤ 0.001). Reprinted with permission.[57]

1.3 STRATEGIES TO ENHANCE CROSS-PRESENTATION

1.3.1 Utilizing pH-responsive biomaterials for endosomal membrane disruption

Many peptide-based vaccine formulations enter cells through endocytosis and therefore need to escape the endosome and reach the cytosolic compartment for MHC Class I presentation to $CD8^{+}$ T cells. As endosomes mature into lysosomes, pH levels drop from 6.5 in early endosomes to 4.5 in lysosomes to activate lysosomal enzymes (**Figure 1.3a**).[60] Various biomaterials have been designed to leverage the acidification within the endosome-lysosome system, leading to the development of pH-responsive biomaterials(**Figure 1.3b**). Ideally vaccine formulations will selectively facilitate endosomal membrane disruption and avoid toxicity associated with cell membrane disruption.

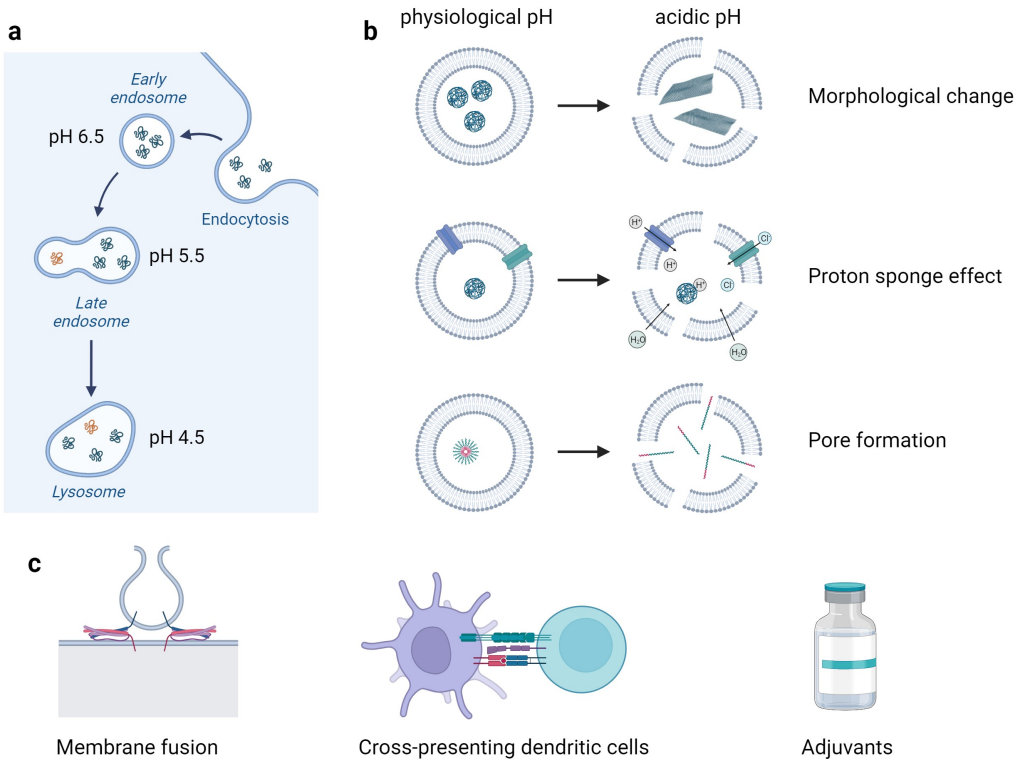

Figure 1.3 Strategies to enhance cross-presentation

(a) pH drops as endosomes mature into lysosomes. (b) pH-responsive biomaterials that utilize the acidification within the endosome-lysosome system to disrupt membranes. (c) Other methods to enhance cross-presentation, including membrane fusion for direct cytosolic delivery, targeting cross-presenting DCs and using adjuvants with cross-presenting activity. Created with BioRender.com.

One method to facilitate endosomal escape involves inducing morphological changes to mechanically disrupt the endosome. Gong et al. developed a proton-driven nanotransformer-based vaccine (NTV), by conjugating pyrene-conjugated D-peptide (PDP) to an amphiphilic block copolymer via an acid-cleavable acetal bond.[61] Under physiological pH conditions, these polymer-peptide conjugates self-assemble into nanospheres about 100 nm in size. As the pH drops in the endosome, the acetal bond hydrolyzes, releasing PDP molecules that assemble into nanosheets due to strong π–π interactions. The nanosheets are several micrometers in length or width and mechanically disrupt the endosomal membrane to release peptide antigens into the

cytosol. Another method employs changes in hydrophobicity to promote endosomal escape. The Stayton group employed endosomolytic polymers to deliver antigens, improving $CD8^+$ T cell response compared to control formulations.[62] The Wilson group developed electrostatically-stabilized nanoparticles by mixing decalysine-modified peptides with poly (propylacrylic acid) (pPAA).[63] At acidic pH, pPAA switched from hydrophilic to hydrophobic and destabilized the endosomal membrane to promote cytosolic delivery of the peptide antigen.

Another method to disrupt the endosomal membrane is through the "proton sponge" effect. This concept posits that buffering polycations swell as they are protonated and induce more protons and chloride ions to the endosome. The resulting osmotic pressure and polymer swelling cause endosomal rupture,[64] although the exact mechanism remains a subject of debate. Cationic polymers with secondary or tertiary amines are often used to create a proton sponge effect.[65] Luo et al. generated a library of pH-sensitive nanoparticles containing copolymers with tertiary amines in linear or cyclic side chains and discovered that a polymer called PC7A, with an tertiary amine in a cyclic seven-membered ring exhibited a high level of cross-presentation when applied for vaccine delivery.[42] This polymer also demonstrates adjuvant activity. Zhou et al. synthesized an amphiphilic diblock copolymer, PEG-b-PDPA, with a sharp pH transition at 6.3, and combined it with a cationic polymer, OEI-C14, to facilitate endosomal escape through the proton sponge effect.[55]

Finally, molecules like perforin can form pores in the endosomal membrane to release biomolecules into the cytosol.[66] This process naturally occurs in conventional DC1 (cDC1) for cross-presentation. Pore-forming molecules such as lytic peptides can be used to facilitate endosomal disruption. In a recent study in the Pun group, a bee-derived lytic peptide D-melittin was conjugated to a pH-sensitive polymer that self-assembled at physiological pH and

dissociated at acidic endosomal pH.[67] As pH drops in the endosome, the lytic peptide is exposed destabilizing the endosomal membrane, facilitate peptide antigen release, and promote cross-presentation.

1.3.2 Reactive Oxygen Species (ROS)

Reactive oxygen species (ROS) cause lipid peroxidation in DCs, which disrupts the endosomal membrane and facilitates antigen release into the cytosol for cross-presentation.[68] Xu et al. developed a PEGylated reduced graphene oxide nanosheet (RGO-PEG) and conjugated neoantigen peptides through maleimide reactions and adsorbed CpG to the nanosheet via π–π stacking.[69] RGO-PEG increased intracellular reactive oxygen species (ROS) levels in DCs and enhanced cross-presentation of the neoantigen peptides.

1.3.3 Direct cytosolic delivery

Peptides that are delivered directly to the cytosol through membrane fusion may avoid endosomal entrapment. SNARE proteins mediate synaptic vesicles and plasma membrane fusion during exocytosis.[70] Yang et al. developed complementary lipidated coiled-coil peptides and modified cell membranes and liposomes with the complementary to achieve targeted membrane fusion and intracellular delivery.[71] However, as cell membrane fusion requires modification to the cells, further progress is needed for *in vivo* applications like cancer vaccines.

1.3.4 Targeting cross-presenting DCs

DCs have two subtypes: conventional DCs (cDCs) and plasmacytoid DCs (pDCs).[72] cDCs are further divided into two subsets: cDC1 and cDC2. cDC1 are known to be potent at cross-presentation.[73] Their high expression of MHCI, high ROS production and low pH contribute to enhanced cross-presentation.[72] In addition, a recent study showed that cDC1 expresses perforin-

2, which forms pores in the endosomes to facilitate antigen delivery to the cytosol and enhance cross-presentation.[74] cDC1 express certain markers, including XCR1 (chemokine receptor), DNGR-1/CLEC9A (C-type lectin receptor), CD103 in mice (integrin αE) and BDCA3 in humans, which can be used to target cDC1.[75] Yan et al. identified a peptide, WH, that binds to Clec9a.[76] They fused the WH peptide or a control peptide with the OVA antigenic peptide and observed enhanced activation of OVA-specific $CD8^+$ T cells with the WH-fused peptide compared to the control peptide. This study demonstrated that peptide WH could bind to Clec9a and targeting cDC1 for enhanced cross-presentation. Similarly, Arabpour et al. developed fusion vaccines by fusing antigens with anti-CD103 antibodies, specifically targeting $CD103^+$ cDC1, and demonstrated that CD103 targeting increased the number of antigen-specific $CD8^+$ T cells.[77]

1.3.5 Adjuvants to enhance cross-presentation

Certain adjuvants facilitate antigen cross-presentation. Aluminum-containing adjuvants have been used clinically for many years and demonstrate excellent safety profiles. Although traditional aluminum adjuvant is insufficient for cross-presentation, Li et al. found that when antigens were conjugated to α-Al_2O_3 nanoparticles, cross-presentation significantly improved through the autophagy pathway.[78] Nanoparticles such as α-Al_2O_3 can induce autophagy[79] and the activation of autophagy promotes DCs to cross-present antigens to $CD8^+$ T cells.[80] Saponin-based adjuvants (SBAs), glycosides isolated from the South American soapbark tree, also induce cross-presentation. Huis in 't Veld et al. showed that SBAs promote cross-presentation through the induction of lipid bodies and activation of the PKR-like endoplasmic reticulum kinase (PERK) pathway.[81] Some adjuvants targeting the Toll-like receptors (TLRs) and nucleotide-binding and oligomerization domain (NOD)-like receptors (NLRs) expressed by DCs promote cross-presentation. Zhao et al. utilized *meso*-2,6-diaminopimelic acid (DAP), a NOD1 agonist, in

their polymeric vaccine formulation vaccine design to promote antigen cross-presentation in DCs .[82]

1.4 CONSIDERATIONS IN DESIGNING VACCINE ADJUVANTS

Adjuvants have long played a critical role in enhancing the antigen-specific responses in vaccines, and are particularly important for peptide-cancer vaccines since peptide antigens are usually non-immunogenic on their own. While some delivery platforms such as the previously described PC7A polymer inherently possess adjuvant properties,[42] other platforms require the incorporation of adjuvants to augment the immune response. Commonly-used cancer vaccine adjuvants are summarized in **Table 1.1**. Aluminum salts and incomplete Freund's adjuvant (IFA) were often used in earlier vaccine formulations to generate an antigen depot at the injection site to prolong antigen presentation. However, their adjuvant effect is relatively weak, and they promote Th2 responses, which is less suitable for cancer vaccine applications.[83] Toll-like receptor (TLR) agonists and stimulator of interferon genes (STING) agonists are used in more recent vaccine formulations and enhance the immune responses by generating pro-inflammatory cytokines,[84] contributing to DC maturation,[85] enhancing cross-presentation,[86] and improving antigen-specific $CD8^+$ T cell survival.[87] However, high levels of pro-inflammatory cytokines in the systemic circulation raise safety concerns. To develop effective vaccine adjuvants, the following important considerations need to be taken into account to maximize adjuvant benefits while minimizing potential drawbacks: controlling the delivery of adjuvants, optimizing adjuvant co-delivery with antigens, and exploring combinations of multiple adjuvants.

Table 1.1 Common cancer vaccine adjuvants, pathways, receptor locations and applications in peptide-based cancer vaccines.

Adjuvants	Pathway / mechanism of action	Receptor location	Peptide cancer vaccine applications

Aluminum salts	Depot effect[88], NLRP3 inflammasome[89]	N/A	[90]
Incomplete Freund's adjuvant (IFA) (e.g. Montanide ISA-51)	Depot effect, cytokine and chemokine induction[91]	N/A	[92]
Granulocyte-macrophage colony stimulating factor (GM-CSF)	DC maturation, T cell activation[93]	Cell surface	[9]
CpG oligodeoxynucleotides (CpG ODNs)	TLR 9 pathway	Endosome	[51,94]
polyinosinic acid: polycytidylic acid Poly(I:C)	TLR 3 pathway	Endosome	[95,96]
Imidazoquinoline derivatives (IMDs) (e.g. resiquimod, imiquimod and gardiquimod)	TLR 7/8 pathway	Endosome	[45,97]
Stimulator of interferon genes (STING) agonists (e.g. cGAMP, ADU-S100)	STING pathway	Endoplasmic reticulum	[55,98]

1.4.1 Controlled delivery of adjuvants

Despite recent advances in adjuvant development, uncontrolled delivery of adjuvants may generate pro-inflammatory cytokines in the systemic circulation and cause toxicity.[99] To address this problem, researchers have developed pH-responsive and redox-responsive materials to control the release of adjuvants. Aichhorn et al. developed a pH-sensitive polymeric prodrug with hydrazide linkers that releases TLR 7/8 agonist in the acidic endosomal environment.[100] This polymer accumulated in endosomal and lysosomal vesicles and adjuvant release was greatly enhanced at pH 5 compared to pH 7.4. Similarly, Zhou et al. developed a dendritic cell-targeted diblock copolymer that formed micelles at physiological pH, but disassembled when pH was below 6.3.[55] Nguyen and Song et al. reported a polymeric STING adjuvant formulation with STING Agonist-3 conjugated to the polymer backbone via a cathepsin substrate which is cleaved in endosomal compartments.[101] They conjugated DMXAA, a STING agonist to the polymer backbone through an esterase-labile bond so that the STING agonist is released inside DCs rather than in the blood circulation. Bhagchandani et al. expanded on this concept by creating a library

of R848 bottlebrush prodrugs with different aryl ester linkers to achieve release half-life ranging from 4 to 40 days.[102] They noticed that the fast release prodrug had similar maximum tolerable dose (MTD) compared to free R848, while the medium and slow release prodrug had MTDs four and eight times higher than the free drug when administered intravenously. The medium and slow release prodrugs slowed tumor progression and improved survival compared to free R848 and displayed no signs of toxicity.

1.4.2 Co-delivery of antigen and adjuvant

Since antigen recognition by TCR in the absence of the co-stimulatory signal can induce T cell anergy,[103] efficient T cell activation relies on the colocalized delivery of both antigen and adjuvant to the same DC to ensure that antigen is presented along with the necessary co-stimulatory molecules to activate T cells. Delivering antigens with tolerogenic immunomodulators can even induce antigen-specific immune tolerance and inhibition of T cell activation.[104] Fischer et al. showed that colocalized delivery of antigen and adjuvant generated higher antibody titers compared to coadministration of antigen and adjuvant.[105] In addition, they were able to reduce the adjuvant doses by 10-fold with colocalized delivery, potentially reducing the side effects associated with adjuvants. Antigens and adjuvants can be co-delivered by co-encapsulation[58,98] or by covalent conjugation on the same delivery platform[45,54].

1.4.3 Combination of multiple adjuvants

Multiple adjuvants can be combined to activate different immune pathways to boost the immune response. Tom et al. conjugated pyrimido-indole (TLR4 agonist), loxoribine (TLR7 agonist) and CpG-ODN (TLR9 agonist) together to form a tri-agonist compound.[106] The tri-agonist compound generated higher immune cell activation and antibody responses compared to di-agonist compounds and unconjugated mixture of the agonists, perhaps due to the proximity of agonists

with covalent conjugation. Controlling the spatial arrangement of multiple adjuvants generated synergistic effects and shifted the immune response. Besides spatial control, temporal control of multiple adjuvants also plays an important role. Jin et al. developed a liposome platform to co-deliver poly(I:C), a TLR3 agonist, and resiquimod, a TLR7/8 agonist.[95] Resiquimod was delivered as an inactive prodrug by conjugation to cholesterol. Poly(I:C) rapidly activated the TLR3 pathway, while TLR7/8 pathway activation was delayed for 4-6 h as resiquimod activity was restored by γ-interferon-inducible lysosomal thiol reductase (GILT) in the endolysosome through linker cleavage. This optimized order and kinetics of pathway activation generated non-exhausted DCs and $CD8^+$ T cells and created strong antitumor immunity.

1.5 ROUTES OF ADMINISTRATION

1.5.1 Subcutaneous and intramuscular administration

Subcutaneous administration is the most commonly used method for delivering peptide-based cancer vaccines in recent preclinical studies. Many studies have demonstrated that nanoparticles with diameter less than 100 nm accumulate in the lymph nodes without any active-targeting strategies when administered through the subcutaneous route.[42,69,94,95,98,107] In addition, vaccines can benefit from the depot effect of this route, which prolongs the release of antigens to enhance the immune response.[108] Baharom et al. developed a polymer-based nanoparticle platform delivering neoantigens and TLR7/8 agonists and found that subcutaneously administered nanoparticles can be detected at the injection site as well as lymph nodes for up to two weeks, resulting in prolonged antigen presentation and a high magnitude of antigen-specific $CD8^+$ T cells.[109] However, vaccine depots can be a double-edged sword. Hailemichael et al. showed that chronic antigen presentation by antigenic peptide in incomplete Freund's adjuvant (IFA) induced T cell sequestration and deletion at the vaccination site and was less effective than a short-lived

water-based formulation.[110] While the subcutaneous route is often used for preclinical cancer vaccine studies, the intramuscular route is preferred in clinical settings as it allows for rapid absorption, large injection volume and reduced irritation. Kuai et al. evaluated a cancer nanodisc vaccine platform by both subcutaneous and intramuscular injections, and demonstrated that cancer vaccines administered through the subcutaneous route had higher LN delivery and induced more antigen-specific T cells compared to the intramuscular route.[111] Currently, subcutaneous delivery of cancer vaccines is still the preferred route for most preclinical studies.

1.5.2 Intradermal administration

Intradermal delivery is another suitable option for peptide-based cancer vaccines. The papillary dermis, where this route targets, is highly vascularized and contains many APCs such as Langerhans cells and dendritic cells, which are good targets for cancer vaccines.[112] Kim et al. developed dissolving microneedles with amphiphilic triblock copolymer, Pluronic F127, hydrophobic resiquimod adjuvant and hydrophilic antigen.[113] The microneedles dissolve in the intradermal fluid, forming micelles that encapsulate the antigen and adjuvant, and then travel to the lymph nodes to activate the DCs.

1.5.3 Intranodal administration

Intranodal delivery allows cancer vaccines to be delivered directly to the lymph nodes. Senti et al. showed that intranodal delivery of allergens generated less side effects compared to subcutaneous delivery in a clinical trial.[114] Intranodal injection of peptide antigens generated a higher $CD8^+$ T cell response compared to subcutaneous and intradermal vaccinations possibly due to short half-life and inefficient delivery of free peptides when administered outside of the lymphatic system.[115] It also induced a higher IgG2a response and IFN-γ production compared to subcutaneous, intramuscular and intradermal administrations.[116] However, this method requires

ultrasound guidance in patients[117] or requires surgically exposing the lymph nodes in mice [118] and is more invasive than subcutaneous and intradermal injections.

1.5.4 Intravenous administration

Treatments using the intravenous route offers some advantages for vaccine applications but pose higher risk of systemic toxicity. Baharom et al. compared intravenous and subcutaneous routes for delivery of a nanoparticle containing neoantigen and TLR7/8 agonist.[109] At the same antigen dosage, subcutaneous administration generated higher frequency of antigen-specific $CD8^+$ T cells than intravenous administration, which could be due to prolonged antigen retention by the subcutaneous route. However, the intravenous route generated antigen-specific $CD8^+$ T cells that were more stem-like, whereas the subcutaneous route generated antigen-specific $CD8^+$ T cells in the effector state. When the intravenous dosage was increased by four-fold to match the magnitude of $CD8^+$ T cell response generated by the subcutaneous administration, the investigators observed better tumor control in the MC38 colorectal cancer with intravenous injection. This study showed that the vaccine administration route can affect the responding T cell states and that stem-like T cells generated better antitumoral effect compared to effector T cells in a therapeutic cancer vaccination. Interestingly, Sultan et al. found out that intravenous route generated a higher T cell response compared to subcutaneous route.[108] They adoptively transferred low numbers of naïve antigen-specific cytotoxic T-lymphocytes (CTLs) and then immunized the mice intravenously, intramuscularly or subcutaneously with peptide antigens and poly-ICLC, anti-CD40 adjuvants. Intravenous vaccination was more efficient at expanding antigen-specific CTLs compared to intramuscular and subcutaneous vaccination. The intravenous route can also be used to target tumors for in situ vaccination. Zhang et al. developed a nanoparticle platform containing poly-[(N-2-hydroxyethyl)-aspartamide]-Pt(IV)/β-cyclodextrin

(PPCD) and CpG that accumulate in the tumor after intravenous administration and dissociate to release PPCD for tumor killing.[119] The resulting tumor antigens and CpG activate DCs and prime T cells.

Other less common routes of peptide-based cancer vaccine delivery include oral delivery[120] and intratumoral delivery[121]. The choice of administration route should be carefully considered to balance between effectiveness and potential side effects.

1.6 EVALUATION OF CANCER VACCINES

1.6.1 Preclinical tumor models

Most tumor models in preclinical cancer vaccine development are implanted subcutaneously for ease of monitoring tumor growth. However, subcutaneous models may not recapitulate the tumor microenvironment as well as orthotopic models. A recent study showed CMT 167, a lung carcinoma model, had fewer immune cells when implanted orthotopically compared to subcutaneously. However, no immune cell difference was observed in the 4T1 breast cancer model between orthotopic and subcutaneous tumors.[122] The commonly-used preclinical tumor models for vaccine evaluation are summarized in Table 1.2.

Some tumor cell lines such as B16 and E.G7 are modified to express the ovalbumin (OVA), a commonly used model antigen in cancer research that is well-characterized with defined epitopes. In addition, many *in vitro* and *in vivo* assays have been developed for OVA-derived antigens. However, OVA is a foreign antigen that is not naturally present in mice and humans, and therefore is less clinically relevant. Two neoantigens that have been validated for the B16F10 melanoma model are gp100 and Trp2.[123,124] The Sahin group used next-generation sequencing to identify mutations in the B16F10, CT26 and 4T1 tumors and demonstrated tumor

control with immunization of some synthetic 27-mer peptides, including B16-M30.[125] For the MC38 tumor model, Adpgk and Reps1 are commonly used neoantigens. Yadav et al. discovered mutations in the neo-epitopes within adpgk and resp1 proteins and demonstrated that immunization with the mutated peptides slowed MC38 tumor growth.[126]

Among the different preclinical tumor models, TC-1 cervical carcinoma is relatively easy to treat; several vaccines generated long-term survival in mice bearing TC-1 tumors.[9,45] However, B16F10 tumors are highly aggressive, immunosuppressive and can metastasize to distant sites. While a few studies showed initial control of tumor growth after vaccination, tumors continued to grow after treatment cessation.[55,127] Poorly immunogenic tumors like B16 express lower levels of T cell costimulatory molecules and respond poorly to immunotherapies.[128] Cancer vaccines often need to be combined with immune checkpoint blockade such as anti-PD-1, anti-PD-L1 or anti-CTLA-4 antibodies in these tumor models.[82,94]

The antitumor response can be examined in either a prophylactic model, whereby tumors are inoculated after vaccination, or a therapeutic model, whereby vaccination is given to treat established tumors. Most research focuses on therapeutic models for clinical relevance, although some formulations have been reported to be effective in both the prophylactic and therapeutic settings.[109,127]

Table 1.2 Common preclinical models for cancer vaccine development.

Cell line	Tumor type	Mouse strain	Antigen	Sequence for MHCI epitope	Sequence for MHCII epitope
B16-OVA	Melanoma	C57BL/6	OVA	SIINFEKL[129]	ISQAVHAAHAEINEAGR
E.G7-OVA	Lymphoma	C57BL/6	OVA	SIINFEKL	ISQAVHAAHAEINEAGR
B16F10	Melanoma	C57BL/6	gp100, Trp2	Trp2: VYDFFVWL[124] gp100: EGSRNQDWL[130] B16-M27: REGVELCP	Trp1: CRPGWRGAACNQKI B16-M30: PSKPSFQE FVDWENVSPELNSTDQPFL

				GNKYEMRRHGTTHSLVIHD[125]	
MC38	Colon carcinoma	C57BL/6	Adpgk, Reps1	Adpgk: ASMTNMELM Resp1: AQLANDVVL[126]	Ddr2: SEASEWEPHAVYFPLVLDDVNPS Pcdh18: SPWAYITTVTATDPDL Zmiz1: RPPADFTQPAASAAAAA[131]
TC1	Cervical carcinoma	C57BL/6	E7	E7: RAHYNIVTF[132]	E7: EQLNDSSEEEDTDEID[133]

1.6.2 DC cross-presentation and activation

In vitro DC cross-presentation assays using T cell hybridomas can be used as initial screening of vaccine candidates. B3Z cell is a T cell hybridoma that recognizes SIINFEKL, an OVA MHCI epitope, in the context of H-2K^b and produces β-galactosidase, which can be detected by adding fluorogenic or chromogenic substrates.[134] Similarly, BUSA14 is a T cell hybridoma that recognizes both human and mouse gp100$_{25\text{-}33}$ peptides and produces β-galactosidase, and can be used in evaluating vaccines with gp100 neoantigen.[135] *In vivo* DC cross-presentation is evaluated by analyzing the amount of antigen-specific CD8$^+$ T cells generated after vaccinations, and will be discussed in the next section.

DC activation is another important criterion for vaccine efficiency. DCs upregulate the expression of costimulatory molecules, such as CD80, CD86, CD83 and MHCII upon activation.[136,137] CD80 and CD86 are the most commonly evaluated DC activation markers that belong to the B7 family, and bind to CD28 on T cells to enhance T cell activation by promoting T cell survival, expansion and differentiation.[138] CD40 is another DC activation marker that binds to CD40L (CD154) on T cells and contributes to Th1 differentiation in CD4$^+$ T cells.[139]

1.6.3 Antigen-specific T cells and T cell subsets

Cancer vaccines stimulate the adaptive immune system to generate T cells that can recognize cancer antigens. Therefore, the magnitude of antigen-specific T cells is an important indicator for cancer vaccine efficiency. The MHC multimer assay (usually tetramers or pentamers), with multiple MHC molecules held together with specific peptides to increase the avidity between the MHC/peptide complexes and T cell receptors (TCRs), is often used to evaluate the frequency of antigen-specific T cells. ELISpot and intracellular cytokine staining (ICS) are often used together with the MHC multimer assay to evaluate the functionality of antigen-specific T cells. After isolation from immunized mice, T cells are cultured *in vitro* and stimulated with antigens to evaluate antigen-specific cytokine-producing T cells.

We investigated twenty recently published peptide-based vaccine papers but did not observe an obvious correlation between the percentage of antigen-specific T cells and antitumor capacity.[9,42,43,45,51,52,54,55,58,61,63,69,82,94,96–98,107,127,140] A number of different factors could contribute to this. First, the percentage of antigen-specific $CD8^+$ T cells over total $CD8^+$ T cells was reported from various sources, including blood, spleen, lung and lymph node. The antigen-specific T cell frequency is usually higher in blood samples/peripheral blood mononuclear cells (PBMCs) than in spleens.[140,141] T cells in the blood are circulating and thus have a higher chance to encounter antigens presented by the antigen-presenting cells (APCs) and in the peripheral tissues. However, within the same study, the percentage of antigen-specific T cells does correlate with outcome.[43,51] In a study with albumin-binding vaccines, Zhu et al. showed that the albumin/vaccine nanocomplexes containing CpG and Adpgk neoantigen showed a 14.1- and 13.6- fold higher frequency of antigen-specific $CD8^+$ T cells compared to CpG + Adpgk and IFA(CpG + Adpgk) controls, and only albumin/vaccine nanocomplexes generated long-term survival in a MC38 tumor model, with 2 out of 16 mice surviving more than 30 days. The

number of immunizations, treatment schedules, and time of T cell evaluation also affect the magnitude of T cell responses. The frequency of antigen-specific $CD8^+$ T cells increases as more immunizations are given.[94,107] For instance, Kuai et al. demonstrated that the frequency of antigen-specific $CD8^+$ T cells in PBMCs increased from 3% to 30% one week after the 1st immunization compared to one week after the 3rd immunization.[94] The number gradually decreased after the treatment stopped.[69,94] Therefore, optimizing the dosing schedule could generate a better immune response. We suggest that the field could standardize one of the time points of evaluation, such as 7 days after the 2nd immunization, for better comparison between formulations from different research groups.

T cell states and subsets also affect therapeutic efficacy. Baharom et al. used different injection routes to generate similar magnitude of antigen-specific T cell responses, but demonstrated better therapeutic efficacy when T cells were more stem-like.[109] Similarly, Ramirez-Valdez et al. also found that the extent of $CD8^+$ T cell response was not the only factor determining tumor control.[141] They either primed the mice with nanoparticles containing irrelevant antigen followed by boosting with adenoviral vector containing cancer antigen, or primed the mice with nanoparticles containing cancer antigen followed by adenoviral vector containing irrelevant antigen. They observed that the two methods generated similar magnitudes of antigen-specific $CD8^+$ T cell response one week post the vaccine boost, but differed significantly in a therapeutic MC38 tumor model, suggesting that the innate immunity could play a role. $CD8^+$ T cells have different subsets, and only Tc1, Tc2 and Tc22 have cytotoxic function.[142] Regulatory T (Treg) cells, a subset of $CD4^+$ T cells, hinder antitumor responses by secreting inhibitory cytokines, suppressing cytolysis and impeding DC maturation.[143] To account for the immunosuppressive T cells, some people used the $CD8^+$ T cells to the Tregs ratio for analysis.[55] Therefore, it is

important to examine both the magnitude of T cell response and T cell states to predict the therapeutic outcome.

1.7 CONCLUSION AND PERSPECTIVES

Peptide-based cancer vaccines hold great promise as a novel cancer immunotherapy. Peptides are safe, easy to make, cost-effective and have good storage stability. With the development in bioinformatics and machine learning, neoantigens can be selected and personalized for different patients for optimal care. Development of new delivery platforms enhances antigen delivery and presentation, resulting in improved antigen-specific T cell responses and antitumoral efficiency. Discovery of new adjuvants boosts the immune response and further enhances the activity of the cancer vaccines.

Despite recent progress in cancer vaccine development, most formulations are still in the preclinical stage. Many cancer vaccine studies use the model antigen ovalbumin to test the delivery platforms, but its translational value is limited. To bring cancer vaccines into the clinical stage, more research needs to be done to identify antigens that can effectively bind to the MHC molecules and are specific to tumors. In addition, cancer vaccines have limited efficacy in some preclinical models, especially in non-immunogenic and aggressive tumor models. While many vaccines slow tumor growth, they may not lead to tumor elimination. Cancer vaccines may need to be combined with traditional cancer treatment methods, such as chemotherapy or radiation therapy to induce cancer cell death and release antigens to further boost the immune response. In addition, cancer vaccines may be combined with immune checkpoint inhibitors such as anti-PD-1 and anti-CTLA-4 to enhance T cells' capacity to fight against cancer cells. Because T cell exclusion in the TME might also contribute to vaccine failures, approaches for promoting T cell infiltration into tumors is paramount. Many cancer vaccine studies focus on the quantity of

antigen-specific T cells, but investigation into the quality of the T cells will provide more insights for future vaccine development. T cells are not the only players in tumor immunity; the TME contains other immune cells such as myeloid-derived suppressor cells (MDSCs), regulatory T (Treg) cells and tumor-associated macrophages (TAMs) that are immunosuppressive. It is critical to eliminate or reprogram the immune-suppressive cells to turn a “cold” tumor into a “hot” tumor to optimize the activity of antigen-specific T cells. Furthermore, optimizing vaccine adjuvant dosing, timing and combinations can yield additional benefits. Although studies have shown the benefits of combining multiple adjuvants, it is not clear what combination yields the best results and what the best timing is for activating the innate immune pathways. Achieving these goals will be important for developing more effective cancer vaccines and translating them into clinical therapies.

1.8 ACKNOWLEDGEMENTS

This work was supported by the U.S. National Institutes of Health, National Cancer Institute Grant R01CA257563.

1.9 REFERENCES

(1) Kantoff, P. W.; Higano, C. S.; Shore, N. D.; Berger, E. R.; Small, E. J.; Penson, D. F.; Redfern, C. H.; Ferrari, A. C.; Dreicer, R.; Sims, R. B.; Xu, Y.; Frohlich, M. W.; Schellhammer, P. F. Sipuleucel-T Immunotherapy for Castration-Resistant Prostate Cancer. *New England Journal of Medicine* **2010**, *363* (5), 411–422. https://doi.org/10.1056/NEJMoa1001294.

(2) Rojas, L. A.; Sethna, Z.; Soares, K. C.; Olcese, C.; Pang, N.; Patterson, E.; Lihm, J.; Ceglia, N.; Guasp, P.; Chu, A.; Yu, R.; Chandra, A. K.; Waters, T.; Ruan, J.; Amisaki, M.; Zebboudj, A.; Odgerel, Z.; Payne, G.; Derhovanessian, E.; Müller, F.; Rhee, I.; Yadav, M.; Dobrin, A.; Sadelain, M.; Łuksza, M.; Cohen, N.; Tang, L.; Basturk, O.; Gönen, M.; Katz, S.; Do, R. K.; Epstein, A. S.; Momtaz, P.; Park, W.; Sugarman, R.; Varghese, A. M.; Won, E.; Desai, A.; Wei, A. C.; D'Angelica, M. I.; Kingham, T. P.; Mellman, I.; Merghoub, T.; Wolchok, J. D.; Sahin, U.; Türeci, Ö.; Greenbaum, B. D.; Jarnagin, W. R.; Drebin, J.; O'Reilly, E. M.; Balachandran, V. P. Personalized RNA Neoantigen Vaccines Stimulate T Cells in Pancreatic Cancer. *Nature* **2023**, *618* (7963), 144–150. https://doi.org/10.1038/s41586-023-06063-y.

(3) Morse, M. A.; Crosby, E. J.; Force, J.; Osada, T.; Hobeika, A. C.; Hartman, Z. C.; Berglund, P.; Smith, J.; Lyerly, H. K. Clinical Trials of Self-Replicating RNA-Based Cancer Vaccines. *Cancer Gene Ther* **2023**, *30* (6), 803–811. https://doi.org/10.1038/s41417-023-00587-1.

(4) Maslak, P. G.; Dao, T.; Bernal, Y.; Chanel, S. M.; Zhang, R.; Frattini, M.; Rosenblat, T.; Jurcic, J. G.; Brentjens, R. J.; Arcila, M. E.; Rampal, R.; Park, J. H.; Douer, D.; Katz, L.; Sarlis, N.; Tallman, M. S.; Scheinberg, D. A. Phase 2 Trial of a Multivalent WT1 Peptide Vaccine (Galinpepimut-S) in Acute Myeloid Leukemia. *Blood Adv* **2018**, *2* (3), 224–234. https://doi.org/10.1182/bloodadvances.2017014175.

(5) Callmann, C. E.; Cole, L. E.; Kusmierz, C. D.; Huang, Z.; Horiuchi, D.; Mirkin, C. A. Tumor Cell Lysate-Loaded Immunostimulatory Spherical Nucleic Acids as Therapeutics for Triple-Negative Breast Cancer. *Proceedings of the National Academy of Sciences* **2020**, *117* (30), 17543–17550. https://doi.org/10.1073/pnas.2005794117.

(6) Kawahara, M.; Takaku, H. A Tumor Lysate Is an Effective Vaccine Antigen for the Stimulation of CD4+ T-Cell Function and Subsequent Induction of Antitumor Immunity Mediated by CD8+ T Cells. *Cancer Biol Ther* **2015**, *16* (11), 1616–1625. https://doi.org/10.1080/15384047.2015.1078027.

(7) Viborg, N.; Pavlidis, M. A.; Barrio-Calvo, M.; Friis, S.; Trolle, T.; Sørensen, A. B.; Thygesen, C. B.; Kofoed, S. V.; Kleine-Kohlbrecher, D.; Hadrup, S. R.; Rønø, B. DNA Based Neoepitope Vaccination Induces Tumor Control in Syngeneic Mouse Models. *npj Vaccines* **2023**, *8* (1), 1–16. https://doi.org/10.1038/s41541-023-00671-5.

(8) Li, J.; Wu, Y.; Xiang, J.; Wang, H.; Zhuang, Q.; Wei, T.; Cao, Z.; Gu, Q.; Liu, Z.; Peng, R. Fluoroalkane Modified Cationic Polymers for Personalized mRNA Cancer Vaccines. *Chemical Engineering Journal* **2023**, *456*, 140930. https://doi.org/10.1016/j.cej.2022.140930.

(9) Li, A. W.; Sobral, M. C.; Badrinath, S.; Choi, Y.; Graveline, A.; Stafford, A. G.; Weaver, J. C.; Dellacherie, M. O.; Shih, T.-Y.; Ali, O. A.; Kim, J.; Wucherpfennig, K. W.; Mooney, D. J. A Facile Approach to Enhance Antigen Response for Personalized Cancer Vaccination. *Nature Mater* **2018**, *17* (6), 528–534. https://doi.org/10.1038/s41563-018-0028-2.

(10) Choi, B.; Moon, H.; Hong, S. J.; Shin, C.; Do, Y.; Ryu, S.; Kang, S. Effective Delivery of Antigen–Encapsulin Nanoparticle Fusions to Dendritic Cells Leads to Antigen-Specific Cytotoxic T Cell Activation and Tumor Rejection. *ACS Nano* **2016**, *10* (8), 7339–7350. https://doi.org/10.1021/acsnano.5b08084.

(11) Liu, J.; Fu, M.; Wang, M.; Wan, D.; Wei, Y.; Wei, X. Cancer Vaccines as Promising Immuno-Therapeutics: Platforms and Current Progress. *J Hematol Oncol* **2022**, *15*, 28. https://doi.org/10.1186/s13045-022-01247-x.

(12) Saxena, M.; van der Burg, S. H.; Melief, C. J. M.; Bhardwaj, N. Therapeutic Cancer Vaccines. *Nat Rev Cancer* **2021**, *21* (6), 360–378. https://doi.org/10.1038/s41568-021-00346-0.

(13) Hu, Z.; Ott, P. A.; Wu, C. J. Towards Personalized, Tumour-Specific, Therapeutic Vaccines for Cancer. *Nat Rev Immunol* **2018**, *18* (3), 168–182. https://doi.org/10.1038/nri.2017.131.
(14) Lin, M. J.; Svensson-Arvelund, J.; Lubitz, G. S.; Marabelle, A.; Melero, I.; Brown, B. D.; Brody, J. D. Cancer Vaccines: The next Immunotherapy Frontier. *Nat Cancer* **2022**, *3* (8), 911–926. https://doi.org/10.1038/s43018-022-00418-6.
(15) Slamon, D. J.; Godolphin, W.; Jones, L. A.; Holt, J. A.; Wong, S. G.; Keith, D. E.; Levin, W. J.; Stuart, S. G.; Udove, J.; Ullrich, A.; Press, M. F. Studies of the HER-2/Neu Proto-Oncogene in Human Breast and Ovarian Cancer. *Science* **1989**, *244* (4905), 707–712. https://doi.org/10.1126/science.2470152.
(16) You, Z.; Zhou, W.; Weng, J.; Feng, H.; Liang, P.; Li, Y.; Shi, F. Application of HER2 Peptide Vaccines in Patients with Breast Cancer: A Systematic Review and Meta-Analysis. *Cancer Cell International* **2021**, *21* (1), 489. https://doi.org/10.1186/s12935-021-02187-1.
(17) Baba, T.; Sato-Matsushita, M.; Kanamoto, A.; Itoh, A.; Oyaizu, N.; Inoue, Y.; Kawakami, Y.; Tahara, H. Phase I Clinical Trial of the Vaccination for the Patients with Metastatic Melanoma Using Gp100-Derived Epitope Peptide Restricted to HLA-A*2402. *Journal of Translational Medicine* **2010**, *8* (1), 84. https://doi.org/10.1186/1479-5876-8-84.
(18) Schwartzentruber, D. J.; Lawson, D. H.; Richards, J. M.; Conry, R. M.; Miller, D. M.; Treisman, J.; Gailani, F.; Riley, L.; Conlon, K.; Pockaj, B.; Kendra, K. L.; White, R. L.; Gonzalez, R.; Kuzel, T. M.; Curti, B.; Leming, P. D.; Whitman, E. D.; Balkissoon, J.; Reintgen, D. S.; Kaufman, H.; Marincola, F. M.; Merino, M. J.; Rosenberg, S. A.; Choyke, P.; Vena, D.; Hwu, P. Gp100 Peptide Vaccine and Interleukin-2 in Patients with Advanced Melanoma. *N Engl J Med* **2011**, *364* (22), 2119–2127. https://doi.org/10.1056/NEJMoa1012863.
(19) Peng, M.; Mo, Y.; Wang, Y.; Wu, P.; Zhang, Y.; Xiong, F.; Guo, C.; Wu, X.; Li, Y.; Li, X.; Li, G.; Xiong, W.; Zeng, Z. Neoantigen Vaccine: An Emerging Tumor Immunotherapy. *Molecular Cancer* **2019**, *18* (1), 128. https://doi.org/10.1186/s12943-019-1055-6.
(20) Lang, F.; Schrörs, B.; Löwer, M.; Türeci, Ö.; Sahin, U. Identification of Neoantigens for Individualized Therapeutic Cancer Vaccines. *Nat Rev Drug Discov* **2022**, *21* (4), 261–282. https://doi.org/10.1038/s41573-021-00387-y.
(21) Keskin, D. B.; Anandappa, A. J.; Sun, J.; Tirosh, I.; Mathewson, N. D.; Li, S.; Oliveira, G.; Giobbie-Hurder, A.; Felt, K.; Gjini, E.; Shukla, S. A.; Hu, Z.; Li, L.; Le, P. M.; Allesøe, R. L.; Richman, A. R.; Kowalczyk, M. S.; Abdelrahman, S.; Geduldig, J. E.; Charbonneau, S.; Pelton, K.; Iorgulescu, J. B.; Elagina, L.; Zhang, W.; Olive, O.; McCluskey, C.; Olsen, L. R.; Stevens, J.; Lane, W. J.; Salazar, A. M.; Daley, H.; Wen, P. Y.; Chiocca, E. A.; Harden, M.; Lennon, N. J.; Gabriel, S.; Getz, G.; Lander, E. S.; Regev, A.; Ritz, J.; Neuberg, D.; Rodig, S. J.; Ligon, K. L.; Suvà, M. L.; Wucherpfennig, K. W.; Hacohen, N.; Fritsch, E. F.; Livak, K. J.; Ott, P. A.; Wu, C. J.; Reardon, D. A. Neoantigen Vaccine Generates Intratumoral T Cell Responses in Phase Ib Glioblastoma Trial. *Nature* **2019**, *565* (7738), 234–239. https://doi.org/10.1038/s41586-018-0792-9.
(22) Ott, P. A.; Hu-Lieskovan, S.; Chmielowski, B.; Govindan, R.; Naing, A.; Bhardwaj, N.; Margolin, K.; Awad, M. M.; Hellmann, M. D.; Lin, J. J.; Friedlander, T.; Bushway, M. E.; Balogh, K. N.; Sciuto, T. E.; Kohler, V.; Turnbull, S. J.; Besada, R.; Curran, R. R.; Trapp, B.; Scherer, J.; Poran, A.; Harjanto, D.; Barthelme, D.; Ting, Y. S.; Dong, J. Z.; Ware, Y.; Huang, Y.; Huang, Z.; Wanamaker, A.; Cleary, L. D.; Moles, M. A.; Manson, K.; Greshock, J.; Khondker, Z. S.; Fritsch, E.; Rooney, M. S.; DeMario, M.; Gaynor, R. B.; Srinivasan, L. A Phase Ib Trial of Personalized Neoantigen Therapy Plus Anti-PD-1 in Patients with Advanced Melanoma, Non-Small Cell Lung Cancer, or Bladder Cancer. *Cell* **2020**, *183* (2), 347-362.e24. https://doi.org/10.1016/j.cell.2020.08.053.
(23) Hu, Z.; Leet, D. E.; Allesøe, R. L.; Oliveira, G.; Li, S.; Luoma, A. M.; Liu, J.; Forman, J.; Huang, T.; Iorgulescu, J. B.; Holden, R.; Sarkizova, S.; Gohil, S. H.; Redd, R. A.; Sun, J.; Elagina, L.; Giobbie-Hurder, A.; Zhang, W.; Peter, L.; Ciantra, Z.; Rodig, S.; Olive, O.; Shetty, K.; Pyrdol, J.; Uduman, M.; Lee, P. C.; Bachireddy, P.; Buchbinder, E. I.; Yoon, C. H.; Neuberg, D.; Pentelute, B. L.; Hacohen, N.; Livak, K. J.; Shukla, S. A.; Olsen, L. R.; Barouch, D. H.; Wucherpfennig, K. W.; Fritsch, E. F.; Keskin, D. B.; Wu, C. J.; Ott, P. A. Personal Neoantigen Vaccines Induce Persistent

Memory T Cell Responses and Epitope Spreading in Patients with Melanoma. *Nat Med* **2021**, *27* (3), 515–525. https://doi.org/10.1038/s41591-020-01206-4.
(24) Dhatchinamoorthy, K.; Colbert, J. D.; Rock, K. L. Cancer Immune Evasion Through Loss of MHC Class I Antigen Presentation. *Frontiers in Immunology* **2021**, *12*.
(25) Cornel, A. M.; Mimpen, I. L.; Nierkens, S. MHC Class I Downregulation in Cancer: Underlying Mechanisms and Potential Targets for Cancer Immunotherapy. *Cancers (Basel)* **2020**, *12* (7), 1760. https://doi.org/10.3390/cancers12071760.
(26) Upadhyay, R.; Boiarsky, J. A.; Pantsulaia, G.; Svensson-Arvelund, J.; Lin, M. J.; Wroblewska, A.; Bhalla, S.; Scholler, N.; Bot, A.; Rossi, J. M.; Sadek, N.; Parekh, S.; Lagana, A.; Baccarini, A.; Merad, M.; Brown, B. D.; Brody, J. D. A Critical Role for Fas-Mediated Off-Target Tumor Killing in T-Cell Immunotherapy. *Cancer Discovery* **2021**, *11* (3), 599–613. https://doi.org/10.1158/2159-8290.CD-20-0756.
(27) Lerner, E. C.; Woroniecka, K. I.; D'Anniballe, V. M.; Wilkinson, D. S.; Mohan, A. A.; Lorrey, S. J.; Waibl-Polania, J.; Wachsmuth, L. P.; Miggelbrink, A. M.; Jackson, J. D.; Cui, X.; Raj, J. A.; Tomaszewski, W. H.; Cook, S. L.; Sampson, J. H.; Patel, A. P.; Khasraw, M.; Gunn, M. D.; Fecci, P. E. CD8+ T Cells Maintain Killing of MHC-I-Negative Tumor Cells through the NKG2D–NKG2DL Axis. *Nat Cancer* **2023**, *4* (9), 1258–1272. https://doi.org/10.1038/s43018-023-00600-4.
(28) Wculek, S. K.; Cueto, F. J.; Mujal, A. M.; Melero, I.; Krummel, M. F.; Sancho, D. Dendritic Cells in Cancer Immunology and Immunotherapy. *Nat Rev Immunol* **2020**, *20* (1), 7–24. https://doi.org/10.1038/s41577-019-0210-z.
(29) Villadangos, J. A.; Schnorrer, P. Intrinsic and Cooperative Antigen-Presenting Functions of Dendritic-Cell Subsets in Vivo. *Nat Rev Immunol* **2007**, *7* (7), 543–555. https://doi.org/10.1038/nri2103.
(30) Philip, M.; Schietinger, A. CD8+ T Cell Differentiation and Dysfunction in Cancer. *Nat Rev Immunol* **2022**, *22* (4), 209–223. https://doi.org/10.1038/s41577-021-00574-3.
(31) Tay, R. E.; Richardson, E. K.; Toh, H. C. Revisiting the Role of CD4+ T Cells in Cancer Immunotherapy—New Insights into Old Paradigms. *Cancer Gene Ther* **2021**, *28* (1), 5–17. https://doi.org/10.1038/s41417-020-0183-x.
(32) Blum, J. S.; Wearsch, P. A.; Cresswell, P. Pathways of Antigen Processing. *Annu Rev Immunol* **2013**, *31*, 443–473. https://doi.org/10.1146/annurev-immunol-032712-095910.
(33) Sckisel, G. D.; Bouchlaka, M. N.; Monjazeb, A. M.; Crittenden, M.; Curti, B. D.; Wilkins, D. E. C.; Alderson, K. A.; Sungur, C. M.; Ames, E.; Mirsoian, A.; Reddy, A.; Alexander, W.; Soulika, A.; Blazar, B. R.; Longo, D. L.; Wiltrout, R. H.; Murphy, W. J. Out-of-Sequence Signal 3 Paralyzes Primary CD4+ T-Cell-Dependent Immunity. *Immunity* **2015**, *43* (2), 240–250. https://doi.org/10.1016/j.immuni.2015.06.023.
(34) Acuto, O.; Michel, F. CD28-Mediated Co-Stimulation: A Quantitative Support for TCR Signalling. *Nat Rev Immunol* **2003**, *3* (12), 939–951. https://doi.org/10.1038/nri1248.
(35) *T Cell Anergy | Annual Review of Immunology*. https://www.annualreviews.org/doi/10.1146/annurev.immunol.21.120601.141110 (accessed 2023-09-22).
(36) Pham, N.-L.; Badovinac, V.; Harty, J. Differential Role of "Signal 3" Inflammatory Cytokines in Regulating CD8 T Cell Expansion and Differentiation in Vivo. *Frontiers in Immunology* **2011**, *2*.
(37) Wilson, N. S.; El-Sukkari, D.; Belz, G. T.; Smith, C. M.; Steptoe, R. J.; Heath, W. R.; Shortman, K.; Villadangos, J. A. Most Lymphoid Organ Dendritic Cell Types Are Phenotypically and Functionally Immature. *Blood* **2003**, *102* (6), 2187–2194. https://doi.org/10.1182/blood-2003-02-0513.
(38) Swartz, M. A.; Hubbell, J. A.; Reddy, S. T. Lymphatic Drainage Function and Its Immunological Implications: From Dendritic Cell Homing to Vaccine Design. *Seminars in Immunology* **2008**, *20* (2), 147–156. https://doi.org/10.1016/j.smim.2007.11.007.
(39) Ryan, G. M.; Kaminskas, L. M.; Porter, C. J. H. Nano-Chemotherapeutics: Maximising Lymphatic Drug Exposure to Improve the Treatment of Lymph-Metastatic Cancers. *Journal of Controlled Release* **2014**, *193*, 241–256. https://doi.org/10.1016/j.jconrel.2014.04.051.

(40) Trevaskis, N. L.; Kaminskas, L. M.; Porter, C. J. H. From Sewer to Saviour — Targeting the Lymphatic System to Promote Drug Exposure and Activity. *Nat Rev Drug Discov* **2015**, *14* (11), 781–803. https://doi.org/10.1038/nrd4608.
(41) Schudel, A.; Francis, D. M.; Thomas, S. N. Material Design for Lymph Node Drug Delivery. *Nat Rev Mater* **2019**, *4* (6), 415–428. https://doi.org/10.1038/s41578-019-0110-7.
(42) Luo, M.; Wang, H.; Wang, Z.; Cai, H.; Lu, Z.; Li, Y.; Du, M.; Huang, G.; Wang, C.; Chen, X.; Porembka, M. R.; Lea, J.; Frankel, A. E.; Fu, Y.-X.; Chen, Z. J.; Gao, J. A STING-Activating Nanovaccine for Cancer Immunotherapy. *Nature Nanotech* **2017**, *12* (7), 648–654. https://doi.org/10.1038/nnano.2017.52.
(43) Kim, Y.; Kang, S.; Shin, H.; Kim, T.; Yu, B.; Kim, J.; Yoo, D.; Jon, S. Sequential and Timely Combination of a Cancer Nanovaccine with Immune Checkpoint Blockade Effectively Inhibits Tumor Growth and Relapse. *Angewandte Chemie International Edition* **2020**, *59* (34), 14628–14638. https://doi.org/10.1002/anie.202006117.
(44) An, M.; Li, M.; Xi, J.; Liu, H. Silica Nanoparticle as a Lymph Node Targeting Platform for Vaccine Delivery. *ACS Appl. Mater. Interfaces* **2017**, *9* (28), 23466–23475. https://doi.org/10.1021/acsami.7b06024.
(45) Lynn, G. M.; Sedlik, C.; Baharom, F.; Zhu, Y.; Ramirez-Valdez, R. A.; Coble, V. L.; Tobin, K.; Nichols, S. R.; Itzkowitz, Y.; Zaidi, N.; Gammon, J. M.; Blobel, N. J.; Denizeau, J.; de la Rochere, P.; Francica, B. J.; Decker, B.; Maciejewski, M.; Cheung, J.; Yamane, H.; Smelkinson, M. G.; Francica, J. R.; Laga, R.; Bernstock, J. D.; Seymour, L. W.; Drake, C. G.; Jewell, C. M.; Lantz, O.; Piaggio, E.; Ishizuka, A. S.; Seder, R. A. Peptide–TLR-7/8a Conjugate Vaccines Chemically Programmed for Nanoparticle Self-Assembly Enhance CD8 T-Cell Immunity to Tumor Antigens. *Nat Biotechnol* **2020**, *38* (3), 320–332. https://doi.org/10.1038/s41587-019-0390-x.
(46) Mueller, S. N.; Tian, S.; DeSimone, J. M. Rapid and Persistent Delivery of Antigen by Lymph Node Targeting PRINT Nanoparticle Vaccine Carrier To Promote Humoral Immunity. *Mol. Pharmaceutics* **2015**, *12* (5), 1356–1365. https://doi.org/10.1021/mp500589c.
(47) O'Melia, M. J.; Rohner, N. A.; Manspeaker, M. P.; Francis, D. M.; Kissick, H. T.; Thomas, S. N. Quality of CD8+ T Cell Immunity Evoked in Lymph Nodes Is Compartmentalized by Route of Antigen Transport and Functional in Tumor Context. *Science Advances* **2020**. https://doi.org/10.1126/sciadv.abd7134.
(48) Gerner, M. Y.; Torabi-Parizi, P.; Germain, R. N. Strategically Localized Dendritic Cells Promote Rapid T Cell Responses to Lymph-Borne Particulate Antigens. *Immunity* **2015**, *42* (1), 172–185. https://doi.org/10.1016/j.immuni.2014.12.024.
(49) Zhang, Y.-N.; Lazarovits, J.; Poon, W.; Ouyang, B.; Nguyen, L. N. M.; Kingston, B. R.; Chan, W. C. W. Nanoparticle Size Influences Antigen Retention and Presentation in Lymph Node Follicles for Humoral Immunity. *Nano Lett.* **2019**, *19* (10), 7226–7235. https://doi.org/10.1021/acs.nanolett.9b02834.
(50) Zhang, Y.-N.; Poon, W.; Sefton, E.; Chan, W. C. W. Suppressing Subcapsular Sinus Macrophages Enhances Transport of Nanovaccines to Lymph Node Follicles for Robust Humoral Immunity. *ACS Nano* **2020**, *14* (8), 9478–9490. https://doi.org/10.1021/acsnano.0c02240.
(51) Zhu, G.; Lynn, G. M.; Jacobson, O.; Chen, K.; Liu, Y.; Zhang, H.; Ma, Y.; Zhang, F.; Tian, R.; Ni, Q.; Cheng, S.; Wang, Z.; Lu, N.; Yung, B. C.; Wang, Z.; Lang, L.; Fu, X.; Jin, A.; Weiss, I. D.; Vishwasrao, H.; Niu, G.; Shroff, H.; Klinman, D. M.; Seder, R. A.; Chen, X. Albumin/Vaccine Nanocomplexes That Assemble in Vivo for Combination Cancer Immunotherapy. *Nat Commun* **2017**, *8* (1), 1954. https://doi.org/10.1038/s41467-017-02191-y.
(52) Liu, H.; Moynihan, K. D.; Zheng, Y.; Szeto, G. L.; Li, A. V.; Huang, B.; Van Egeren, D. S.; Park, C.; Irvine, D. J. Structure-Based Programming of Lymph-Node Targeting in Molecular Vaccines. *Nature* **2014**, *507* (7493), 519–522. https://doi.org/10.1038/nature12978.
(53) van der Zande, H. J. P.; Nitsche, D.; Schlautmann, L.; Guigas, B.; Burgdorf, S. The Mannose Receptor: From Endocytic Receptor and Biomarker to Regulator of (Meta)Inflammation. *Frontiers in Immunology* **2021**, *12*.

(54) Wilson, D. S.; Hirosue, S.; Raczy, M. M.; Jeanbart, L.; Wang, R.; Kwissa, M.; Franetich, J.-F.; Broggi, M. A. S.; Diaceri, G.; Quaglia-Thermes, X.; Mazier, D.; Swartz, M. A.; Hubbell, J. A. Antigens Reversibly Conjugated to a Polymeric Glyco-Adjuvant Induce Protective Humoral and Cellular Immunity. *Nature Mater* **2019**, *18* (2), 175–185. https://doi.org/10.1038/s41563-018-0256-5.
(55) Zhou, L.; Hou, B.; Wang, D.; Sun, F.; Song, R.; Shao, Q.; Wang, H.; Yu, H.; Li, Y. Engineering Polymeric Prodrug Nanoplatform for Vaccination Immunotherapy of Cancer. *Nano Lett.* **2020**, *20* (6), 4393–4402. https://doi.org/10.1021/acs.nanolett.0c01140.
(56) Yu, J.; Wang, S.; Qi, J.; Yu, Z.; Xian, Y.; Liu, W.; Wang, X.; Liu, C.; Wei, M. Mannose-Modified Liposome Designed for Epitope Peptide Drug Delivery in Cancer Immunotherapy. *International Immunopharmacology* **2021**, *101*, 108148. https://doi.org/10.1016/j.intimp.2021.108148.
(57) Lv, S.; Song, K.; Yen, A.; Peeler, D. J.; Nguyen, D. C.; Olshefsky, A.; Sylvestre, M.; Srinivasan, S.; Stayton, P. S.; Pun, S. H. Well-Defined Mannosylated Polymer for Peptide Vaccine Delivery with Enhanced Antitumor Immunity. *Advanced Healthcare Materials n/a* (n/a), 2101651. https://doi.org/10.1002/adhm.202101651.
(58) Rosalia, R. A.; Cruz, L. J.; van Duikeren, S.; Tromp, A. T.; Silva, A. L.; Jiskoot, W.; de Gruijl, T.; Löwik, C.; Oostendorp, J.; van der Burg, S. H.; Ossendorp, F. CD40-Targeted Dendritic Cell Delivery of PLGA-Nanoparticle Vaccines Induce Potent Anti-Tumor Responses. *Biomaterials* **2015**, *40*, 88–97. https://doi.org/10.1016/j.biomaterials.2014.10.053.
(59) Trabbic, K. R.; Kleski, K. A.; Barchi, J. J. Jr. Stable Gold-Nanoparticle-Based Vaccine for the Targeted Delivery of Tumor-Associated Glycopeptide Antigens. *ACS Bio Med Chem Au* **2021**, *1* (1), 31–43. https://doi.org/10.1021/acsbiomedchemau.1c00021.
(60) Hu, Y.-B.; Dammer, E. B.; Ren, R.-J.; Wang, G. The Endosomal-Lysosomal System: From Acidification and Cargo Sorting to Neurodegeneration. *Transl Neurodegener* **2015**, *4*, 18. https://doi.org/10.1186/s40035-015-0041-1.
(61) Gong, N.; Zhang, Y.; Teng, X.; Wang, Y.; Huo, S.; Qing, G.; Ni, Q.; Li, X.; Wang, J.; Ye, X.; Zhang, T.; Chen, S.; Wang, Y.; Yu, J.; Wang, P. C.; Gan, Y.; Zhang, J.; Mitchell, M. J.; Li, J.; Liang, X.-J. Proton-Driven Transformable Nanovaccine for Cancer Immunotherapy. *Nat. Nanotechnol.* **2020**, *15* (12), 1053–1064. https://doi.org/10.1038/s41565-020-00782-3.
(62) Wilson, J. T.; Keller, S.; Manganiello, M. J.; Cheng, C.; Lee, C.-C.; Opara, C.; Convertine, A.; Stayton, P. S. pH-Responsive Nanoparticle Vaccines for Dual-Delivery of Antigens and Immunostimulatory Oligonucleotides. *ACS Nano* **2013**, *7* (5), 3912–3925. https://doi.org/10.1021/nn305466z.
(63) Qiu, F.; Becker, K. W.; Knight, F. C.; Baljon, J. J.; Sevimli, S.; Shae, D.; Gilchuk, P.; Joyce, S.; Wilson, J. T. Poly(Propylacrylic Acid)-Peptide Nanoplexes as a Platform for Enhancing the Immunogenicity of Neoantigen Cancer Vaccines. *Biomaterials* **2018**, *182*, 82–91. https://doi.org/10.1016/j.biomaterials.2018.07.052.
(64) Behr, J.-P. The Proton Sponge: A Trick to Enter Cells the Viruses Did Not Exploit. *CHIMIA* **1997**, *51* (1–2), 34–34. https://doi.org/10.2533/chimia.1997.34.
(65) Vermeulen, L. M. P.; De Smedt, S. C.; Remaut, K.; Braeckmans, K. The Proton Sponge Hypothesis: Fable or Fact? *European Journal of Pharmaceutics and Biopharmaceutics* **2018**, *129*, 184–190. https://doi.org/10.1016/j.ejpb.2018.05.034.
(66) Thiery, J.; Keefe, D.; Boulant, S.; Boucrot, E.; Walch, M.; Martinvalet, D.; Goping, I. S.; Bleackley, R. C.; Kirchhausen, T.; Lieberman, J. Perforin Pores in the Endosomal Membrane Trigger Release of Endocytosed Granzyme B to the Cytosol of Target Cells. *Nat Immunol* **2011**, *12* (8), 770–777. https://doi.org/10.1038/ni.2050.
(67) Song, K.; Nguyen, D. C.; Luu, T.; Yazdani, O.; Roy, D.; Stayton, P. S.; Pun, S. H. A Mannosylated Polymer with Endosomal Release Properties for Peptide Antigen Delivery. *Journal of Controlled Release* **2023**, *356*, 232–241. https://doi.org/10.1016/j.jconrel.2023.03.004.
(68) Dingjan, I.; Verboogen, D. R.; Paardekooper, L. M.; Revelo, N. H.; Sittig, S. P.; Visser, L. J.; Mollard, G. F. von; Henriet, S. S.; Figdor, C. G.; ter Beest, M.; van den Bogaart, G. Lipid

Peroxidation Causes Endosomal Antigen Release for Cross-Presentation. *Sci Rep* **2016**, *6* (1), 22064. https://doi.org/10.1038/srep22064.
(69) Xu, C.; Hong, H.; Lee, Y.; Park, K. S.; Sun, M.; Wang, T.; Aikins, M. E.; Xu, Y.; Moon, J. J. Efficient Lymph Node-Targeted Delivery of Personalized Cancer Vaccines with Reactive Oxygen Species-Inducing Reduced Graphene Oxide Nanosheets. *ACS Nano* **2020**, *14* (10), 13268–13278. https://doi.org/10.1021/acsnano.0c05062.
(70) Han, J.; Pluhackova, K.; Böckmann, R. A. The Multifaceted Role of SNARE Proteins in Membrane Fusion. *Frontiers in Physiology* **2017**, *8*.
(71) Yang, J.; Bahreman, A.; Daudey, G.; Bussmann, J.; Olsthoorn, R. C. L.; Kros, A. Drug Delivery via Cell Membrane Fusion Using Lipopeptide Modified Liposomes. *ACS Cent. Sci.* **2016**, *2* (9), 621–630. https://doi.org/10.1021/acscentsci.6b00172.
(72) Embgenbroich, M.; Burgdorf, S. Current Concepts of Antigen Cross-Presentation. *Frontiers in Immunology* **2018**, *9*.
(73) Brown, C. C.; Gudjonson, H.; Pritykin, Y.; Deep, D.; Lavallée, V.-P.; Mendoza, A.; Fromme, R.; Mazutis, L.; Ariyan, C.; Leslie, C.; Pe'er, D.; Rudensky, A. Y. Transcriptional Basis of Mouse and Human Dendritic Cell Heterogeneity. *Cell* **2019**, *179* (4), 846-863.e24. https://doi.org/10.1016/j.cell.2019.09.035.
(74) Rodríguez-Silvestre, P.; Laub, M.; Krawczyk, P. A.; Davies, A. K.; Schessner, J. P.; Parveen, R.; Tuck, B. J.; McEwan, W. A.; Borner, G. H. H.; Kozik, P. Perforin-2 Is a Pore-Forming Effector of Endocytic Escape in Cross-Presenting Dendritic Cells. *Science* **2023**, *380* (6651), 1258–1265. https://doi.org/10.1126/science.adg8802.
(75) Böttcher, J. P.; Reis e Sousa, C. The Role of Type 1 Conventional Dendritic Cells in Cancer Immunity. *Trends Cancer* **2018**, *4* (11), 784–792. https://doi.org/10.1016/j.trecan.2018.09.001.
(76) Yan, Z.; Wu, Y.; Du, J.; Li, G.; Wang, S.; Cao, W.; Zhou, X.; Wu, C.; Zhang, D.; Jing, X.; Li, Y.; Wang, H.; Gao, Y.; Qi, Y. A Novel Peptide Targeting Clec9a on Dendritic Cell for Cancer Immunotherapy. *Oncotarget* **2016**, *7* (26), 40437–40450. https://doi.org/10.18632/oncotarget.9624.
(77) Arabpour, M.; Paul, S.; Grauers Wiktorin, H.; Kaya, M.; Kiffin, R.; Lycke, N.; Hellstrand, K.; Martner, A. An Adjuvant-Containing cDC1-Targeted Recombinant Fusion Vaccine Conveys Strong Protection against Murine Melanoma Growth and Metastasis. *OncoImmunology* **2022**, *11* (1), 2115618. https://doi.org/10.1080/2162402X.2022.2115618.
(78) Li, H.; Li, Y.; Jiao, J.; Hu, H.-M. Alpha-Alumina Nanoparticles Induce Efficient Autophagy-Dependent Cross-Presentation and Potent Antitumour Response. *Nature Nanotech* **2011**, *6* (10), 645–650. https://doi.org/10.1038/nnano.2011.153.
(79) Panzarini, E.; Dini, L. Nanomaterial-Induced Autophagy: A New Reversal MDR Tool in Cancer Therapy? *Mol. Pharmaceutics* **2014**, *11* (8), 2527–2538. https://doi.org/10.1021/mp500066v.
(80) Ravindran, R.; Khan, N.; Nakaya, H. I.; Li, S.; Loebbermann, J.; Maddur, M. S.; Park, Y.; Jones, D. P.; Chappert, P.; Davoust, J.; Weiss, D. S.; Virgin, H. W.; Ron, D.; Pulendran, B. Vaccine Activation of the Nutrient Sensor GCN2 in Dendritic Cells Enhances Antigen Presentation. *Science* **2014**, *343* (6168), 313–317. https://doi.org/10.1126/science.1246829.
(81) Huis in 't Veld, L. G. M.; Ho, N. I.; Wassink, M.; den Brok, M. H.; Adema, G. J. Saponin-Based Adjuvant-Induced Dendritic Cell Cross-Presentation Is Dependent on PERK Activation. *Cell. Mol. Life Sci.* **2022**, *79* (5), 231. https://doi.org/10.1007/s00018-022-04253-x.
(82) Zhao, H.; Xu, J.; Li, Y.; Guan, X.; Han, X.; Xu, Y.; Zhou, H.; Peng, R.; Wang, J.; Liu, Z. Nanoscale Coordination Polymer Based Nanovaccine for Tumor Immunotherapy. *ACS Nano* **2019**, *13* (11), 13127–13135. https://doi.org/10.1021/acsnano.9b05974.
(83) Khong, H.; Overwijk, W. W. Adjuvants for Peptide-Based Cancer Vaccines. *J Immunother Cancer* **2016**, *4* (1), 56. https://doi.org/10.1186/s40425-016-0160-y.
(84) El-Zayat, S. R.; Sibaii, H.; Mannaa, F. A. Toll-like Receptors Activation, Signaling, and Targeting: An Overview. *Bulletin of the National Research Centre* **2019**, *43* (1), 187. https://doi.org/10.1186/s42269-019-0227-2.

(85) Simmons, D. P.; Wearsch, P. A.; Canaday, D. H.; Meyerson, H. J.; Liu, Y. C.; Wang, Y.; Boom, W. H.; Harding, C. V. Type I IFN Drives a Distinctive Dendritic Cell Maturation Phenotype That Allows Continued Class II MHC Synthesis and Antigen Processing. *The Journal of Immunology* **2012**, *188* (7), 3116–3126. https://doi.org/10.4049/jimmunol.1101313.
(86) Lorenzi, S.; Mattei, F.; Sistigu, A.; Bracci, L.; Spadaro, F.; Sanchez, M.; Spada, M.; Belardelli, F.; Gabriele, L.; Schiavoni, G. Type I IFNs Control Antigen Retention and Survival of CD8α+ Dendritic Cells after Uptake of Tumor Apoptotic Cells Leading to Cross-Priming. *The Journal of Immunology* **2011**, *186* (9), 5142–5150. https://doi.org/10.4049/jimmunol.1004163.
(87) Boukhaled, G. M.; Harding, S.; Brooks, D. G. Opposing Roles of Type I Interferons in Cancer Immunity. *Annu Rev Pathol* **2021**, *16*, 167–198. https://doi.org/10.1146/annurev-pathol-031920-093932.
(88) Marrack, P.; McKee, A. S.; Munks, M. W. Towards an Understanding of the Adjuvant Action of Aluminium. *Nat Rev Immunol* **2009**, *9* (4), 287–293. https://doi.org/10.1038/nri2510.
(89) Ruwona, T. B.; Xu, H.; Li, X.; Taylor, A. N.; Shi, Y.; Cui, Z. Toward Understanding the Mechanism Underlying the Strong Adjuvant Activity of Aluminum Salt Nanoparticles. *Vaccine* **2016**, *34* (27), 3059–3067. https://doi.org/10.1016/j.vaccine.2016.04.081.
(90) Bai, S.; Jiang, H.; Song, Y.; Zhu, Y.; Qin, M.; He, C.; Du, G.; Sun, X. Aluminum Nanoparticles Deliver a Dual-Epitope Peptide for Enhanced Anti-Tumor Immunotherapy. *Journal of Controlled Release* **2022**, *344*, 134–146. https://doi.org/10.1016/j.jconrel.2022.02.027.
(91) Billiau, A.; Matthys, P. Modes of Action of Freund's Adjuvants in Experimental Models of Autoimmune Diseases. *Journal of Leukocyte Biology* **2001**, *70* (6), 849–860. https://doi.org/10.1189/jlb.70.6.849.
(92) Kenter, G. G.; Welters, M. J. P.; Valentijn, A. R. P. M.; Lowik, M. J. G.; Berends-van der Meer, D. M. A.; Vloon, A. P. G.; Essahsah, F.; Fathers, L. M.; Offringa, R.; Drijfhout, J. W.; Wafelman, A. R.; Oostendorp, J.; Fleuren, G. J.; van der Burg, S. H.; Melief, C. J. M. Vaccination against HPV-16 Oncoproteins for Vulvar Intraepithelial Neoplasia. *New England Journal of Medicine* **2009**, *361* (19), 1838–1847. https://doi.org/10.1056/NEJMoa0810097.
(93) Kaufman, H. L.; Ruby, C. E.; Hughes, T.; Slingluff, C. L. Current Status of Granulocyte–Macrophage Colony-Stimulating Factor in the Immunotherapy of Melanoma. *J Immunother Cancer* **2014**, *2* (1), 11. https://doi.org/10.1186/2051-1426-2-11.
(94) Kuai, R.; Ochyl, L. J.; Bahjat, K. S.; Schwendeman, A.; Moon, J. J. Designer Vaccine Nanodiscs for Personalized Cancer Immunotherapy. *Nature Mater* **2017**, *16* (4), 489–496. https://doi.org/10.1038/nmat4822.
(95) Jin, S. M.; Yoo, Y. J.; Shin, H. S.; Kim, S.; Lee, S. N.; Lee, C. H.; Kim, H.; Kim, J.-E.; Bae, Y.-S.; Hong, J.; Noh, Y.-W.; Lim, Y. T. A Nanoadjuvant That Dynamically Coordinates Innate Immune Stimuli Activation Enhances Cancer Immunotherapy and Reduces Immune Cell Exhaustion. *Nat. Nanotechnol.* **2023**, *18* (4), 390–402. https://doi.org/10.1038/s41565-022-01296-w.
(96) Peeler, D. J.; Yen, A.; Luera, N.; Stayton, P. S.; Pun, S. H. Lytic Polyplex Vaccines Enhance Antigen-Specific Cytotoxic T Cell Response through Induction of Local Cell Death. *Adv. Therap.* **2021**, 2100005. https://doi.org/10.1002/adtp.202100005.
(97) Ni, Q.; Zhang, F.; Liu, Y.; Wang, Z.; Yu, G.; Liang, B.; Niu, G.; Su, T.; Zhu, G.; Lu, G.; Zhang, L.; Chen, X. A Bi-Adjuvant Nanovaccine That Potentiates Immunogenicity of Neoantigen for Combination Immunotherapy of Colorectal Cancer. *Science Advances* **2020**, *6* (12), eaaw6071. https://doi.org/10.1126/sciadv.aaw6071.
(98) Shae, D.; Baljon, J. J.; Wehbe, M.; Becker, K. W.; Kumar, A.; Suryadevara, N.; Carson, C. S.; Palmer, C. R.; Knight, F. C.; Joyce, S.; Wilson, J. T. Co-Delivery of Peptide Neoantigens and Stimulator of Interferon Genes Agonists Enhances Response to Cancer Vaccines. *ACS Nano* **2020**, *14* (8), 9904–9916. https://doi.org/10.1021/acsnano.0c02765.
(99) Manik, M.; Singh, R. K. Role of Toll-like Receptors in Modulation of Cytokine Storm Signaling in SARS-CoV-2-induced COVID-19. *J Med Virol* **2022**, *94* (3), 869–877. https://doi.org/10.1002/jmv.27405.

(100) Aichhorn, S.; Linhardt, A.; Halfmann, A.; Nadlinger, M.; Kirchberger, S.; Stadler, M.; Dillinger, B.; Distel, M.; Dohnal, A.; Teasdale, I.; Schöfberger, W. A pH-Sensitive Macromolecular Prodrug as TLR7/8 Targeting Immune Response Modifier. *Chemistry – A European Journal* **2017**, *23* (70), 17721–17726. https://doi.org/10.1002/chem.201702942.
(101) Nguyen, D. C.; Song, K.; Jokonya, S.; Yazdani, O.; Sellers, D. L.; Pun, S. H.; Stayton, P. S. Mannosylated STING Agonist Drugamers For Dendritic Cell-Mediated Cancer Immunotherapy.
(102) Bhagchandani, S. H.; Vohidov, F.; Milling, L. E.; Tong, E. Y.; Brown, C. M.; Ramseier, M. L.; Liu, B.; Fessenden, T. B.; Nguyen, H. V.-T.; Kiel, G. R.; Won, L.; Langer, R. S.; Spranger, S.; Shalek, A. K.; Irvine, D. J.; Johnson, J. A. Engineering Kinetics of TLR7/8 Agonist Release from Bottlebrush Prodrugs Enables Tumor-Focused Immune Stimulation. *Science Advances* **2023**, *9* (16), eadg2239. https://doi.org/10.1126/sciadv.adg2239.
(103) Sharpe, A. H. Mechanisms of Costimulation. *Immunol Rev* **2009**, *229* (1), 5–11. https://doi.org/10.1111/j.1600-065X.2009.00784.x.
(104) Maldonado, R. A.; LaMothe, R. A.; Ferrari, J. D.; Zhang, A.-H.; Rossi, R. J.; Kolte, P. N.; Griset, A. P.; O'Neil, C.; Altreuter, D. H.; Browning, E.; Johnston, L.; Farokhzad, O. C.; Langer, R.; Scott, D. W.; von Andrian, U. H.; Kishimoto, T. K. Polymeric Synthetic Nanoparticles for the Induction of Antigen-Specific Immunological Tolerance. *Proc Natl Acad Sci U S A* **2015**, *112* (2), E156–E165. https://doi.org/10.1073/pnas.1408686111.
(105) Fischer, N. O.; Rasley, A.; Corzett, M.; Hwang, M. H.; Hoeprich, P. D.; Blanchette, C. D. Colocalized Delivery of Adjuvant and Antigen Using Nanolipoprotein Particles Enhances the Immune Response to Recombinant Antigens. *J. Am. Chem. Soc.* **2013**, *135* (6), 2044–2047. https://doi.org/10.1021/ja3063293.
(106) Tom, J. K.; Dotsey, E. Y.; Wong, H. Y.; Stutts, L.; Moore, T.; Davies, D. H.; Felgner, P. L.; Esser-Kahn, A. P. Modulation of Innate Immune Responses via Covalently Linked TLR Agonists. *ACS Cent. Sci.* **2015**, *1* (8), 439–448. https://doi.org/10.1021/acscentsci.5b00274.
(107) Wei, L.; Zhao, Y.; Hu, X.; Tang, L. Redox-Responsive Polycondensate Neoepitope for Enhanced Personalized Cancer Vaccine. *ACS Cent. Sci.* **2020**, *6* (3), 404–412. https://doi.org/10.1021/acscentsci.9b01174.
(108) Sultan, H.; Kumai, T.; Nagato, T.; Wu, J.; Salazar, A. M.; Celis, E. The Route of Administration Dictates the Immunogenicity of Peptide-Based Cancer Vaccines in Mice. *Cancer Immunol Immunother* **2019**, *68* (3), 455–466. https://doi.org/10.1007/s00262-018-02294-5.
(109) Baharom, F.; Ramirez-Valdez, R. A.; Tobin, K. K. S.; Yamane, H.; Dutertre, C.-A.; Khalilnezhad, A.; Reynoso, G. V.; Coble, V. L.; Lynn, G. M.; Mulè, M. P.; Martins, A. J.; Finnigan, J. P.; Zhang, X. M.; Hamerman, J. A.; Bhardwaj, N.; Tsang, J. S.; Hickman, H. D.; Ginhoux, F.; Ishizuka, A. S.; Seder, R. A. Intravenous Nanoparticle Vaccination Generates Stem-like TCF1+ Neoantigen-Specific CD8+ T Cells. *Nat Immunol* **2021**, *22* (1), 41–52. https://doi.org/10.1038/s41590-020-00810-3.
(110) Hailemichael, Y.; Dai, Z.; Jaffarzad, N.; Ye, Y.; Medina, M. A.; Huang, X.-F.; Dorta-Estremera, S. M.; Greeley, N. R.; Nitti, G.; Peng, W.; Liu, C.; Lou, Y.; Wang, Z.; Ma, W.; Rabinovich, B.; Sowell, R. T.; Schluns, K. S.; Davis, R. E.; Hwu, P.; Overwijk, W. W. Persistent Antigen at Vaccination Sites Induces Tumor-Specific CD8+ T Cell Sequestration, Dysfunction and Deletion. *Nat Med* **2013**, *19* (4), 465–472. https://doi.org/10.1038/nm.3105.
(111) Kuai, R.; Sun, X.; Yuan, W.; Xu, Y.; Schwendeman, A.; Moon, J. J. Subcutaneous Nanodisc Vaccination with Neoantigens for Combination Cancer Immunotherapy. *Bioconjugate Chem.* **2018**, *29* (3), 771–775. https://doi.org/10.1021/acs.bioconjchem.7b00761.
(112) Migliore, A.; Gigliucci, G.; Di Marzo, R.; Russo, D.; Mammucari, M. Intradermal Vaccination: A Potential Tool in the Battle Against the COVID-19 Pandemic? *Risk Manag Healthc Policy* **2021**, *14*, 2079–2087. https://doi.org/10.2147/RMHP.S309707.
(113) Kim, N. W.; Kim, S.-Y.; Lee, J. E.; Yin, Y.; Lee, J. H.; Lim, S. Y.; Kim, E. S.; Duong, H. T. T.; Kim, H. K.; Kim, S.; Kim, J.-E.; Lee, D. S.; Kim, J.; Lee, M. S.; Lim, Y. T.; Jeong, J. H. Enhanced

Cancer Vaccination by In Situ Nanomicelle-Generating Dissolving Microneedles. *ACS Nano* **2018**, *12* (10), 9702–9713. https://doi.org/10.1021/acsnano.8b04146.
(114) Senti, G.; Prinz Vavricka, B. M.; Erdmann, I.; Diaz, M. I.; Markus, R.; McCormack, S. J.; Simard, J. J.; Wüthrich, B.; Crameri, R.; Graf, N.; Johansen, P.; Kündig, T. M. Intralymphatic Allergen Administration Renders Specific Immunotherapy Faster and Safer: A Randomized Controlled Trial. *Proceedings of the National Academy of Sciences* **2008**, *105* (46), 17908–17912. https://doi.org/10.1073/pnas.0803725105.
(115) Johansen, P.; Häffner, A. C.; Koch, F.; Zepter, K.; Erdmann, I.; Maloy, K.; Simard, J. J.; Storni, T.; Senti, G.; Bot, A.; Wüthrich, B.; Kündig, T. M. Direct Intralymphatic Injection of Peptide Vaccines Enhances Immunogenicity. *European Journal of Immunology* **2005**, *35* (2), 568–574. https://doi.org/10.1002/eji.200425599.
(116) Mohanan, D.; Slütter, B.; Henriksen-Lacey, M.; Jiskoot, W.; Bouwstra, J. A.; Perrie, Y.; Kündig, T. M.; Gander, B.; Johansen, P. Administration Routes Affect the Quality of Immune Responses: A Cross-Sectional Evaluation of Particulate Antigen-Delivery Systems. *Journal of Controlled Release* **2010**, *147* (3), 342–349. https://doi.org/10.1016/j.jconrel.2010.08.012.
(117) Morisaki, T.; Morisaki, T.; Kubo, M.; Onishi, H.; Hirano, T.; Morisaki, S.; Eto, M.; Monji, K.; Takeuchi, A.; Nakagawa, S.; Tanaka, H.; Koya, N.; Umebayashi, M.; Tsujimura, K.; Yew, P. Y.; Yoshimura, S.; Kiyotani, K.; Nakamura, Y. Efficacy of Intranodal Neoantigen Peptide-Pulsed Dendritic Cell Vaccine Monotherapy in Patients With Advanced Solid Tumors: A Retrospective Analysis. *Anticancer Research* **2021**, *41* (8), 4101–4115. https://doi.org/10.21873/anticanres.15213.
(118) Joe, P. T.; Christopoulou, I.; van Hoecke, L.; Schepens, B.; Ysenbaert, T.; Heirman, C.; Thielemans, K.; Saelens, X.; Aerts, J. L. Intranodal Administration of mRNA Encoding Nucleoprotein Provides Cross-Strain Immunity against Influenza in Mice. *Journal of Translational Medicine* **2019**, *17* (1), 242. https://doi.org/10.1186/s12967-019-1991-3.
(119) Zhang, Y.; Ma, S.; Liu, X.; Xu, Y.; Zhao, J.; Si, X.; Li, H.; Huang, Z.; Wang, Z.; Tang, Z.; Song, W.; Chen, X. Supramolecular Assembled Programmable Nanomedicine As In Situ Cancer Vaccine for Cancer Immunotherapy. *Advanced Materials* **2021**, *33* (7), 2007293. https://doi.org/10.1002/adma.202007293.
(120) Calderón-Colón, X.; Zhang, Y.; Tiburzi, O.; Wang, J.; Hou, S.; Raimondi, G.; Patrone, J. Design and Characterization of Lipid Nanocarriers for Oral Delivery of Immunotherapeutic Peptides. *Journal of Biomedical Materials Research Part A* **2023**, *111* (7), 938–949. https://doi.org/10.1002/jbm.a.37477.
(121) Francian, A.; Namen, S.; Stanley, M.; Mann, K.; Martinson, H.; Kullberg, M. Intratumoral Delivery of Antigen with Complement C3-Bound Liposomes Reduces Tumor Growth in Mice. *Nanomedicine* **2019**, *18*, 326–335. https://doi.org/10.1016/j.nano.2018.10.009.
(122) Snipstad, S.; Bremnes, F.; Dehli Haugum, M.; Sulheim, E. Characterization of Immune Cell Populations in Syngeneic Murine Tumor Models. *Cancer Medicine* **2023**, *12* (10), 11589–11601. https://doi.org/10.1002/cam4.5784.
(123) Overwijk, W. W.; Tsung, A.; Irvine, K. R.; Parkhurst, M. R.; Goletz, T. J.; Tsung, K.; Carroll, M. W.; Liu, C.; Moss, B.; Rosenberg, S. A.; Restifo, N. P. Gp100/Pmel 17 Is a Murine Tumor Rejection Antigen: Induction of "Self"-Reactive, Tumoricidal T Cells Using High-Affinity, Altered Peptide Ligand. *The Journal of Experimental Medicine* **1998**, *188* (2), 277. https://doi.org/10.1084/jem.188.2.277.
(124) Bloom, M. B.; Perry-Lalley, D.; Robbins, P. F.; Li, Y.; El-Gamil, M.; Rosenberg, S. A.; Yang, J. C. Identification of Tyrosinase-Related Protein 2 as a Tumor Rejection Antigen for the B16 Melanoma. *J Exp Med* **1997**, *185* (3), 453–460.
(125) Kreiter, S.; Vormehr, M.; van de Roemer, N.; Diken, M.; Löwer, M.; Diekmann, J.; Boegel, S.; Schrörs, B.; Vascotto, F.; Castle, J. C.; Tadmor, A. D.; Schoenberger, S. P.; Huber, C.; Türeci, Ö.; Sahin, U. Mutant MHC Class II Epitopes Drive Therapeutic Immune Responses to Cancer. *Nature* **2015**, *520* (7549), 692–696. https://doi.org/10.1038/nature14426.

(126) Yadav, M.; Jhunjhunwala, S.; Phung, Q. T.; Lupardus, P.; Tanguay, J.; Bumbaca, S.; Franci, C.; Cheung, T. K.; Fritsche, J.; Weinschenk, T.; Modrusan, Z.; Mellman, I.; Lill, J. R.; Delamarre, L. Predicting Immunogenic Tumour Mutations by Combining Mass Spectrometry and Exome Sequencing. *Nature* **2014**, *515* (7528), 572–576. https://doi.org/10.1038/nature14001.

(127) Xu, J.; Lv, J.; Zhuang, Q.; Yang, Z.; Cao, Z.; Xu, L.; Pei, P.; Wang, C.; Wu, H.; Dong, Z.; Chao, Y.; Wang, C.; Yang, K.; Peng, R.; Cheng, Y.; Liu, Z. A General Strategy towards Personalized Nanovaccines Based on Fluoropolymers for Post-Surgical Cancer Immunotherapy. *Nature Nanotechnology* **2020**, *15* (12), 1043–1052. https://doi.org/10.1038/s41565-020-00781-4.

(128) Lechner, M. G.; Karimi, S. S.; Barry-Holson, K.; Angell, T. E.; Murphy, K. A.; Church, C. H.; Ohlfest, J. R.; Hu, P.; Epstein, A. L. Immunogenicity of Murine Solid Tumor Models as a Defining Feature of in Vivo Behavior and Response to Immunotherapy. *J Immunother* **2013**, *36* (9), 477–489. https://doi.org/10.1097/01.cji.0000436722.46675.4a.

(129) Rötzschke, O.; Falk, K.; Stevanovic, S.; Jung, G.; Walden, P.; Rammensee, H.-G. Exact prediction of a natural T cell epitope. *European Journal of Immunology* **1991**, *21* (11), 2891–2894. https://doi.org/10.1002/eji.1830211136.

(130) Finkelstein, S. E.; Heimann, D. M.; Klebanoff, C. A.; Antony, P. A.; Gattinoni, L.; Hinrichs, C. S.; Hwang, L. N.; Palmer, D. C.; Spiess, P. J.; Surman, D. R.; Wrzesiniski, C.; Yu, Z.; Rosenberg, S. A.; Restifo, N. P. Bedside to Bench and Back Again: How Animal Models Are Guiding the Development of New Immunotherapies for Cancer. *J Leukoc Biol* **2004**, *76* (2), 333–337. https://doi.org/10.1189/jlb.0304120.

(131) Hos, B. J.; Tondini, E.; Camps, M. G. M.; Rademaker, W.; van den Bulk, J.; Ruano, D.; Janssen, G. M. C.; de Ru, A. H.; van den Elsen, P. J.; de Miranda, N. F. C. C.; van Veelen, P. A.; Ossendorp, F. Cancer-Specific T Helper Shared and Neo-Epitopes Uncovered by Expression of the MHC Class II Master Regulator CIITA. *Cell Reports* **2022**, *41* (2), 111485. https://doi.org/10.1016/j.celrep.2022.111485.

(132) Feltkamp, M. C. W.; Smits, H. L.; Vierboom, M. P. M.; Minnaar, R. P.; De Jongh, B. M.; Drijfhout, J. W.; Schegget, J. T.; Melief, C. J. M.; Kast, W. M. Vaccination with Cytotoxic T Lymphocyte Epitope-Containing Peptide Protects against a Tumor Induced by Human Papillomavirus Type 16-Transformed Cells. *European Journal of Immunology* **1993**, *23* (9), 2242–2249. https://doi.org/10.1002/eji.1830230929.

(133) Bahmani, B.; Amini-bayat, Z.; Ranjbar, M. M.; Bakhtiari, N.; Zarnani, A.-H. HPV16-E7 Protein T Cell Epitope Prediction and Global Therapeutic Peptide Vaccine Design Based on Human Leukocyte Antigen Frequency: An In-Silico Study. *Int J Pept Res Ther* **2021**, *27* (1), 365–378. https://doi.org/10.1007/s10989-020-10089-5.

(134) Karttunen, J.; Sanderson, S.; Shastri, N. Detection of Rare Antigen-Presenting Cells by the lacZ T-Cell Activation Assay Suggests an Expression Cloning Strategy for T-Cell Antigens. *Proceedings of the National Academy of Sciences* **1992**, *89* (13), 6020–6024. https://doi.org/10.1073/pnas.89.13.6020.

(135) Cafri, G.; Sharbi-Yunger, A.; Tzehoval, E.; Eisenbach, L. Production of LacZ Inducible T Cell Hybridoma Specific for Human and Mouse Gp10025–33 Peptides. *PLOS ONE* **2013**, *8* (2), e55583. https://doi.org/10.1371/journal.pone.0055583.

(136) Kim, M. K.; Kim, J. Properties of Immature and Mature Dendritic Cells: Phenotype, Morphology, Phagocytosis, and Migration. *RSC Adv.* **2019**, *9* (20), 11230–11238. https://doi.org/10.1039/C9RA00818G.

(137) Mbongue, J. C.; Nieves, H. A.; Torrez, T. W.; Langridge, W. H. R. The Role of Dendritic Cell Maturation in the Induction of Insulin-Dependent Diabetes Mellitus. *Front. Immunol.* **2017**, *8*. https://doi.org/10.3389/fimmu.2017.00327.

(138) Sharpe, A. H.; Freeman, G. J. The B7–CD28 Superfamily. *Nat Rev Immunol* **2002**, *2* (2), 116–126. https://doi.org/10.1038/nri727.

(139) Ma, D. Y.; Clark, E. A. The Role of CD40 and CD154/CD40L in Dendritic Cells. *Seminars in Immunology* **2009**, *21* (5), 265–272. https://doi.org/10.1016/j.smim.2009.05.010.

(140) Cheng, K.; Zhao, R.; Li, Y.; Qi, Y.; Wang, Y.; Zhang, Y.; Qin, H.; Qin, Y.; Chen, L.; Li, C.; Liang, J.; Li, Y.; Xu, J.; Han, X.; Anderson, G. J.; Shi, J.; Ren, L.; Zhao, X.; Nie, G. Bioengineered Bacteria-Derived Outer Membrane Vesicles as a Versatile Antigen Display Platform for Tumor Vaccination via Plug-and-Display Technology. *Nat Commun* **2021**, *12* (1), 2041. https://doi.org/10.1038/s41467-021-22308-8.
(141) Ramirez-Valdez, R. A.; Baharom, F.; Khalilnezhad, A.; Fussell, S. C.; Hermans, D. J.; Schrager, A. M.; Tobin, K. K. S.; Lynn, G. M.; Khalilnezhad, S.; Ginhoux, F.; Van den Eynde, B. J.; Leung, C. S. K.; Ishizuka, A. S.; Seder, R. A. Intravenous Heterologous Prime-Boost Vaccination Activates Innate and Adaptive Immunity to Promote Tumor Regression. *Cell Reports* **2023**, *42* (6), 112599. https://doi.org/10.1016/j.celrep.2023.112599.
(142) St. Paul, M.; Ohashi, P. S. The Roles of CD8+ T Cell Subsets in Antitumor Immunity. *Trends in Cell Biology* **2020**, *30* (9), 695–704. https://doi.org/10.1016/j.tcb.2020.06.003.
(143) Vignali, D. A. A.; Collison, L. W.; Workman, C. J. How Regulatory T Cells Work. *Nat Rev Immunol* **2008**, *8* (7), 523–532. https://doi.org/10.1038/nri2343.

Chapter 2 : Well-Defined Mannosylated Polymer for Peptide Vaccine Delivery with Enhanced Antitumor Immunity[2]

Shixian Lv, Kefan Song,* Albert Yen, David J. Peeler, Dinh Chuong Nguyen, Audrey Olshefsky, Meilyn Sylvestre, Selvi Srinivasan, Patrick S. Stayton, and Suzie H. Pun*

ABSTRACT

Peptide-based cancer vaccines offer production and safety advantages but have had limited clinical success due to their intrinsic instability, rapid clearance, and low cellular uptake. Nanoparticle-based delivery vehicles can improve the in vivo stability and cellular uptake of peptide antigens. Here, a well-defined, self-assembling mannosylated polymer is developed for anticancer peptide antigen delivery. The amphiphilic polymer is prepared by reversible addition-fragmentation chain transfer (RAFT) polymerization, and the peptide antigens are conjugated to the pH-sensitive hydrophobic block through the reversible disulfide linkage for selective release after cell entry. The polymer–peptide conjugates self-assemble into sub-100 nm micelles at physiological pH and dissociate at endosomal pH. The mannosylated micellar corona increases the accumulation of vaccine cargoes in the draining inguinal lymph nodes and facilitates nanoparticle uptake by professional antigen presenting cells. In vivo studies demonstrate that the mannosylated micelle formulation improves dendritic cell activation and enhances antigen-specific T cell responses, resulting in higher antitumor immunity in tumor-bearing mice compared to free peptide antigen. The mannosylated polymer is therefore a simple and promising platform for the delivery of peptide cancer vaccines.[3]

[2] Chapter reproduced from: Lv, S., Song, K. *et al*. Well-Defined Mannosylated Polymer for Peptide Vaccine Delivery with Enhanced Antitumor Immunity. *Advanced healthcare materials* vol. 11,9 (2022): e2101651.

2.1 INTRODUCTION

The recent clinical translation of multiple immunotherapies is the largest paradigm shift in oncology since the use of chemo-drugs in the 1940s.[1-5] The major types of cancer immunotherapy include immune checkpoint blocking (ICB) monoclonal antibodies, chimeric antigen receptor T cells (CAR T cells), and cancer vaccines.[6-10] Cancer vaccines, which educate the immune system to recognize and remove cancer cells, are a powerful approach among various cancer immunotherapies.[11-13] Therapeutic cancer vaccines that stimulate both CD8+ cytotoxic T lymphocytes (CTLs) and CD4+ T-helper (Th) cells by inducing antigen-presenting cells (APCs) like dendritic cells (DCs) to present antigens through MHC class I (MHC-I) and MHC class II (MHC-II) pathways can generate specific and effective antitumor responses. Cancer vaccines offer the possibility to eliminate cancer cells with sustained protection against recurrence. As a result, cancer vaccines have attracted great attention in recent years, and several therapeutic vaccines have been used in the treatment of different types of cancers.[14,15]

Antigen sources in cancer vaccines include (i) tumor cells and cell lysates, (ii) recombinant, purified or in situ-expressed proteins, and (iii) peptide epitopes.[1,3] Peptide antigens are particularly attractive given their direct and natural function as T-cell epitopes, well-defined structures, ease of manufacturing and modifications, low cost, and long-term storage stability.[16-19] Despite these advantages, the application of peptide-based cancer vaccines in anticancer clinical trials only achieved modest benefit, which is mainly attributed to the intrinsic drawbacks from peptides themselves. Soluble peptide vaccines suffer from poor in vivo stability due to degradation, fast clearance, low DC uptake, and inefficient delivery to lymph nodes (LNs).[20-22]

Nanoparticle (NP)-based delivery systems can overcome the aforementioned pharmacokinetic challenges of soluble peptides.[2, 23-26] NPs can protect encapsulated peptide antigens against

enzymatic degradation, enhance cellular uptake, and improve the accumulation in the lymphatic systems (e.g., LNs).[27-29] In addition, peptide antigens can be co-formulated with immunoregulatory molecules such as active adjuvants in one nanocarrier for better immunostimulation.[16, 30-32] Among various nanoparticulate systems, polymers are the most widely used carriers because they can be synthesized with a broad range of chemical and structural functionality.[23, 33-36] The size, particle shape, surface properties of polymeric carriers can be tuned to optimize peptide vaccine efficacy. Polymers can also be functionalized with targeting ligands (such as mannose, and CD40) to enhance DC uptake and LN accumulation.[27, 37-39] The most commonly used polymer carrier is poly(lactic-co-glycolic acid) (PLGA) which has limited capacity for functionalization with targeting ligands or other components that promote intracellular delivery.[24] There remains a need for simple and scalable polymeric systems for peptide antigen delivery.

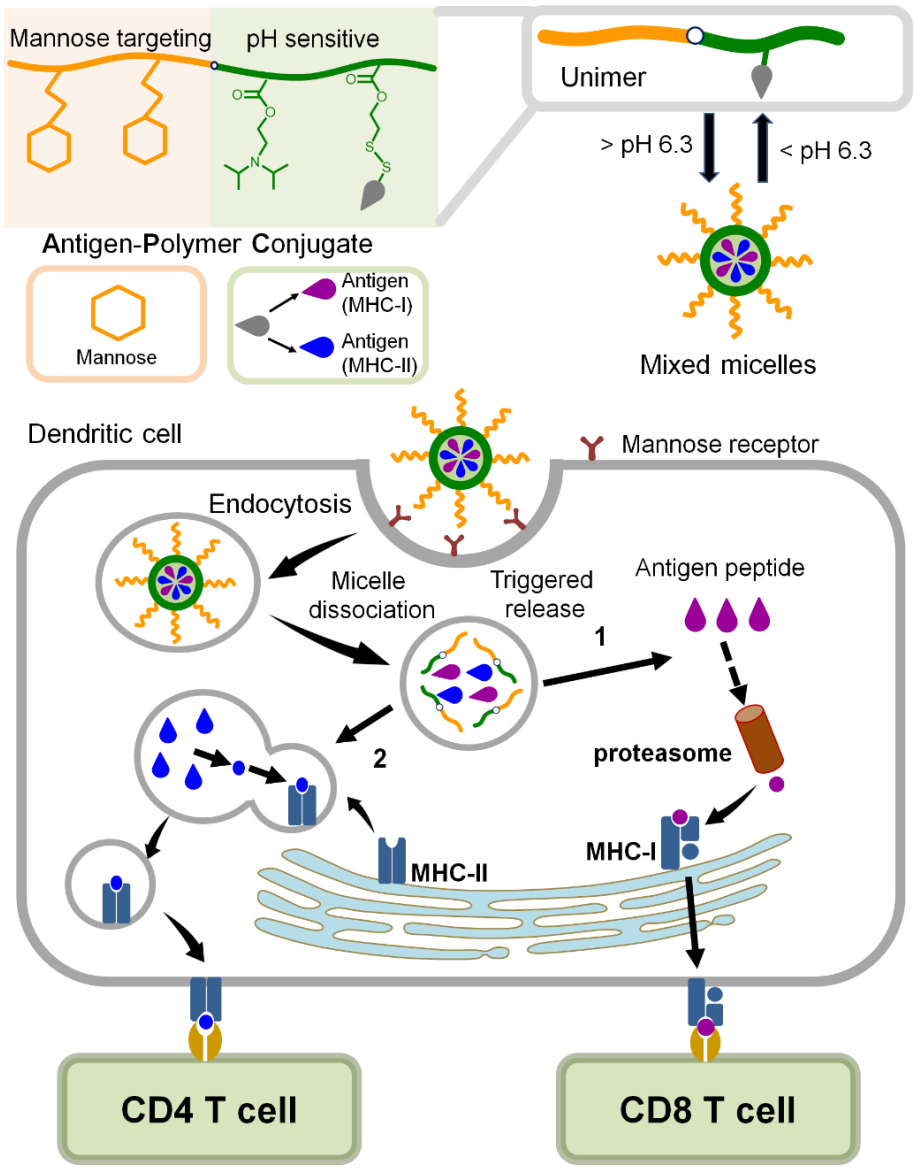

Figure 2.1 Schematic illustration of a mannosylated block copolymer for the delivery of both MHC-I and MHC-II epitopes to dendritic cells.

This work reports mannosylated polymer as an effective delivery platform for reversibly-conjugated peptide in cancer vaccine applications. The amphiphilic polymer is easily prepared by reversible addition-fragmentation chain transfer (RAFT) polymerization. The poly(mannose) block serves as the hydrophilic domain for micellization as well as the targeting ligand for improved LN accumulation. Peptides of both MHC-I and MHC-II epitopes were conjugated to the pH-sensitive block via disulfide bonds. In this design, polymers shield antigens at

physiological pH and rapidly disassemble into unimers at endosomal pH after cellular uptake to facilitate antigen release (**Figure 2.1**). In vivo LN accumulation studies demonstrate that the mannosylated micelles improve the DC uptake compared with free peptides and non-targeted NPs. The mannosylated micelles display improved DC activation, enhanced antigen-specific T cell response and higher antitumor immunity compared to free peptide, revealing a simple and effective platform for peptide cancer vaccine design.

2.2 RESULTS AND DISCUSSION

2.2.1 Synthesis of Mannosylated Polymer Platform for Peptide Delivery

The mannosylated polymer (MAN-P) was synthesized by RAFT polymerization (Figure 2.2a). The mannose block was first prepared by polymerization of mannose methacrylate (MMA). The resulting polymer (PMMA) had a degree of polymerization (DP) of 38 and low dispersity (Đ = 1.08) determined by gel permeation chromatography (GPC) (**Figure S2.1** and **S2.2**). The MAN-P diblock polymer was obtained by copolymerization of 2-diisopropylaminoethyl methacrylate (DIPAMA) and pyridyl disulfide ethyl methacrylate (PDSEMA) using PMMA as the macro chain transfer agent (mCTA) (Figure 2.2a). The DP of DIPAMA and PDSEMA were 47 and 3, respectively (**Figure S2.3**). GPC trace of MAN-P demonstrated a mono-model distribution and relatively low dispersity (Đ = 1.21, **Figure S2.4**). The DIPAMA block provides pH-sensitivity for the copolymer, and PDSEMA enables conjugation with thiol-containing peptide antigens. Therefore, peptides conjugated to MAN-P are protected inside the micellar core in extracellular environments but are exposed after cellular internalization.

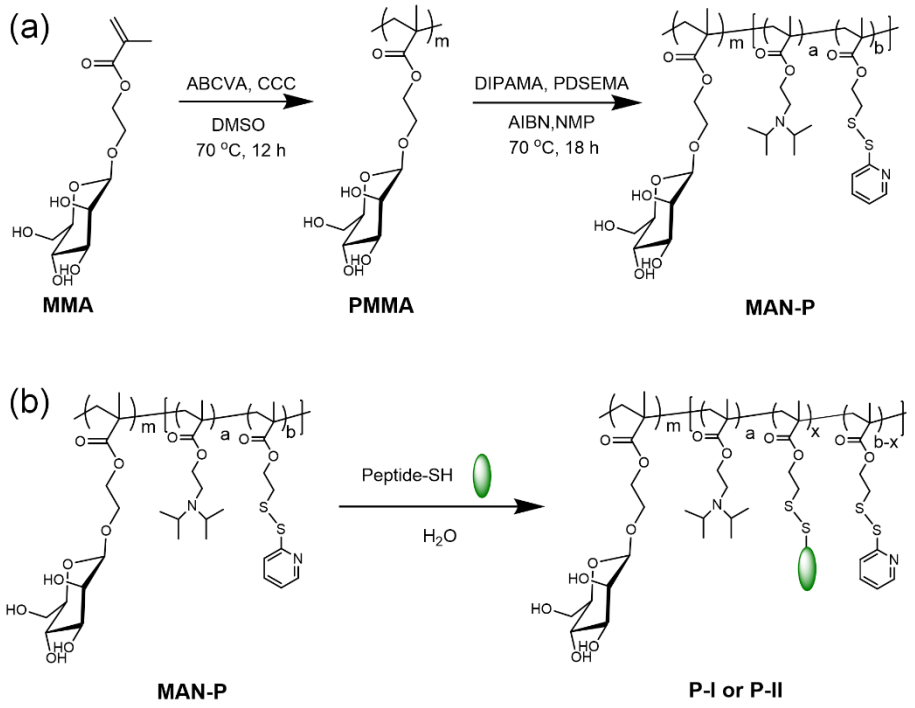

Figure 2.2 Polymer synthesis pathway

a) Synthetic pathway of the mannosylated block copolymer MAN-P. b) Conjugation of peptide antigens to MAN-P.

Peptide antigens were conjugated separately to MAN-P through the disulfide exchange reaction of thiolated peptides with PDSEMA (**Figure 2.2b**). CSSSIINFEKL, a variant of the chicken ovalbumin (OVA) MHC-I epitope, and CSSISQAVHAAHAEINEAGR, a variant of the OVA MHC-II epitope, were selected as the model antigens.[40] Both the peptides were conjugated to MAN-P with at least 50% efficiency by simply mixing the peptides and polymer in the aqueous solution (**Table 2.1**). The obtained polymer-MHC-I and polymer-MHC-II conjugates are denoted as P-I and P-II, respectively.

Table 2.1 Conjugation of MHC-I and MHC-II peptides to the MAN-P polymer.

Entry	Peptide per polymer	Peptide loading efficiency (%)	Peptide loading content (wt%)
P-I	2.0	67%	9.0
P-II	1.5	50%	11

P-I and P-II can self-assemble into micellar NPs in phosphate buffer saline (PBS) at physiological pH = 7.4. Both P-I and P-II micelles had diameters of 30-50 nm with narrow size distribution (**Figure 2.3a, b**, **Table 2.2**), which were smaller than the blank vehicle control (**Figure S5**). NPs encapsulating MHC-I and MHC-II peptides (P-I/II) are prepared by simply mixing P-I and P-II conjugates during the micelle fabrication process. The P-I/II mixed micelles demonstrated similar size distribution as compared to P-I and P-II micelles (**Figure 2.3c**). In addition, all of these micelles disassemble into free polymer unimers at acidic pH (**Figure 2.4**), exposing peptides after cellular internalization in endosomes.

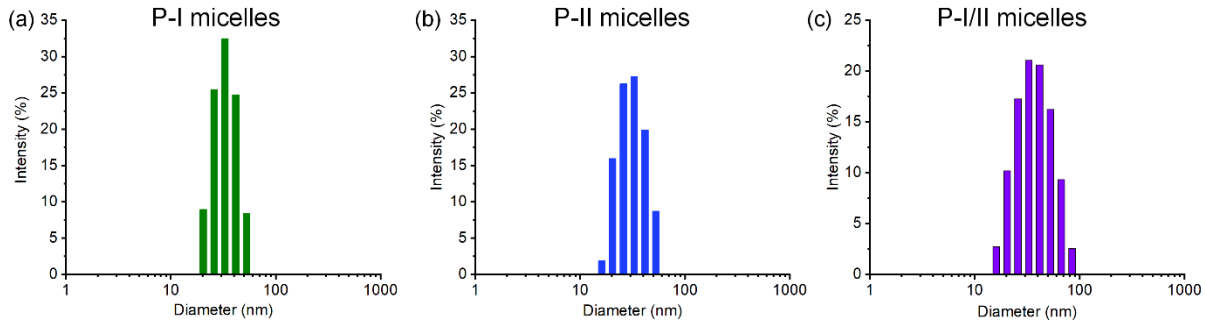

Figure 2.3 Size distribution of P-I, P-II and P-I/II micelles in PBS (pH = 7.4).

Table 2.2 Diameter and dispersity of various micelle formulations.

Entry	Diameter (nm)	PDI
P-I micelles	33.7	0.26
P-II micelles	32.1	0.3
P-I/II mixed micelles	39.4	0.4

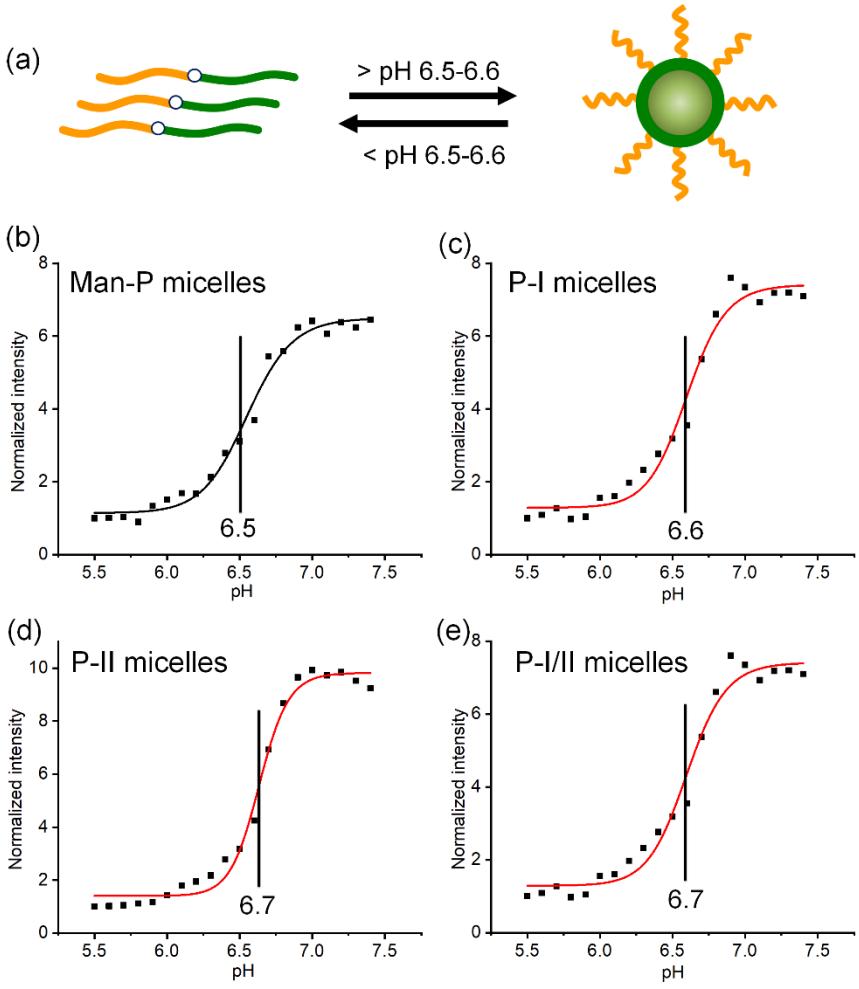

Figure 2.4 pH transition study for Man-P, P-I, P-II and P-I/II micelles.

2.2.2 LN Accumulation

To test the effect of mannose functionalization on *in vivo* delivery of nanovaccines to DCs, the CSSSIINFEKL antigen was rhodamine-labeled and injected as free peptide or peptide-conjugated micelles subcutaneously at the right tail base of the mice. In addition to the free peptide control, two non-targeted micelles with the same micellar core but different coronas (PEGylated or cationic)[41-43] were also utilized as control groups (**Figure 2.5a**). Fluorescent imaging of harvested lymph nodes 48 h after injection showed that the mannosylated micelles were retained more efficiently in draining inguinal lymph nodes (ILNs) than the other formulations, with preferential localization of micelles into the right ILN that corresponded with the injection site (**Figure 2.5b**). Flow cytometry analysis of lymph node-resident cells verified that mannosylated micelles and their antigen cargoes were primarily internalized by $CD11c^{+}MHCII^{+}$ DCs (**Figure 2.5c**). Mannosylated micelles generated an average of 16-, 79- and 36- fold increase in the number of DCs internalizing the rhodamine-labeled peptides in the lymph nodes compared with neutral micelles, cationic micelles and free peptide respectively. Taken together, these results confirm that display of mannose at micellar surface significantly improved the LN targeting and DC uptake *in vivo*.

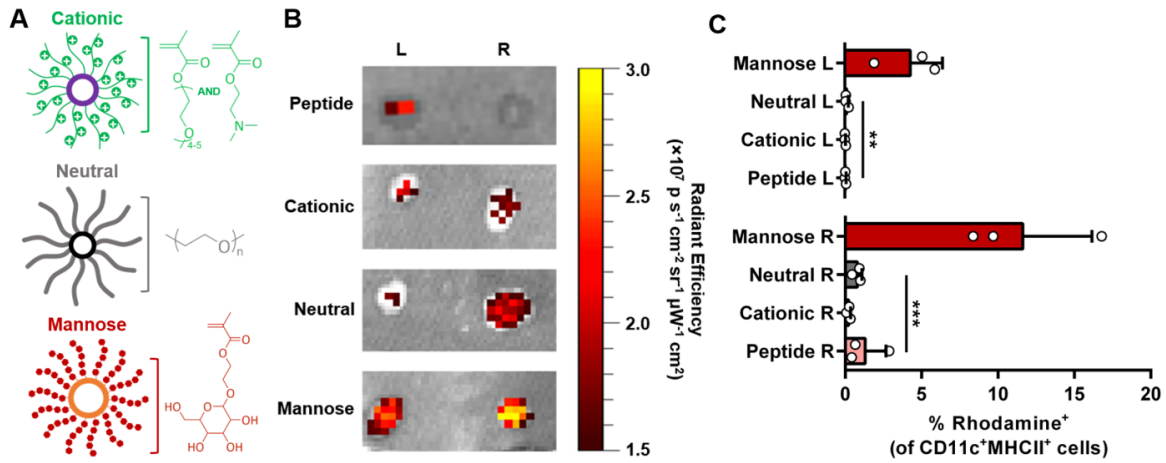

Figure 2.5 LN targeting and DC uptake

a) Cationic, neutral and mannose micelle structures. b) Fluorescence imaging of right and left draining ILNs (48 h post-treatment). Mannosylated micelles are retained more efficiently in lymph nodes. c) Flow cytometry analysis of lymph node-resident cells confirms that mannose-micelle formulations are internalized by $CD11c^{+}MHCII^{+}$ DCs. Data are presented as mean ± SD. N = 3 biological replicates. Statistical significance was calculated using one-way ANOVA with post-hoc Fisher's LSD test (**$P \leq 0.01$, ***$P \leq 0.001$).

2.2.3 *In Vivo* DC maturation

DC maturation is a critical step for T cell activation and immune responses.[44] Hallmarks of DC maturation include increased expression of MHC II molecules and costimulatory molecules such as CD86.[45,46] To assess whether the mannosylated micelles enhance DC maturation *in vivo*, P-I/II micelles, free peptides and PBS were injected subcutaneously in mice at the tail base followed by ILN analysis 24 h post-immunization. All the formulations were confirmed to have low levels of endotoxin (**Table S2.1**). P-I/II micelles increased the percentage of $CD86^{+}MHCII^{+}$ cells in the lymph nodes to a greater extent than free peptides (**Figure 2.6a**). In addition, P-I/II micelles increased the expression of maturation marker CD86 in both the total DC population and the $CD8^{+}$ DC subset (**Figure 2.6b,c**). $CD8^{+}$ DCs are a special subset of DCs that can present antigens on

MHC I molecules through cross-presentation,[47] a process that is essential for the activation of $CD8^+$ T cells that directly kill tumor cells.[48] P-I/II micelles significantly increased the expression of costimulatory molecule CD86 in $CD8^+$ DCs, whereas free peptides had no effect on CD86 expression (**Figure 2.6c**). The higher amount of activated $CD8^+$ DCs could lead to enhanced activation of $CD8^+$ T cells and robust antitumor responses. It is important to note that DC maturation in response to eh formulations was not observed *in vitro*. Immature bone marrow-derived dendritic cells (BMDCs) were incubated with PBS, free peptides, MAN-P and P-I/II micelles for 24 h. Minimal change in expression of CD86, CD40 and MHCII MFI was observed upon treatment with either peptides, control polymer or P-I/II micelles (**Figure S2.6**). Collectively, these data suggest that the micelles do not on their own have an adjuvant effect, but likely promote DC maturation in vivo by facilitating higher DC uptake through mannose targeting. The vaccine formulation can therefore be further improved in the future by combining with adjuvants like the stimulator of interferon genes (STING) agonists.[49]

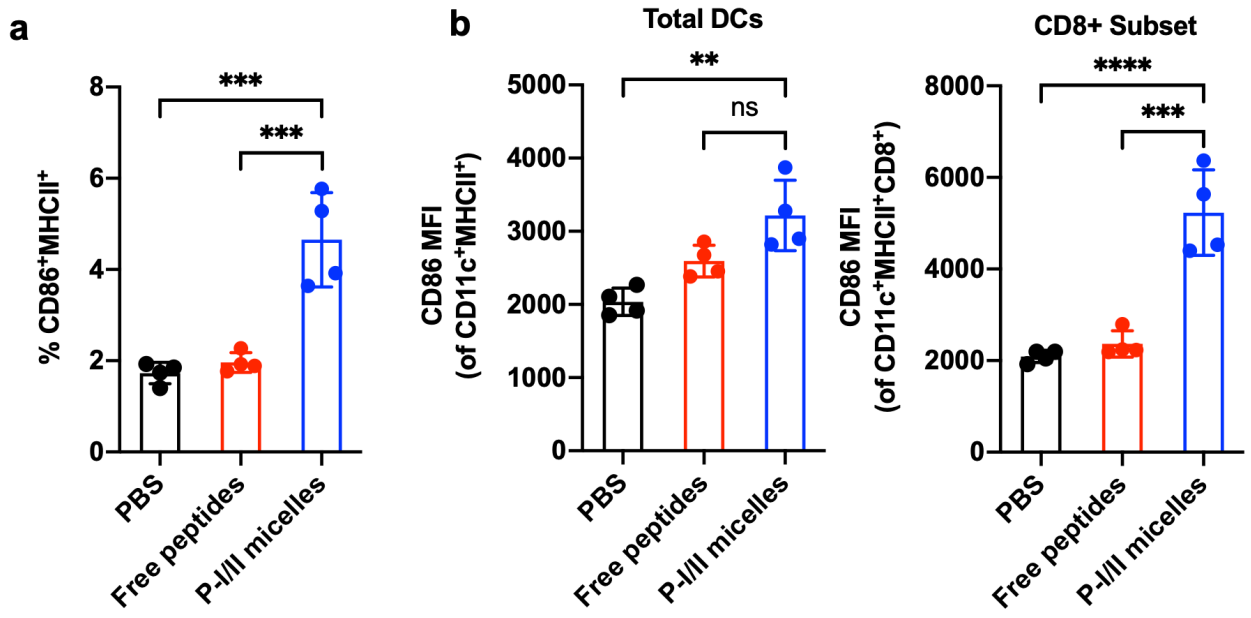

Figure 2.6 P-I/II micelles enhance DC maturation in vivo.

a) Percentage of $CD86^+$ $MHCII^+$ antigen-presenting cells in the ILNs 24 h after subcutaneous injection of PBS, free peptides and P-I/II micelles at the tail base. b) Median fluorescence intensity (MFI) of CD86 in $CD11c^+$ $MHCII^+$ DCs by flow cytometry 24 h after immunization. c) Median fluorescence intensity (MFI) of CD86 in $CD8^+$ DC subset by flow cytometry 24 h after immunization. Data are presented as mean ± SD. N=4 biological replicates. Statistical significance was calculated using one-way ANOVA with post-hoc Tukey HSD test (**P ≤ 0.01, ***P ≤ 0.001, ****P ≤ 0.0001, ns: not significant).

2.2.4 *In Vivo* T Cell Activation

We next evaluated whether P-I/II micelles could generate antigen-specific T cell responses *in vivo*. Mice were immunized with PBS, free peptides and P-I/II micelles on day 0 and 14, and splenocytes were collected and analyzed on day 21 (**Figure 2.7a**). H-$2K^b$/SIINFEKL tetramer staining was used to analyze the population of antigen-specific T cells in the splenocytes. P-I/II micelles generated a significantly higher SIINFEKL-specific T cell response, with a 6.8-fold increase of SIINFEKL-specific $CD8^+$ T cells in the splenocytes compared with that in the free peptides treatment group (**Figure 2.7b,c**). Intracellular cytokine staining (ICCS) was used to analyze cytokine production upon antigen restimulation.[50] P-I/II micelles induced a significant increase in the number of IFN-γ- and TNF-α-producing $CD8^+$ T cells in the splenocytes when stimulated with SIINFEKL, whereas free peptides only induced cytokine producing cells similar to the PBS control (**Figure 2.7d, Figure S2.7**). Similarly, P-I/II micelles induced a higher number of IFN-γ- and IL-2-producing $CD4^+$ T cells when stimulated with OVA antigen, although the increase was not statistically significant (**Figure 2.7e**). Collectively, these results demonstrate that the P-I/II micelles generate a large amount of antigen-specific $CD8^+$ T cells and robust cytokine production in both $CD8^+$ and $CD4^+$ T cells, a desirable trait as a peptide antigen carrier for cancer vaccines. The data also support the correlation between DC maturation and T cell activation, where more activated DCs lead to more robust T cell responses.

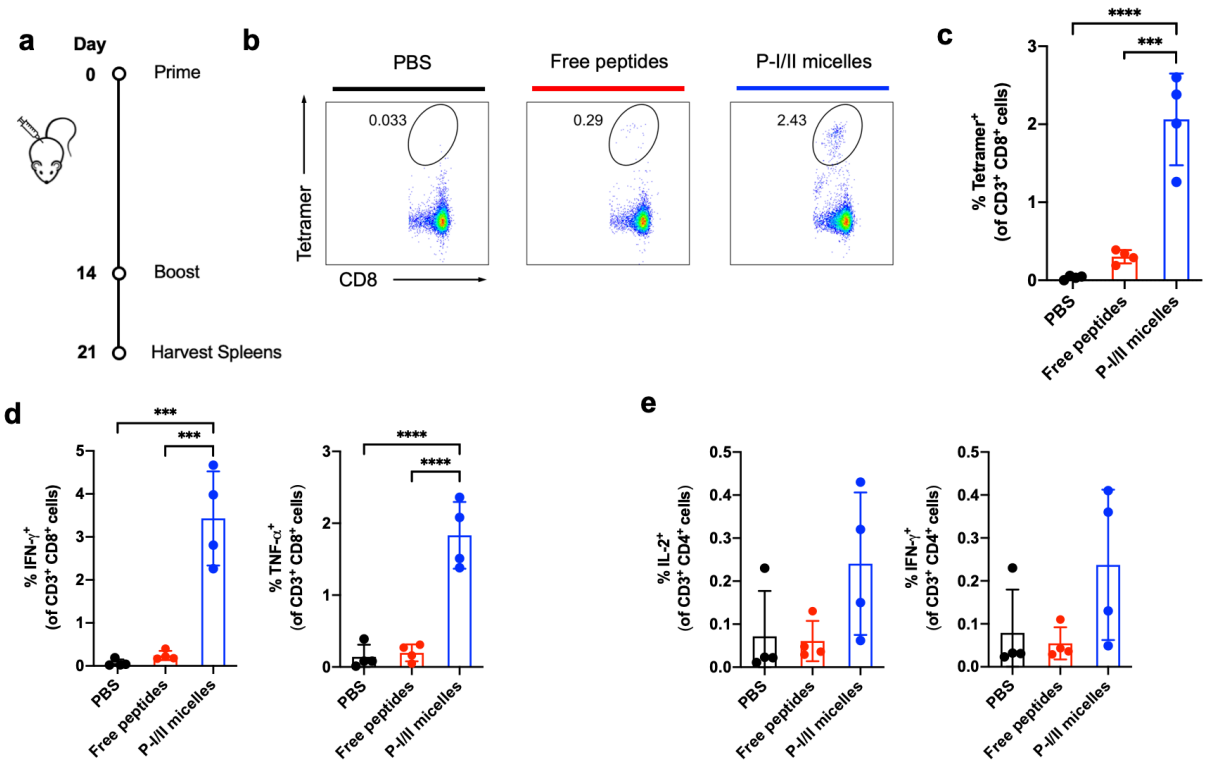

Figure 2.7 In vivo T cell activation

a) Schematic of the study timeline. Female C57BL/6 mice were immunized on days 0 and 14 via subcutaneous injection at the tail base with PBS, free peptides or P-I/II micelles. Spleens were collected on day 21. b) Representative flow data of H-2K^b/SIINFEKL tetramer staining in CD8$^+$ T cells. c) Percentage of SIINFEKL-specific CD8$^+$ T cells in the spleens. d) Percentage of IFN-γ$^+$ and TNF-α$^+$ CD8$^+$ T cells after restimulation with SIINFEKL peptide. e) Percentage of IFN-γ$^+$ and IL-2$^+$ CD4$^+$ T cells after restimulation with OVA protein. Data are presented as mean ± SD. N=4 biological replicates. Statistical significance was calculated using one-way ANOVA with post-hoc Tukey HSD test (***P ≤ 0.001, ****P ≤ 0.0001).

2.2.5 Therapeutic Vaccination

Given the enhanced T cell activation generated by P-I/II micelles, we next evaluated the therapeutic effects of the vaccines. B16F10-OVA tumor-bearing mice were injected with PBS, free peptides, MAN-P micelles (vehicle control), and P-I/II micelles four days post tumor inoculation, followed by two boost injections at one week intervals (**Figure 2.8a**). Immune

checkpoint blockade (ICB) anti-PD1 was given one day after vaccination through intraperitoneal injection to increase the efficacy of the treatments. P-I/II micelles delayed tumor growth compared with free peptides and MAN-P (**Figure 2.8b**). In addition, P-I/II micelles significantly prolonged the survival of tumor-bearing mice compared with free peptides (**Figure 2.8c**). These results align with the other *in vivo* data, further demonstrating the potential of P-I/II micelles as a therapeutic cancer vaccine. A similar trend was observed in the combination treatment with ICB. ICB alone was not able to achieve a therapeutic effect. However, the combination of ICB with free peptides or P-I/II micelles slowed tumor growth and prolonged survival (**Figure 2.8d,e**). The difference in tumor volume and survival between ICB + free peptides and ICB + P-I/II micelles was significant, substantiating the efficacy of the mannosylated-polymer delivery system in rodent tumor models. Both P-I/II micelles and ICB + P-I/II micelles inhibited tumor growth compared with other groups (**Figure 2.8f**). The inclusion of ICB slightly improved the efficacy of the P-I/II micelles (**Figure S2.8**). However, the difference was not significant as the B16F10 melanoma model is poorly immunogenic.[51,52] The treatment could be potentially improved by combining the anti-PD1 and anti-CTLA4 treatments to overcome the immune suppression in both the early and the late stages of an immune response.[53] In addition, anti-PD1 was administered once between weekly vaccinations. Increasing the dosage frequency to two doses between weekly vaccinations could improve the efficacy of the vaccine.[54]

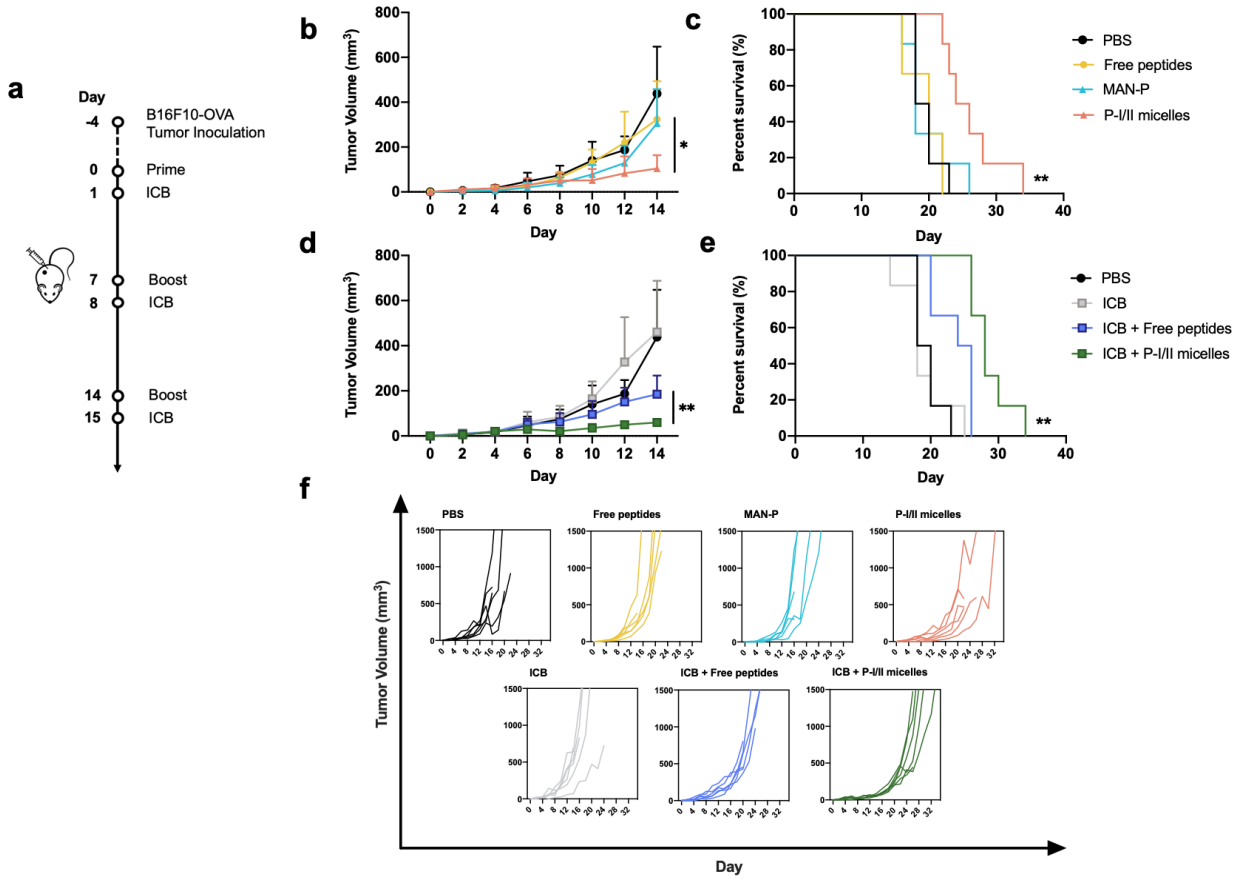

Figure 2.8 P-I/II micelles inhibit tumor growth and prolong survival in B16F10 tumor-bearing mice.

a) Schematic of the study timeline. Female C57BL/6 mice were inoculated with B16F10-OVA cells on day -4 and immunized on day 0, 7 and 14 via subcutaneous injection at the tail base with PBS, free peptides, MAN-P or P-I/II micelles. Immune checkpoint blockade (ICB) anti-PD1 was given 1 day post immunization in some of the groups. b, c) Tumor growth curve and survival curve of mice treated with PBS, free peptides, polymer and P-I/II micelles. d, e) Tumor growth curve and survival of mice treated with PBS, ICB, ICB + free peptides and ICB + P-I/II micelles. f) Individual tumor growth curves. Data are presented as mean ± SD. N=6 biological replicates. Statistical significance of tumor volume was calculated using unpaired t-test. Survival analysis was performed using the log-rank test (*P ≤ 0.05, **P ≤ 0.01).

2.3 CONCLUSION

In summary, we report the development of mannosylated polymeric NPs for peptide cancer delivery. The polymer carrier design possesses several advantages including defined chemical structures, multiple functionalities, and ease of manufacturing. Various peptide antigens can be readily conjugated to the polymer under mild conditions. The obtained polymer-antigen peptide conjugates can self-assemble into sub-100 nm micelles at physiological environments and dissociate at endosomal acidic conditions. The mannose displayed on the surface of the micelles facilitates LN accumulation and DC uptake. The mannosylated micelles demonstrate significantly enhanced antitumor immunity. With a simple design and multi-functional capability for targeted delivery, peptide protection and triggered peptide release, this mannosylated polymer provides a useful and practical platform for the peptide cancer vaccine delivery. The combination of this mannosylated vaccine with immune-stimulating molecules will be investigated in the future studies.

2.4 MATERIALS AND METHODS

2.4.1 Materials, polymer synthesis, and characterization

RAFT chain transfer agent 4-((((2-Carboxyethyl)thio)carbonothioyl)thio)-4-cyanopentanoic acid (CCC), azobisisobutyronitrile (AIBN), 4,4'-azobis(4-cyanovaleric acid) (ABCVA), and PDSEMA were purchased from Sigma-Aldrich and used as received. Mannose ethylmethacrylate (MMA) was purchased from Omm Scientific. DIPAMA was purchased from Sigma-Aldrich and was purified by passing through a column filled with basic alumina to remove the inhibitor prior to polymerization. Anhydrous *N*-Methyl-2-pyrrolidone (NMP, 99.5%), and dimethylsulfoxide (DMSO, > 99%) were purchased from Sigma-Aldrich and stored with activated molecular sieves.

Endotoxin level was measured using the limulus amebocyte lysate (LAL) endosafe PTS assay from Charles River.

2.4.2 Characterization

Polymer characterization. All ^{1}H NMR spectra were recorded on a Bruker AV 300 (Bruker Corporation, Billerica, MA) nuclear magnetic resonance (NMR) instrument in various deuterated solvents as described below. Polydispersity index ($Đ = M_w/M_n$) of the polymers were determined by gel permeation chromatography (GPC). The mobile phase consisted of DMF containing 0.1 M LiBr at a flow rate of 1 mL min^{-1}. Samples were filtered through a 0.45 μm PTFE filter before analysis. Size and distribution of micelles were recorded on a dynamic light scattering (DLS) system (DynaPro NanoStar, Wyatt technology).

2.4.3 Polymer synthesis

The mannose macro chain transfer agent PMMA was prepared through RAFT polymerization of MMA (40 mol equiv) using ABCVA (0.1 mol equiv) as initiator and CCC (1 mol equiv) as chain transfer agent in DMSO. All reaction components were dissolved in DMSO at 35% wt/wt final concentration in a round bottom flask. After purging with argon through a sealed septum for 15 minutes, the flask was vigorously stirred at 70 °C for 18 h before the reaction was terminated by perfusion of air. The reaction solution was diluted by *N*,*N*'-dimethylacetamide (DMAc) and then precipitated into acetone and ether mixture (1:1, v/v). PMMA was obtained as white powder after high vacuum and used without further purification. Yield: 70%. Then, PMMA (1 mol equiv), AIBN (0.25 mol equiv), DIPAMA (60 mol equiv), and PDSEMA (10 mol equiv) were dissolved in NMP at 20% wt/wt in a round bottom flask. After purging with argon through a sealed septum for 15 minutes, the flask was vigorously stirred at 70 °C for 18 h. The reaction was terminated by

perfusion of air and the product purified through serial dialysis in NMP and deionized (DI) water before lyophilization. MAN-P was dissolved in DMSO-d_6 for ^{1}H NMR spectroscopy and block 2 degree of polymerization was confirmed relative to known block 1 MMA content. Yield: 90%.

2.4.4 Peptide synthesis and conjugation

Antigen peptides (CSSSIINFEKL and CSSISQAVHAAHAEINEAGR) were synthesized using a Liberty Blue (CEM) microwave peptide synthesizer on Rink Amide resin (Millipore) before purification with reverse phase HPLC as in our previous work.[43] Synthesized peptides were conjugated to polymers through disulfide exchange between cysteine and PDSEMA and conjugates were purified as in previous work.[43] Briefly, both polymer and peptide were dissolved in DI water at > 40 mg/mL and incubated at room temperature until Abs343 nm due to pyridyl-2-thione displacement plateaued (~24 h), indicating completion of disulfide exchange. Then, the reaction solution was put into a MWCO 10000 dialysis bag and dialyzed against DI water for 3 days. P-I and P-II conjugates were obtained after lyophilization.

2.4.5 Micelle formation

The vaccine micelles were prepared by a pH-transition method. Briefly, 10-20 mg of P-I and P-II was dissolved in 190 μL of 200 mM monobasic sodium phosphate (~pH 5.4), followed by addition of 810 μL of 200 mM dibasic sodium phosphate to bring the pH to 7.4. Micelles were allowed to form overnight before buffer exchange to nanopure distilled water on a 10 kDa cutoff Amicon centrifugal filter (Millipore) and stored at 4 °C before use. The pH transition point of the micelles was determined using a Nile Red assay as in previous work.[43]

2.4.6 Cell lines and animals

B16F10-OVA cells (gift of Prof. Amanda Lund) were cultured in DMEM supplemented with 10% FBS and 1% P/S at 37°C and 5% CO2. All studies with animals were carried out in accordance with protocols approved by the Institutional Animal Care and Use Committee at the University of Washington. Female C57BL/6 mice, aged between 6 and 8 weeks, were purchased from Charles River Laboratories.

2.4.7 In vitro dendritic cell activation

BMDCs were generated by culturing bone marrow cells from the femur and tibia of female C57BL/6 mice. Cells were cultured in RPMI supplemented with 10% HI-FBS, 1% P/S, 2mM L-glutamine, 50uM β-mercaptoethanol and 20 ng/mL GM-CSF. Medium was half replaced on day 3 and day 6. Non-adherent and loosely adherent immature BMDCs were harvested on day 8. BMDCs were plated in 6-well non-TC treated plates at $3 * 10^5$ cells per well. PBS, free peptides containing 1μg/ml CSSSIINFEKL and 1μg/ml CSSISQAVHAAHAEINEAGR, P-I/II micelles containing equivalent antigen and MAN-P containing equivalent polymer were added to the cell culture and incubated for 24 h at 37°C and 5% CO2. After incubation, cells were stained with Zombie NIR viability kit, incubated with anti-CD16/32 and with anti-CD86-BV510, anti-MHC II-eFluor450, anti-CD11c-APC and anti-CD40-FITC. Flow data were acquired on the Attune NxT flow cytometer and analyzed using FlowJo software.

2.4.8 Vaccine localization to LN and DCs.

Mice were injected subcutaneously in the right tail base with various CSSSIINFEKL formulations (20 μg CSSSIINFEKL, 10% rhodamine-labeled) in 40 μL of 5% (w/v) glucose. The following formulations were used: (i) soluble CSSSIINFEKL, (ii) Cationic micelles, (iii) PEGylated micelles, and (iv) mannosylated micelles (n = 3 per treatment group). The cationic and PEGylated

polymers were synthesized according to previous reports.[41, 42] CSSSIINFEKL and rhodamine-labeled CSSSIINFEKL were conjugated to these polymers using the same reaction conditions as described above. Rhodamine fluorescence at the injection site was monitored by Xenogen (Caliper Life Sciences) over a period of 48 hours. After 48 hours, mice were sacrificed and ILNs were removed. Rhodamine fluorescence in the ILNs was visualized by Xenogen. Lymph node-resident cells were subsequently harvested as described above. Harvested cells were spun down, transferred to a 96-well U-bottom plate, and stained with Zombie Violet live/dead staining buffer for 15 minutes at room temperature After live/dead staining, cells were washed with mouse anti-CD16/CD32 for 10 minutes at 4 °C. After blocking, cells were stained for 30 minutes at 4 °C with the following antibodies: FITC-anti-CD45, CD11c-APC, and PerCP/Cy5.5-anti-MHCII. After antibody staining, cells were washed and resuspended in 250 μL of PBS + 1% bovine serum albumin. Flow cytometry was used to analyze DC populations. DCs from untreated mice were used as assay baselines.

2.4.9 In vivo dendritic cell activation

Female C57BL/6 mice were injected subcutaneously at the tail base with PBS, free peptides containing 25 μg CSSSIINFEKL and 25 μg CSSISQAVHAAHAEINEAGR, or P-I/II micelles containing equivalent antigen. ILNs were harvested 24 h post injection. LNs were digested in RPMI 1640, 10% FBS, collagenase type IV (50 U/mL) and DNase I (100 U/mL). Tissues were mashed against a 70 μm cell strainer to obtain single-cell suspension. Cells were stained with Zombie NIR viability kit for 15 min at room temperature. Afterwards, cells were incubated with anti-CD16/32 for 30 min at 4°C. After blocking, cells were incubated with anti-CD86-BV510, anti-MHC II-PerCP/Cy5.5, anti-CD11c-APC, anti-CD8-AF488 for 20 min at 4°C. Flow data were acquired on the Attune NxT flow cytometer and analyzed using FlowJo software.

2.4.10 In vivo immunization and T cell responses

Female C57BL/6 mice were immunized on day 0 and 14 via subcutaneous injection at the tail base with PBS, free peptides containing 25 μg CSSSIINFEKL and 25 μg CSSISQAVHAAHAEINEAGR, or P-I/II micelles containing equivalent antigen. On day 21, spleens were collected and passed through a 70 μm cell strainer to obtain single-cell suspension. The splenocytes were treated with ACK lysis buffer, washed and transferred to 96-well plates for tetramer staining and intracellular cytokine staining (ICCS). To analyze antigen-specific T cell responses, splenocytes were stained with Zombie NIR viability kit for 15 min at room temperature, followed by 15 min incubation with PE-labeled H-2K^b/SIINFEKL tetramer (NIH Tetramer Core). Cells were then incubated with anti-CD16/32 and stained with anti-CD3-eFluor450 and anti-CD8-FITC. Flow cytometry was used to determine the percentage of SIINFEKL-specific CD8$^+$ T cells. Data were analyzed using FlowJo software. To analyze cytokine production, splenocytes were cultured in IMDM with 10% FBS and 1% P/S and restimulated with 5 μg/mL SIINFEKL peptide or 5 mg/mL OVA protein. After 3 h incubation at 37 °C and 5% CO_2, Protein Transport Inhibitor Cocktail (eBioscience) was added and cells were incubated for an additional 3 h. After restimulation, cells were incubated with Zombie NIR, anti-CD16/32, followed by anti-CD3-eFluor450, anti-CD8-FITC or anti-CD4-FITC. Fixation and permeabilization of cells were carried out using BD Cytofix/Cytoperm kit. ICCS was performed with anti-TNF-α-PE and anti-IFN-γ-APC for CD8$^+$ T cells and anti-IL-2-PE and anti-IFN-γ-APC for CD4$^+$ T cells. Flow data were acquired on the Attune NxT flow cytometer and analyzed using FlowJo software.

2.4.11 Tumor studies

Female C57BL/6 mice were inoculated with 10^5 B16F10-OVA cells in the right hind flank on day -4. On day 0, 7 and 14, mice were immunized with PBS, free peptides containing 25 μg

CSSSIINFEKL and 25 μg CSSISQAVHAAHAEINEAGR, P-I/II micelles containing equivalent antigen or MAN-P containing equivalent polymer at the tail base via subcutaneous injection. 100ug anti PD-1 was given via intraperitoneal injection on day 1, 8 and 15. Tumor volume was measured every other day using a caliper and the volume was calculated using the equation Volume = $Width^2$ * Length / 2. Mice were euthanized if tumor volume exceeded 1500 mm^3, body weight loss exceeded 20%, or tumor discharge was observed.

2.4.12 Statistical analysis

All statistical analyses were carried out in GraphPad Prism software. Unpaired t-test was used for comparisons with two groups. One-way ANOVA with post-hoc Tukey HSD test or post-hoc Fisher's LSD test was used for comparisons with more than two groups. Survival analysis was performed using the log-rank test.

2.5 ACKNOWLEDGEMENTS

S. L. and K. S. contributed equally to this work. This work was supported by the U.S. National Institutes of Health (NIH R01CA17727, R01 AI134729 and R01CA257563). We are grateful to Prof. Amanda Lund for providing B16-OVA cells. We thank the NIH Tetramer Core Facility for providing the PE-labeled H-$2K^b$/SIINFEKL tetramer. We thank the Prof. Kim Woodrow for use of her DLS particle sizer.

2.6 REFERENCES

[1] H. Wang, D.J. Mooney, Biomaterial-assisted targeted modulation of immune cells in cancer treatment, Nat Mater, 17 (2018) 761-772.

[2] K. Shao, S. Singha, X. Clemente-Casares, S. Tsai, Y. Yang, P. Santamaria, Nanoparticle-Based Immunotherapy for Cancer, Acs Nano, 9 (2015) 16-30.

[3] W.T. Song, S.N. Musetti, L. Huang, Nanomaterials for cancer immunotherapy, Biomaterials, 148 (2017) 16-30.

[4] I. Mellman, G. Coukos, G. Dranoff, Cancer immunotherapy comes of age, Nature, 480 (2011) 480-489.

[5] W.J. Lesterhuis, J. Haanen, C.J.A. Punt, Cancer immunotherapy - revisited, Nat Rev Drug Discov, 10 (2011) 591-600.

[6] P. Sharma, K. Wagner, J.D. Wolchok, J.P. Allison, Novel cancer immunotherapy agents with survival benefit: recent successes and next steps, Nat Rev Cancer, 11 (2011) 805-812.

[7] N.P. Restifo, M.E. Dudley, S.A. Rosenberg, Adoptive immunotherapy for cancer: harnessing the T cell response, Nat Rev Immunol, 12 (2012) 269-281.

[8] D.F. McDermott, M.B. Atkins, PD-1 as a potential target in cancer therapy, Cancer Medicine, 2 (2013) 662-673.

[9] T. Okazaki, S. Chikuma, Y. Iwai, S. Fagarasan, T. Honjo, A rheostat for immune responses: the unique properties of PD-1 and their advantages for clinical application, Nat Immunol, 14 (2013) 1212-1218.

[10] K. Palucka, J. Banchereau, Cancer immunotherapy via dendritic cells, Nat Rev Cancer, 12 (2012) 265-277.

[11] J.R. Zhou, A.V. Kroll, M. Holay, R.H. Fang, L.F. Zhang, Biomimetic Nanotechnology toward Personalized Vaccines, Adv Mater, 32 (2020).

[12] D. Shae, J.J. Baljon, M. Wehbe, K.W. Becker, T.L. Sheehy, J.T. Wilson, At the bench: Engineering the next generation of cancer vaccines, J Leukocyte Biol, (2019).

[13] R.J. Malonis, J.R. Lai, O. Vergnolle, Peptide-Based Vaccines: Current Progress and Future Challenges, Chem Rev, 120 (2020) 3210-3229.

[14] Y. Zhao, Y.G. Guo, L. Tang, Engineering cancer vaccines using stimuli-responsive biomaterials, Nano Res, 11 (2018) 5355-5371.

[15] R.E. Hollingsworth, K. Jansen, Turning the corner on therapeutic cancer vaccines, Npj Vaccines, 4 (2019).

[16] S.Y. Kim, Y.W. Noh, T.H. Kang, J.E. Kim, S. Kim, S.H. Um, D.B. Oh, Y.M. Park, Y.T. Lim, Synthetic vaccine nanoparticles target to lymph node triggering enhanced innate and adaptive antitumor immunity, Biomaterials, 130 (2017) 56-66.

[17] T.P. Hogervorst, R.J.E. Li, L. Marino, S.C.M. Bruijns, N.J. Meeuwenoord, D.V. Filippov, H.S. Overkleeft, G.A. van der Marel, S.J. van Vliet, Y. van Kooyk, J.D.C. Codee, C-Mannosyl Lysine for Solid Phase Assembly of Mannosylated Peptide Conjugate Cancer Vaccines, Acs Chem Biol, 15 (2020) 728-739.

[18] M. Glaffig, B. Palitzsch, S. Hartmann, C. Schull, L. Nuhn, B. Gerlitzki, E. Schmitt, H. Frey, H. Kunz, A Fully Synthetic Glycopeptide Antitumor Vaccine Based on Multiple Antigen Presentation on a Hyperbranched Polymer, Chem-Eur J, 20 (2014) 4232-4236.

[19] M. Luo, H. Wang, Z.H. Wang, H.C. Cai, Z.G. Lu, Y. Li, M.J. Du, G. Huang, C.S. Wang, X. Chen, M.R. Porembka, J. Lea, A.E. Frankel, Y.X. Fu, Z.J.J. Chen, J.M. Gao, A STING-activating nanovaccine for cancer immunotherapy, Nat Nanotechnol, 12 (2017) 648-+.

[20] G.M. Lynn, C. Sedlik, F. Baharom, Y.L. Zhu, R.A. Ramirez-Valdez, V.L. Coble, K. Tobin, S.R. Nichols, Y. Itzkowitz, N. Zaidi, J.M. Gammon, N.J. Blobel, J. Denizeau, P. de la Rochere, B.J. Francica, B. Decker, M. Maciejewski, J. Cheung, H. Yamane, M.G. Smelkinson, J.R. Francica, R. Laga, J.D. Bernstock, L.W. Seymour, C.G. Drake, C.M. Jewell, O. Lantz, E. Piaggio, A.S. Ishizuka, R.A. Seder, Peptide-TLR-7/8a conjugate vaccines chemically programmed for nanoparticle self-assembly enhance CD8 T-cell immunity to tumor antigens, Nat Biotechnol, (2020).

[21] L. Nuhn, S. Hartmann, B. Palitzsch, B. Gerlitzki, E. Schmitt, R. Zentel, H. Kunz, Water-Soluble Polymers Coupled with Glycopeptide Antigens and T-Cell Epitopes as Potential Antitumor Vaccines, Angew Chem Int Edit, 52 (2013) 10652-10656.

[22] L.X. Wei, Y. Zhao, X.M. Hu, L. Tang, Redox-Responsive Polycondensate Neoepitope for Enhanced Personalized Cancer Vaccine, Acs Central Sci, 6 (2020) 404-412.

[23] H. Yue, G.H. Ma, Polymeric micro/nanoparticles: Particle design and potential vaccine delivery applications, Vaccine, 33 (2015) 5927-5936.

[24] V. Pavot, M. Berthet, J. Resseguier, S. Legaz, N. Handke, S.C. Gilbert, S. Paul, B. Verrier, Poly(lactic acid) and poly(lactic-co-glycolic acid) particles as versatile carrier platforms for vaccine delivery, Nanomedicine-Uk, 9 (2014) 2703-2718.

[25] Y.C. Fan, J.J. Moon, Nanoparticle Drug Delivery Systems Designed to Improve Cancer Vaccines and Immunotherapy, Vaccines-Basel, 3 (2015) 662-685.

[26] H. Dewitte, R. Verbeke, K. Breckpot, S.C. De Smedt, I. Lentacker, Nanoparticle design to induce tumor immunity and challenge the suppressive tumor microenvironment, Nano Today, 9 (2014) 743-758.

[27] J. Conniot, A. Scomparin, C. Peres, E. Yeini, S. Pozzi, A.I. Matos, R. Kleiner, L.I.F. Moura, E. Zupancic, A.S. Viana, H. Doron, P.M.P. Gois, N. Erez, S. Jung, R. Satchi-Fainaro, H.F.

Florindo, Immunization with mannosylated nanovaccines and inhibition of the immune-suppressing microenvironment sensitizes melanoma to immune checkpoint modulators, Nat Nanotechnol, 14 (2019) 891-+.

[28] S.T. Reddy, A.J. Van Der Vlies, E. Simeoni, V. Angeli, G.J. Randolph, C.P. O'Neil, L.K. Lee, M.A. Swartz, J.A. Hubbell, Exploiting lymphatic transport and complement activation in nanoparticle vaccines, Nat Biotechnol, 25 (2007) 1159-1164.

[29] A. Francian, S. Namen, M. Stanley, K. Mann, H. Martinson, M. Kullberg, Intratumoral delivery of antigen with complement C3-bound liposomes reduces tumor growth in mice, Nanomed-Nanotechnol, 18 (2019) 326-335.

[30] Y.Y. Guo, D. Wang, Q.L. Song, T.T. Wu, X.T. Zhuang, Y.L. Bao, M. Kong, Y. Qj, S.W. Tan, Z.P. Zhang, Erythrocyte Membrane-Enveloped Polymeric Nanoparticles as Nanovaccine for Induction of Antitumor Immunity against Melanoma, Acs Nano, 9 (2015) 6918-6933.

[31] C.G. Da Silva, M.G.M. Camps, T.M.W.Y. Li, A.B. Chan, F. Ossendorp, L.J. Cruz, Co-delivery of immunomodulators in biodegradable nanoparticles improves therapeutic efficacy of cancer vaccines, Biomaterials, 220 (2019).

[32] F. Coumes, C.Y. Huang, C.H. Huang, J. Coudane, D. Domurado, S.M. Li, V. Darcos, M.H. Huang, Design and Development of Immunomodulatory Antigen Delivery Systems Based on Peptide/PEG-PLA Conjugate for Tuning Immunity, Biomacromolecules, 16 (2015) 3666-3673.

[33] G.Z. Zhao, S. Chandrudu, M. Skwarczynski, I. Toth, The application of self-assembled nanostructures in peptide-based subunit vaccine development, Eur Polym J, 93 (2017) 670-681.

[34] E.S. Lee, J.M. Shin, S. Son, H. Ko, W. Um, S.H. Song, J.A. Lee, J.H. Park, Recent Advances in Polymeric Nanomedicines for Cancer Immunotherapy, Adv Healthc Mater, 8 (2019).

[35] S. Eskandari, T. Guerin, I. Toth, R.J. Stephenson, Recent advances in self-assembled peptides: Implications for targeted drug delivery and vaccine engineering, Adv Drug Deliver Rev, 110 (2017) 169-187.

[36] S.B. Du, S.S. Liew, L. Li, S.Q. Yao, Bypassing Endocytosis: Direct Cytosolic Delivery of Proteins, J Am Chem Soc, 140 (2018) 15986-15996.

[37] R.H. Fang, C.M.J. Hu, B.T. Luk, W.W. Gao, J.A. Copp, Y.Y. Tai, D.E. O'Connor, L.F. Zhang, Cancer Cell Membrane-Coated Nanoparticles for Anticancer Vaccination and Drug Delivery, Nano Lett, 14 (2014) 2181-2188.

[38] S.X. Li, X.R. Feng, J.X. Wang, W.G. Xu, M.A. Islam, T.M. Sun, Z.G. Xie, C.X. Wang, J.X. Ding, X.S. Chen, Multiantigenic Nanoformulations Activate Anticancer Immunity Depending on Size, Adv Funct Mater, 29 (2019).

[39] H.P. Liu, K.D. Moynihan, Y.R. Zheng, G.L. Szeto, A.V. Li, B. Huang, D.S. Van Egeren, C. Park, D.J. Irvine, Structure-based programming of lymph-node targeting in molecular vaccines, Nature, 507 (2014) 519-+.

[40] S. Hirosue, I.C. Kourtis, A.J. van der Vlies, J.A. Hubbell, M.A. Swartz, Antigen delivery to dendritic cells by poly(propylene sulfide) nanoparticles with disulfide conjugated peptides: Cross-presentation and T cell activation, Vaccine, 28 (2010) 7897-7906.

[41] Y.L. Cheng, R.C. Yumul, S.H. Pun, Virus-Inspired Polymer for Efficient In Vitro and In Vivo Gene Delivery, Angew Chem Int Edit, 55 (2016) 12013-12017.

[42] M. Sylvestre, S. Lv, L.F. Yang, N. Luera, D.J. Peeler, B.M. Chen, S.R. Roffler, S.H. Pun, Replacement of L-amino acid peptides with D-amino acid peptides mitigates anti-PEG antibody generation against polymer-peptide conjugates in mice, J controlled release, 331 (2021) 142-153.

[43] D.J. Peeler, S.N. Thai, Y.L. Cheng, P.J. Horner, D.L. Sellers, S.H. Pun, pH-sensitive polymer micelles provide selective and potentiated lytic capacity to venom peptides for effective intracellular delivery, Biomaterials, 192 (2019) 235-244.

[44] I. Mellman, R.M. Steinman, Dendritic cells: Specialized and regulated antigen processing machines, Cell, 106 (2001) 255-258.

[45] K. Palucka, J. Banchereau, Dendritic-Cell-Based Therapeutic Cancer Vaccines, Immunity, 39 (2013) 38-48.

[46] J.C. Mbongue, H.A. Nieves, T.W. Torrez, W.H.R. Langridge, The Role of Dendritic Cell Maturation in the induction of insulin-Dependent Diabetes Mellitus, Front Immunol, 8 (2017).

[47] J.A. Villadangos, P. Schnorrer, Intrinsic and cooperative antigen-presenting functions of dendritic-cell subsets in vivo, Nat Rev Immunol, 7 (2007) 543-555.

[48] O.P. Joffre, E. Segura, A. Savina, S. Amigorena, Cross-presentation by dendritic cells, Nat Rev Immunol, 12 (2012) 557-569.

[49] M.C. Hanson, M.R. Crespo, W. Abraham, K.D. Moynihan, G.L. Szeto, S.H. Chen, M.B. Melo, S. Mueller, D.J. Irvine, Nanoparticu late STING agonists are potent lymph node-targeted vaccine adjuvants, J Clin Invest, 125 (2015) 2532-2546.

[50] D.S. Wilson, S. Hirosue, M.M. Raczy, L. Bonilla-Ramirez, L. Jeanbart, R.Y. Wang, M. Kwissa, J.F. Franetich, M.A.S. Broggi, G. Diaceri, X. Quaglia-Thermes, D. Mazier, M.A. Swartz, J.A. Hubbell, Antigens reversibly conjugated to a polymeric glyco-adjuvant induce protective humoral and cellular immunity, Nat Mater, 18 (2019) 175-+.

[51] J.W. Yu, S. Bhattacharya, N. Yanamandra, D. Kilian, H. Shi, S. Yadavilli, Y. Katlinskaya, H. Kaczynski, M. Conner, W. Benson, A. Hahn, L. Seestaller-Wehr, M.X. Bi, N.J. Vitali, L. Tsvetkov, W. Halsey, A. Hughes, C. Traini, H. Zhou, J.P. Jing, T. Lee, D.J. Figueroa, S. Brett, C.B. Hopson, J.F. Smothers, A. Hoos, R. Srinivasan, Tumor-immune profiling of murine syngeneic tumor models as a framework to guide mechanistic studies and predict therapy response in distinct tumor microenvironments, Plos One, 13 (2018).

[52] M.G. Lechner, S.S. Karimi, K. Barry-Holson, T.E. Angell, K.A. Murphy, C.H. Church, J.R. Ohlfest, P.S. Hu, A.L. Epstein, Immunogenicity of Murine Solid Tumor Models as a Defining

Feature of In Vivo Behavior and Response to Immunotherapy, J Immunother, 36 (2013) 477-489.

[53] E.I. Buchbinder, A. Desai, CTLA-4 and PD-1 Pathways Similarities, Differences, and Implications of Their Inhibition, Am J Clin Oncol-Canc, 39 (2016) 98-106.

[54] R. Kuai, L.J. Ochyl, K.S. Bahjat, A. Schwendeman, J.J. Moon, Designer vaccine nanodiscs for personalized cancer immunotherapy, Nat Mater, 16 (2017) 489-+.

2.7 SUPPORTING INFORMATION

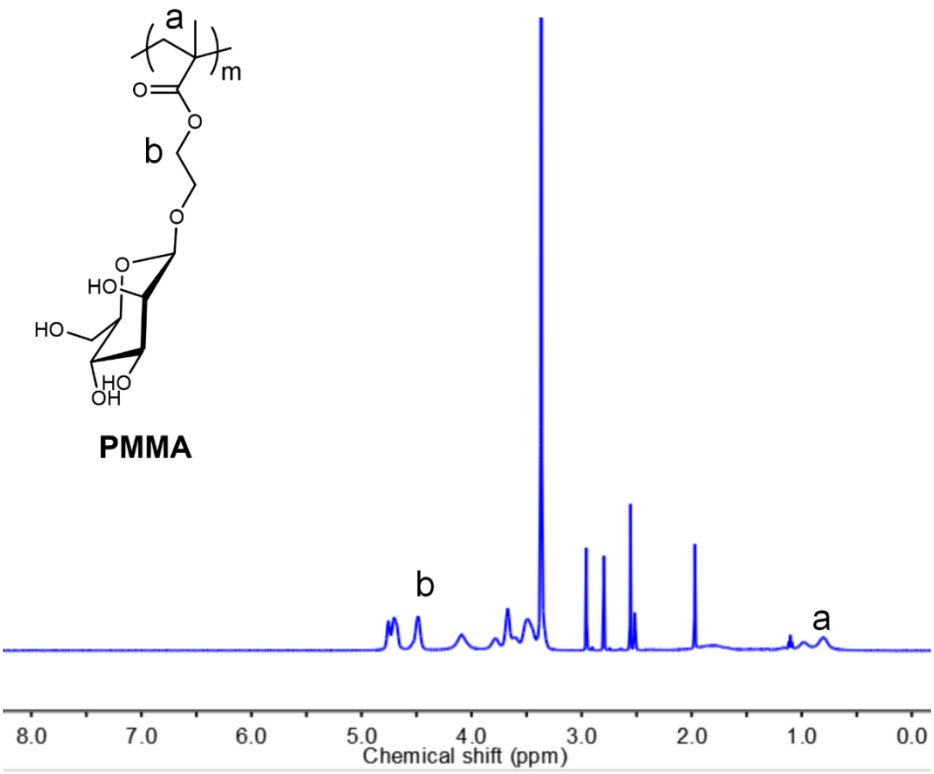

Figure S 2.1 ^{1}H NMR spectrum of PMMA in DMSO-d_6

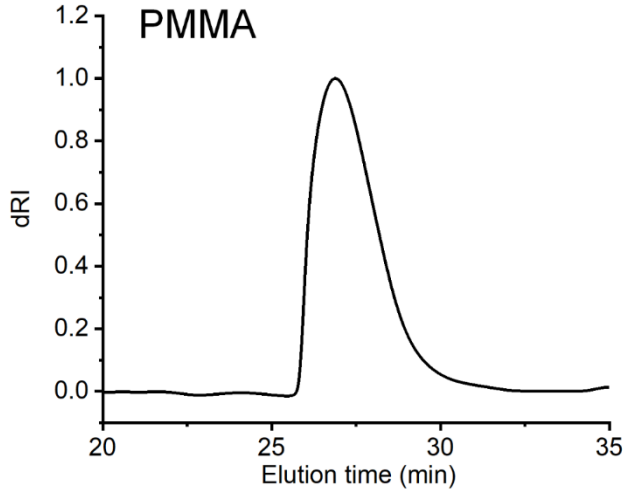

Figure S 2.2 GPC dRI traces of the PMMA.

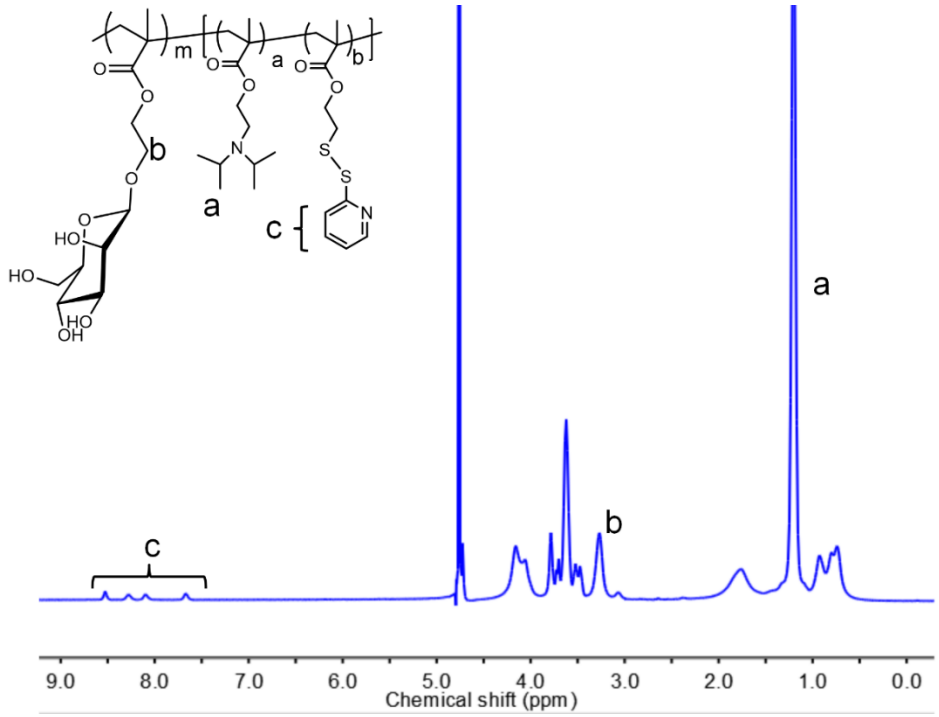

Figure S 2.3 ^{1}H NMR spectrum of MAN-P in D_2O containing 5% TFA-d.

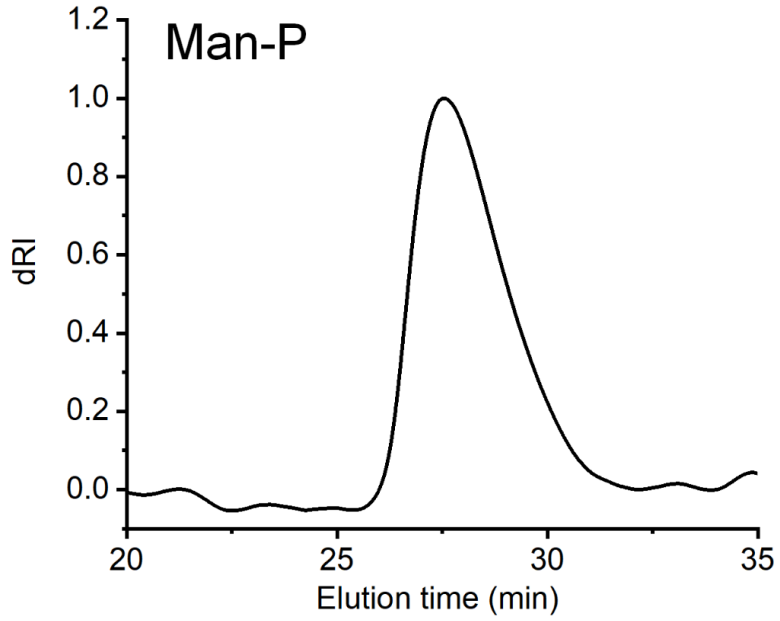

Figure S 2.4 GPC dRI traces of the MAN-P.

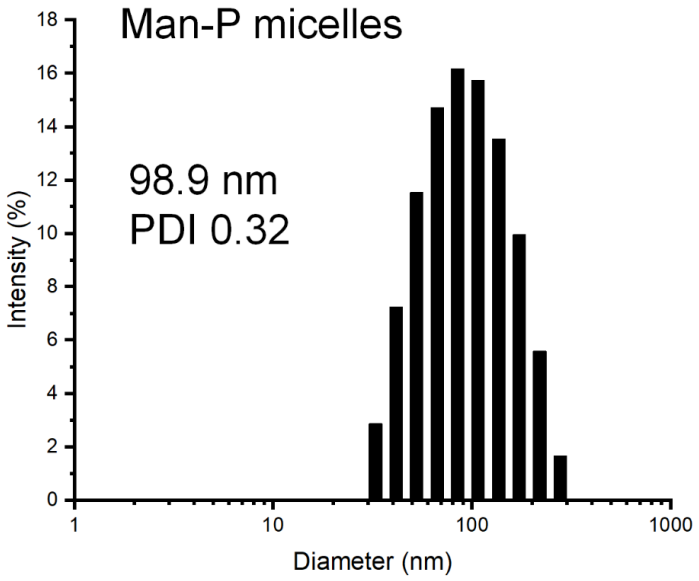

Figure S 2.5 Size distribution of the MAN-P micelles in PBS (pH = 7.4).

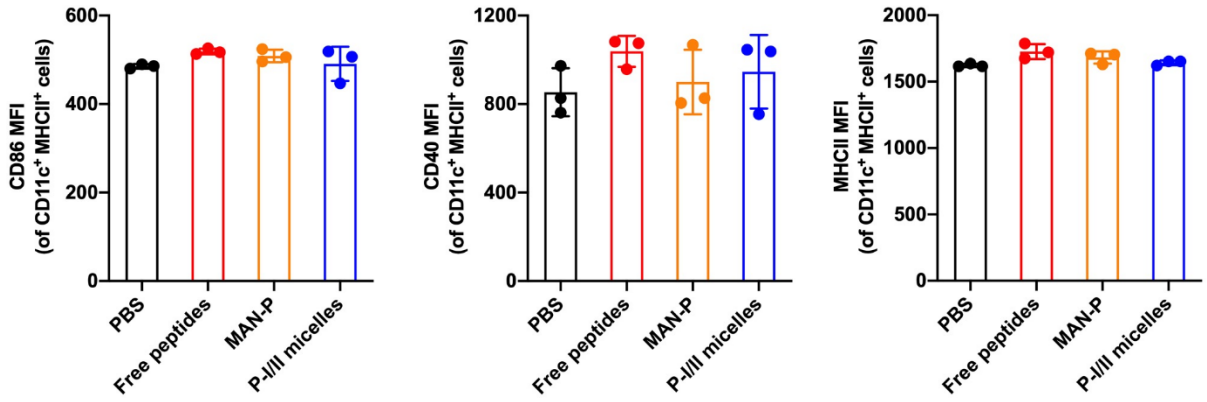

Figure S 2.6 *In vitro* BMDC maturation.

Median fluorescence intensity (MFI) of CD86, CD40 and MHCII in $CD11c^{+}MHCII^{+}$ BMDCs by flow cytometry 24 h after treatment. Data are presented as mean ± SD.

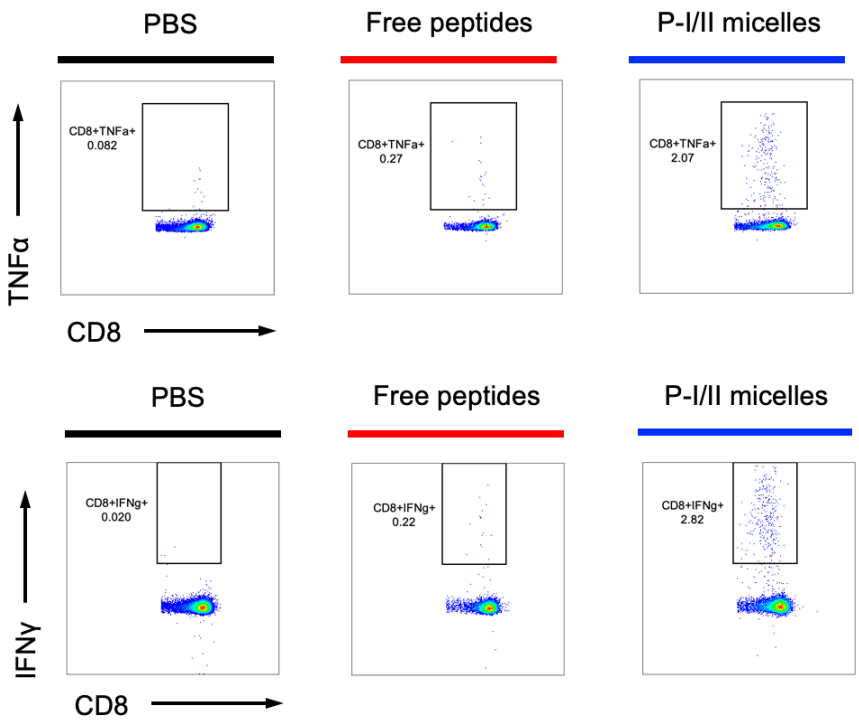

Figure S 2.7 Representative scatter plots of cytokine-producing $CD8^+$ T cells in SIINFEKL-restimulated splenocytes.

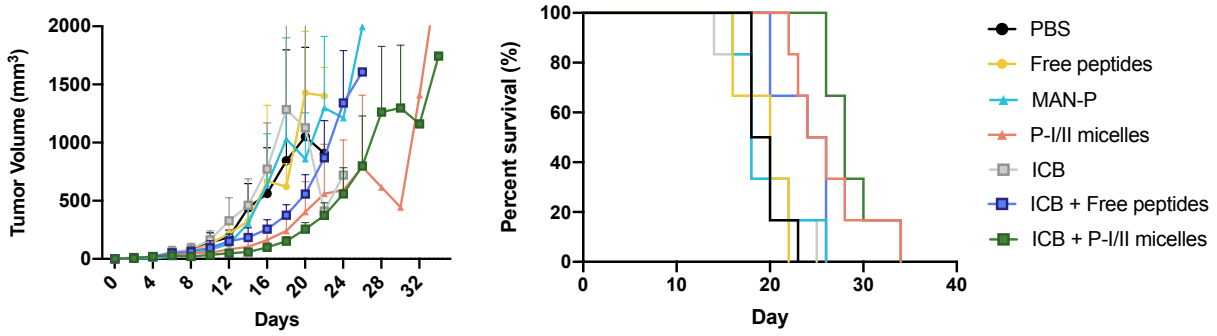

Figure S 2.8 Tumor volume and survival curve of B16F10-OVA tumor-bearing mice.

Sample	Endotoxin concentration	Amount of endotoxin injected
Free peptides	<0.1 EU/ml	<0.01 EU
MAN-P	<0.1 EU/ml	<0.01 EU
P-I/II micelles	<1 EU/ml	<0.1 EU

Table S 2.1 Endotoxin level of the formulations.

Endotoxin level was determined by the limulus amebocyte lysate (LAL) endosafe PTS assay from Charles River. All the formulations have endotoxin below the preclinical research limit of 5 EU per kg.

Chapter 3 : A Mannosylated Polymer with Endosomal Release Properties for Peptide Antigen Delivery[4]

Kefan Song, Dinh Chuong Nguyen,* Tran Luu, Omeed Yazdani, Debashish Roy, Patrick S. Stayton, Suzie H. Pun*

ABSTRACT

Peptide cancer vaccines have had limited clinical success despite their safety, characterization and production advantages. We hypothesize that the poor immunogenicity of peptides can be surmounted by delivery vehicles that overcome the systemic, cellular and intracellular drug delivery barriers faced by peptides. Here, we introduce Man-VIPER, a self-assembling (40-50nm micelles), pH-sensitive, mannosylated polymeric peptide delivery platform that targets dendritic cells in the lymph nodes, encapsulates peptide antigens at physiological pH, and facilitates endosomal release of antigens at acidic endosomal pH through a conjugated membranolytic peptide melittin. We used D-melittin to improve the safety profile of the formulation without compromising the lytic properties. We evaluated polymers with both releasable (Man-VIPER-R) or non-releasable (Man-VIPER-NR) D-melittin. Both Man-VIPER polymers exhibited superior endosomolysis and antigen cross-presentation compared to non-membranolytic D-melittin-free analogues (Man-AP) *in vitro*. *In vivo*, Man-VIPER polymers demonstrated an adjuvanting effect, induced the proliferation of antigen-specific cytotoxic T cells and helper T cells compared to free peptides and Man-AP. Remarkably, antigen delivery with Man-VIPER-NR generated significantly

[4] Chapter reproduced from: Song K, Nguyen DC, *et al*. A mannosylated polymer with endosomal release properties for peptide antigen delivery. *J Control Release*. 2023 Apr; 356:232-241.

more antigen-specific cytotoxic T cells than Man-VIPER-R *in vivo*. As our candidate for a therapeutic vaccine, Man-VIPER-NR exerted superior efficacy in a B16F10-OVA tumor model. These results highlight Man-VIPER-NR as a safe and powerful peptide cancer vaccine platform for cancer immunotherapy.

3.1 INTRODUCTION

Cancer subunit vaccines utilize neoantigens to train the immune system to recognize and attack tumor cells.[1] Among multiple tumor antigen sources, peptide antigens have garnered significant attention for multiple reasons: improved safety compared to whole antigens, facile incorporation of multiple epitopes, low cost, manufacturing ease, shelf stability and well-defined structures[1]. Peptide antigen sequences can be identified empirically by mass spectrometry and sequencing or computationally designed and validated.[2] Despite these salient features, peptide antigen vaccines have only met moderate clinical success, and even less so in the context of cancer vaccines due to peptides' poor immunogenicity.[3]

Cytotoxic T-cells ($CD8^+$) T-cells are most prominently credited for tumor-killing responses. As $CD8^+$ T cell priming requires antigen presentation through the MHC class I (MHC-I) pathway (called "cross-presentation"), providing access to the MHC-I presentation is important to cancer peptide vaccines' ability to induce tumor clearance.[4] There are three major barriers to MHC-I presentation for peptide subunit vaccine formulations – systemic, cellular and intracellular. Systemically, peptides need to preferentially localize into lymph nodes (LNs) where T-cell priming takes place,[5] while facing risk of degradation due to peptidases in circulation.[6] Cellularly, peptides need to be internalized by antigen-presenting cells (APCs) in order to be properly processed for antigen presentation. Intracellularly, peptides need to access the cytosolic compartment in order to

access the MHC-I presentation pathway.[7] All of these pose significant barriers to generating efficient antitumor responses that peptide formulations alone cannot surmount.

Various drug delivery platforms have been proposed to surmount these barriers with impressive results. Antigens can either be conjugated to targeting moieties or formulated into sub-50 nm nanoparticles that can traffic to LNs from the interstitium.[8-10] For instance, soluble antigen-mannose conjugates,[11] and self-assembling antigen micelles,[12] or antigen-protein complexes[13] have both been demonstrated to preferentially accumulate in the LNs. Interestingly, the same technology could be leveraged to overcome the cellular barrier - APC-targeting moieties and nanoparticle formulation have both been shown to promote endocytosis.[14,15] These can be in turn incorporated into controlled-release platforms such as hydrogels to impart additional benefits.[16] To surmount the intracellular barriers, strategies such as 'proton-sponge' cationic materials,[17] pH-responsive solubility-switching anionic polymers and combinations thereof,[18,19] amphiphilic polymers,[20,21] or membrane-perforating biomolecules[22] have been employed to facilitate endosomal release. Successful integration of technologies to overcome these three barriers have resulted in preclinically efficacious formulations.[23]

We previously reported two formulations for cancer peptide subunit vaccine applications. Our first report utilizes our well-developed Virus-Inspired Polymers for Endosomal Release (VIPER) platform.[24] The VIPER platform is a self-assembling pH-responsive cationic amphiphilic polymer conjugated to the membranolytic peptide melittin.[25] Melittin is sequestered in the self-assembled structure at physiological conditions, but is bioavailable in the acidic endosome where it can lyse the endosomal membrane to release disulfide-conjugated peptide cargo into the cytosol for MHC-I presentation. We co-formulated a cationic VIPER conjugated to antigen peptide with the nucleic acid adjuvant poly(I:C) to form polyplexes.[26] This formulation relied on non-specific, charge-

mediated uptake to local dendritic cells after subcutaneous injection. The VIPER formulation improved antigen cross-presentation when tested *in vitro* and increased generation of antigen-specific cytotoxic T cells, but had modest effects on tumor growth rate and overall survival, possibly due to poor LN localization. In our second report, we focused on targeting dendritic cells (DCs) in the draining LN and synthesized a diblock copolymer that self-assembles into ~30 nm micelles with a poly(mannose) corona for targeting mannose receptor (CD206) expressed on DCs.[27] We demonstrated that the targeted micelles were effective in LN localization and induction of DC maturation. In summary, our first formulation surmounted the intracellular and cellular barriers, but not the systemic barrier while our second surmounted the systemic and cellular barrier, but leaves the intracellular barrier unchallenged.

In this work, we addressed the aforementioned shortcomings with a mannosylated VIPER platform that self-assembles into sub-60nm micelles that allows for efficient LN draining and DC targeting. Upon endocytosis and acidification, the VIPER design with the pH-responsive, melittin-conjugated inner block induces endosomal rupture and antigen release into the cytosol and thus the MHC-I antigen presentation pathway in addition to MHC-II presentation from intact matured endosomes (**Figure 3.1**). We also used D-amino acids instead of L-amino acids to synthesize the melittin peptide (D-Melittin) to prevent antibody generation against the VIPER carrier.[28] In addition, we explored stable conjugation of melittin to the polymeric backbone using a pentafluorobenzyl-thiol reaction to form a thioether bond to improve the endosomal release properties of VIPER[29] compared to our previously-employed disulfide conjugation strategy. Our previous work established that polymer-conjugated melittin is considerably more membranolytic,[25] which can translate to improved endosomal release of antigen and MHC-I antigen presentation. Therefore, in this work, we evaluated a form of VIPER that retains melittin

as a polymer-bound species within the endosome (VIPER-NR) as well as a form of VIPER for which melittin can be reduced and released in as a monomeric peptide (VIPER-R). The mannosylated VIPER formulation induced efficient endosomal release and MHC-I antigen presentation *in vitro*, and potent T-cell responses against a model antigen *in vivo*. Ultimately, this platform significantly slowed tumor growth and prolonged survival in an aggressive melanoma model, demonstrating the utility of our platform as a cancer peptide subunit vaccine formulation.

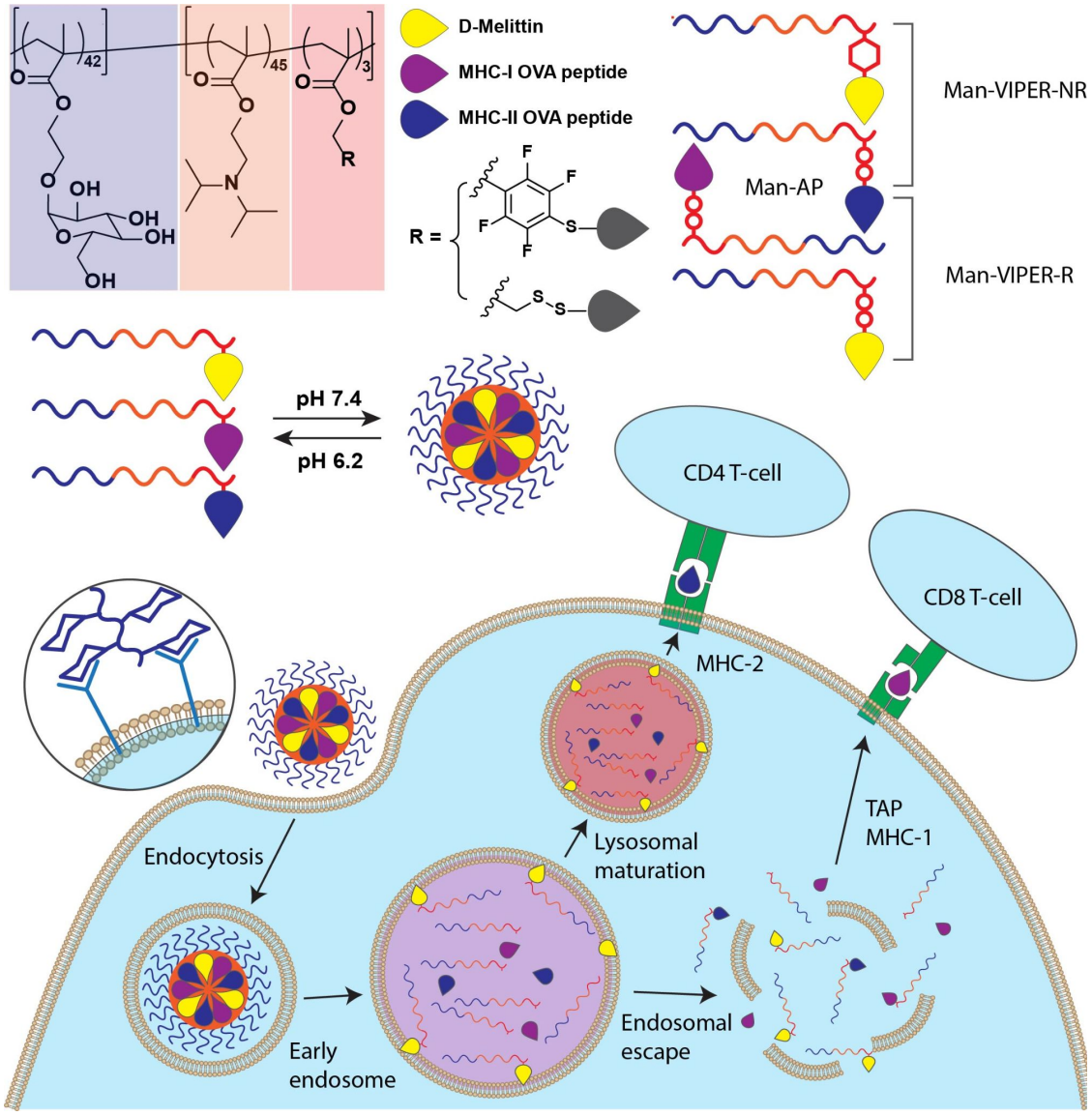

Figure 3.1 Schematic illustration of Man-VIPER delivery systems.

The Man-VIPER formulations consist of releasable disulfide conjugated OVA antigens, and either releasable disulfide conjugated membranolytic melittin (Man-VIPER-R) or non-releasable pentafluorobenzyl conjugated melittin (Man-VIPER-NR). The formulations self-assemble into well-defined micelles, which are preferentially endocytosed via the mannosylated hydrophilic segment. The micelles disassemble upon endosomal maturation, and either results in endosomal disruption and cross-presentation of MHC-1 epitopes, or lysosomal maturation and presentation of MHC-2 epitopes, to their own respective T-cell subsets.

3.2 RESULTS AND DISCUSSION

3.2.1 Polymer synthesis and characterization

Polymers were synthesized by RAFT polymerization in a two-step process. Mannose ethyl methacrylate (ManEMA) was polymerized first to make a macro-RAFT chain transfer agent (ManCTA), followed by copolymerization of diisopropylamino ethyl methacrylate (DIPAMA) with either pyridyl disulfide ethyl methacrylate (PDSEMA) or pentafluorobenzyl methacrylate (PFBzMA), to form well-defined diblock copolymers with low dispersity (**Table S3.1, Figure S3.1-S3.2**). The polymers without any conjugated peptides are denoted as CP, or control polymer, in accordance with previous nomenclature. To differentiate between polymers synthesized with the PDSEMA and PFBzMA monomers, which result in a labile disulfide or a nonlabile thioether bond upon peptide conjugation respectively, we denote polymers as CP-R (CP-Releasable) and CP-NR (CP-Non-Releasable).

We selected the model antigen OVA and the lytic peptide D-Melittin for conjugation. OVA is highly immunogenic and its MHC-I and MHC-II epitope sequences are well-defined, so we chose these peptide sequences with an N-terminal Cys-Ser-Ser sequence for conjugation (CSSIINFEKL and CSSISQAVHAAHAEINEAG, respectively). Melittin was chosen for its effective membrane-lytic capability and used in its D-amino acid form, which retains lytic activity without the adverse

immunogenicity of L-melittin.[28] Both antigens were conjugated through disulfide exchange with PDSEMA on CP-R, while D-melittin was conjugated through either PDSEMA on CP-R or a base-catalyzed thiol-PFBzMA substitution reaction on CP-NR.[29] We decided to explore different conjugation strategies solely for D-Melittin because of its direct role in endosomal escape induction in VIPER, as well as the need to retain releasability for conjugated antigen. All peptides were conjugated with >50% efficiency as measured by the amount of conjugated peptides. The antigen-functionalized polymers without D-Melittin are denoted AP-1 and AP-2 for "Antigen Polymer", demarcated by the MHC epitope identity. The melittin-functionalized polymers are denoted MP-R and MP-NR for "Melittin Polymer" in accordance with the CP-R and CP-NR nomenclature. The peptide conjugation results are displayed in **Table 3.1**. ^{19}F-NMR was also performed to confirm conjugation for MP-NR (**Figure S3.3**).

Table 3.1 Characterization of peptide conjugation in constituents of Man-VIPER formulations

Polymer name	Conjugated peptide	Approx. peptide/polymer[a]	Peptide wt%[a]
Man-AP-1	OVA MHC-I epitope	2.9	14.1
Man-AP-2	OVA MHC-II epitope	3.0	22.7
Man-MP-R	D-melittin	2.2	22.3
Man-MP-NR	D-melittin	1.8	19.4

a - Calculated by determining residual conjugating groups - quantifying PDS release with DTT reduction (AP-1, AP-2, MP-R) or cysteamine depletion with Ellman's assay (MP-NR)

The full formulation (visualized in **Figure 3.1**) of AP-1 coformulated with AP-2 and either MP-R (Man-VIPER-R) or MP-NR (Man-VIPER-NR) self-assembles into micelles with narrowly-distributed sizes at physiological pH (**Figure 3.2a**). Melittin-containing formulations (i.e. Man-

VIPER-R and Man-VIPER-NR) had larger micelle sizes (51.6 nm and 40 nm in diameter, respectively) compared to non-melittin (i.e. Man-AP, 27.6 nm), likely due to additional peptide in the micelle core. The size difference is consistent with our previous work showing that formulations with higher peptide loading exhibit larger micelle sizes.[27] Man-VIPER-NR formed smaller micelle sizes than Man-VIPER-R, possibly due to pi-pi stacking interactions from the pentafluorobenzyl linkers within the micelle core, which has been observed with other polymeric micellar systems in the literature.[33] All formulations exhibited pH-dependent micelle disassembly with a transition point around pH 6.2 as determined by a Nile Red assay (**Figure 3.2b**). Interestingly, Man-VIPER-NR exhibits disassembly over a broader pH range compared to Man-VIPER-NR or Man-AP, also possibly due to pi-pi stacking interactions within the reversibly hydrophobic polymer blocks. To determine whether or not Man-VIPER-NR might have a lower critical micelle concentration (CMC) than Man-VIPER-R due to aforementioned additional pi-pi interactions within the core, we measured CMC by evaluating micellization at various polymer concentrations using the Nile Red Assay but observed no difference between the two formulations (**Figure S3.4**). These results demonstrate that Man-VIPER-R and Man-VIPER-NR exhibit desired self-assembly and pH-responsive properties for antigen delivery.

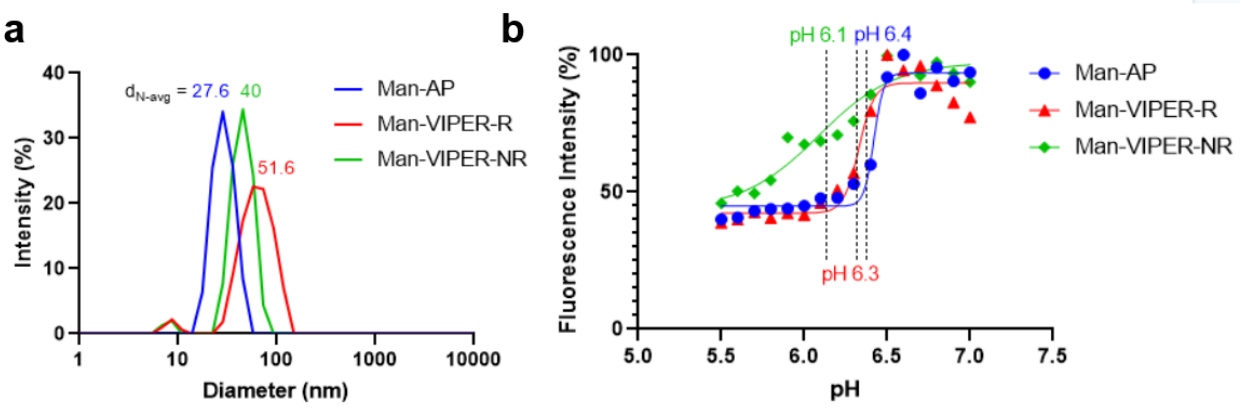

Figure 3.2 Polymer characterization.

(a) Size distribution of Man-AP, Man-VIPER-R and Man-VIPER-NR characterized by dynamic light scattering (d_{mean} = 27.6nm, 51.6nm, 40nm respectively). (b) pH-dependent micellization of Man-AP, Man-VIPER-R and Man-VIPER-NR (transition pH = 6.4, 6.3, 6.1, respectively).

3.2.2 Man-VIPER-R and Man-VIPER-NR enhances antigen cross-presentation through endosomolytic activity

The lytic properties of Man-VIPER-R and Man-VIPER-NR were examined using a hemolysis assay. The polymers were incubated with human red blood cells (RBCs) at various concentrations at pH 7.4, 6.2, and 5.6, representing the pH of the extracellular environment, early endosomes, and late endosomes/lysosomes (**Figure 3.3a**). Both Man-VIPER-R and Man-VIPER-NR showed no lytic activity pH 7.4, confirming full encapsulation and inactivation of D-melittin at physiological pH.[24-26] Man-VIPER-R showed pH-dependent lytic activity at acidic endosomal pHs (HC_{50} = 0.090 μg/ml at pH 6.2, 0.068 μg/ml at pH 5.6), while Man-VIPER-NR showed similar lytic activity at pH 5.6 and pH 6.2 (HC_{50} = 0.045 μg/ml at pH 6.2, HC_{50} = 0.043 μg/ml at pH 5.6). Man-AP showed negligible hemolysis compared to Man-VIPER-R and Man-VIPER-NR at pH 5.6, emphasizing the role of D-melittin in hemolysis induction.

Next, we directly evaluated the endosomal disruption ability of Man-VIPER-R and Man-VIPER-NR using a Gal8-GFP assay developed by the Duvall group.[34] Gal8 is a protein that is dispersed in the cytoplasm but redistributes to the inner membrane of the endosomes upon its disruption, resulting in visualizable "punctaes" of redistributed Gal8-GFP. We used the dendritic cell DC2.4 cell line that stably expresses the Gal8-GFP fusion protein (DC 2.4 Gal8-GFP) and treated the cells for 18 hours with the nanoparticles before imaging Gal8 punctae by confocal microscopy. Man-VIPER-R-treated cells exhibit more punctae (~10% of cells) compared to Man-AP and Man-VIPER-NR (**Figure 3.3b-d**). All formulations showed no cytotoxicity at the tested concentrations.

We observed a similar but more striking trend with the same experiment using a HeLa-Gal8-GFP cell line (**Figure 3.3e**). Most cells (>90%) treated with Man-VIPER-R had multiple disrupted endosomes. These results suggest that Man-VIPER-R is more capable of inducing endosomal disruption than Man-VIPER-NR, which is contrary to our initial expectations given previous data showing higher hemolysis with polymer-conjugated melittin.[25]

As antigen cross-presentation towards MHC-1 is desired, we evaluated *in vitro* cross-presentation using a DC2.4 and B3Z cell co-culture assay. B3Z is a T cell hybridoma that specifically recognizes the MHC I-SIINFEKL complex and produces measurable β-galactosidase upon binding.[35] We tested Man-VIPER-R and Man-VIPER-NR with different antigen to melittin molar ratios to optimize for our *in vivo* studies (1:1, 1:3 and 1:5). Both Man-VIPER-R and Man-VIPER-NR demonstrated higher cross-presentation compared to Man-AP in a melittin dose-dependent manner (**Figure 3.3f**). Interestingly, no significant differences in the cross-presentation of Man-VIPER-R and Man-VIPER-NR was observed despite their different endosomal disruption properties. There are several possible explanations for this difference. For example, the Gal8 assay evaluated endosomal disruption at 18 hours post-incubation, and the two formulations may have different kinetics of peptide display and endosomal release unresolvable through the single timepoint. The cross-presentation assay evaluates display of antigen peptide on MHC-I complexes which is downstream of uptake and endosomal disruption and thus less susceptible to kinetic differences in endosomal release. The discrepancy in these two assays observed may also reflect differences in other steps in the cross-presentation process. We chose the 1:5 molar ratio of antigen to melittin for the *in vivo* studies due to the higher cross-presentation at this ratio.

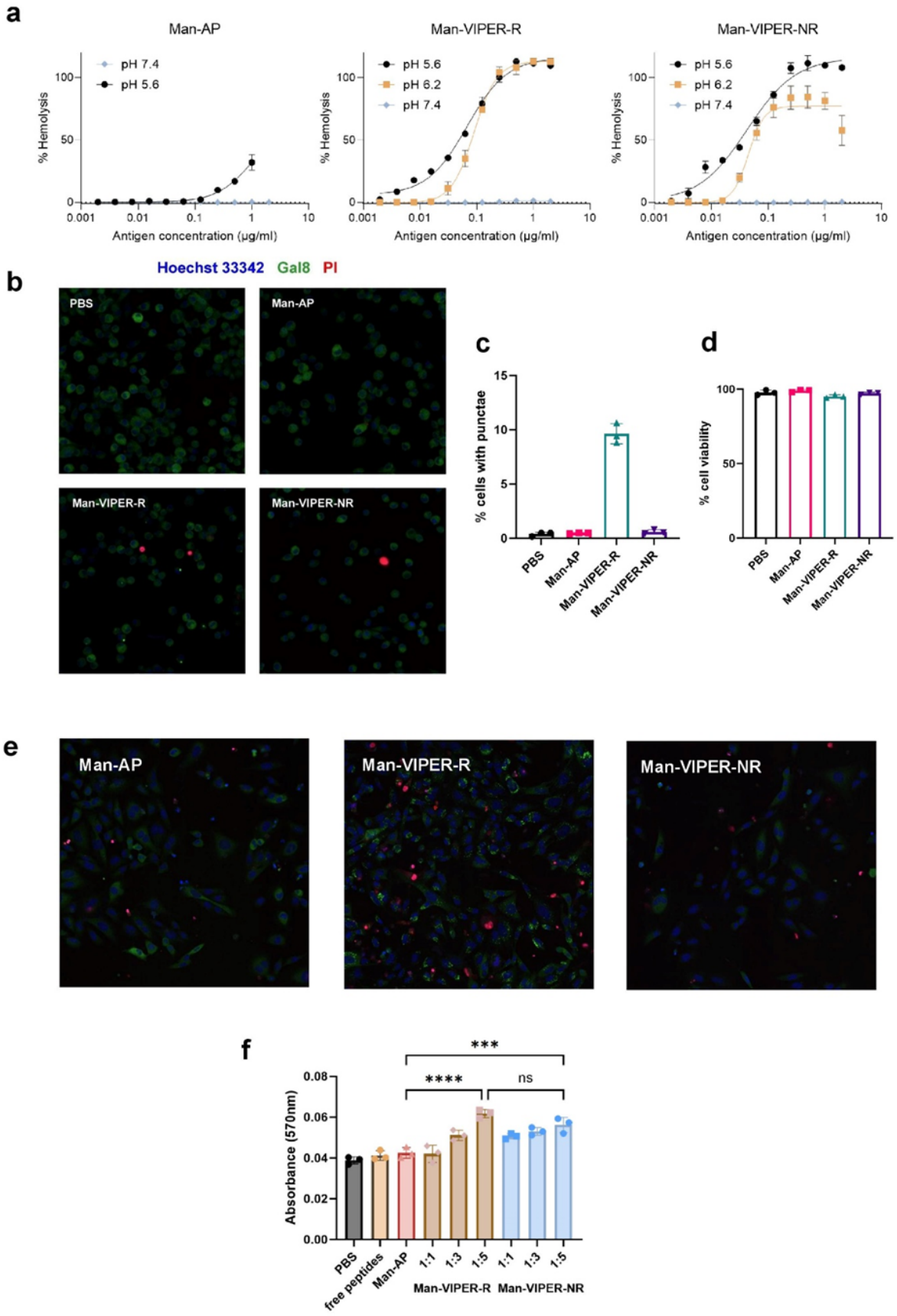
a
Man-AP
Man-VIPER-R
Man-VIPER-NR
pH 7.4
pH 5.6
pH 6.2
% Hemolysis
Antigen concentration (μg/ml)
b
Hoechst 33342 Gal8 PI
PBS
Man-AP
Man-VIPER-R
Man-VIPER-NR
c
% cells with punctae
d
% cell viability
e
Man-AP
Man-VIPER-R
Man-VIPER-NR
f
Absorbance (570nm)
***
****
ns
PBS
free peptides
Man-AP
1:1
1:3
1:5
Man-VIPER-R
Man-VIPER-NR

Figure 3.3 *In vitro* characterization of Man-AP and Man-VIPER.

(a) Hemolytic activity of the micelles against human RBCs at pH 5.6, pH 6.2 and pH 7.4. (b-d) Endosomal disruption in DC2.4-Gal8-GFP cells. (b) Representative images of DC2.4-Gal8 cells. Hoechst 33342 was used to stain the nucleus in blue. Gal8-GFP in green was dispersed in the cytosol and localized to the disrupted endosomes. Propidium iodide in red stained dead cells. (c) Percentage of cells with disrupted endosomes. (d) Percentage cell viability (e) Endosomal disruption in Hela-Gal8-GFP cells. (f) Cross-presentation of Man-AP and Man-VIPER at different antigen to melittin ratios. DC2.4 cells were treated with vaccine formulations and co-cultured with B3Z cells. Production of β-galactosidase was quantified using a CPRG assay kit by measuring the absorbance at 570 nm. Data are represented as mean ± SD. N = 3 biological replicates. Statistical analysis was performed using one-way ANOVA with post-hoc Tukey HSD test (***$p \leq 0.001$, **** $p \leq 0.0001$).

3.2.3 Man-VIPER enhances DC maturation in vivo

DC activation is a fundamental step in mounting a T-cell-based immune response. We therefore assessed the effect of Man-VIPER formulations on dendritic cell (DC) activation *in vivo* by measuring expression of co-stimulatory molecules CD86 and CD40 in lymph node DCs.[36] Mice were injected subcutaneously at the tail base with vaccine formulations (free peptides, Man-AP, Man-VIPER-R and Man-VIPER-NR), followed by cell isolation from the inguinal lymph nodes (ILNs) 24 hours later and analysis with flow cytometry. Both Man-VIPER-R and Man-VIPER-NR significantly increased CD86 and CD40 expression in $CD11c^+$ DCs compared to Man-AP and free peptides (**Figure 3.4, Figure S3.5**), suggesting that Man-VIPER formulations exhibit adjuvant activity. Melittin has been shown to activate the NLRP3 inflammasome,[37] which in DCs triggers the secretion of interleukin-1β (IL-1β) and helps in priming $CD8^+$ T cells.[38] Our previous studies have shown that D-Melittin also exhibits similar activity,[39] corroborating these results. DCs from animals treated with free peptides or Man-AP showed no difference in CD86 and CD40 expression compared to PBS. This is contrary to our previous study in which Man-AP increased the expression

of CD86.[27] The lower expression of the costimulatory molecules reported here might be due to the reduced antigen dosage employed in this study. We decreased the antigen dosage from 25 µg to 15 µg per mouse due to co-formulation with melittin-containing polymers for endosomal release.

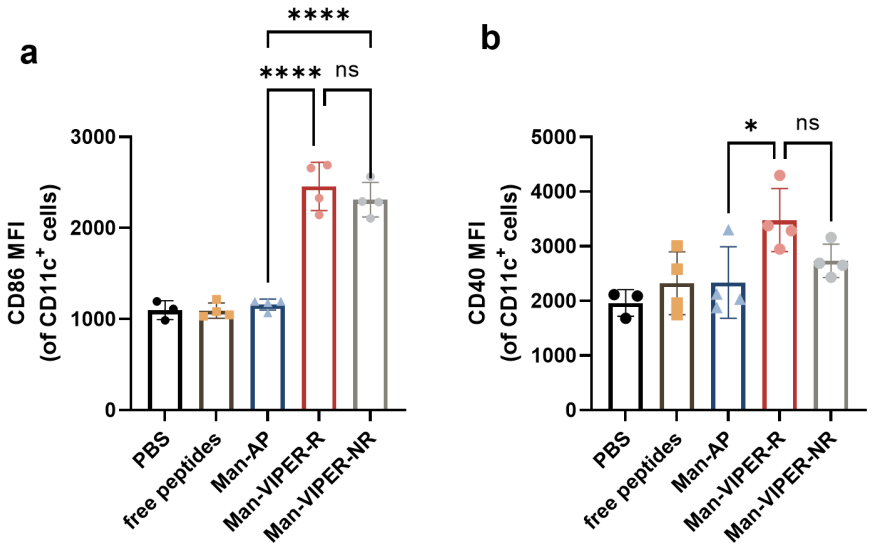

Figure 3.4 Evaluation of the expression of the co-stimulatory molecules in DCs *in vivo*.

(a) Median fluorescence intensity of CD86 in $CD11c^+$ DCs characterized by flow cytometry 24 h post immunization (b) Median fluorescence intensity of CD40 in $CD11c^+$ DCs. Data are represented as mean ± SD. N = 4 biological replicates. Statistical analysis was performed using one-way ANOVA with post-hoc Tukey HSD test (*$p \leq 0.05$, ****$p \leq 0.0001$)

3.2.4 Man-VIPER induces superior in vivo adaptive immune responses compared to non-endosomolytic carriers

Encouraged by these results, we then assessed immunogenicity in a vaccination context. Mice were immunized twice with all formulations on days 0 and 14, and splenocytes were collected, isolated and analyzed on day 21 for antigen-specific T cell responses. The amount of antigen-specific cytotoxic T cells was assessed with SIINFEKL tetramer staining, while the cellular response to antigen was evaluated using intracellular cytokine staining upon restimulation with the

antigens. All three polymeric nanoparticles, Man-AP, Man-VIPER-R and Man-VIPER-NR generated more antigen-specific $CD8^+$ T cells compared to free peptides, suggesting that the mannosylated polymeric delivery vehicle enhances antigen delivery to DCs and promotes antigen-specific T cell proliferation (**Figure 3.5**). Notably, immunization with Man-VIPER-NR generated 2.7-fold more SIINFEKL-specific $CD8^+$ T cells compared to Man-AP and Man-VIPER-R, which may indicate more robust $CD8^+$ T-cell activation (**Figure 3.5a**). Particles with sizes around 40 nm enter the lymphatic system most efficiently in some reports.[9] Man-VIPER-NR has a diameter of 40 nm, while Man-VIPER-R has a slightly larger size of 51.6 nm, which might explain the higher number of antigen-specific $CD8^+$ T generated by Man-VIPER-NR. As mentioned previously, we attribute the small diameter in Man-VIPER-NR nanoparticles to the presence of the pentafluorobenzyl linker. Animals treated with Man-VIPER-R or Man-VIPER-NR had significantly higher numbers of antigen-specific cytokine-producing $CD8^+$ and $CD4^+$ T cells compared to animals treated with Man-AP, although similar numbers of antigen-specific $CD8^+$ T cells were observed in animals treated with Man-AP and Man-VIPER-R (**Figure 3.5b, Figure S3.6**). Man-AP generated an average of 6-fold more cytokine-producing T cells compared to free peptides, while Man-VIPER-R and Man-VIPER-NR generated 41- and 42- fold more compared to free peptides. This phenomenon can be attributed to the higher expression of co-stimulatory molecules CD86 and CD40 in DCs generated by Man-VIPER compared to Man-AP in the DC maturation study (**Figure 3.4**). It has been reported that CD28, the T-cell cognate receptor for CD80/CD86, can amplify early TCR signaling.[40] Therefore, it is possible that T cells in Man-VIPER treated mice require less antigens to be activated. Both Man-VIPER-R and Man-VIPER-NR generated similar levels of IFNγ-, TNFα-producing $CD8^+$ T cells and IFNγ-producing $CD4^+$ T cells upon antigen restimulation (**Figure 3.5c**). Man-VIPER-R generated more IL-2-producing

$CD4^+$ T cells than Man-VIPER-NR, indicating that Man-VIPER-R generates a more robust $CD4^+$ T cell response. The higher $CD4^+$ T cell activation induced by Man-VIPER-R could be attributed to the slightly higher expression of CD40 on DCs (**Figure 3.4b**), which is critical for activation of $CD4^+$ T cells.[41] However, as $CD8^+$ T cells are directly associated with tumor cell elimination, we used Man-VIPER-NR in the tumor reduction study as it induced a higher antigen-specific $CD8^+$ T cell proliferation compared to Man-VIPER-R.

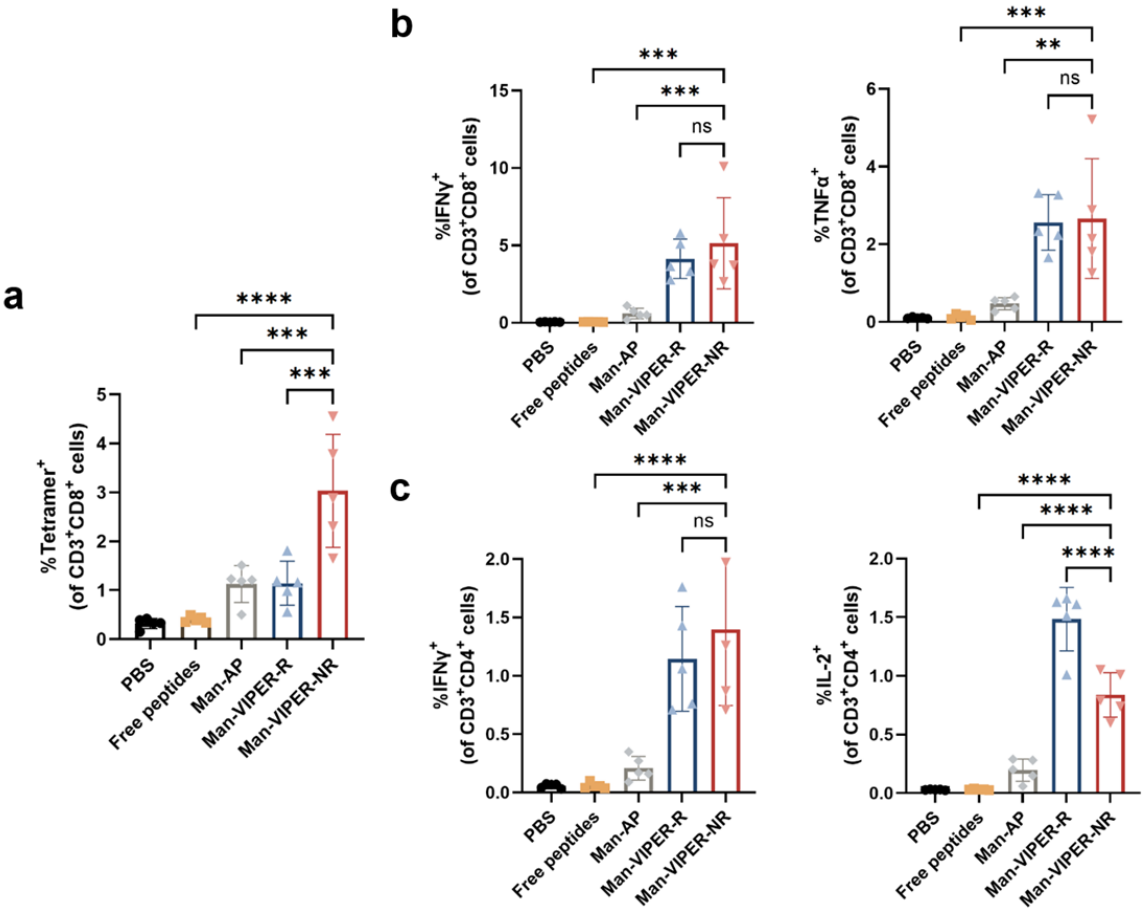

Figure 3.5 Evaluation of the antigen-specific T cell responses *in vivo*.

(a) Percentage of SIINFEKL-tetramer$^+$ $CD8^+$ T cells in spleens after immunization. (b-c) Intracellular cytokine staining of the splenocytes. (b) Splenocytes were restimulated with SIINFEKL peptide and percentage of IFNγ^+ and TNFα^+ $CD8^+$ T cells were characterized by flow cytometry (c) Splenocytes were restimulated with OVA protein and percentage of IFNγ^+ and IL-2^+ $CD4^+$ T cells were characterized by flow cytometry. Data are represented as mean ± SD. N =

5 biological replicates. Statistical analysis was performed using one-way ANOVA with post-hoc Tukey HSD test (**p ≤ 0.01, ***p ≤ 0.001, **** p ≤ 0.0001).

3.2.5 Man-VIPER-NR slowed tumor growth and improved survival in an antigen-expressing melanoma model

We evaluated the utility of Man-VIPER-NR as a therapeutic vaccine against an aggressive, poorly-immunogenic B16F10 murine melanoma model. Mice were subcutaneously injected with B16F10 cells engineered to express the OVA antigen (B16F10-OVA) on day 0. On days 3, 10 and 19, mice were immunized subcutaneously at the tail base with either PBS, free peptides, Man-AP or Man-VIPER-NR. Anti PD-1 immune checkpoint blockade (ICB) was given to some of the mice one day after each immunization through intraperitoneal injection (**Figure 3.6a**). ICB had no effect on tumor growth compared to PBS, likely because the B16F10-OVA tumor model is poorly immunogenic and inefficient in activating antigen-specific cytotoxic T cells.[42] Man-VIPER-NR significantly delayed tumor growth and improved survival compared to free peptides and Man-AP, while Man-AP exhibited modest tumor growth delay and survival benefits consistent with our previous data (**Figure 3.6b,c, Figure S3.7**).[27] Co-treatment with ICB interestingly did not result in increased therapeutic efficacy (**Figure S3.8**). The immunosuppressive tumor microenvironment, T cell exhaustion and other inhibitory signaling can all lead to the resistance in the ICB therapy.[43] The tumor response to immunization might be further improved by administration of TGF-β blockade,[44] blocking other inhibitory pathways by combining with anti-CTLA-4,[45] and increasing T cell infiltration.[46] We also noticed 5%-10% weight loss in mice treated with Man-VIPER-NR two days after vaccination, but the mice recovered weight later and demonstrated no other side effects (**Figure S3.9**). These results establish Man-VIPER-NR as a promising therapeutic cancer peptide vaccine platform. There exists avenues to improve this Man-

VIPER-NR, which includes co-formulation with known adjuvants such as STING, TLR or NLR agonists.

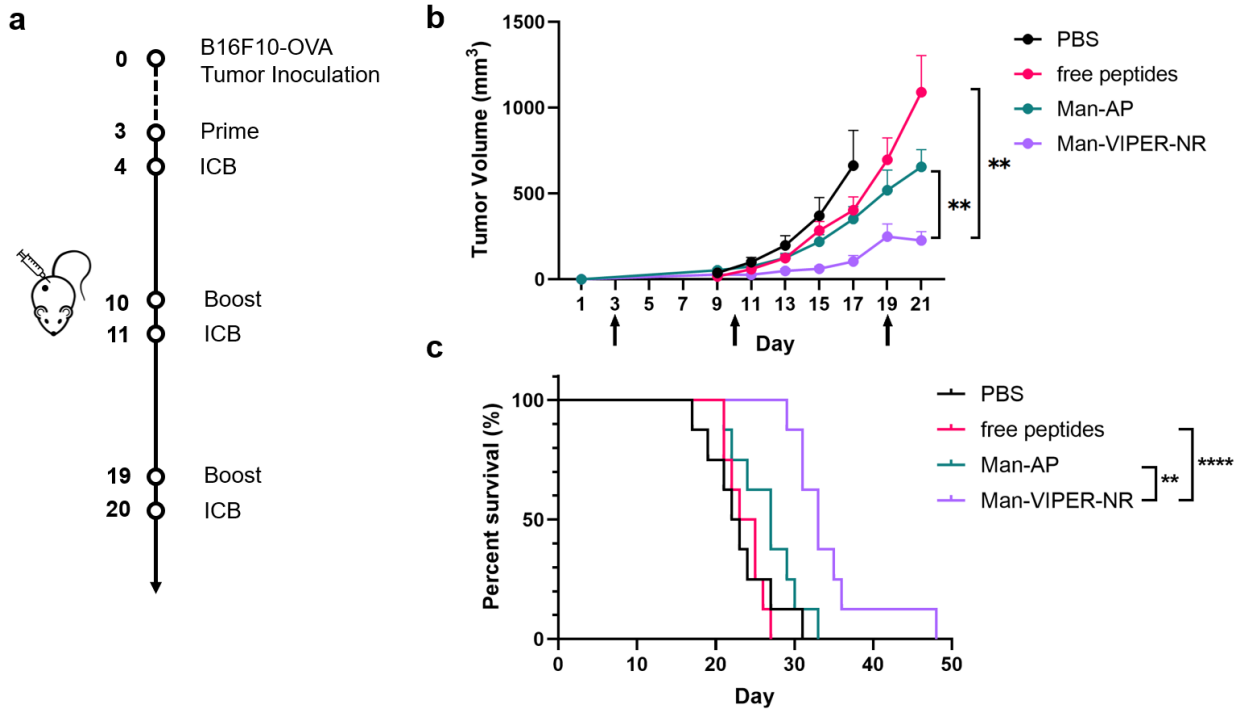

Figure 3.6 Evaluation of the antitumor effect in a B16F10-OVA tumor model.

(a) Study timeline. Mice were inoculated with B16F10-OVA cells on day 0, vaccinated on days 3, 10, 19, and treated with ICB on days 4, 11, 20. (b) Tumor growth curve. Tumor was measured every other day. Data are represented as mean ± SEM. N = 8 biological replicates. Statistical analysis was performed using unpaired t test on day 21 (**$p \leq 0.01$). (c) Kaplan-Meier survival curve. Survival analysis was performed using the log-rank test (**$p \leq 0.01$, **** $p \leq 0.0001$).

3.3 CONCLUSIONS

In this work, we developed a mannosylated endosomolytic cancer peptide vaccine platform building from our previous mannosylated peptide delivery work and our established Virus-Inspired Polymers for Endosomal Release (VIPER) system. Man-VIPER-NR self-assembles into micelles suitable for lymph node trafficking and efficiently delivers peptide antigens to the cytosol through endosomal lysis induction, resulting in superior antigen cross-presentation, cytotoxic T-cell

priming and potent antitumor response. This culminates into superior efficacy as a therapeutic vaccine compared to non-endosomolytic formulations in an aggressive, poorly immunogenic murine melanoma model.

3.4 MATERIALS AND METHODS

3.4.1 Materials

RAFT chain transfer agent 4-((((2-Carboxyethyl)thio)carbonothioyl)thio)-4-cyanopentanoic acid (CCC) was purchased from Boron Molecular. Azobisisobutyronitrile (AIBN), 4,4'-azobis(4-cyanovaleric acid) (ABCVA), cysteamine hydrochloride, piperidine, triisopropylsilane (TIPS) and ethanedithiol (EDT) were purchased from Sigma-Aldrich. Mannose ethyl methacrylate (ManEMA) was purchased from Omm Scientific. Diisopropylcarbodiimide (DIC) and ethyl cyanohydroxyiminoacetate (Oxyma) were purchased from Chem-Impex. Dimethoxybenzene (DMB), trifluoroacetic acid (TFA), acetic acid (AcOH), acetonitrile (ACN) and Ellman's reagent were purchased from Fisher Scientific. Dithiothreitol (DTT) was purchased from Enzo Life Sciences. All were used as received. Diisopropyl ethyl methacrylate (DIPAMA) was purchased from Sigma-Aldrich. Pyridyl disulfide ethyl methacrylate (PDSEMA, also known as 2-(2-pyridinyldithio)ethyl methacrylate) and pentafluorobenzyl methacrylate (PFBzMA) was purchased from Tokyo Chemical Industries Ltd. These aforementioned monomers were purified by passing through a basic alumina column to remove any existing inhibitor prior to polymerization. Anhydrous N-methyl-2-pyrrolidone (NMP, 99.5%), and dimethylsulfoxide (DMSO, > 99%) were purchased from Sigma-Aldrich and stored with activated molecular sieves. Protected amino acids were purchased from Novabiochem and used as received. Buffers were prepared in-house using endotoxin-free water and salts purchased from Fisher Scientific.

3.4.2 Polymer synthesis

All polymers were synthesized by RAFT polymerization. Briefly, the mannose hydrophilic block (ManCTA) was synthesized by RAFT polymerization of ManEMA. ManEMA was combined with CCC, ABCVA (CCC:ManEMA = 1:44.4, CCC:ABCVA = 1:20) in dry DMSO (2.5 wt% monomer), purged with argon for 30 minutes, and reacted at 70°C for 3h with vigorous stirring. ManCTA was purified by 3x precipitation in 1:1 (v/v) acetone and diethyl ether, dissolving in DMF in-between, and dried *in vacuo* for 2 days. To synthesize CP-R and CP-NR, ManCTA was combined with AIBN (ManCTA:AIBN = 1:10), DIPAMA and either PDSEMA for CP-R (ManCTA:DIPAMA:PDSEMA = 1:8:45) or PFBzMA for CP-NR (ManCTA:DIPAMA:PFBzMA = 1:5:45) in NMP (20 wt% monomer), purged with argon for 30 minutes, and reacted at 70°C in NMP solvent (20 wt% monomer) for 18h with vigorous stirring. CP-R was purified through serial dialysis in NMP for 1 day and deionized (DI) water for 3 days. CP-NR was dialyzed in NMP for 1 day, and 30x AIBN used in polymerization was added directly to the solution and reacted at 70°C overnight to remove CTA head-groups,[30] which can interfere with the conjugation reaction from aminolyzed thiols on the head-groups (data not shown). CP-NR is then purified in a similar manner to CP-R. All polymers were lyophilized post-dialysis and stored at -20°C until used.

3.4.3 Polymer Characterization

All ^{1}H NMR spectra were recorded on a Bruker AV 300 (Bruker Corporation, Billerica, MA) nuclear magnetic resonance (NMR) instrument in deuterated DMSO (DMSO-d6). Polymer molecular weights (Mw, Mn) and polydispersity index (Đ = Mw/Mn) were determined by gel permeation chromatography (GPC). The system consisted of an Agilent 1260 HPLC stack running heated LiBr-supplemented (0.1% w/v) DMF mobile phase at a flow rate of 1 mL min^{-1} through a semi-prep three-column setup (Phenogel-TSKgel). Samples (5 mg/mL) were filtered through a 0.2

μm PTFE filter before analysis. We observed a difference between the theoretical Mn calculated by NMR and the Mn calculated by GPC, as well as a lower-than-expected shift in retention time for the block copolymers. This may be caused the presence of bimolecular termination products in the mannose macro-CTA owing to high conversion masking the retention time shift, as well as differences in the molecular weight-hydrodynamic radii relationship between mannose-CTA and CP polymers. The size distribution profiles of micelles were recorded on a dynamic light scattering (DLS) system (DynaPro NanoStar, Wyatt technology) at a micelle concentration of 1 mg/mL.

3.4.4 Peptide synthesis and conjugation

MHC-1 OVA epitope peptide (CSSSIINFEKL, or OVA-1), MHC-2 OVA epitope peptide (CSSISQAVHAAHAEINEAG, or OVA-2) and D-Melittin (GIGAVLKVLTTGLPALISWIKRKRQQC, or D-Mel) were synthesized using a Liberty Blue (CEM) microwave peptide synthesizer on Rink Amide resin (Millipore) using Fmoc-piperidine deprotection and DIC-Oxyma activation chemistry before cleavage and deprotection (5% DMB, 2.5% TIPS, 2.5% EDT, 0.5% H2O in TFA), and purification with reverse-phase HPLC (TFA-supplemented H2O:ACN).

AP-1, AP-2 and VIPER-R were synthesized by conjugating OVA-1, OVA-2 and D-Melittin to CP-R using disulfide exchange chemistry. Briefly, CP-R and peptides were dissolved in separate solutions of 2% (v/v) AcOH in DMSO at a CP-R concentration equivalent to 12.5 mM PDSEMA and 14-19 mM peptide. The two solutions were combined in equal volumes and allowed to react overnight at room temperature. The reaction solution was then dialyzed against DMSO (SpectraPor 6-8 kDa MWCO) for 2 days, against MilliQ water for 3 days to remove free peptides, and lyophilized over the weekend. Peptide loading was assessed by reacting conjugated polymers

with DTT for 30 minutes at 37°C and comparing 2-mercaptopyridine release (Abs_{max} = 347 nm) compared to unconjugated polymers as previously reported by our group[25].

VIPER-NR was synthesized by conjugating D-Melittin to CP-NR using a recently-described pentafluorobenzyl-thiol (PFB-thiol) reaction[29]. Briefly, D-Melittin was dissolved with CP-NR at a CP-NR concentration equivalent to 30 mM PFB and 10 mM peptide. The concentrations were adjusted to achieve a theoretical peptide loading of 19% by weight of the final conjugate. DBU (2 mmol) was added in excess to counteract acidic counterions present in D-Melittin and the reaction allowed to proceed overnight at room temperature. The reaction was quenched by addition of TFA, and dialyzed as above to remove free peptides. Peptide loading was assessed by reacting conjugated and unconjugated polymers with a 2-fold excess of cysteamine hydrochloride (50 mM in dry DMSO) in a similar manner to conjugation, and comparing cysteamine depletion using Ellman's reagent to determine extent of PFB conjugation. ^{19}F-NMR was also used to determine PFB substitution extent, but was disfavored due to low solubility of polymers in NMR solvents coupled with low mass sensitivity of ^{19}F-NMR.

3.4.5 Micelle formulation

We utilized our previously-described pH-switch method to formulate our micelles with slight modifications.[27] Briefly, individual polymer conjugates were dissolved in endotoxin-free water. The polymer solutions were combined at equal volumes. HCl (0.6% to 2.5% of 1 N solution) was added to the mixture until a clear solution was obtained. The solution was probe-sonicated for 30 seconds to ensure complete dissolution. A solution of 0.2 M pH 5.0 monobasic sodium phosphate was added, followed by 0.2 M pH 9.0 dibasic sodium phosphate to obtain the final pH in the range of 6.6-7.4. The formulations were prepared at ambient conditions. The critical micellar concentration (CMC) and transition point of the micelles were determined using the Nile Red

assay.[31] Briefly, micelles with different concentrations or pH were mixed with 1μM Nile Red. Fluorescence intensity was measured using a plate reader (ex. 556 nm, em. 625 nm).

3.4.6 Hemolysis assay for endosomal rupture quantification

The polymers' ability to disrupt endosomal membranes in a pH-dependent manner was evaluated using a hemolysis assay as previously described.[32] Briefly, red blood cells (RBCs) isolated from de-identified human whole blood samples (Bloodworks Northeast) were pelleted at 500g and washed three times with 150 mM NaCl and once with pH 7.4 PBS. The washed RBCs were resuspended in PBS of various pHs (pH 7.4, 6.2, and 5.6). RBCs were then treated with polymers at various concentrations of melittin or equivalent melittin-free polymer concentrations (polymer:RBC 10:190 v/v) in V-bottom well-plates and incubated at 37°C for 1 h. Cells were then pelleted and the supernatant was transferred to flat-bottom well-plates. The amount of hemoglobin leakage into the supernatant was quantified via absorbance spectroscopy (Tecan, $\lambda = 575$ nm) and normalized to 100% hemolysis with 20% Triton X-100 and 0% hemolysis with PBS at its respective pHs.

3.4.7 Cell lines and animals

The B16F10-OVA cell line (gift of Prof. Amanda Lund) was cultured in DMEM supplemented with 10% FBS and 1% P/S. The DC2.4-Gal8-GFP and Hela-Gal8-GFP cell lines were generated as previously described.[26] DC2.4-Gal8-GFP cells were cultured in RPMI supplemented with 10% heat-inactivated FBS, 1% P/S, 1x nonessential amino acids, 10 mM HEPES buffer and 55 μM β-mercaptoethanol. Hela-Gal8-GFP cells were cultured in DMEM supplemented with 10% FBS and 1% P/S. The B3Z cell line (gift of Prof. Nilabh Shastri) was cultured in RPMI supplemented with 10% heat-inactivated FBS, 1% P/S, 1 mM sodium pyruvate and 50 μM β-mercaptoethanol. Cells

were incubated at 37°C and 5% CO_2. Female C57BL/6 mice aged 6 to 8 weeks were purchased from Charles River Laboratories. All animal studies were approved by the University of Washington Institutional Animal Care and Use Committee (IACUC).

3.4.8 Gal8 endosomal disruption assay

DC2.4-Gal8-GFP and Hela-Gal8-GFP cells were cultured in TC-treated 96-well imaging plates overnight. Cells were incubated with polymers containing 2 μg/ml CSSSIINFEKL, 2 μg/ml CSSISQAVHAAHAEINEAGR, 38 μg/ml D-Melittin peptide for 18 hr. Media was replaced with Fluorobrite DMEM supplemented with 10% FBS, 25 mM HEPES. Hoechst 33342 was used to stain the nucleus and propidium iodide was used to stain the dead cells. Images were obtained using a Leica SP8X confocal microscope using a 20x objective.

3.4.9 DC2.4 Cross-Presentation and Viability Assays

The DC2.4 cell line was seeded into U-bottom TC-treated 96 well plates at 20,000 cells per well and incubated at 37°C and 5% CO2 overnight. To assess cross-presentation, cells were treated with the ovalbumin protein or polymers containing 2 μg/ml CSSSIINFEKL and 2 μg/ml CSSISQAVHAAHAEINEAGR with different amounts of D-Melittin peptide. After 4 hours, cells were washed twice with PBS and co-cultured with 100,000 B3Z cells for an additional 18-20 hours in the incubator. After co-culture, cells were pelleted by centrifugation and resuspended in 150 μL CPRG lysis buffer (0.15 mM chlorophenol red-β-D-galactopyranoside + 0.1% Triton-X100 + 9 mM MgCl2 + 100 μM β-mercaptoethanol + PBS). Cells were incubated at 37°C in the dark for 90 minutes. The supernatant was transferred to a flat-bottom 96-well plate and the absorbance was measured at 570 nm (reference 650 nm) using a plate reader. Cell viability was analyzed using the MTS/PMS assay 24 hours post-treatment (Promega).

3.4.10 In vivo dendritic cell activation

Female C57BL/6 mice were injected subcutaneously at the tail base with PBS or with 15 μg CSSSIINFEKL and 15 μg CSSISQAVHAAHAEINEAGR antigen peptides either in free peptide form or in Man-VIPER-R or Man-VIPER-NR formulations. Polymer formulations also contained 286 μg D-Melittin peptide (1:5 molar ratio of antigen and melittin). Twenty-four hours-post immunization, inguinal lymph nodes were harvested and digested in 50 U/mL type IV collagenase + 100 U/mL DNase I. Single-cell suspension was obtained by mashing the tissue through a 70 μm cell strainer. Cells were stained for viability with Zombie NIR viability kit, blocked with anti-CD16/32, and then stained with anti-CD86-BV510, anti-CD40-FITC, anti-CD11c-APC and anti-SIINFEKL-PE. An Attune NxT flow cytometer was used to analyze the data.

3.4.11 In vivo T cell responses

Female C57BL/6 mice were immunized with PBS, free peptides, AP, Man-VIPER-R and Man-VIPER-NR on day 0 and day 14. Spleens were harvested on day 21. Tissues were passed through 70 μm cell strainers and treated with ACK lysis buffer. Splenocytes were resuspended in IMDM and plated in separate 96-well plates for tetramer staining and intracellular cytokine staining (ICCS). For the tetramer staining, splenocytes were stained with Zombie NIR for viability and then stained with PE-labeled H-2Kb/SIINFEKL tetramer (NIH Tetramer Core). Cells were blocked with anti-CD16/32 and stained with anti-CD3-eFluor450 and anti-CD8-FITC. For ICCS, splenocytes were either restimulated with 5 μg/ml SIINFEKL peptide or 5 mg/ml OVA protein. 3 hr later, Protein Transport Inhibitor Cocktail (PTIC) was added and cells were incubated for another 3 hr. After incubation, cells were stained with Zombie NIR for viability, blocked with anti-CD16/32 and stained with either anti-CD3-eFluor450 + anti-CD8-FITC for $CD8^+$ T cells or anti-CD3-eFluor450 + anti-CD4-FITC for $CD4^+$ T cells. Cells were then treated with the BD

Cytofix/Cytoperm Fixation/Permeabilization Kit and stained with either anti-TNFα-PE and anti-IFNγ-APC for $CD8^+$ T cells and anti-IL-2-PE and anti-IFNγ-APC for $CD4^+$ T cells. Data was collected using the Attune NxT flow cytometer and analyzed using Flowjo.

3.4.12 Tumor studies

Female C57BL/6 mice (N=8) were inoculated with 1.5×10^5 B16F10-OVA cells in the right-hind flank on day 0. On days 3, 10, and 19, mice were immunized with PBS, free peptides containing 15 μg CSSSIINFEKL and 15 μg CSSISQAVHAAHAEINEAGR, AP or MAN-VIPER-NR containing the same amount of peptides. On days 4, 11, and 20, mice were injected with 100 μg of anti PD-1 ICB (Clone 29F.1A12, BioXCell) via intraperitoneal injection. Tumor length and width were then measured every other day using a vernier caliper, and volume was subsequently calculated using the formula: Volume = $(\text{Width}^2 \times \text{Length}) \div 2$. Weight was also measured every other day. Mice were euthanized if total tumor volume exceeded 1500 mm^3, visible discharge was observed on ulcers of the tumors, or the body weight loss exceeded 20%.

3.4.12 Statistical analysis

Statistical analysis was performed using the Graphpad Prism software. One-way ANOVA with post-hoc Tukey HSD test was used to compare more than two groups. Log-rank test was used for survival analysis.

3.5. ACKNOWLEDGEMENTS

K.S. and D.C.N. contributed equally to this work. This work was supported by the U.S. National Institutes of Health, National Cancer Institute Grant R01CA257563. Confocal microscopy was completed at the UW Keck Microscopy Center; the Leica SP8X microscope and software was funded by NIH S10 OD016240 and the UW Student Technology Fee (UWSTF). We thank the

Institute for Protein Design (IPD) at the University of Washington for the use of Dynamic Light Scattering, as well as the Mass Spectrometry Core at the University of Washington for the use of MALDI. We thank Prof. Amanda Lund for providing the B16F10-OVA cell line, Prof. Nilabh Shastri (Johns Hopkins University) for providing the B3Z cells, and the NIH Tetramer Core Facility for providing the PE-labeled H-2Kb/SIINFEKL tetramer. We thank Prof. Jordan Green (Johns Hopkins University) for the Gal8-GFP and PiggyBac transposon plasmids and Prof. Craig Duvall (Vanderbilt University) for the MATLAB code for Gal8 quantification.

3.6. REFERENCES

[1] Hu, Z., Ott, P. A. & Wu, C. J. Towards personalized, tumour-specific, therapeutic vaccines for cancer. Nat. Rev. Immunol. 18, 168–182 (2018).

[2] Parvizpour, S., Pourseif, M. M., Razmara, J., Rafi, M. A. & Omidi, Y. Epitope-based vaccine design: a comprehensive overview of bioinformatics approaches. Drug Discov. Today 25, 1034–1042 (2020).

[3] Liu, W. et al. Peptide-based therapeutic cancer vaccine: Current trends in clinical application. Cell Prolif. 54, e13025 (2021).

[4] Durgeau, A., Virk, Y., Corgnac, S. & Mami-Chouaib, F. Recent Advances in Targeting CD8 T-Cell Immunity for More Effective Cancer Immunotherapy. Front. Immunol. 9, 14 (2018).

[5] Mempel, T. R., Henrickson, S. E. & von Andrian, U. H. T-cell priming by dendritic cells in lymph nodes occurs in three distinct phases. Nature 427, 154–159 (2004).

[6] Acar, H., M. Ting, J., Srivastava, S., L. LaBelle, J. & V. Tirrell, M. Molecular engineering solutions for therapeutic peptide delivery. Chem. Soc. Rev. 46, 6553–6569 (2017).

[7] Joffre, O. P., Segura, E., Savina, A. & Amigorena, S. Cross-presentation by dendritic cells. Nat. Rev. Immunol. 12, 557–569 (2012).

[8] Reddy, S. T., Rehor, A., Schmoekel, H. G., Hubbell, J. A. & Swartz, M. A. In vivo targeting of dendritic cells in lymph nodes with poly(propylene sulfide) nanoparticles. J. Controlled Release 112, 26–34 (2006).

[9] Bachmann, M. F. & Jennings, G. T. Vaccine delivery: a matter of size, geometry, kinetics and molecular patterns. Nat. Rev. Immunol. 10, 787–796 (2010).

[10] Oussoren, C., Zuidema, J., Crommelin, D. J. A. & Storm, G. Lymphatic uptake and biodistribution of liposomes after subcutaneous injection.: II. Influence of liposomal size, lipid composition and lipid dose. Biochim. Biophys. Acta BBA - Biomembr. 1328, 261–272 (1997).

[11] Wilson, D. S. et al. Antigens reversibly conjugated to a polymeric glyco-adjuvant induce protective humoral and cellular immunity. Nat. Mater. 18, 175–185 (2019).

[12] Lynn, G. M. et al. Peptide–TLR-7/8a conjugate vaccines chemically programmed for nanoparticle self-assembly enhance CD8 T-cell immunity to tumor antigens. Nat. Biotechnol. 38, 320–332 (2020).

[13] He, Y. et al. Peptide-Based Cancer Vaccine Delivery via the STINGΔTM-cGAMP Complex. Adv. Healthc. Mater. 11, 2200905 (2022).

[14] Akinc, A. & Battaglia, G. Exploiting Endocytosis for Nanomedicines. Cold Spring Harb. Perspect. Biol. 5, a016980 (2013).

[15] Liang, W., Shi, X., Deshpande, D., Malanga, C. J. & Rojanasakul, Y. Oligonucleotide targeting to alveolar macrophages by mannose receptor-mediated endocytosis. Biochim. Biophys. Acta BBA - Biomembr. 1279, 227–234 (1996).

[16] Liu, X. et al. Co-localized delivery of nanomedicine and nanovaccine augments the postoperative cancer immunotherapy by amplifying T-cell responses. Biomaterials 230, 119649 (2020).

[17] Shen, C. et al. Polyethylenimine-based micro/nanoparticles as vaccine adjuvants. Int. J. Nanomedicine 12, 5443–5460 (2017).

[18] Flanary, S., Hoffman, A. S. & Stayton, P. S. Antigen Delivery with Poly(Propylacrylic Acid) Conjugation Enhances MHC-1 Presentation and T-Cell Activation. Bioconjug. Chem. 20, 241–248 (2009).

[19] Foster, S., Duvall, C. L., Crownover, E. F., Hoffman, A. S. & Stayton, P. S. Intracellular Delivery of a Protein Antigen with an Endosomal-Releasing Polymer Enhances CD8 T-Cell Production and Prophylactic Vaccine Efficacy. Bioconjug. Chem. 21, 2205–2212 (2010).

[20] Wilson, J. T. et al. pH-Responsive Nanoparticle Vaccines for Dual-Delivery of Antigens and Immunostimulatory Oligonucleotides. ACS Nano 7, 3912–3925 (2013).

[21] Lin, W. et al. Co-Delivery of Imiquimod and Plasmid DNA via an Amphiphilic pH-Responsive Star Polymer that Forms Unimolecular Micelles in Water. Polymers 8, 397 (2016).

[22] Derouazi, M. et al. Novel Cell-Penetrating Peptide-Based Vaccine Induces Robust CD4+ and CD8+ T Cell–Mediated Antitumor Immunity. Cancer Res. 75, 3020–3031 (2015).

[23] Shae, D. et al. Co-delivery of Peptide Neoantigens and Stimulator of Interferon Genes Agonists Enhances Response to Cancer Vaccines. ACS Nano 14, 9904–9916 (2020).

[24] Cheng, Y., Yumul, R. C. & Pun, S. H. Virus-Inspired Polymer for Efficient In Vitro and In Vivo Gene Delivery. Angew. Chem. Int. Ed. 55, 12013–12017 (2016).

[25] Peeler, D. J. et al. pH-sensitive polymer micelles provide selective and potentiated lytic capacity to venom peptides for effective intracellular delivery. Biomaterials 192, 235–244 (2019).

[26] Peeler, D. J., Yen, A., Luera, N., Stayton, P. S. & Pun, S. H. Lytic Polyplex Vaccines Enhance Antigen-Specific Cytotoxic T Cell Response through Induction of Local Cell Death. Adv. Ther. n/a, 2100005.

[27] Lv, S. et al. Well-Defined Mannosylated Polymer for Peptide Vaccine Delivery with Enhanced Antitumor Immunity. Adv. Healthc. Mater. 11, 2101651 (2022).

[28] Sylvestre, M. et al. Replacement of L-amino acid peptides with D-amino acid peptides mitigates anti-PEG antibody generation against polymer-peptide conjugates in mice. J. Controlled Release 331, 142–153 (2021).

[29] Noy, J.-M. et al. Para-Fluoro Postpolymerization Chemistry of Poly(pentafluorobenzyl methacrylate): Modification with Amines, Thiols, and Carbonylthiolates. Macromolecules 50, 7028–7040 (2017).

[30] Perrier, S., Takolpuckdee, P. & Mars, C. A. Reversible Addition−Fragmentation Chain Transfer Polymerization: End Group Modification for Functionalized Polymers and Chain Transfer Agent Recovery. Macromolecules 38, 2033–2036 (2005).

[31] Prossnitz, A. N. & Pun, S. H. Modulating Boronic Ester Stability in Block Copolymer Micelles via the Neighbor Effect of Copolymerized Tertiary Amines for Controlled Release of Polyphenolic Drugs. ACS Macro Lett. 11, 276–283 (2022).

[32] Evans, B. C. et al. Ex Vivo Red Blood Cell Hemolysis Assay for the Evaluation of pH-responsive Endosomolytic Agents for Cytosolic Delivery of Biomacromolecular Drugs. JoVE J. Vis. Exp. e50166 (2013) doi:10.3791/50166.

[33] Li, S. et al. Pi-Stacking Enhances Stability, Scalability of Formation, Control over Flexibility, and Circulation Time of Polymeric Filamentous Nanocarriers. Adv. NanoBiomed Res. 1, 2100063 (2021).

[34] Kilchrist, K. V. et al. Gal8 Visualization of Endosome Disruption Predicts Carrier-Mediated Biologic Drug Intracellular Bioavailability. ACS Nano 13, 1136–1152 (2019).

[35] Karttunen, J. & Shastri, N. Measurement of ligand-induced activation in single viable T cells using the lacZ reporter gene. Proc. Natl. Acad. Sci. 88, 3972–3976 (1991).

[36] Tai, Y., Wang, Q., Korner, H., Zhang, L. & Wei, W. Molecular Mechanisms of T Cells Activation by Dendritic Cells in Autoimmune Diseases. Front. Pharmacol. 9, 642 (2018).

[37] Martín-Sánchez, F. et al. Lytic cell death induced by melittin bypasses pyroptosis but induces NLRP3 inflammasome activation and IL-1β release. Cell Death Dis. 8, e2984–e2984 (2017).

[38] Ghiringhelli, F. et al. Activation of the NLRP3 inflammasome in dendritic cells induces IL-1β–dependent adaptive immunity against tumors. Nat. Med. 15, 1170–1178 (2009).

[39] Lv, S., Sylvestre, M., Song, K. & Pun, S. H. Development of D-melittin polymeric nanoparticles for anti-cancer treatment. Biomaterials 277, 121076 (2021).

[40] Zumerle, S., Molon, B. & Viola, A. Membrane Rafts in T Cell Activation: A Spotlight on CD28 Costimulation. Front. Immunol. 8, 1467 (2017).

[41] Grewal, I. S. & Flavell, R. A. The Role of CD40 Ligand in Costimulation and T-Cell Activation. Immunological Reviews 153, 85–106 (1996).

[42] Chen, S. et al. Combination of 4-1BB agonist and PD-1 antagonist promotes antitumor effector/memory CD8 T cells in a poorly immunogenic tumor model. Cancer Immunol. Res. 3, 149–160 (2015).

[43] Lei, Q., Wang, D., Sun, K., Wang, L. & Zhang, Y. Resistance Mechanisms of Anti-PD1/PDL1 Therapy in Solid Tumors. Front. Cell Dev. Biol. 8, 672 (2020).

[44] Martin, C. J. et al. Selective inhibition of TGFβ1 activation overcomes primary resistance to checkpoint blockade therapy by altering tumor immune landscape. Sci. Transl. Med. 12, eaay8456 (2020).

[45] Curran, M. A., Montalvo, W., Yagita, H. & Allison, J. P. PD-1 and CTLA-4 combination blockade expands infiltrating T cells and reduces regulatory T and myeloid cells within B16 melanoma tumors. Proc. Natl. Acad. Sci. 107, 4275–4280 (2010).

[46] Tang, H. et al. Facilitating T cell infiltration in tumor microenvironment overcomes resistance to PD-L1 blockade. Cancer Cell 29, 285–296 (2016).

3.7 SUPPORTING INFORMATION

Polymer name	Conversion by NMR (%)[a]	DP (NMR)[b]	NMR Mn (kDa)[c]	GPC Mw (kDa)[d]	GPC Mn (kDa)[d]	GPC Dispersity (Đ = Mw/Mn)[d]
ManCTA	96	43 Man	12.4	14.5	13.8	1.12
CP-R	87	44 DIPAMA, 4 PDSEMA	23.0	45.2	44.8	1.14
CP-NR	84	44 DIPAMA, 4 PFBzMA	23.1	31.1	30.2	1.15

Table S 3.1 Characterization of Man-VIPER polymeric backbones

a - Calculated by vinyl peak depletion (5.5-6 ppm) in NMR spectroscopy. b - Calculated by a combination of conversion NMR and either downfield PDSEMA peaks (7-9ppm) for CP-R or F-NMR for CP-NR. c - Calculated from DP. d - Calculated from GPC using light scattering

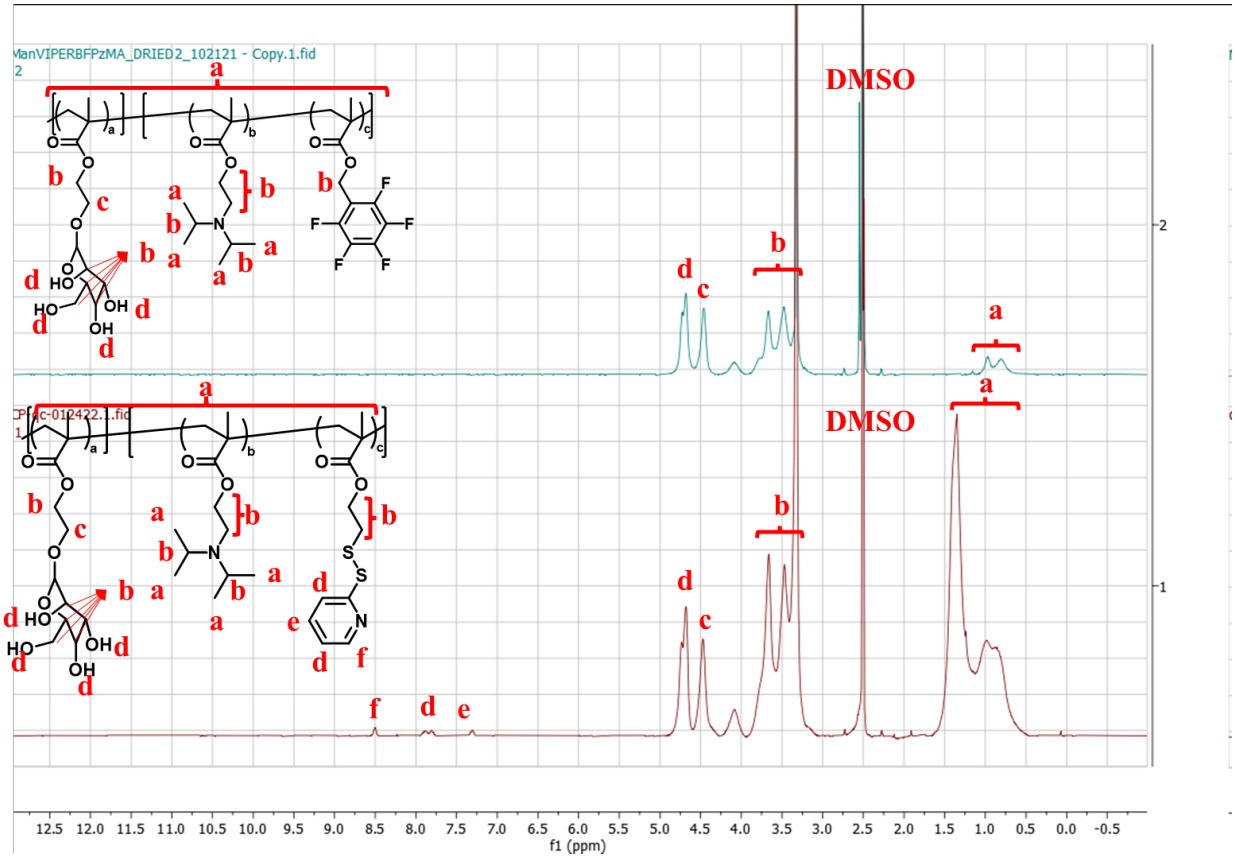

Figure S 3.1 ^{1}H-NMR of CP-NR (top) and CP-R (bottom) in DMSO-d6

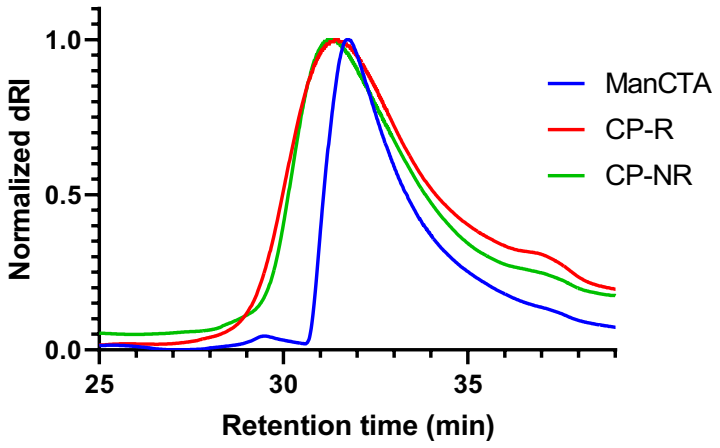

Figure S 3.2 GPC traces of CP polymers and mannose CTA

Obtained from an Agilent 1260 HPLC stack running heated LiBr-supplemented (0.1% w/v) DMF mobile phase at a flow rate of 1 mL min^{-1} through a semi-prep three-column setup (Phenogel-TSKgel) with filtered 5 mg/mL samples

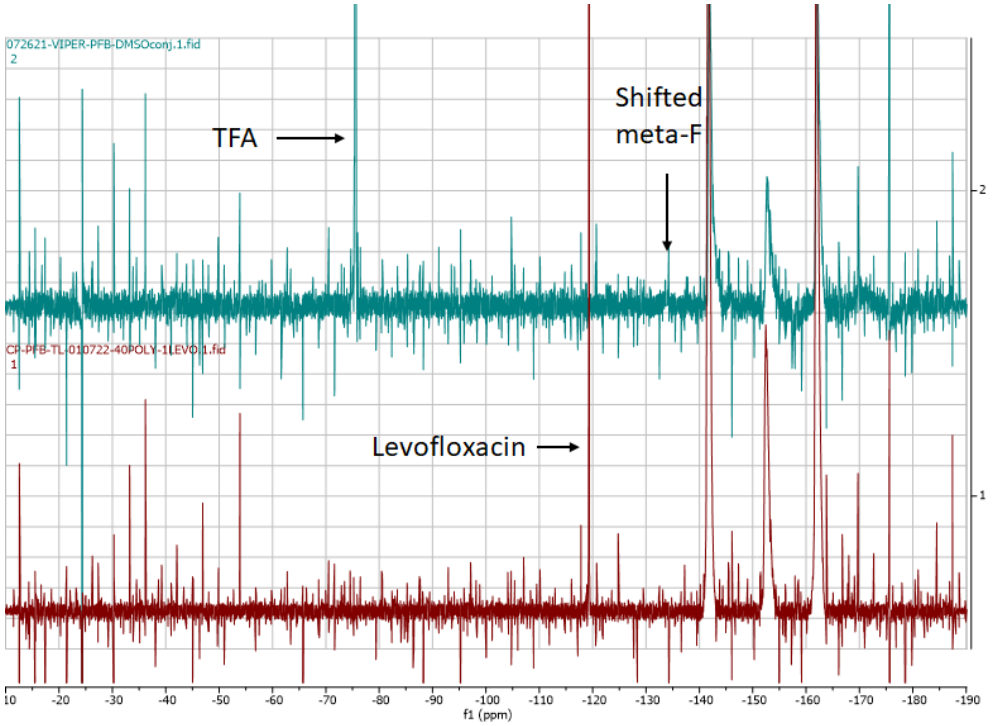

Figure S 3.3 ^{19}F-NMR of MP-NR (top) and CP-NR (bottom) in DMSO-d6.

TFA in MP-NR represents TFA counterions in synthesized peptides. Levofloxacin in CP-NR is an internal standard used to determine PFB wt%

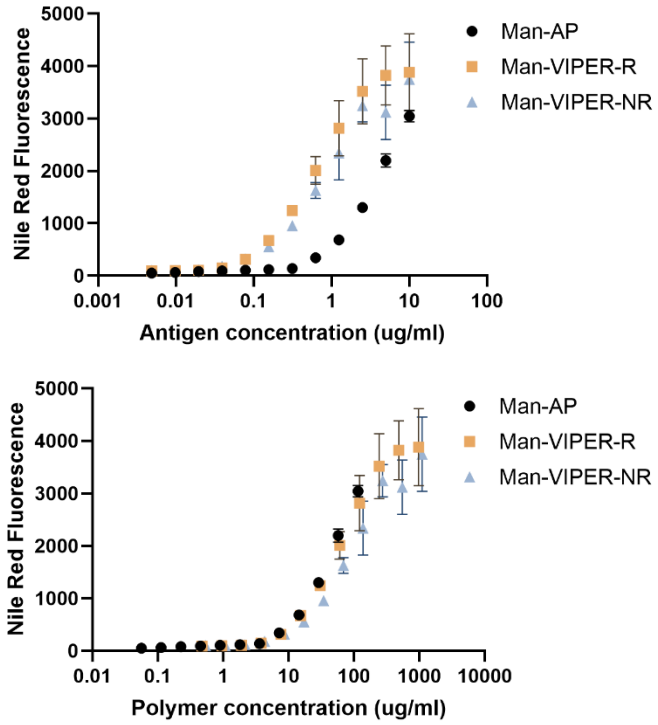

Figure S 3.4 Critical micelle concentration (CMC) was determined by the Nile Red fluorescence assay.

The left panel shows the concentration of the peptide antigens and the right panel shows the concentration of the polymers.

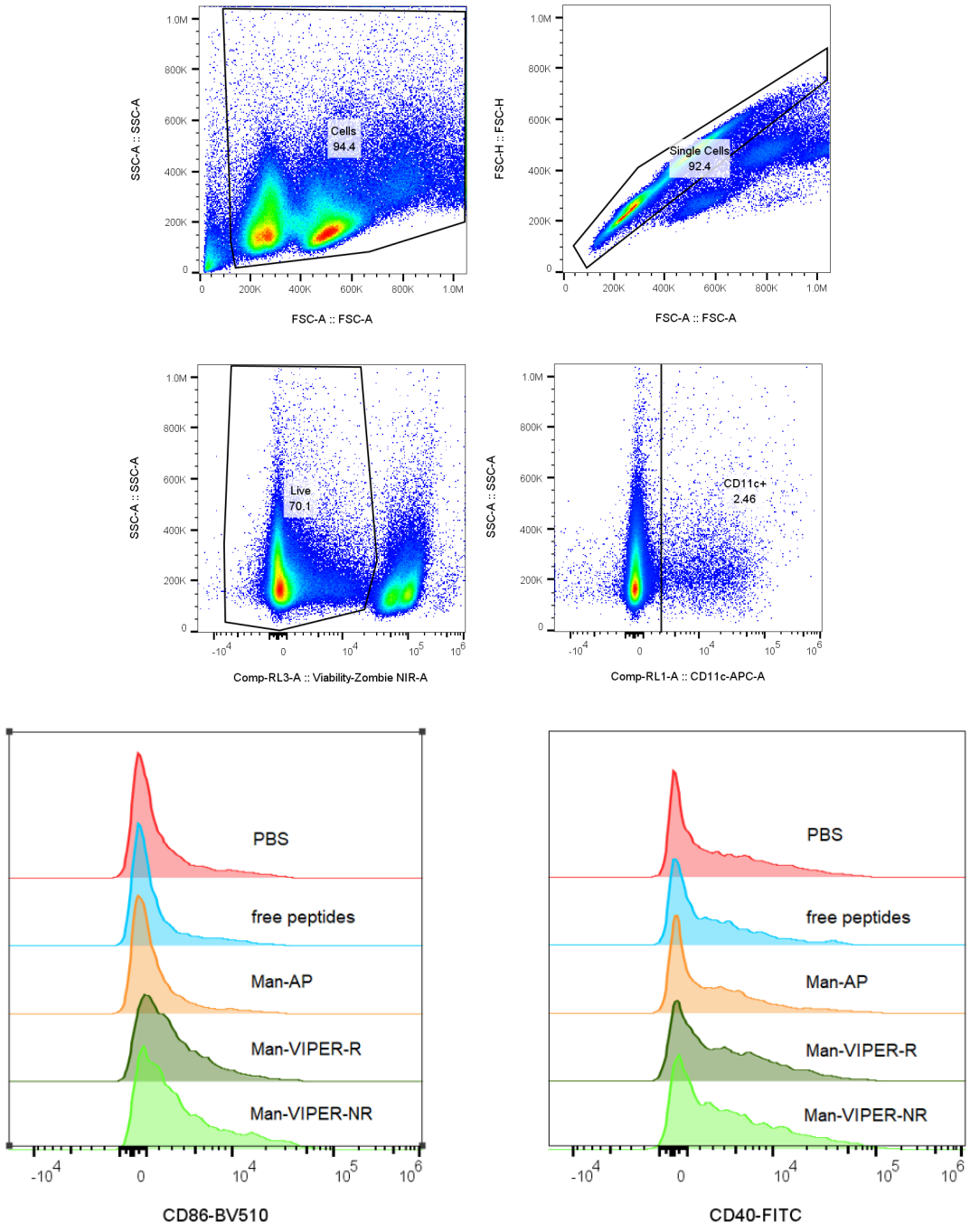

Figure S 3.5 Flow cytometry gating

(a) Gating for CD11c$^+$ DCs in the ILNs. (b) Representative histograms of CD86-BV510 and CD40-FITC in CD11c$^+$ cells.

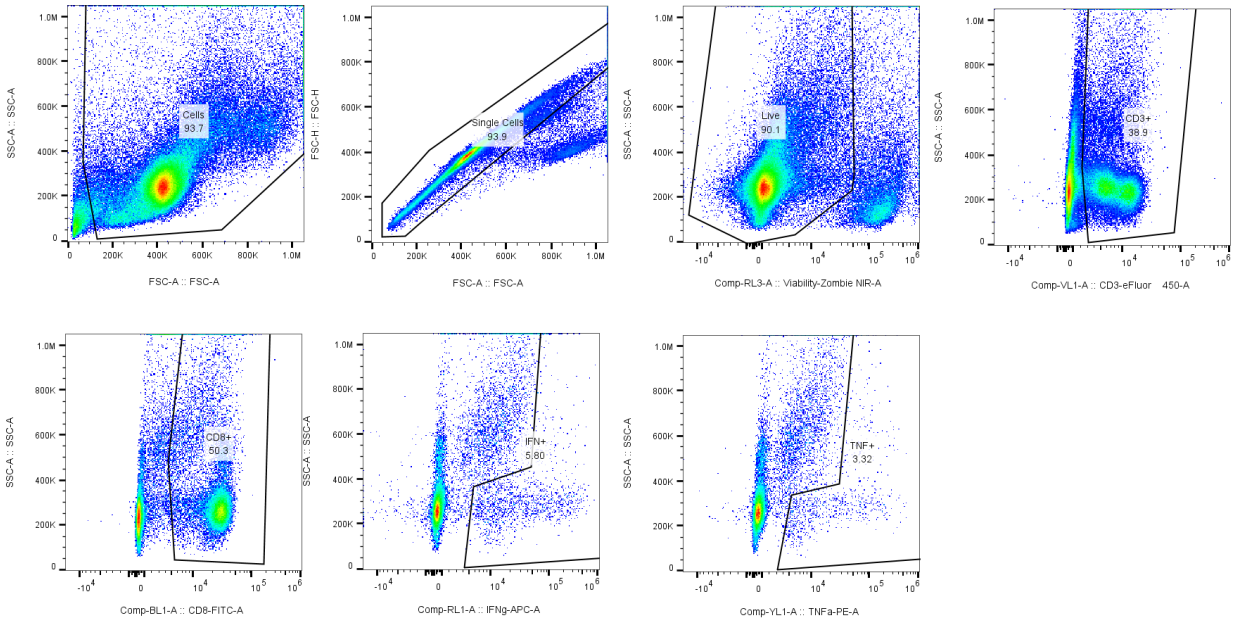

Figure S 3.6 Gating for IFNγ$^+$ and TNFα$^+$ CD8$^+$ T in the splenocytes.

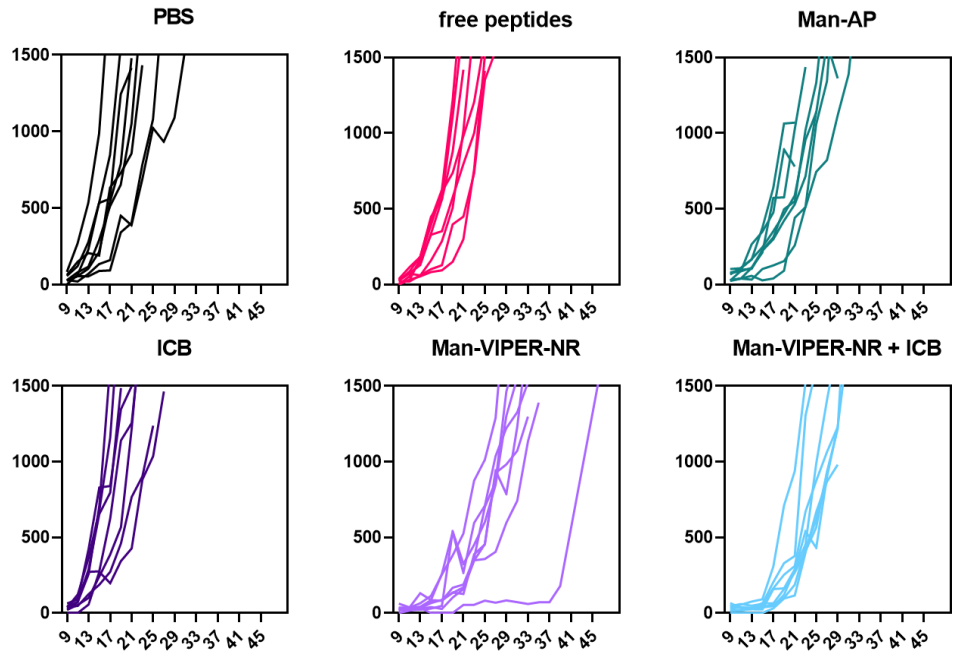

Figure S 3.7 Individual tumor growth curves (N=8).

Y-axis: tumor volume mm^3, x-axis: days post tumor inoculation.

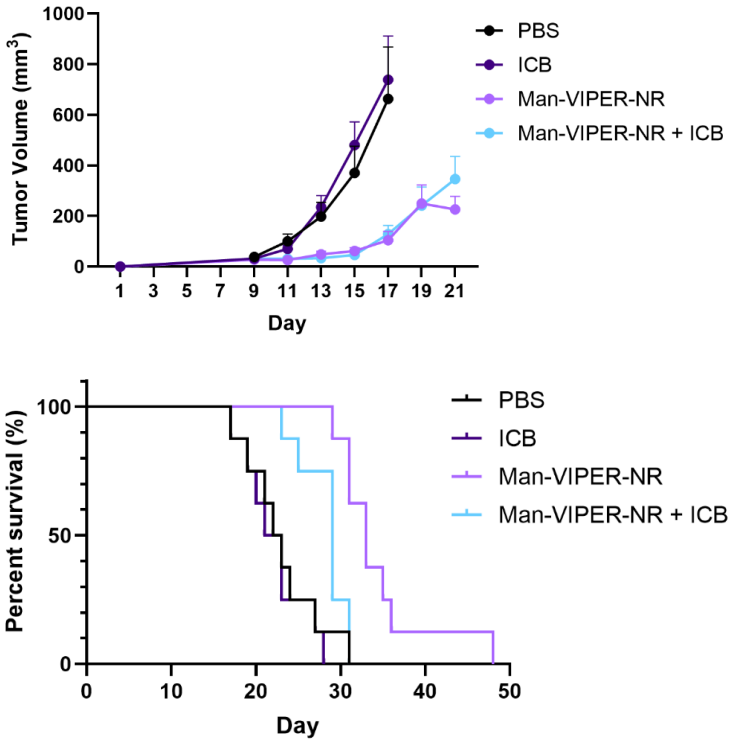

Figure S 3.8 Tumor growth curve and Kaplan-Meier survival curves.

Tumor growth curve and Kaplan-Meier survival curve of mice treated with anti-PD-1 ICB and Man-VIPER-NR. Data are represented as mean ± SEM. N = 8 biological replicates.

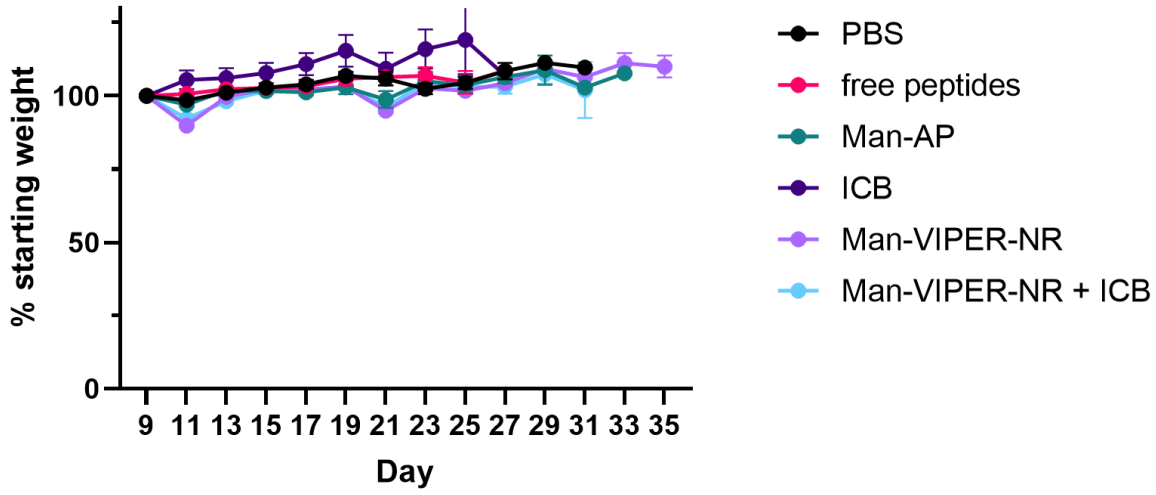

Figure S 3.9 Weight change in the tumor reduction study (N=8).

Mice were treated with PBS, free peptides, Man-AP and Man-VIPER-NR on days 3, 10 and 19. Mice were treated with ICB on days 4, 11, and 20.

Chapter 4 : Mannosylated STING agonist 'drugamers' for dendritic cell-mediated cancer immunotherapy[5]

Dinh Chuong Nguyen, Kefan Song*, Simbarashe Jokonya, Omeed Yazdani, Drew L. Sellers, Suzie H. Pun, Patrick S. Stayton*

ABSTRACT

The Stimulator of Interferon Genes (STING) pathway is a promising target for cancer immunotherapy. Despite recent advances, therapies targeting the STING pathway are often limited by routes of administration, sub-optimal STING activation or off-target toxicity. Here, we report a dendritic cell (DC)-targeted polymeric prodrug platform (polySTING) that is designed to optimize intracellular delivery of a diamidobenzimidazole (diABZI) small molecule STING agonist, while minimizing off-target toxicity after parenteral administration. PolySTING incorporates mannose targeting ligands as a comonomer, which facilitates its uptake in $CD206^+$/mannose $receptor^+$ professional antigen-presenting cells (APCs) in the tumor microenvironment (TME). The STING agonist is conjugated through a cathepsin B-cleavable Valine-Alanine (VA) linker for selective intracellular drug release after receptor-mediated endocytosis. When administered intravenously in tumor-bearing mice, polySTING selectively targeted $CD206^+$/mannose $receptor^+$ APCs in the TME, resulting in increased cross-presenting $CD8^+$ DCs, infiltrating $CD8^+$ T cells in the TME, as well as maturation across multiple DC subtypes in the tumor-draining lymph node (TDLN). Systemic administration of polySTING slowed tumor growth in a B16-F10 murine melanoma model, as well as a 4T1 murine breast cancer

[5] Chapter reproduced from: Nguyen, DC., Song, K. *et al*. (2024). Mannosylated STING Agonist Drugamers for Dendritic Cell-Mediated Cancer Immunotherapy. *ACS central science*, 10(3), 666–675.

model with an acceptable safety profile. Thus, we demonstrate that polySTING delivers STING agonists to professional APCs after systemic administration, generating an efficacious DC-driven anti-tumor immunity with minimal side effects. This new polymeric prodrug platform may offer new opportunities for combining efficient targeted STING agonist delivery with other selective tumor therapeutic strategies.

4.1 INTRODUCTION

Immune therapies that enlist patients' endogenous immune systems are an effective and expanding strategy in treating cancer.[1] While many of the recent innovations such as checkpoint inhibitors[2] and CAR T cell therapies[3] have focused on directly stimulating the adaptive immune system, therapeutics that engage the innate immune system provide an alternative approach to activating both adaptive and innate arms of immunity against cancer.[4] The Stimulator of Interferon Genes (STING) pathway has emerged as a leading target. STING activation elicits a Type-1 interferon-driven response which induces a potent multifaceted innate and adaptive immune response.[5] Systemic administration of STING agonists can jump-start the cancer-immunity cycle.[6] In a tumor-targeted context, initial STING activation in the tumor microenvironment (TME) provides an initial wave of immunogenic ablation through either direct, cell- or cytokine-mediated cytotoxicity. Resultant tumor antigens drain to secondary lymphoid organs, where they are presented by professional antigen-presenting cells (APCs) such as dendritic cells (DCs) to activate adaptive immunity with the help of STING-derived immunogenic cues (e.g. cytokines and co-stimulatory molecules). Activated adaptive immune cells mobilize towards tumors where they further induce immunogenic tumor cell killing to perpetuate the cycle.[7] Indeed, successful STING activation can result in potent tumor suppression, eradication, or even long-term immunity to rechallenge/relapse.[8]

The potential in activating STING in cancer immunotherapy is clear, but drug delivery challenges have limited clinical translation of STING agonists. Canonical STING agonists such as 2'3'-cyclic GMP-AMP (2'3'-cGAMP) face significant systemic, cellular and intracellular barriers in reaching the STING protein,[9] necessitating either toxic high doses or the impractical intratumoral administration route.[10] In addition to the development of alternative small-molecule STING agonists,[11-13] multiple drug delivery platforms have been developed to address STING delivery challenges.[14] Lipid micelles,[15] polymersomes,[16,17] liposomes,[18,19] inorganic nanoparticles,[20] or drug-conjugated polymeric particles[21] have all been employed as systemic STING agonist carriers with potent responses.

Tumor-targeted STING delivery vehicles hold great promise. A reported tumor-targeted STING agonist antibody-drug conjugate (ADC) platform demonstrated an impressive safety profile and good efficacy.[22] However, this platform encounters inherent issues with target availability and scale-up manufacturability.[23] In addition, low-level STING activation in tumors can induce immunosuppressive factors such as indoleamine-2,3-deoxygenase (IDO) causing pathogenesis.[24] As tumor cells can downregulate STING,[25] agonist delivery to tumor cells can either be ineffective or counterproductive through this mechanism. Conversely, overactivation of STING can result in unproductive non-immunogenic cell ablation,[26,27] rendering patients vulnerable to relapse or metastasis. In light of this, targeted STING delivery to intratumoral APCs such as dendritic cells (DCs) may induce antitumor immunity without the aforementioned shortcomings. In tumor rejection models with or without immunotherapy, DC subsets such as type-1 conventional DCs (cDC1) play indispensable roles in antigen transport, cross-priming, and lymphocyte recruitment and maintenance in the TME.[28-32] STING activation in DCs strongly induces DC maturation,[33] and activation in cDC1 was crucial to the function of a intratumoral viral vector STING delivery

platform.[27] We hypothesize that a STING delivery platform targeting tumoral APCs can induce potent antitumor responses with minimal toxicity. A Clec9a$^+$ DC-targeted STING delivery platform showcased this possibility.[34]

Here, we report a DC-targeted STING polymeric prodrug platform that elicits a robust DC-driven antitumor response after systemic intravenous administration. We synthesized a polymerizable STING agonist prodrug monomer by conjugating a diamidobenzimidazole (diABZI) type agonist[11] "STING Agonist-3" to a polymerizable methacrylate via an intracellular cathepsin-cleavable Valine-Alanine (VA) linker. The monomer was co-polymerized with a targeting mannose methacrylate monomer[35] to produce the targeted macromolecular STING agonist prodrug 'drugamer', termed polySTING. We showed that polySTING targets CD206$^+$/mannose receptor$^+$ professional APCs in the TME, activates STING *in vivo*, and is well-tolerated. We confirmed polySTING's efficacy in an aggressive 'cold' B16-F10 murine melanoma model. We examined polySTING's mechanism in the same model and found a strong DC-driven antitumor immune response. Specifically, polySTING strongly enhanced CD8$^+$ cDC1 responses along with TME T-lymphocyte infiltration and CD8$^+$ T cell activation while promoting DC maturation in the tumor-draining lymph nodes (TDLN). PolySTING also reduced tumor growth kinetics in the aggressive 4T1 breast cancer model of a different murine strain, demonstrating the utility of polySTING as a standalone systemic cancer immunotherapy or especially as a candidate for combination immune-therapy strategies.

4.2 RESULTS AND DISCUSSION

4.2.1 Synthesis and characterization of polySTING

"STING Agonist-3" was selected for our studies because it shows excellent activity,[11] and it has a single hydroxyl group amenable to synthesis of the polymerizable prodrug monomer. The synthetic scheme for the STING Agonist-3 prodrug monomer is summarized in **Figure 4.1a** (more detail in **Scheme S4.1**). Using the polymerizable mono-2-(methacryloyloxy)ethyl succinate (SMA) moiety, the prodrug monomer was synthesized by incorporating the cathepsin B-cleavable Val-Ala linker with a self-immolative para-aminobenzyl alcohol (PABA) moiety that has been validated in the human antibody-conjugate field,[36] to yield SMA-Val-Ala-PABA-STING Agonist-3 (SVA-PAB-STING). The prodrug monomer product was validated using ^{1}H-NMR and mass spectrometry (**Figure S4.1-S4.2**). We then synthesized the targeted polymer prodrug "drugamer" polySTING by co-polymerizing SVA-PAB-STING with mannose ethyl methacrylate (ManEMA) (**Figure 4.1b,** characterization in **Figure S4.3-S4.5**). PolySTING has an average Mw of 12 kDa, with an average degree of polymerization (DP) of 35 for ManEMA and 2 for SVA-PAB-STING. PolySTING is thus designed for internalization by receptor-mediated endocytosis in CD206^{+} APCs, followed by endosomal cathepsin cleavage and release of the membrane-permeable diABZI-type "STING Agonist-3" that can activate the cytosolic STING protein in these APCs (**Figure 4.1c**).

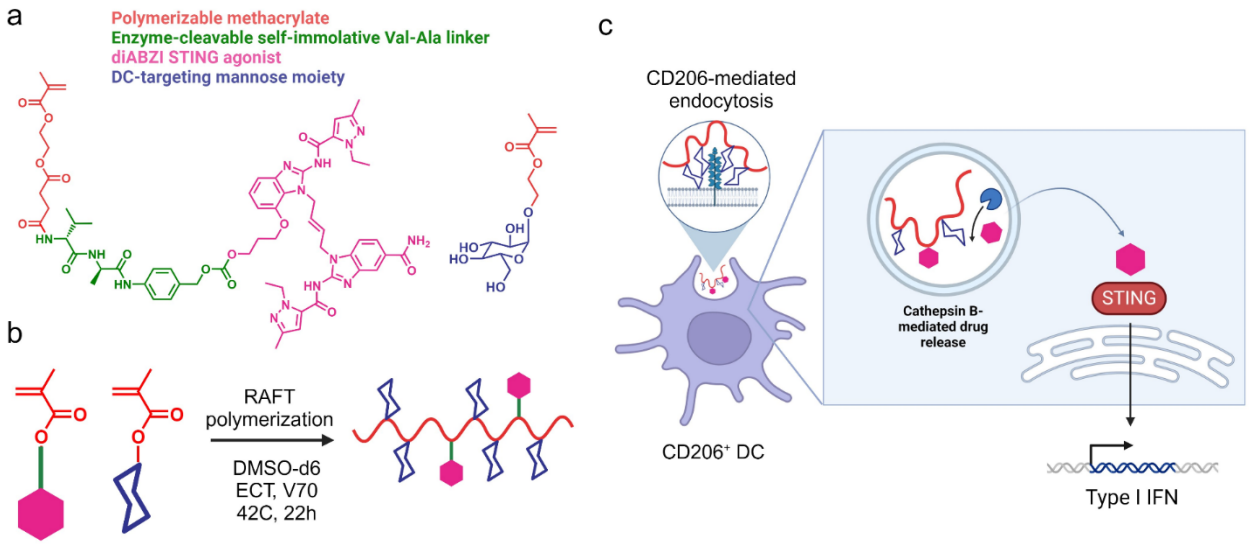

Figure 4.1 Design of polySTING polymeric prodrug.

(a) Structure of the enzyme-cleavable methacrylate-based STING agonist prodrug monomer and mannose ethyl methacrylate monomer. (b) Schematic of polySTING synthesis by RAFT polymerization. (c) Schematic of polySTING uptake by $CD206^+$ DCs, endosomal prodrug cleavage and agonist release, and STING activation in DCs. Created with BioRender.com

4.2.2 PolySTING targets APCs in the TME and activates STING

A fluorescent rhodamine-labelled polySTING (polySTING-Rh) was synthesized to investigate the targeting selectivity of polySTING upon intravenous administration. Professional APCs within the TME was investigated because they play pivotal roles in mounting antitumor responses in immunotherapy.[37,38] PolySTING-Rh was administered to B16-F10-bearing C57BL/6 mice and rhodamine-positive cell subsets in the tumor were characterized. PolySTING was shown to selectively target immune cells ($CD45^+$) including DCs ($CD11c^+$) and macrophages ($F4/80^+$), which all have a significant fraction of polySTING-Rh-positive cells, unlike non-immune $CD45^-$ cells (**Figure 4.2a, b**). PolySTING therefore has a unique TME distribution profile compared to prior non-targeted STING agonist formulations, which all have significant uptake in $CD45^-$

cells.[15,16,21] Thus, by transforming the STING agonist to a mannosylated macromolecular prodrug, we successfully restricted STING agonist delivery to immune cells.

STING activation was also assessed via the expression of STING-related genes Ifnb1 and Cxcl10 in the tumor and the tumor-draining lymph nodes (TDLNs). Tumor STING gene expression was sampled 24 hours after a single treatment, and TDLN STING expression was sampled 24 hours after a second treatment. PolySTING elicited an appreciable increase in both Ifnb1 and Cxcl10 in the tumor compared to free STING agonist and untreated mice (**Figure 4.2c**). In the TDLN, polySTING induced a significant increase in Cxcl10, but not in Ifnb1 (**Figure 4.2d**). This modest activation is in line with some reports of low increases in STING gene expression in DCs upon *in vitro* STING agonist pulsing.[33] This data also reflects a snapshot in time; others have reported the STING-mediated elevated expression levels of Ifnb1 and Cxcl10 decrease over time.[39,40] Nevertheless, these results establish that polySTING preferentially targets APCs, resulting in STING pathway activation in the TME and in the TDLNs.

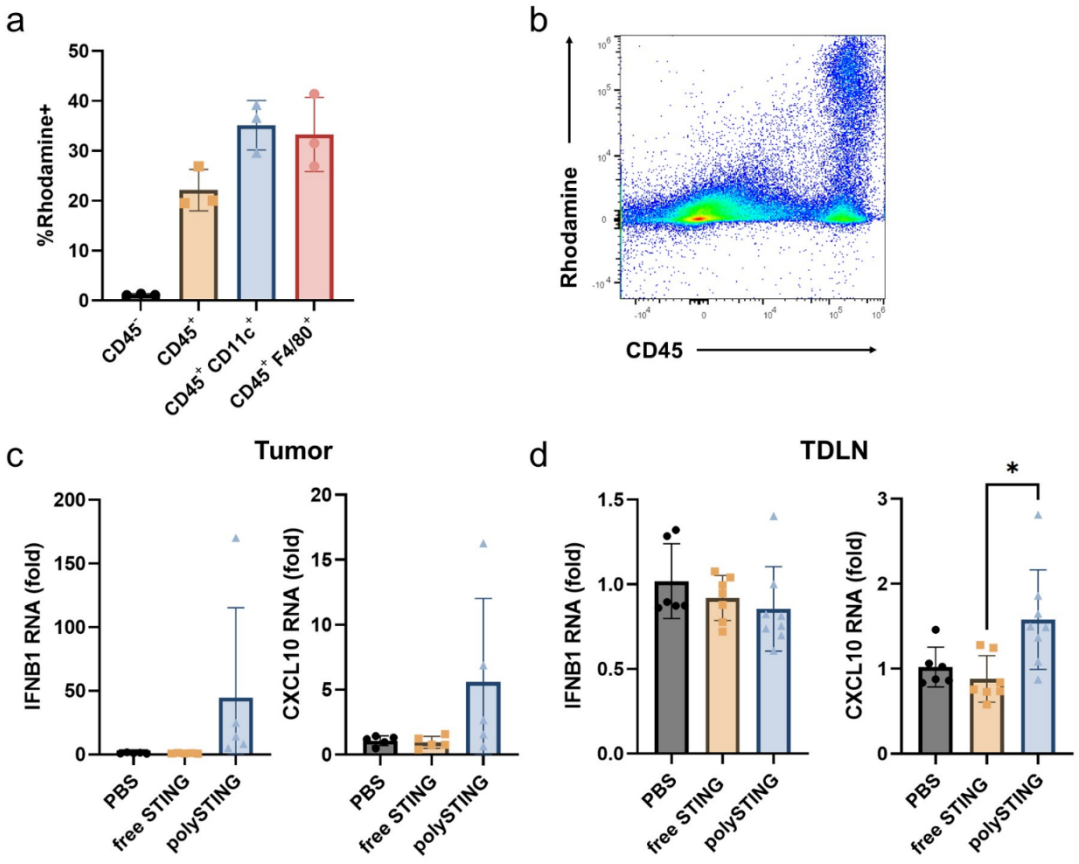

Figure 4.2 PolySTING targets immune cells and activates the STING pathway.

(a) B16F10 tumor-bearing C57BL/6 mice were treated with polySTING-Rh intravenously and tumors (100-200 mm^3) were harvested 30 min post injection. Percentage of rhodamine-positive cells in different cell subsets were quantified by flow cytometry (N=3). (b) Representative flow dot plot of rhodamine and CD45 expression in tumor. (c) Expression levels of interferon-stimulated genes IFNB1 and CXCL10 in the tumor 24 h post treatment by RT-qPCR (N=5). Gene expression was normalized to the GAPDH housekeeping gene. (d) Expression levels of interferon-stimulated genes Ifnb1 and Cxcl10 in the TDLN 24 h post 2nd treatment by RT-qPCR (N=6-8). Gene expression was normalized to the GAPDH housekeeping gene. Data are represented as mean ± SD. Statistical analysis was performed using one-way ANOVA with post-hoc Tukey HSD test (*$p \leq 0.05$).

Because polySTING was shown to localize to both macrophages and DCs in the TME, downstream activation markers were investigated in each cell type. In macrophages, STING activation has been reported to drive polarization towards the pro-inflammatory M1 phenotype over the tolerogenic, tumorigenic M2 phenotype.[41] Surprisingly, polySTING slightly increased

M1 marker CD80 expression in tumor-associated macrophages (TAMs) compared to free STING agonist and untreated mice, but had no effect on M2 marker CD206 expression **(Figure S4.6)**. STING agonists and formulations are usually reported to polarize M2 macrophages towards M1 phenotypes,[22,42] which was not in line with our findings. We observed the same trend *in vitro* with bone marrow-derived macrophages (BMDM) incubated with STING agonists and formulations (**Figure S4.7**). In contrast, polySTING induced significant DC maturation across all markers (CD86, CD80 and CD40) in the DC-enriched TDLN (**Figure S4.8).** The potent DC response suggests the potential for a strong DC-mediated adaptive antitumor immune response. We therefore moved to therapeutic evaluation *in vivo*.

4.2.3 Systemic therapy of polySTING is tolerable and results in potent suppression of melanoma growth

Neither intravenous administration of polySTING nor the free drug resulted in significant weight loss in mice, and polySTING exhibited dose-dependent IFNβ stimulation **(Figure S4.9-S4.10).** These indications of tolerability permitted the subsequent evaluation of polySTING's anti-cancer efficacy in the aggressive, poorly immunogenic murine melanoma model B16-F10.[43] polySTING significantly inhibited B16-F10 tumor growth and prolonged survival compared to vehicle control (**Figure 4.3a, b.** Individual curves in **Figure S4.11)**. Free-form STING Agonist-3 did not yield any therapeutic effect over control. The diABZI family from which "STING Agonist-3" was derived already has an efficacy track record in the CT-26 colon cancer model;[11] these striking results reflect the aggressiveness of B16-F10 model and highlights the therapeutic utility of polySTING. In the same study, a stronger IFNβ response and higher weight loss upon either polySTING or free drug treatment was observed compared to healthy mice, likely due to inflammation in the tumor causing weight loss from ablation (**Figure 4.3c, d**, compared with

Figure S4.9-S4.10). Weight loss increased with subsequent administrations; however, it remained below 10% loss up to the 3rd injection, a treatment regime comparable with many other reported systemic STING delivery platforms.[16,18,21]

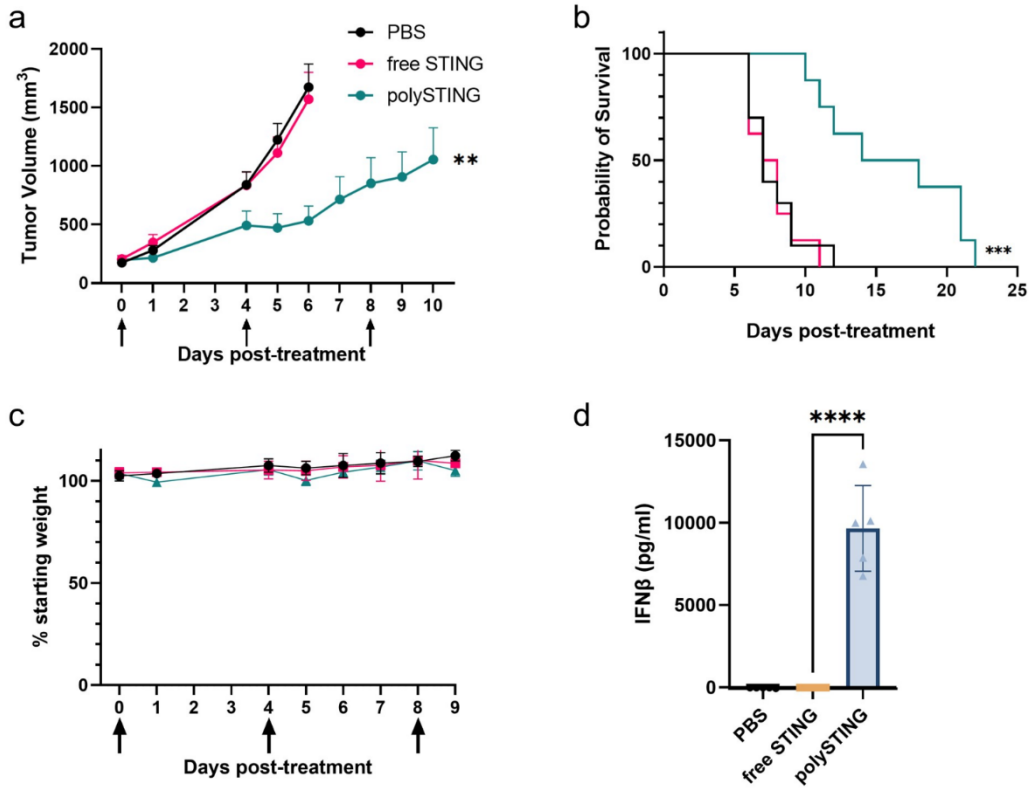

Figure 4.3 PolySTING inhibits tumor growth and prolongs survival in tumor-bearing mice.

(a) Tumor growth curve in B16F10 tumor-bearing C57BL/6 mice. B16F10 cells were inoculated on day -8, and STING treatments were given on days 0, 4 and 8 through tail vein injections. Data are represented as mean ± SEM (N = 8-10). Statistical analysis was performed using unpaired t test on day 10 (**$p \leq 0.01$). (b) Kaplan-Meier survival curve (N=8-10). Survival analysis was performed using the log-rank test (*** $p \leq 0.001$). (c) Weight change in B16F10 tumor-bearing C57BL/6 mice. Data are represented as mean ± SD (N = 8-10). (d) Plasma IFNβ level in 4T1 tumor-bearing BALB/c mice 4 h post treatment with free STING and polySTING (N=5). Data are represented as mean ± SD. Statistical analysis was performed using one-way ANOVA with post-hoc Tukey HSD test (****$p \leq 0.0001$).

4.2.4 Examination of polySTING-treated B16-F10-bearing mice reveals a T-cell-inflamed TME maintained by $CD8^+$ DCs

To better understand the mechanism behind polySTING's efficacy, the immune cell population in the B16-F10 TME was examined after the 2nd injection (**Figure 4.4a**). PolySTING induced more immune cell infiltration into the tumor compared to the free drug (**Figure 4.4b**). As T cells are key contributors in antitumor immunity,[44] we first looked at the T cell infiltration (gating scheme in **Figure S4.12**). In line with the tumor suppression results, polySTING treatment, but not free STING agonist, induced significantly more T cell infiltration (2-fold) in the TME compared to untreated mice (**Figure 4.4c**). More importantly, polySTING treatment increased the percentage of $CD8^+$ T cells in the TME by 4-fold, and could partially explain the antitumor effect of polySTING.

As tumor-infiltrating T cells could still be subject to immunosuppression and therapy failure,[45] DC subset composition was next examined (gating scheme in **Figure S4.13**). cDC1s are critical mediators of antigen transport to TDLNs,[46] chemoattractant producers in the TME (i.e. $CD103^+$ DCs),[30] as well as antigen cross-presentation to T cells both for priming and maintenance (i.e. $CD8^+$ DCs).[29] PolySTING increased $CD8^+$ DCs in the TME compared to untreated or free drug groups, but not overall DC population relative to all cells (**Figure 4.4d**). To our knowledge, this $CD8^+$ DC response without usage of checkpoint blockade therapy has not been reported elsewhere and may represent a novel mechanism for targeted STING immunotherapy. Tumoral DCs have been recognized as crucial in maintaining T-cell activity in the TME through antigen presentation and co-stimulation.[32] Given $CD8^+$ DCs capability for cross-presentation to cytotoxic lymphocytes,[47] their population increase in polySTING-treated groups compared to free drug could better maintain tumoral $CD8^+$ T-cell activity. The increased $CD8^+$ DC population in the

TME without change in the overall $CD11c^+$ DC population may represent either polarization of $CD11c^+$ cells towards $CD8^+$ phenotypes or a migratory equilibrium between $CD8^+$ DCs and other subsets. This is consistent with reports that STING activation and/or its resultant IFN response stimulates $CD8^+$ DC responses.[27,48,49] There were no differences in $CD103^+$ DC populations between treatment groups (**Figure S4.14**).

The quality of infiltrating T-cells was also examined through analysis of PD-1 and TCF-1 expression (gating scheme in **Figure S4.15**). PD-1 is a marker for tumor-reactive $CD8^+$ T cells in melanoma.[50] TCF-1 is a marker indicative of stem-like constitutively-activated T-cells (i.e. exhausted T-cells in the antigen-rich TME) capable of functional rescue,[51] and is mechanistically associated with positive response checkpoint blockade therapy.[52] PolySTING increased the fraction of "tumor-reactive" $PD\text{-}1^+$ $CD8^+$ T cells while the free-form STING agonist did not (**Figure 4.4e**). The increase in $PD\text{-}1^+$ $CD8^+$ T cells may be a consequence of increased T cell infiltration into the tumor, and the heightened persistent antigen exposure associated with it.[53] There was no difference in TCF-1 expression amongst all treatment groups, though the response trended upwards for polySTING (**Figure 4.4e**).

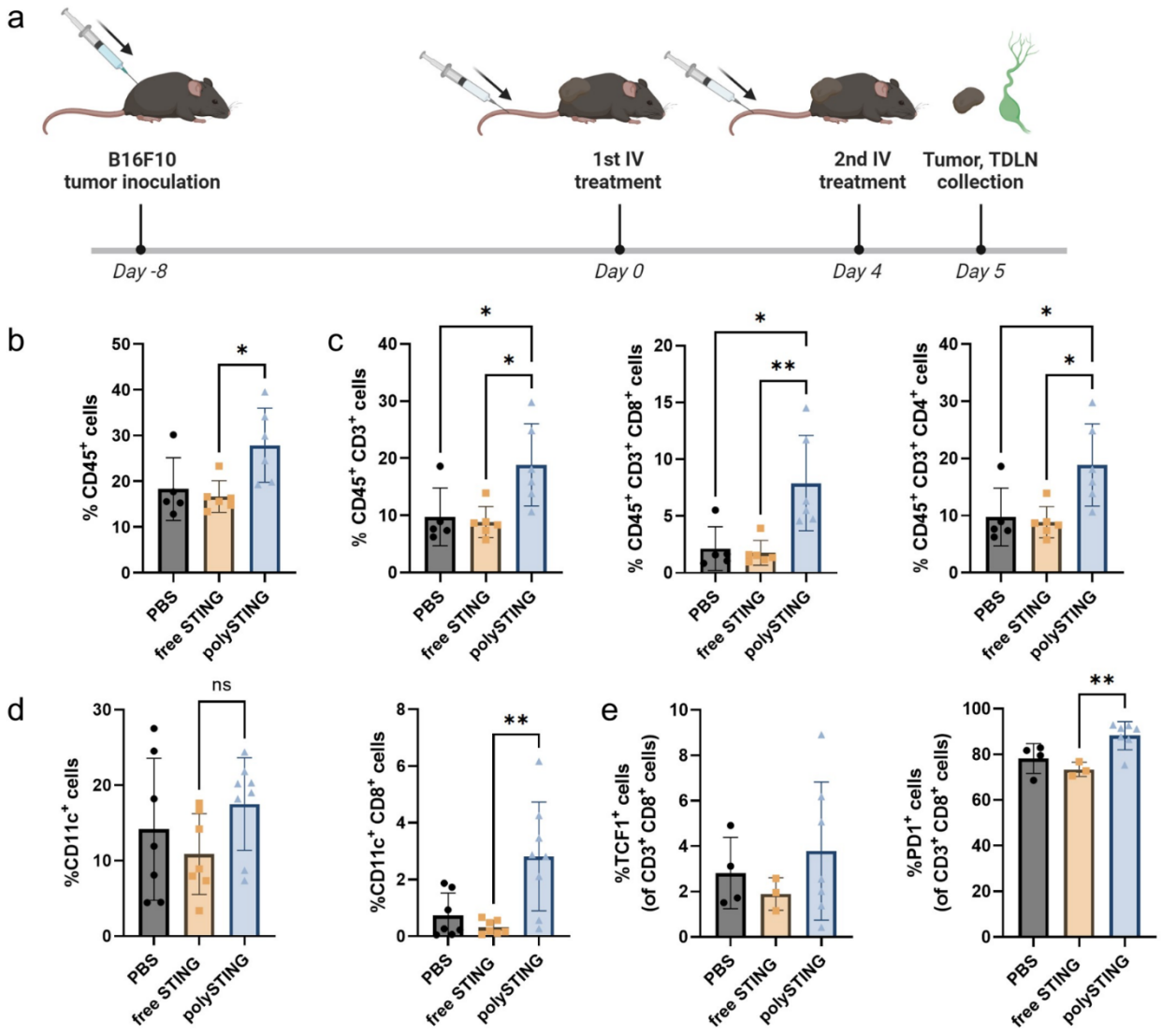

Figure 4.4 PolySTING induces immune cell infiltration into the tumor.

(a) Schematic of polySTING treatment schedule. C57BL/6 mice were inoculated with B16F10 cells on day -8. Treatment was given on day 0 and day 4 intravenously. Tumor and TDLN were harvested 24 h post 2nd injection. (b) Percentage of $CD45^+$ immune cells in the tumor by flow cytometry (N=5-6). (c) Percentage of total T cells, $CD8^+$ T cells and $CD4^+$ T cells in the tumor by flow cytometry (N=5-6). (d) Percentage of total DCs and $CD8^+$ DCs in the tumor by flow cytometry (N=7-8). (e) Percentage of $TCF1^+$ $CD8^+$ T cells and $PD1^+$ $CD8^+$ T cells in the tumor by flow cytometry. Data are represented as mean ± SD. Statistical analysis was performed using one-way ANOVA with post-hoc Tukey HSD test (*$p \leq 0.05$, **$p \leq 0.01$, ns: not significant). Figure 4a created with BioRender.com.

4.2.5 polySTING also positively impacts DC function in the TDLN

Having demonstrated potent downstream effects of polySTING, we next looked upstream at the TDLNs where T cell priming takes place (gating scheme in **Figure S4.16**). In contrast to the TME, there is a noticeable increase $CD11c^+$ DCs in polySTING-treated TDLNs, as well as the cDC1 subsets $CD8^+$ and $CD103^+$ DCs (**Figure 4.5a**). In addition, all DC subsets had a substantial increase in the CD86 maturation marker (**Figure 4.5b**). Consistent with previous data, free-form STING agonist did not induce any appreciable change. The increased maturation marker expression could be due to a combination of type I IFN production due to STING activation and exposure to tumor antigen.[54,55] The indispensable role of secondary lymphoid organ (SLO)-resident $CD8^+$ DCs in priming cytotoxic T-lymphocytes (CTLs) and subsequent cellular responses to both tumors and pathogens is well-established;[29] thus, their expansion brought about by polySTING indicates stronger $CD8^+$ T cell priming. The increase in $CD103^+$ DCs in the TDLN of polySTING-treated animals compared to control animals is in line with a report showing $CD103^+$ DCs passing tumor antigen to CTL-priming $CD8^+$ DCs via synaptic transfer after migration to TDLNs.[56] $CD103^+$ DCs are also potent activators of naive $CD8^+$ T-cells through cross-presentation, complementing this effect.[57] Thus, a more complete image of polySTING's proposed mechanism of action emerges (**Figure 4.5c**): DC-targeted polySTING activates the STING pathway in DCs and results in type I IFN production.[6] Type I IFNs activate DCs and induce the survival and proliferation of $CD8^+$ DCs.[54] Tumor antigens travel to the TDLNs either by themselves or transported by migratory DCs.[58] Migratory $CD103^+$ DCs uptake and transport tumor antigen to the TDLNs for cross-presentation through either self or antigen transfer to $CD8^+$ DCs, both resulting in effective T cell priming. Activated T cells travel to the tumor through the vasculature and type I IFNs promote T cell infiltration in the TME.[59] The strong cytotoxic $CD8^+$

T cell response results in a strong anti-tumor effect. More antigens are generated and transported to the TDLNs to further activate DCs and T cells, perpetuating the cancer-immunity cycle.[7]

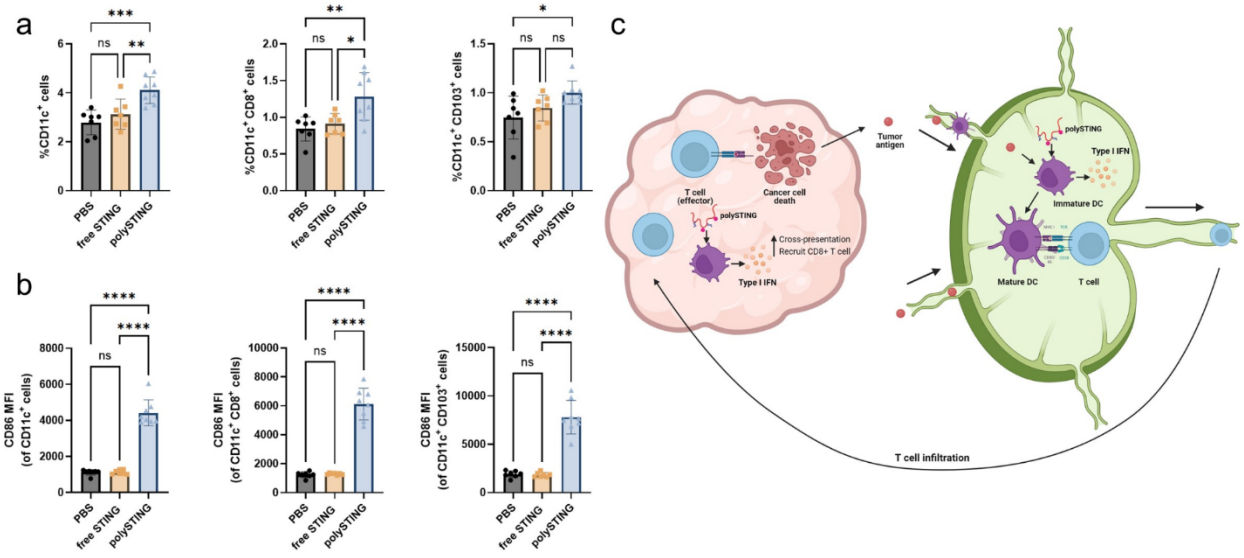

Figure 4.5 PolySTING induces DC proliferation and maturation in the TDLN.

(a) Percentage of total DCs, $CD8^+$ DCs and $CD103^+$ DCs in the TDLN by flow cytometry (N=7-8). (b) CD86 expression on total DCs, $CD8^+$ DCs and $CD103^+$ DCs in the TDLN by flow cytometry (N=7-8). (c) Schematic of polySTING mechanisms in tumor and TDLN. Data are represented as mean ± SD. Statistical analysis was performed using one-way ANOVA with post-hoc Tukey HSD test (*$p \leq 0.05$, **$p \leq 0.01$, ***$p \leq 0.001$, ****$p \leq 0.0001$, ns: not significant). Figure 5c generated with BioRender.com.

4.2.6 Validation of systemic polySTING therapeutic efficacy in the 4T1 breast cancer model

To further demonstrate the utility of polySTING, we evaluated efficacy in another solid tumor type in a different mouse strain. We chose the 4T1 orthotopic breast cancer model in BALB/c mice also for its low immunogenicity and late-stage aggressiveness.[43] In addition, 4T1's resistance to checkpoint blockade therapy in our experience and polySTING's strong induction of PD-1^+ $CD8^+$ T cells makes it a good candidate to test for synergy with anti-PD-1. We also observed tumor growth inhibition and survival benefits with systemic polySTING treatment in this model, with

similar weight loss (**Figure S4.17**) albeit to a more modest therapeutic effect (**Figure 4.6**). Consistent with our previous data, the free-form STING agonist did not exert any measurable therapeutic effect. Interestingly, co-therapy with anti-PD-1 did not further inhibit tumor growth nor improve survival. Other reports of systemic STING delivery therapy in the 4T1 model also reported little to no benefit with anti-PD-1 therapy,[21] suggesting that the primary immunosuppression mechanism lies elsewhere. Regardless, polySTING's efficacy in two different aggressive, non-immunogenic tumor models across two different mouse strains demonstrate its strong utility as a systemic immunotherapy.

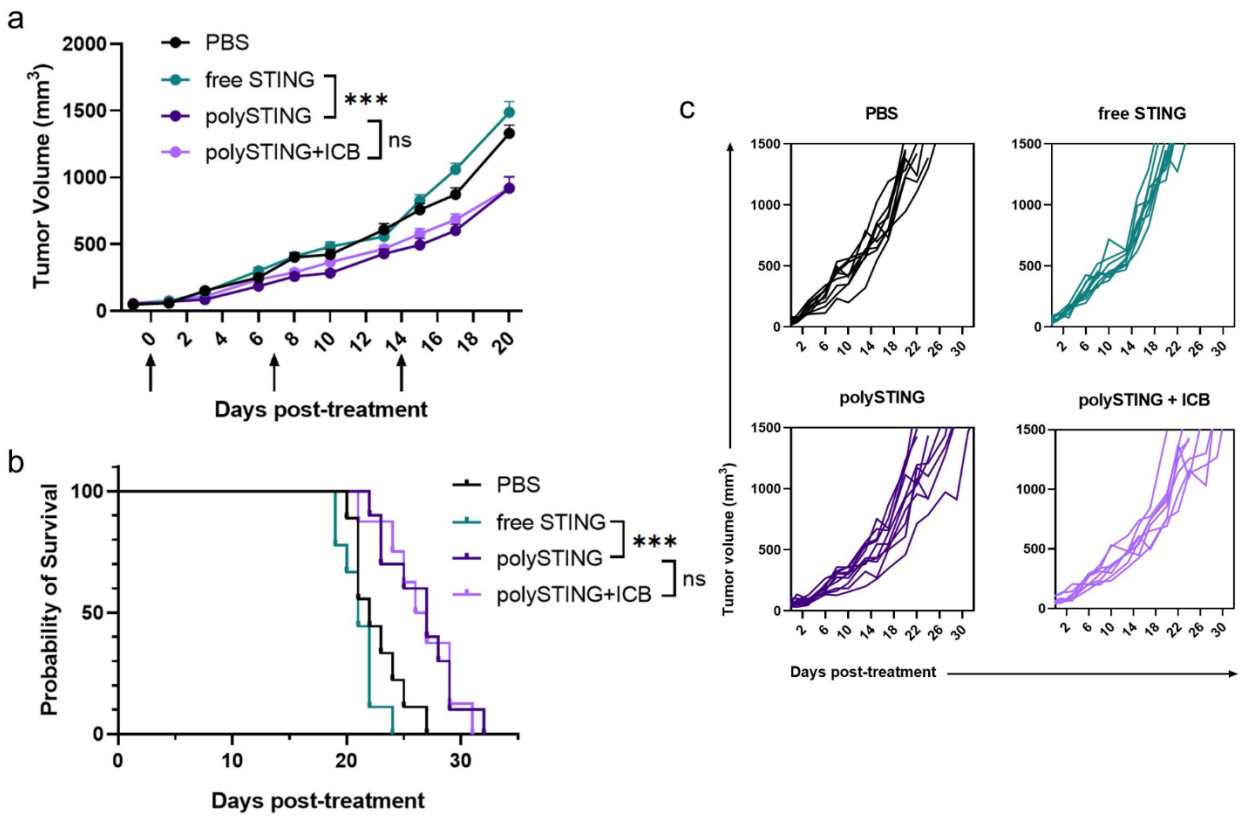

Figure 4.6 PolySTING shows antitumor efficacy in the 4T1 model.

(a) Tumor growth curve in 4T1 tumor-bearing BALB/c mice. 4T1 cells were inoculated on day -8, and STING treatments were given on days 0, 7 and 14. ICB was given on days 1, 8 and 15. Data are represented as mean ± SEM (N = 8-10). Statistical analysis was performed using unpaired t test on day 20 (*** $p \leq 0.001$, ns: no significance). (b) Kaplan-Meier survival curve

(N=8-10). Survival analysis was performed using the log-rank test (*** $p \leq 0.001$, ns: no significance). (c) Individual growth curves.

4.3 CONCLUSIONS

We have developed a novel polymeric platform, polySTING, to deliver STING agonists to DCs through systemic administration. PolySTING was primarily taken up by professional APCs, including DCs, in the TME and resulted in systemic STING activity. PolySTING drove a strong DC-directed immune response through DC activation in the TDLN and induction of cross-presenting $CD8^+$ DCs in both the TDLN and TME. We observed significant therapeutic efficacy in two distinct aggressive non-immunogenic tumor models with a good safety profile as an intravenous immunotherapy. PolySTING is a novel platform for cancer immunotherapy and highlights the potential of targeted STING delivery to DCs.

4.4 MATERIALS AND METHODS

4.4.1 Materials

SMA N-hydroxysuccinimide ester (SMA-NHS, compound 2, **Scheme S4.1**) was synthesized as previously described[1]. The STING agonist "STING Agonist-3" (CAS 2138299-29-1) was purchased from MedChemExpress. L-Valyl-L-Alanine (H-Val-Ala-OH) was purchased from Combi-Blocks. RAFT chain transfer agent 4-(((ethylthio)carbonothioyl)thio)-4-cyanopentanoic acid (ECT) and the monomer mannose ethyl methacrylate (ManEMA) were purchased from Omm Scientific. The rhodamine monomer, methacryloylethyl thiocarbamoyl rhodamine B (RhMA) was purchased from PolySciences Inc. The initiator 2,2'-azobis(4-methoxy-2,4-dimethylvaleronitrile) (also known as V70) was purchased from Wako Fujifilm. N-Ethoxycarbonyl-2-ethoxy-1,2-dihydroquinoline (EEDQ) and 4-nitrophenol chloroformate (PNP-Cl) was purchased from Chem-Impex International Inc.. 4-aminobenzyl alcohol (PABA) was purchased from Tokyo Chemical

Industries. Diisopropylethylamine (DIPEA), triethylamine (TEA) and dimethylaminopyridine (DMAP) were purchased from Sigma-Aldrich. Dimethylformamide (DMF), tetrahydrofuran (THF), dichloromethane (DCM) and chloroform were purchased from Fisher. Argon gas was purchased from Linde Gas & Equipment Inc. All reagents mentioned above were used as received.

Anhydrous deuterated dimethyl sulfoxide (DMSO-d6, > 99%) was purchased from Sigma-Aldrich and stored with activated molecular sieves. Buffers were prepared in-house using endotoxin-free water and salts purchased from Fisher Scientific. All antibodies were purchased from BioLegend, with the exception of anti-TCF1-PE and anti-PD1-eFluor450.

4.4.2 Synthesis of STING agonist prodrug monomer

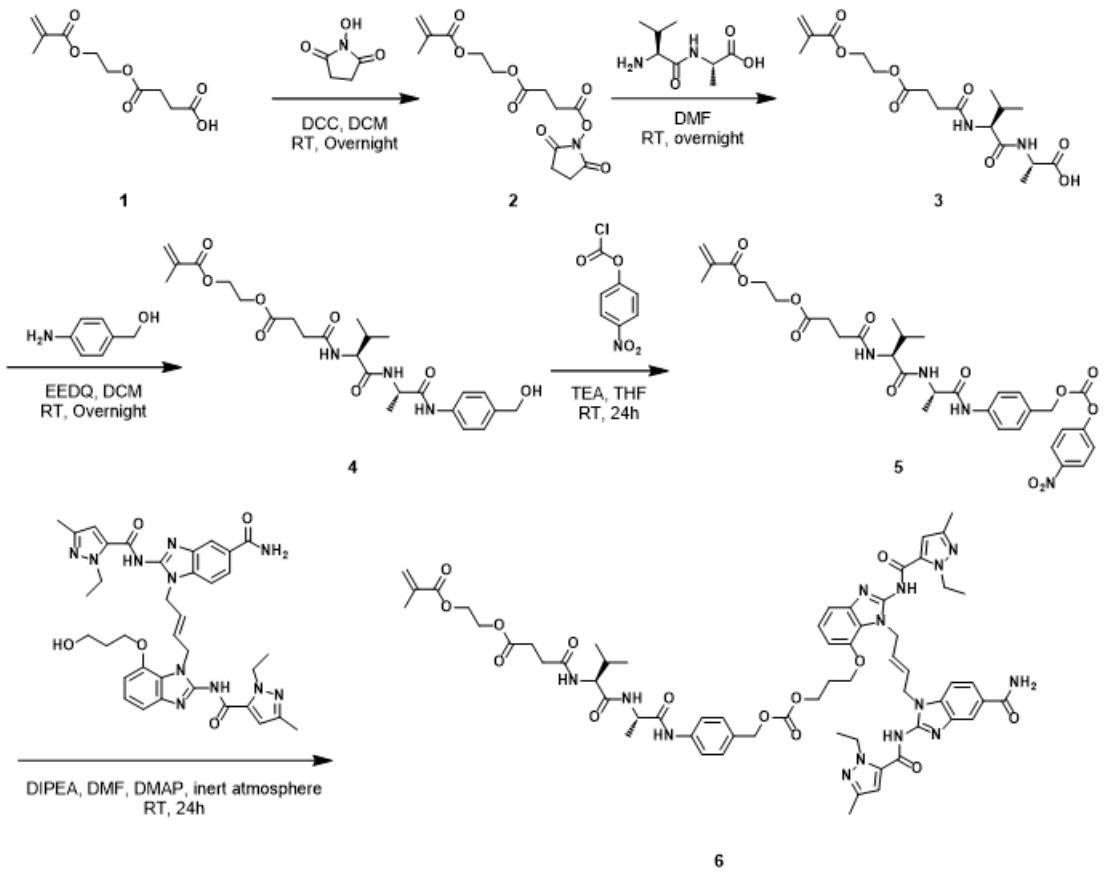

Scheme S4.1 - Synthesis of STING agonist prodrug monomer

Synthesis of SVA (Compound 3)

H-Val-Ala-OH (1.81 g, 9.63 mmol, 1 eq) was dissolved in DMF (22 mL). SMA-NHS/compound 2 (3.27 g, 10.0 mmol, 1.04 eq) was introduced to the stirring solution of VA. The reaction mixture was stirred overnight at room temperature and subsequently diluted with chloroform (300 mL), washed with ice-cold water (200 mL) and brine (15 mL), twice. The aqueous layer was back-extracted with 30 mL of chloroform and the combined organic layers were washed with 100 mL of water and 10 mL of brine. The organic layer was evaporated under reduced pressure to ca. 15 mL and precipitated into 1:1 (v/v) diethyl ether/pentane, and vortexed and centrifuged. SVA was obtained as a white pellet which was dried under in-house vacuum for 24 h to yield 2.81 g of SVA (73.1 % yield).

Synthesis of SVA-PAB-OH (Compound 4)

SVA (2.48g, 6.0 mmol, 1 eq) and PABA (0.88g, 7.2 mmol, 1.2 eq) were added into a round bottom flask and stirred in 50 mL DCM/MeOH (4:1) for 10 minutes. To the stirring solution, EEDQ (2.97g, 12.0 mmol, 2 eq) was slowly added over 5 minutes. The reaction mixture was allowed to stir overnight at room temperature. The reaction mixture was diluted with chloroform (100 mL) and extracted with water (70 mL) and brine (10 mL), twice. The aqueous layers were back-extracted with chloroform (30 mL). The combined organic layers were subsequently extracted with water and brine. The organic layer was concentrated, and the resultant viscous liquid was purified by silica gel column chromatography running 95:5 (v/v) chloroform:methanol. The SVA-PABA fractions (Rf = 0.6) were collected and precipitated into 1:1 (v/v) diethyl ether/pentane. The precipitate was vortexed and centrifuged and the pellet was dried under in-house vacuum overnight.

Synthesis of SVA-PAB-PNP (Compound 5)

SVA-PAB-OH (1.82 g, 3.6 mmol, 1 eq) and PNP-Cl (1.524 g, 7.56 mmol, 2.1 eq) were dissolved in 80 mL of THF. The solution was cooled in an ice bath before the addition of TEA (801.4 mg, 7.92 mmol, 2.2 eq). The mixture was stirred on ice for 30 minutes, and allowed to warm up to room temperature on its own accord for a total reaction time of 24 hours. The resultant reaction mixture was filtered to remove the TEA salt. The filtrate was concentrated to a thick yellow oil via rotary evaporation, precipitated into diethyl ether, vortexed and centrifuged. The pellet was collected by decanting the ether layer, taken up in 150 mL chloroform and washed with 100 mL water and 15 mL brine, respectively. The organic phase was dried over anhydrous sodium sulfate, before concentration and final precipitation in 1:1 (v/v) diethyl ether/pentane. Following centrifugation, the pellet was dried under in-house vacuum to yield 1.74 g of SVA-PAB-PNP (72.5% yield)

Synthesis of STING monomer (SVA-PAB-STING) (Compound 6)

To synthesize the final STING agonist prodrug monomer, STING Agonist-3 (280.8 g, 0.375 mmol, 1 eq) and SVA-PAB-PNP (301.8 mg, 0.45 mmol, 1.5 eq) were dissolved in 8.3 mL of anhydrous DMF (stored under inert atmosphere). The solution was sparged with argon, and cooled on an ice bath before the addition of DIPEA (242.3 mg, 1.875 mmol, 5 eq) and DMAP (45.8 mg, 0.46 mmol, 1.22 eq). The mixture was stirred on ice for 30 minutes, and then at room temperature for 24 hours. Thereafter, the mixture was diluted with 3:1 (v/v) CHCl3:iPrOH (35 mL) and washed three times with cold 2:1 (v/v) saturated NH4Cl:water (19 mL each time). The aqueous wash was back-extracted with 3:1 (v/v) CHCl3:iPrOH (10 mL). The combined organic layers were dried with anhydrous sodium sulfate. The organic phase was concentrated to a thick oil with high-vacuum rotary evaporation with a dry ice cold finger, and combined with 60A silica gel for dry column

loading. The monomer was purified using a CombiFlash NextGen 300 flash chromatography system running a binary dichloromethane and 10:1 (v/v) MeOH:NH4OH mobile phase (0-15% MeOH:NH4OH gradient over 15-20 minutes), collecting the second peak (Rf = 0.5 with 18% MeOH:NH4OH in DCM). The fractions were combined and subject to rotary evaporation to near-dryness (a thick gel) and completely evaporated with in-house vacuum for 2-3 days to yield 150-200 mg (30-40% yield) of SVA-PAB-STING.

It is noted that manual gradient column chromatography can also be employed (5-12% MeOH:NH4OH gradient with 2% increments every 100 mL mobile phase) with some co-eluted fractions. Running the reaction for extended amounts of time (72 h) decreased yield (around 50 mg, 10% yield).

For characterization, mass spectra were recorded on a Bruker EsquireLC Ion Trap (Bruker Corporation, Billerica, MA) Electrospray Ionization Mass Spectrometer instrument with direct injection in methanol (20 μg/mL) in negative ion mode. ^{1}H NMR spectra were recorded on a Bruker NEO 500 (Bruker Corporation, Billerica, MA) autosampler nuclear magnetic resonance (NMR) instrument in deuterated DMSO (DMSO-d6)

^{1}H NMR (500 MHz, DMSO-d6) δ 12.81 (s, 2H), 9.90 (s, 1H), 8.15 (d, *J* = 7.0 Hz, 1H), 8.01 – 7.90 (m, 3H), 7.71 (dd, *J* = 8.4, 1.7 Hz, 1H), 7.66 (s, 1H), 7.62 – 7.56 (m, 2H), 7.41 (d, *J* = 8.4 Hz, 1H), 7.34 – 7.27 (m, 4H), 6.53 (d, *J* = 10.3 Hz, 2H), 6.03 (s, 1H), 5.98 (dd, *J* = 13.3, 7.8 Hz, 1H), 5.76 – 5.66 (m, 2H), 5.01 (s, 2H), 4.94 (d, *J* = 5.3 Hz, 2H), 4.81 (d, *J* = 5.7 Hz, 2H), 4.52 (d, *J* = 6.9 Hz, 4H), 4.38 (p, *J* = 7.1 Hz, 1H), 4.26 (dt, *J* = 8.0, 4.1 Hz, 4H), 4.20 – 4.13 (m, 3H), 4.09 (t, *J* = 6.2 Hz, 2H), 3.78 (p, *J* = 6.1 Hz, 1H), 2.11 (d, *J* = 6.1 Hz, 5H), 1.97 (dt, *J* = 12.1, 6.4 Hz, 3H), 1.87 (d, *J* = 1.3 Hz, 3H), 1.33 – 1.23 (m, 9H), 1.05 (d, *J* = 6.1 Hz, 5H), 0.85 (dd, *J* = 17.6, 6.8 Hz, 6H), -0.06 (s, 1H).

4.4.3 Polymer synthesis

ManEMA (200 mg, 0.68 mmol, 35.7 eq), SVA-PAB-STING (55.9 mg, 0.044 mmol, 2.2 eq), were all dissolved in DMSO-d6 (0.34 mL) in a 5 mL oven-dried pear-shaped flask. Trioxane (15 mg) was added as an internal standard for monomer conversion calculations. Next, a stock solution (20.2 mg/mL in DMSO-d6) of the RAFT chain transfer agent ECT (0.25 mL, 5.05 mg, 0.019 mmol, 1 eq) was added. Thereafter, a stock solution of V70 (17.7 mg/mL in anhydrous DMF) was prepared and quickly added to the solution (0.05 mL, 0.88 mg, 0.0029 mmol, 0.15 eq). After taking a small aliquot (0.02 mL) for NMR conversion analysis, the reaction vessel was sealed with a septa and purged with argon gas for 30 minutes. The flask was then placed into an oil bath set to 42 C, and allowed to react for 22 hours. Upon completion, the reaction mixture was dialyzed against DMSO (500 mL) for 3 days using a SnakeSkin 3.5 kDa MWCO regenerated cellulose membrane, changing the DMSO twice daily. The reaction mixture was then dialyzed against ice-cold water (4C, 4000 mL) in a cold room for 2 days to remove DMSO, changing water twice daily. The dialysate was then lyophilized for 3 days to yield 188 mg (85% gravimetric conversion) of polySTING.

For the synthesis of rhodamine-labelled polySTING (polySTING-Rh), 3.8 mg of RhMA (0.0055 mmol, 0.38 eq) was added to the following: 0.48 mL DMSO-d6, 150 mg of ManEMA (0.51 mmol, 35.3 eq), 42.4 mg of SVA-PAB-STING (0.038 mmol, 2.3 eq), 3.82 mg of ECT (0.015 mmol, 1 eq) and 0.67 mg of V70 (0.0022 mmol, 0.15 eq). Following the addition of RhMA, the above protocol was exactly repeated.

4.4.4 Polymer Characterization

All ^{1}H NMR spectra were recorded on a Bruker NEO 500 (Bruker Corporation, Billerica, MA) autosampler nuclear magnetic resonance (NMR) instrument in deuterated DMSO (DMSO-d6). Drug incorporation into polymers was assessed by ^{1}H NMR analysis of a known polymer mass (typically >10mg in 600 uL solvent) and the internal standard levofloxacin (typically 1 mg/mL in solvent) (Levofloxacin δ 8.9 (s, 1H), STING δ 6.45 (d, 2H)). Polymer molecular weights (Mw, Mn) and polydispersity index (Đ = Mw/Mn) were determined by gel permeation chromatography (GPC). The system consisted of an Agilent 1260 HPLC stack running heated LiBr-supplemented (0.1% w/v) DMF mobile phase at a flow rate of 1 mL min^{-1} through a semi-prep three-column setup (Tosoh TSKGel alpha-4000 to Tosoh TSKGel alpha-300 to Phenomenex Phenogel 10^{3} A). Samples (10 mg/mL) were filtered through a 0.2 μm hydrophilic PTFE filter before analysis.

4.4.5 Formulation of STING treatments

For the free drug STING-3, the received powder was dissolved into sterile DMSO at 4 mg/mL with sonication, and stored at -20C until use, where it is diluted to *in vivo* concentrations with 1X DPBS. For the polymeric STING prodrug polySTING, the lyophilized powder was reconstituted in 1X DPBS at *in vivo* concentrations. All formulations were sterile-filtered through a 0.2 μm PVDF membrane before use.

4.4.6 Cell lines and animals

The B16F10 cell line was cultured in DMEM supplemented with 10% FBS and 1% P/S. The 4T1 cell line was cultured in RPMI supplemented with 10% FBS and 1% P/S. Cells were incubated at 37°C and 5% CO_2. Female C57BL/6 mice and female BALB/c mice aged 6 to 8 weeks were purchased from Charles River Laboratories and The Jackson Laboratories. All animal studies were

approved by the University of Washington Institutional Animal Care and Use Committee (IACUC).

4.4.7 Bone marrow-derived macrophage polarization

Bone marrow cells were extracted from murine femurs and tibias. Cells were seeded in 10 cm non-TC plates with plating media: DMEM + 10% FBS + 1% P/S + 20 ng/ml M-CSF. On day 4, 10 more ml of plating media was added per plate. On day 7, cells were polarized to either M1 using 100 ng/ml LPS + 20 ng/ml IFNγ, or M2 using 20 ng/ml IL-4. After a 48 hour incubation, M1 cells were treated with PBS and M2 cells were treated with either PBS, free STING, or polySTING at a concentration of 20 μg/ml. After a 24 hour incubation, cells were stained for viability with Zombie NIR, blocked with anti-CD16/32, and finally stained with anti-CD206-PerCP-eFluor710, anti-CD11b-FITC, anti-CD163-PE, and anti-CD86-BV510. An Attune NxT flow cytometer was used to analyze the data.

4.4.8 Toxicity study

Female BALB/c mice were injected with free STING at 30μg and polySTING at 10, 20 and 30 μg (STING equivalent) on days 0 and 4, and were observed for signs of decrease in activity, hunched posture and weight loss.

4.4.9 ELISA for cytokine quantification

Female C57BL/6 mice were injected with 30 μg free drug STING agonist-3 or polySTING containing 10, 20 or 30 μg of STING agonist-3 through the tail vein. Blood was collected through tail vein 4 h post injection in EDTA-treated tubes. Blood was spun down for 10 min at 1000 g and upper layer plasma was collected for ELISA to measure IFNβ expression level (Invivogen).

4.4.10 Interferon-stimulated gene expression

Female BALB/c mice with 4T1 tumors around 100-200 mm^3 were injected with PBS or 30 μg free STING agonist-3 or 30 μg (STING equivalent) polySTING through the tail vein. Tumors were collected 24 hr post injection. Female C57BL/6 mice with B16F10 tumors around 100-200 mm^3 were injected with PBS or 10 μg free STING agonist-3 or 10 μg polySTING through the tail vein, twice, 4 days apart. TDLNs were collected 24 hr post 2nd injection. RNA was extracted from tumor tissues or TDLN cells using Trizol or RNeasy mini kit (Qiagen). cDNA was synthesized using the high capacity cDNA reverse transcription kit (Applied Biosystems). qPCR was performed to analyze the amount of cDNA. Ifnb1 and cxcl10 expressions were normalized to the GAPDH housekeeping gene. The DNA primers were used as follows: GAPDH: AATGGATTTGGACGCATTGGT; TTTGCACTGGTACGTGTTGAT. Ifnb1: AGCTCCAAGAAAGGACGAACA; GCCCTGTAGGTGAGGTTGAT. Cxcl10: CCAAGTGCTGCCGTCATTTTC; GGCTCGCAGGGATGATTTCAA.

4.4.11 Tissue processing

Tumors were cut into small pieces, treated with 20 U/mL type IV collagenase + 125 U/mL DNase I, and dissociated with the GentleMACS Dissociator. Tumors were then incubated on a rotating platform at 37 °C for 30 min. Single-cell suspensions were obtained by passing homogenate through a 70 μm cell strainer. Cells were treated with the ACK lysing buffer to remove red blood cells. Inguinal lymph nodes were dissociated with pipette tips and digested with 50 U/mL type IV collagenase + 100 U/mL DNase I. Cells were incubated at 37 °C for 30 min with gentle agitation. Single-cell suspensions were obtained by passing homogenate through a 70 μm cell strainer.

4.4.12 Tumor cellular uptake studies

Female C57BL/6 mice were inoculated with 2×10^5 B16F10 cells in the right-hind flank on day -8. On day 0 (tumor volume approx. 100-200 mm3), they were treated with either PBS or polySTING-Rhod (10 μg STING equivalent) through tail-vein injection. 30 minutes post-administration, tumors were harvested and made into single-cell suspension as described previously. Cells were stained for viability with Zombie Violet viability kit, blocked with Trustain anti-mouse CD16/32, and then stained with anti-CD45-APC/Cy7, anti-CD11c-FITC or anti-F4/80-FITC. An Attune NxT flow cytometer was used to analyze the data.

4.4.13 Tumor-infiltrating lymphocytes (TIL) and TDLN analysis

Female C57BL/6 mice were inoculated with 2×10^5 B16F10 cells in the right-hind flank on day -8. On days 0 (tumor volume approx. 100-200 mm3) and 4, they were treated with either PBS or polySTING (10 μg STING equivalent) through tail-vein injections. On day 5, tumors and the tumor-draining lymph nodes (TDLNs, inguinal LN in the same flank as tumor) were harvested. Tissues were made into single-cell suspension as previously described.

Tumor cells were stained for viability with Zombie Violet viability kit, blocked with Trustain anti-mouse CD16/32, and then stained in three plates for T cells (anti-CD45-APC/Cy7, anti-CD3-PE/Cy5, anti-CD4-PE, anti-CD8-FITC), macrophages (anti-CD45-APC/Cy7, anti-F4/80-FITC, anti-CD80-PE, anti-CD206-BV605), and DCs (anti-CD45-APC/Cy7, anti-CD11c-FITC, anti-CD80-PE, anti-MHCII-PE/Cy5). In a separate study, tumor cells were stained for viability with Zombie NIR viability kit, blocked with Trustain anti-mouse CD16/32, and then stained in two plates for DCs (anti-CD11c-APC, anti-CD8-FITC, anti-CD103-PE, anti-CD86-BV510) and T cells (anti-CD3-PE/Cy5, anti-CD8-FITC, anti-TCF1-PE, anti-PD1-eFluor450).

TDLN cells were stained for viability with Zombie NIR viability kit, blocked with anti-mouse CD16/32, and then stained in two plates for DCs (anti-CD11c-APC, anti-CD8-FITC, anti-CD103-PE, anti-CD86-BV510) and T cells (anti-CD3-eFluor450, anti-CD4-PE, anti-CD8-FITC). In a separate study with 30 μg STING agonists and a single tail-vein injection, TDLN cells were stained for viability with Zombie NIR viability kit, blocked with anti-mouse CD16/32, and then stained in with anti-CD11c-APC, anti-CD86-BV510, anti-CD40-FITC and anti-CD80-PE. An Attune NxT flow cytometer was used to analyze the data.

4.4.14 Therapeutic studies

For the B16F10 tumor model, female C57BL/6 mice were inoculated with 2×10^5 B16F10 cells in the right-hind flank on day -8. On days 0, 4, and 8, mice were treated intravenously (tail vein on days 0, 4, and retro-orbitally on day 8) with PBS, or either free STING or polySTING with an equivalent STING agonist dose of 10 μg. For the 4T1 tumor model, female BALB/c mice were inoculated with 5×10^5 4T1 cells in the mammary fat pad on day -8. On days 0, 7, and 14, mice were treated intravenously (tail vein on days 0, 7, and retro-orbitally on day 14) with PBS, or either free STING or polySTING with an equivalent STING agonist dose of 10 μg. On days 1, 8, and 15, mice were injected with 100 μg of anti PD-1 ICB via intraperitoneal injection. Tumor length and width were then measured using a vernier caliper, and volume was subsequently calculated using the formula: Volume = $(\text{Width}^2 \times \text{Length}) \div 2$. Weight was measured the same time as tumor measurements. Mice were euthanized if total tumor volume exceeded 2000 mm^3 for B16F10 tumors, and 1500 mm^3 for 4T1 tumors, visible discharge was observed on ulcers of the tumors, signs of mortality such as excessive lethargy, or the body weight loss exceeded 20%.

4.4.15 Statistical analysis

Statistical analysis was performed using the Graphpad Prism software. One-way ANOVA with post-hoc Tukey HSD test was used to compare more than two groups. Log-rank test was used for survival analysis.

4.5 ACKNOWLEDGEMENTS

K.S. and D.C.N. contributed equally to this work. This work was supported by the U.S. National Institutes of Health, National Cancer Institute Grant R01CA257563 (S.H.P. and P.S.S.), and the U.S. National Institutes of Health National Institute of Allergy & Infectious Diseases Grant R01AI134729 (P.S.S.). NMR data from this work was also supported by the U.S. National Institutes of Health Grant S10 OD030224-01A1, which funded the NEO 500 instrument used. We thank Prof. Hao Yuan Kueh for providing anti-TCF-1 and anti-PD-1 antibodies.

4.6 REFERENCES

[1] Mellman, I., Coukos, G. & Dranoff, G. Cancer immunotherapy comes of age. Nature 480, 480–489 (2011).

[2] Robert, C. A decade of immune-checkpoint inhibitors in cancer therapy. Nat. Commun. 11, 3801 (2020).

[3] Hong, M., Clubb, J. D. & Chen, Y. Y. Engineering CAR-T Cells for Next-Generation Cancer Therapy. Cancer Cell 38, 473–488 (2020).

[4] Demaria, O. et al. Harnessing innate immunity in cancer therapy. Nature 574, 45–56 (2019).

[5] Chen, Q., Sun, L. & Chen, Z. J. Regulation and function of the cGAS–STING pathway of cytosolic DNA sensing. Nat. Immunol. 17, 1142–1149 (2016).

[6] Zhu, Y. et al. STING: a master regulator in the cancer-immunity cycle. Mol. Cancer 18, 1–15 (2019).

[7] Chen, D. S. & Mellman, I. Oncology Meets Immunology: The Cancer-Immunity Cycle. Immunity 39, 1–10 (2013).

[8] Hines, J. B., Kacew, A. J. & Sweis, R. F. The Development of STING Agonists and Emerging Results as a Cancer Immunotherapy. Curr. Oncol. Rep. 25, 189–199 (2023).

[9] Petrovic, M., Borchard, G. & Jordan, O. Considerations for the delivery of STING ligands in cancer immunotherapy. J. Controlled Release 339, 235–247 (2021).

[10] Meric-Bernstam, F. et al. Phase I Dose-Escalation Trial of MIW815 (ADU-S100), an Intratumoral STING Agonist, in Patients with Advanced/Metastatic Solid Tumors or Lymphomas. Clin. Cancer Res. 28, 677–688 (2022).

[11] Ramanjulu, J. M. et al. Design of amidobenzimidazole STING receptor agonists with systemic activity. Nature 564, 439–443 (2018).

[12] Pan, B.-S. et al. An orally available non-nucleotide STING agonist with antitumor activity. Science 369, (2020).

[13] Chin, E. N. et al. Antitumor activity of a systemic STING-activating non-nucleotide cGAMP mimetic. Science 369, 993–999 (2020).

[14] Garland, K. M., Sheehy, T. L. & Wilson, J. T. Chemical and Biomolecular Strategies for STING Pathway Activation in Cancer Immunotherapy. Chem. Rev. 122, 5977–6039 (2022).

[15] Dane, E. L. et al. STING agonist delivery by tumour-penetrating PEG-lipid nanodiscs primes robust anticancer immunity. Nat. Mater. 21, 710–720 (2022).

[16] Wehbe, M. et al. Nanoparticle delivery improves the pharmacokinetic properties of cyclic dinucleotide STING agonists to open a therapeutic window for intravenous administration. J. Controlled Release 330, 1118–1129 (2021).

[17] Wang-Bishop, L. et al. STING-activating nanoparticles normalize the vascular-immune interface to potentiate cancer immunotherapy. Sci. Immunol. 8, eadd1153 (2023).

[18] Go, E.-J. et al. Systemic Delivery of a STING Agonist-Loaded Positively Charged Liposome Selectively Targets Tumor Immune Microenvironment and Suppresses Tumor Angiogenesis. Small n/a, 2300544 (2023).

[19] Chen, X. et al. Chemically programmed STING-activating nano-liposomal vesicles improve anticancer immunity. Nat. Commun. 14, 4584 (2023).

[20] Sun, X. et al. Amplifying STING activation by cyclic dinucleotide–manganese particles for local and systemic cancer metalloimmunotherapy. Nat. Nanotechnol. 1–11 (2021) doi:10.1038/s41565-021-00962-9.

[21] Dosta, P. et al. Investigation of the enhanced antitumour potency of STING agonist after conjugation to polymer nanoparticles. Nat. Nanotechnol. 1–13 (2023) doi:10.1038/s41565-023-01447-7.

[22] Wu, Y. et al. Tumor-targeted delivery of a STING agonist improves cancer immunotherapy. Proc. Natl. Acad. Sci. 119, e2214278119 (2022).

[23] Gordon, M. R. et al. Field Guide to Challenges and Opportunities in Antibody–Drug Conjugates for Chemists. Bioconjug. Chem. 26, 2198–2215 (2015).

[24] Lemos, H. et al. STING Promotes the Growth of Tumors Characterized by Low Antigenicity via IDO Activation. Cancer Res. 76, 2076–2081 (2016).

[25] Sokolowska, O. & Nowis, D. STING Signaling in Cancer Cells: Important or Not? Arch. Immunol. Ther. Exp. (Warsz.) 66, 125–132 (2018).

[26] Sivick, K. E. et al. Magnitude of Therapeutic STING Activation Determines CD8+ T Cell-Mediated Anti-tumor Immunity. Cell Rep. 25, 3074-3085.e5 (2018).

[27] Jneid, B. et al. Selective STING stimulation in dendritic cells primes antitumor T cell responses. Sci. Immunol. 8, eabn6612 (2023).

[28] Theisen, D. J. et al. Batf3-Dependent Genes Control Tumor Rejection Induced by Dendritic Cells Independently of Cross-Presentation. Cancer Immunol. Res. 7, 29–39 (2019).

[29] Hildner, K. et al. Batf3 Deficiency Reveals a Critical Role for CD8α+ Dendritic Cells in Cytotoxic T Cell Immunity. Science 322, 1097–1100 (2008).

[30] Spranger, S., Dai, D., Horton, B. & Gajewski, T. F. Tumor-Residing Batf3 Dendritic Cells Are Required for Effector T Cell Trafficking and Adoptive T Cell Therapy. Cancer Cell 31, 711-723.e4 (2017).

[31] Sánchez-Paulete, A. R. et al. Cancer Immunotherapy with Immunomodulatory Anti-CD137 and Anti–PD-1 Monoclonal Antibodies Requires BATF3-Dependent Dendritic Cells. Cancer Discov. 6, 71–79 (2016).

[32] Mellman, I., Chen, D. S., Powles, T. & Turley, S. J. The cancer-immunity cycle: Indication, genotype, and immunotype. Immunity 56, 2188–2205 (2023).

[33] Thim-Uam, A. et al. STING Mediates Lupus via the Activation of Conventional Dendritic Cell Maturation and Plasmacytoid Dendritic Cell Differentiation. iScience 23, 101530 (2020).

[34] Doshi, A. S., Cantin, S., Prickett, L. B., Mele, D. A. & Amiji, M. Systemic nano-delivery of low-dose STING agonist targeted to CD103+ dendritic cells for cancer immunotherapy. J. Controlled Release 345, 721–733 (2022).

[35] Lv, S. et al. Well-Defined Mannosylated Polymer for Peptide Vaccine Delivery with Enhanced Antitumor Immunity. Adv. Healthc. Mater. 11, 2101651 (2022).

[36] Tiberghien, A. C. et al. Design and Synthesis of Tesirine, a Clinical Antibody–Drug Conjugate Pyrrolobenzodiazepine Dimer Payload. ACS Med. Chem. Lett. 7, 983–987 (2016).

[37] Christofides, A. et al. The complex role of tumor-infiltrating macrophages. Nat. Immunol. 23, 1148–1156 (2022).

[38] Marciscano, A. E. & Anandasabapathy, N. The role of dendritic cells in cancer and anti-tumor immunity. Semin. Immunol. 52, 101481 (2021).

[39] Pokatayev, V. et al. Homeostatic regulation of STING protein at the resting state by stabilizer TOLLIP. Nat. Immunol. 21, 158–167 (2020).

[40] Wang-Bishop, L. et al. Potent STING activation stimulates immunogenic cell death to enhance antitumor immunity in neuroblastoma. J. Immunother. Cancer 8, e000282 (2020).

[41] Ohkuri, T. et al. Intratumoral administration of cGAMP transiently accumulates potent macrophages for anti-tumor immunity at a mouse tumor site. Cancer Immunol. Immunother. 66, 705–716 (2017).

[42] Downey, C. M., Aghaei, M., Schwendener, R. A. & Jirik, F. R. DMXAA Causes Tumor Site-Specific Vascular Disruption in Murine Non-Small Cell Lung Cancer, and like the Endogenous Non-Canonical Cyclic Dinucleotide STING Agonist, 2′3′-cGAMP, Induces M2 Macrophage Repolarization. PLOS ONE 9, e99988 (2014).

[43] Lechner, M. G. et al. Immunogenicity of murine solid tumor models as a defining feature of in vivo behavior and response to immunotherapy. J. Immunother. Hagerstown Md 1997 36, 477–489 (2013).

[44] Chen, D. S. & Mellman, I. Elements of cancer immunity and the cancer-immune set point. Nature 541, 321–330 (2017).

[45] Xia, A., Zhang, Y., Xu, J., Yin, T. & Lu, X.-J. T Cell Dysfunction in Cancer Immunity and Immunotherapy. Front. Immunol. 10, (2019).

[46] Roberts, E. W. et al. Critical Role for CD103+/CD141+ Dendritic Cells Bearing CCR7 for Tumor Antigen Trafficking and Priming of T Cell Immunity in Melanoma. Cancer Cell 30, 324–336 (2016).

[47] den Haan, J. M. M., Lehar, S. M. & Bevan, M. J. Cd8+ but Not Cd8− Dendritic Cells Cross-Prime Cytotoxic T Cells in Vivo. J. Exp. Med. 192, 1685–1696 (2000).

[48] Liang, Y., Hannan, R. & Fu, Y.-X. Type I IFN Activating Type I Dendritic Cells for Antitumor Immunity. Clin. Cancer Res. 27, 3818–3824 (2021).

[49] Fuertes, M. B. et al. Host type I IFN signals are required for antitumor CD8+ T cell responses through CD8α+ dendritic cells. J. Exp. Med. 208, 2005–2016 (2011).

[50] Inozume, T. et al. Selection of CD8+PD-1+ lymphocytes in fresh human melanomas enriches for tumor-reactive T-cells. J. Immunother. Hagerstown Md 1997 33, 956–964 (2010).

[51] Wen, S. et al. TCF-1 maintains CD8+ T cell stemness in tumor microenvironment. J. Leukoc. Biol. 110, 585–590 (2021).

[52] Im, S. J. et al. Defining CD8+ T cells that provide the proliferative burst after PD-1 therapy. Nature 537, 417–421 (2016).

[53] Jubel, J. M., Barbati, Z. R., Burger, C., Wirtz, D. C. & Schildberg, F. A. The Role of PD-1 in Acute and Chronic Infection. Front. Immunol. 11, (2020).

[54] Li, A. et al. Activating cGAS-STING pathway for the optimal effect of cancer immunotherapy. J. Hematol. Oncol.J Hematol Oncol 12, 35 (2019).

[55] Del Prete, A. et al. Dendritic cell subsets in cancer immunity and tumor antigen sensing. Cell. Mol. Immunol. 20, 432–447 (2023).

[56] Ruhland, M. K. et al. Visualizing Synaptic Transfer of Tumor Antigens among Dendritic Cells. Cancer Cell 37, 786-799.e5 (2020).

[57] Broz, M. L. et al. Dissecting the Tumor Myeloid Compartment Reveals Rare Activating Antigen-Presenting Cells Critical for T Cell Immunity. Cancer Cell 26, 638–652 (2014).

[58] du Bois, H., Heim, T. A. & Lund, A. W. Tumor-draining lymph nodes: At the crossroads of metastasis and immunity. Sci. Immunol. 6, eabg3551 (2021).

[59] Boukhaled, G. M., Harding, S. & Brooks, D. G. Opposing Roles of Type I Interferons in Cancer Immunity. Annu. Rev. Pathol. 16, 167–198 (2021).

4.7 SUPPORTING INFORMATION

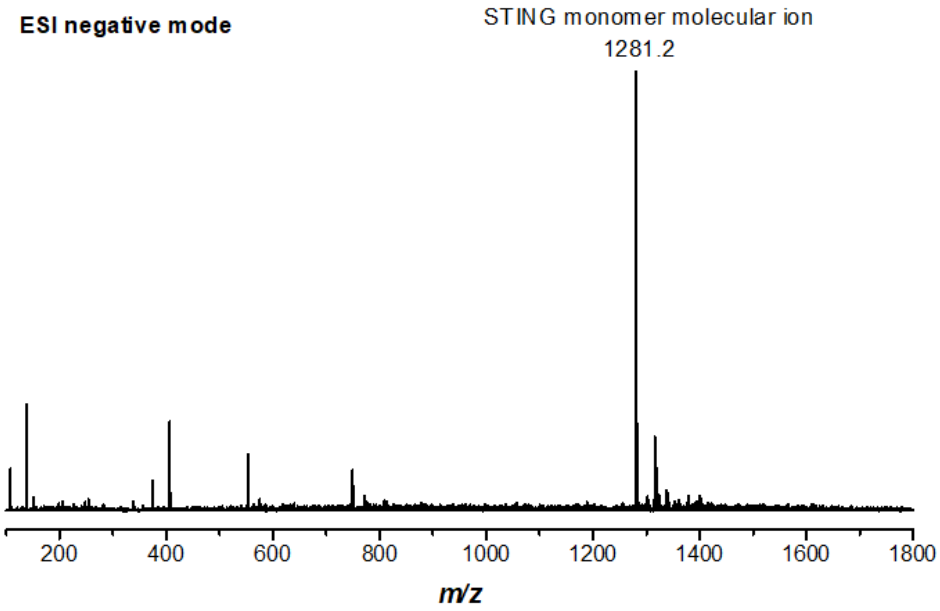

Figure S 4.1 Mass spectrum of SVA-PAB-STING (Compound 6) in methanol.

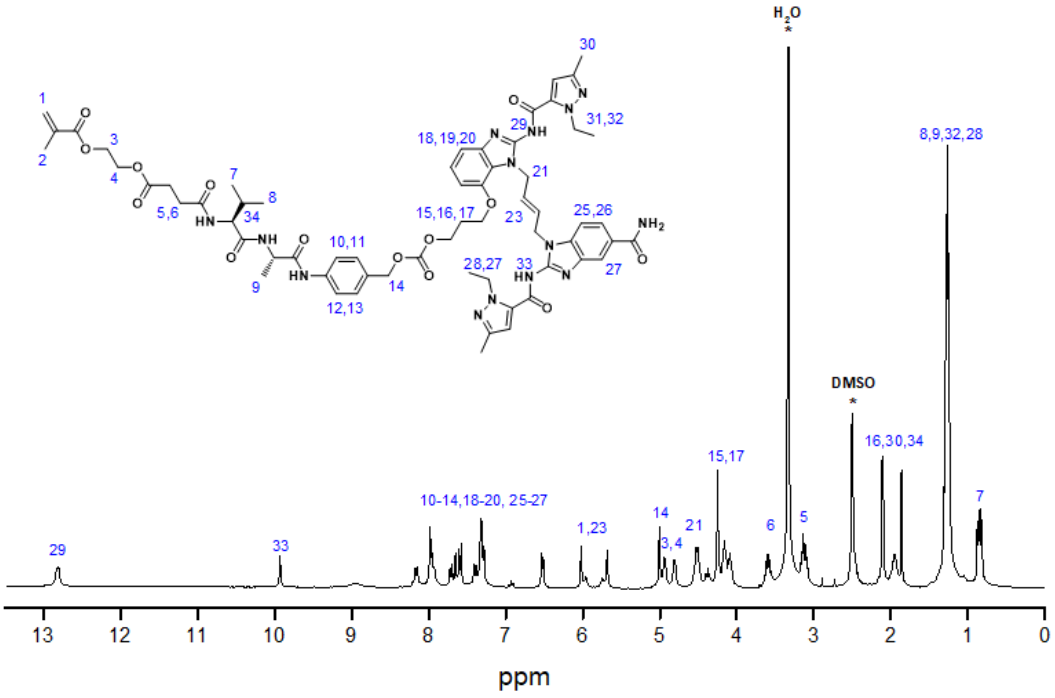

Figure S 4.2 ^{1}H-NMR spectrum of SVA-PAB-STING (Compound 6) in DMSO-d6.

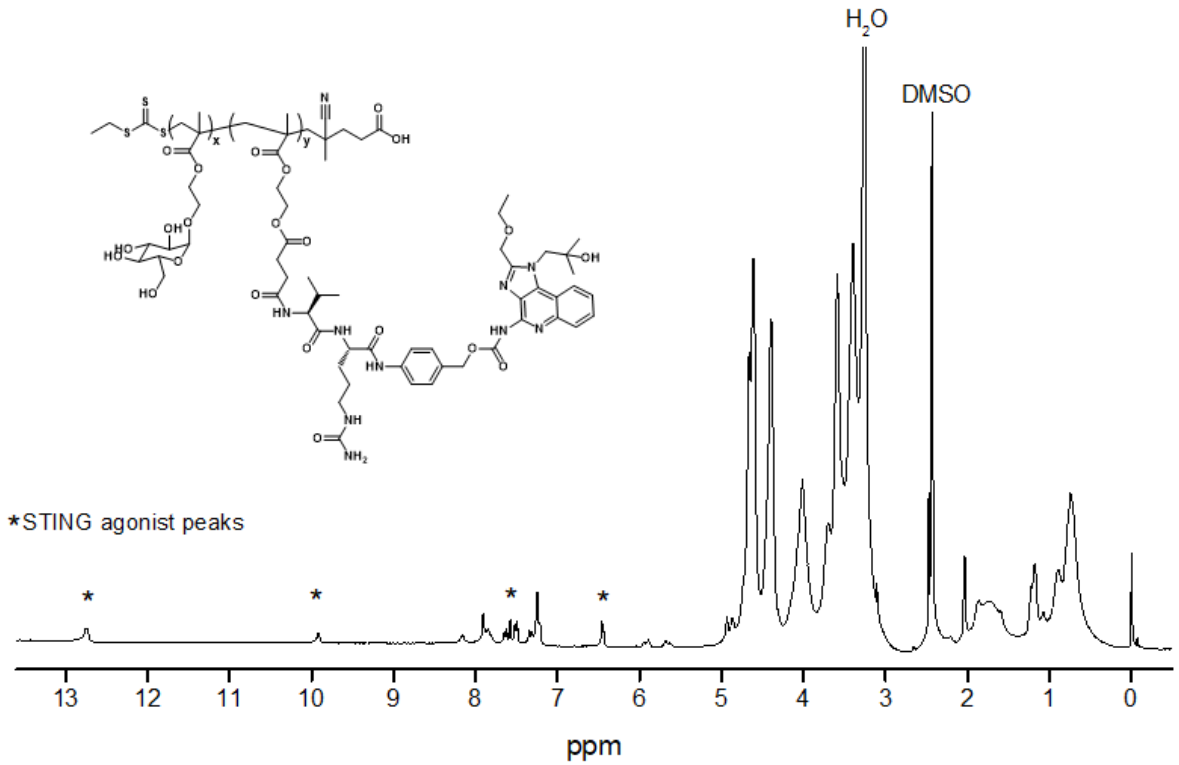

Figure S 4.3 ^{1}H-NMR spectrum of polySTING in DMSO-d6.

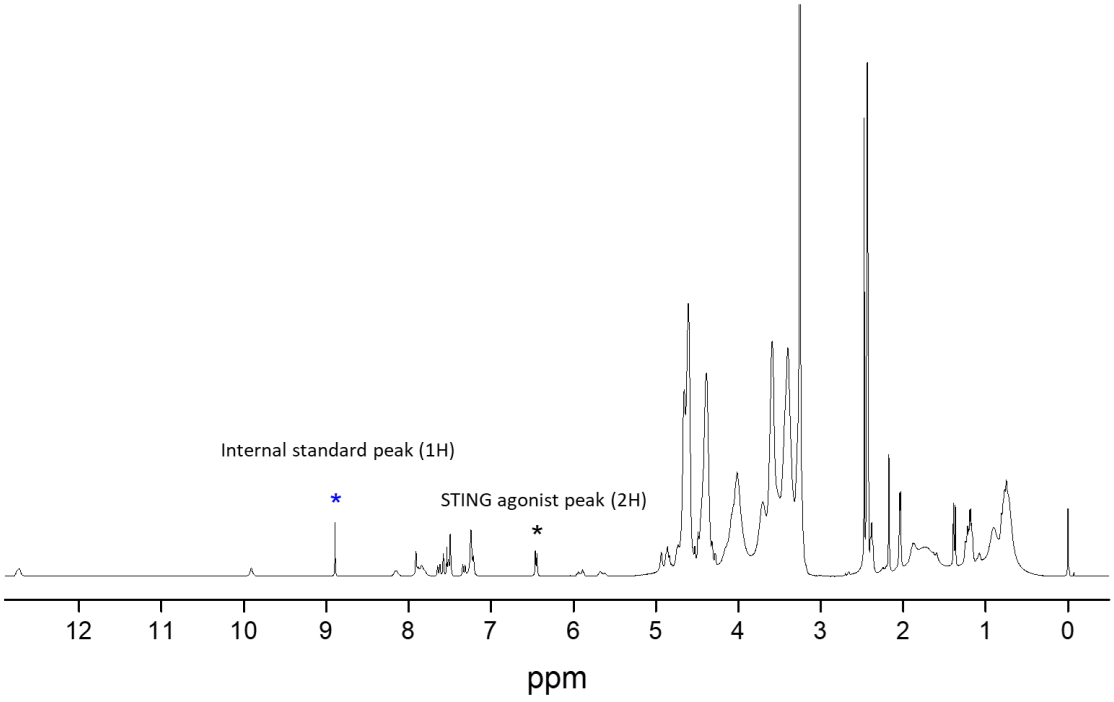

Figure S 4.4 ^{1}H-NMR spectrum of polySTING and levofloxacin internal standard.

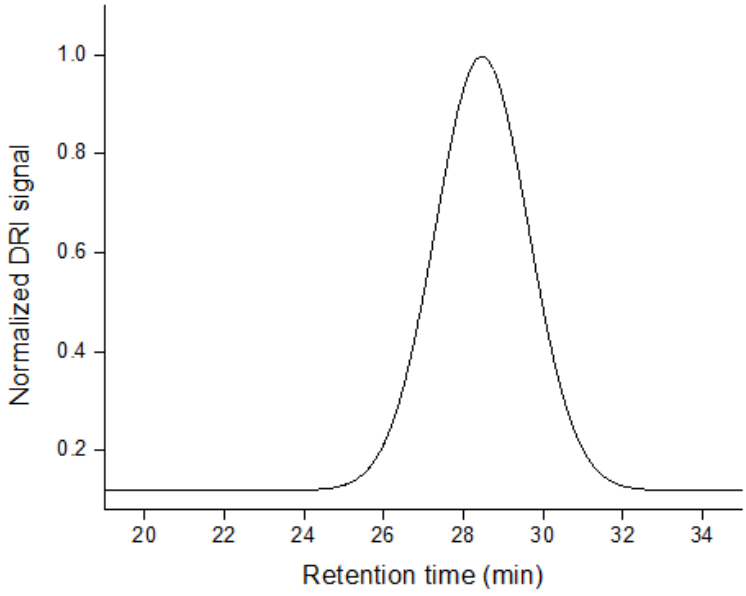

Figure S 4.5 GPC spectrum of polySTING in supplemented DMF (1 g/L LiBr).

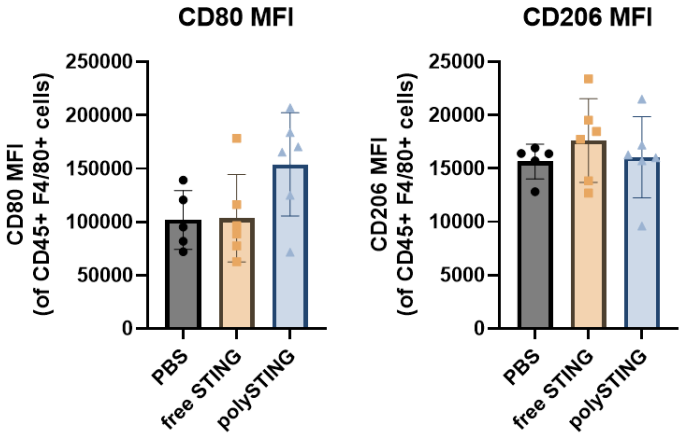

Figure S 4.6 *In vivo* tumor-associated macrophage polarization.

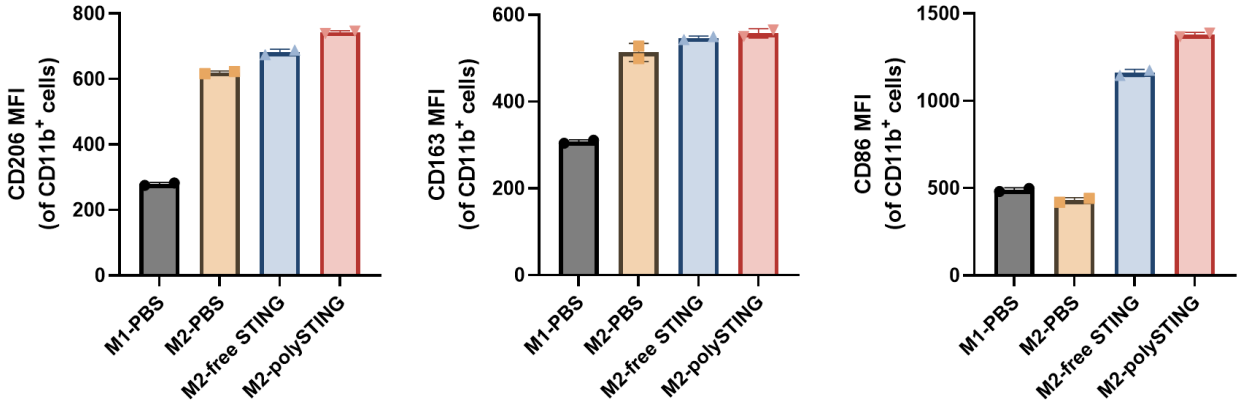

Figure S 4.7 *In vitro* tumor-associated macrophage polarization.

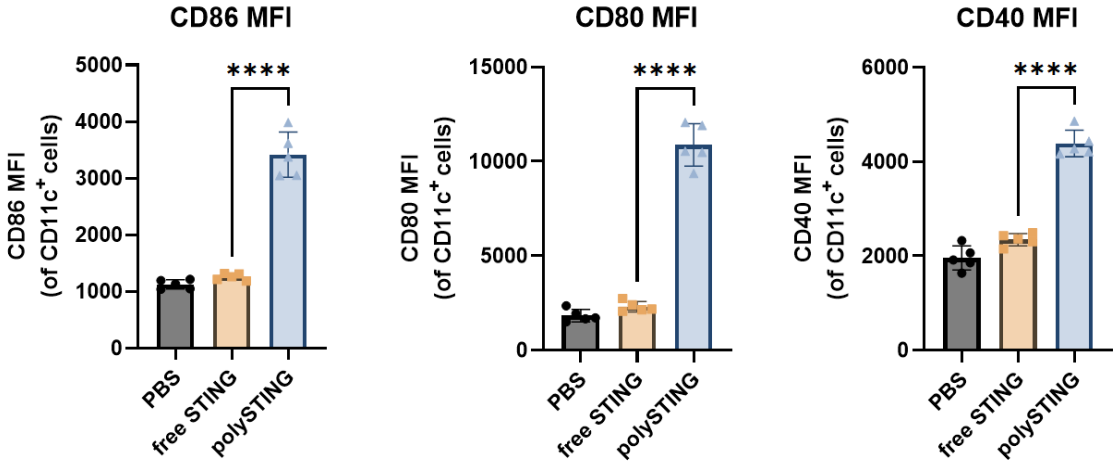

Figure S 4.8 *In vivo* DC maturation in TDLNs

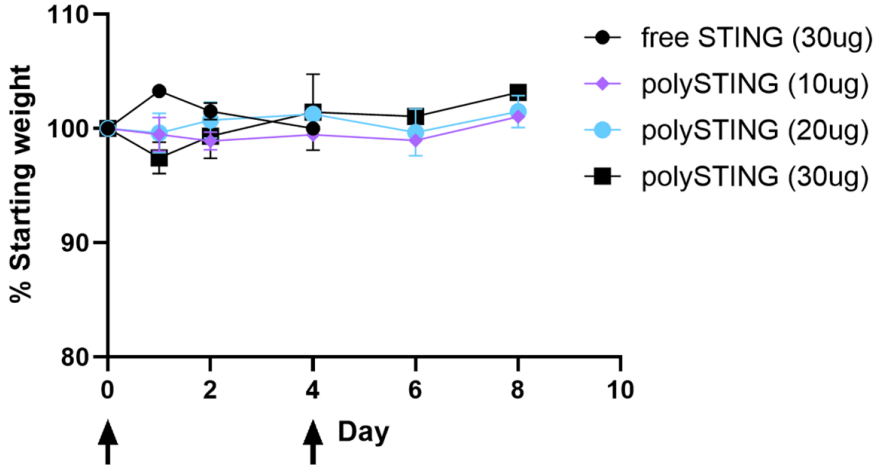

Figure S 4.9 Weight loss in non-tumor bearing mice.

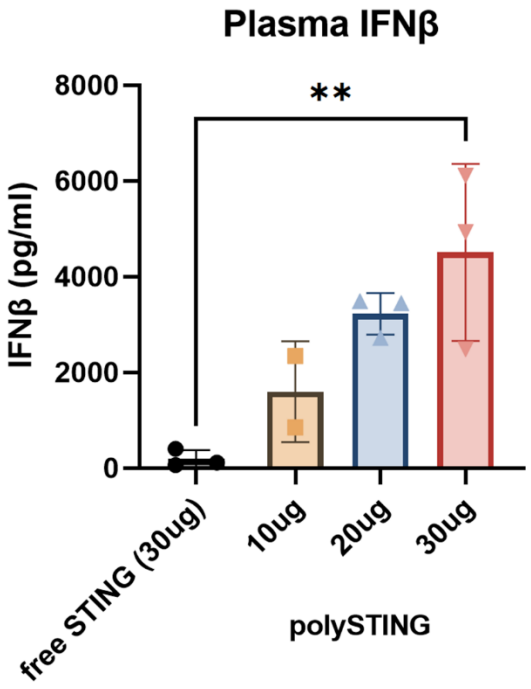

Figure S 4.10 Plasma IFNβ level in healthy C57BL/6 mice 4 h post treatment with free STING and polySTING at different doses (N=3).

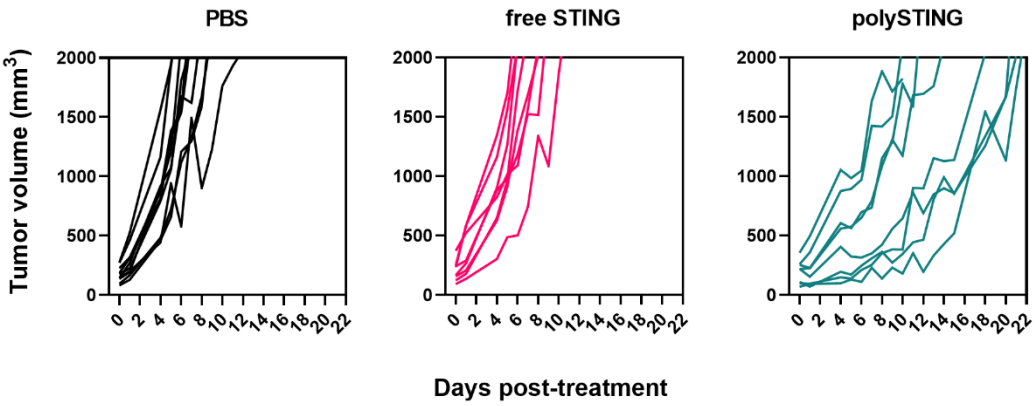

Figure S 4.11 Individual tumor growth curves for B16F10 tumor reduction study.

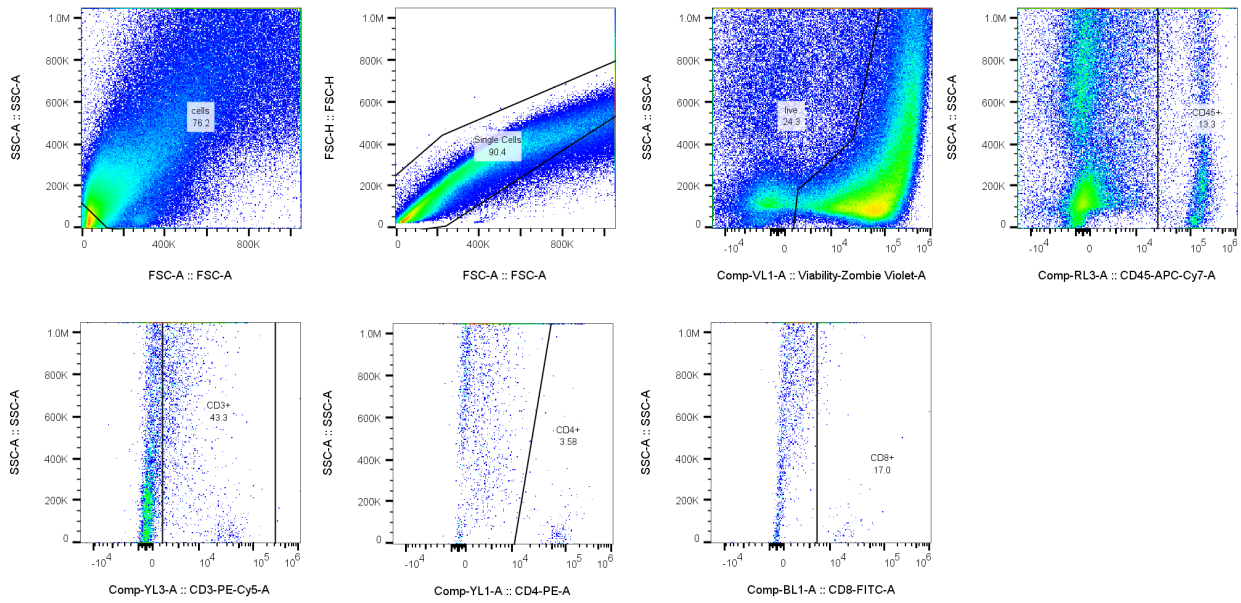

Figure S 4.12 Gating on tumor-infiltrating CD4$^+$ and CD8$^+$ T cells.

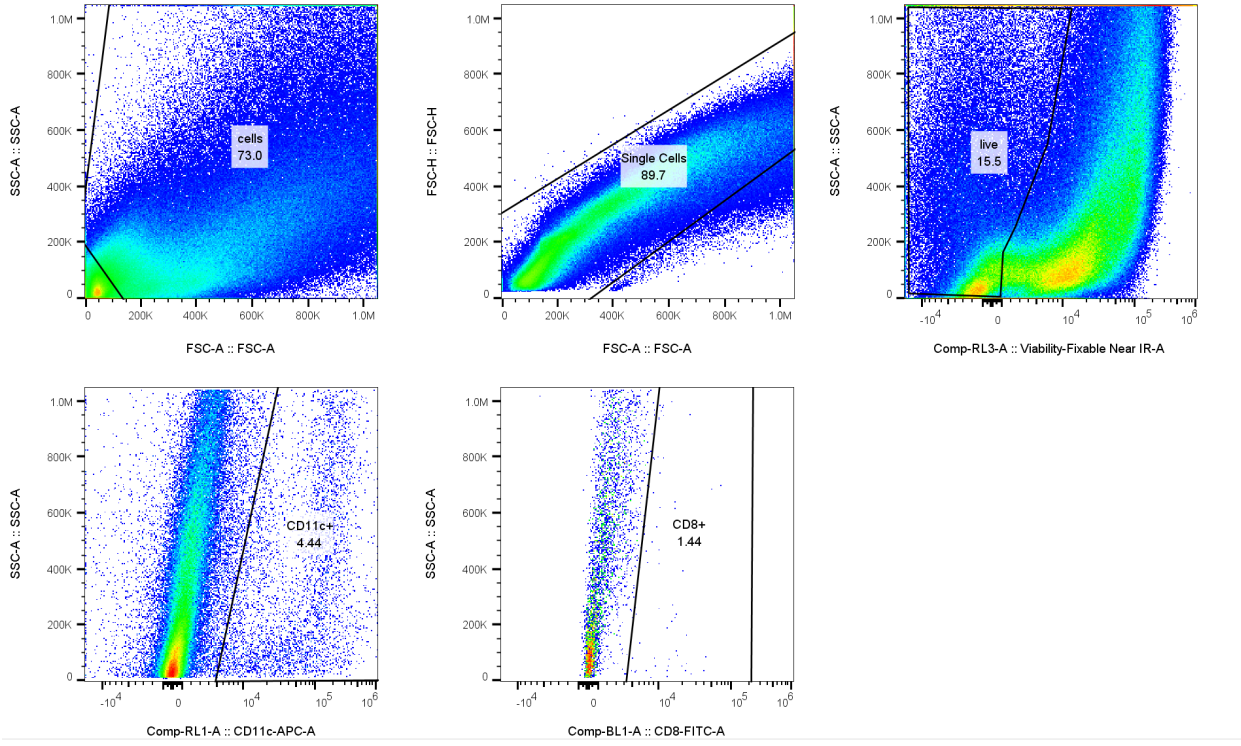

Figure S 4.13 Gating on CD8$^+$ CD11c$^+$ DCs in tumors.

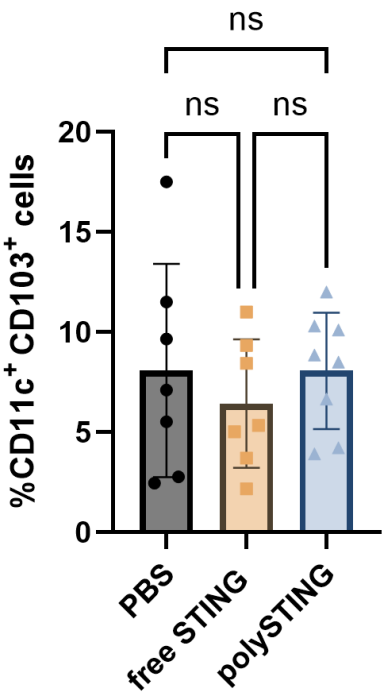

Figure S 4.14 Assessment of CD11c$^+$ CD103$^+$ DCs in the TME

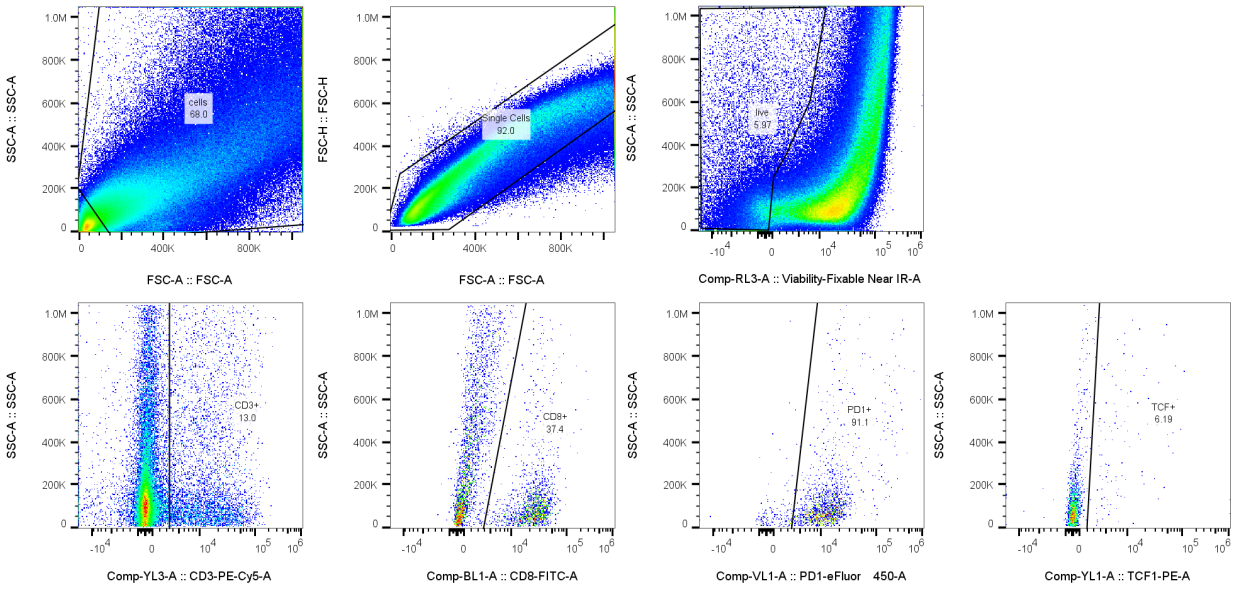

Figure S 4.15 Gating on TCF-1$^+$, PD-1$^+$ CD8$^+$ T cells in tumors.

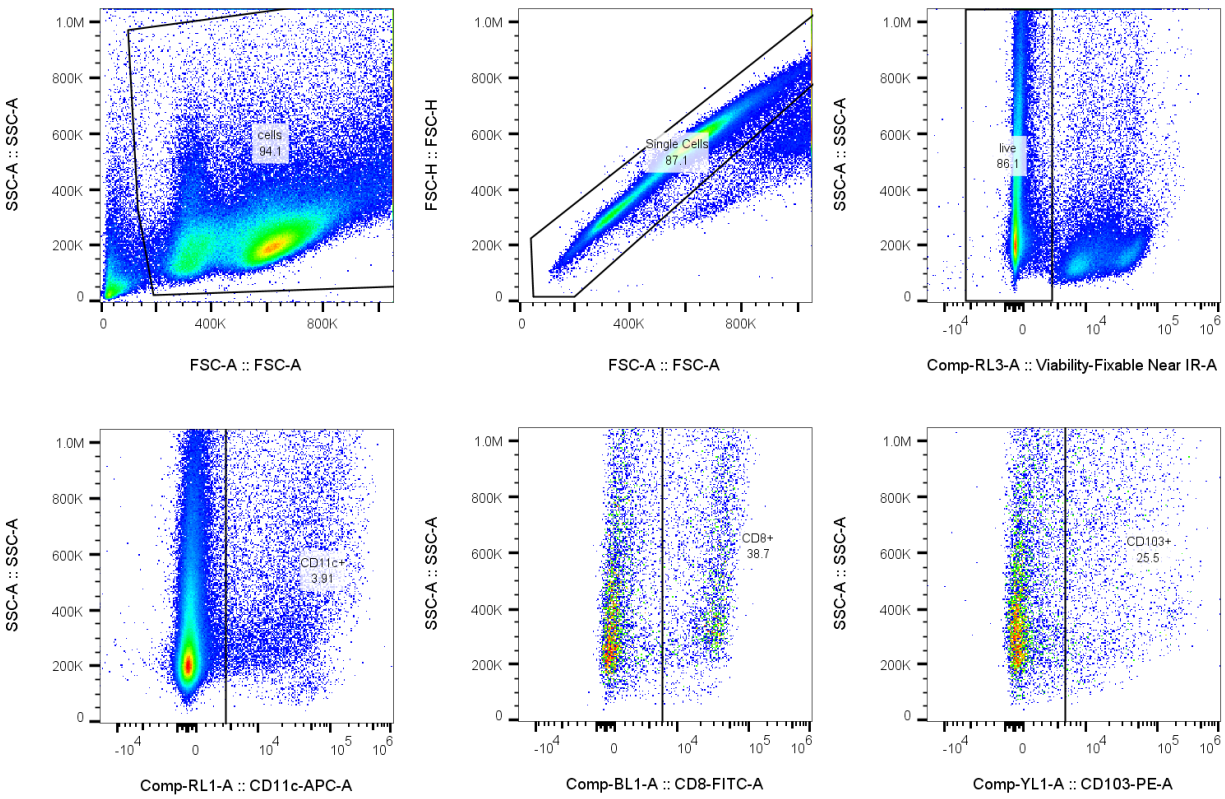

Figure S 4.16 Gating on CD8$^+$, CD103$^+$ DCs in TDLN.

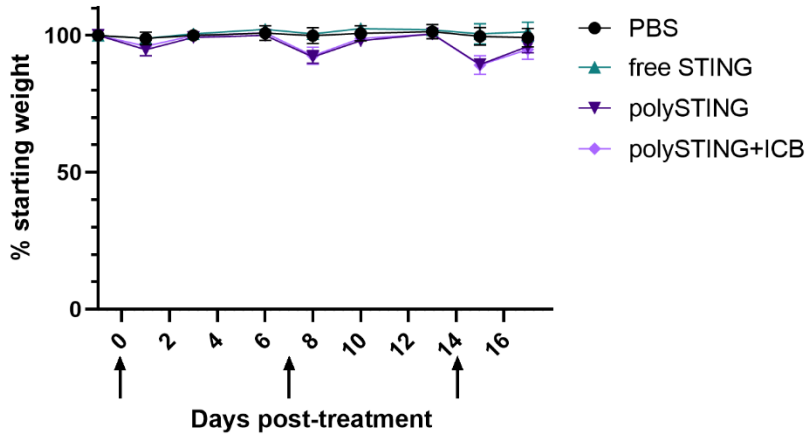

Figure S 4.17 Weight loss in 4T1 study

Chapter 5 : Peptide Vaccine Formulations with Structurally Distinct STING Agonist Drugamers Induce Discrete, Efficacious Antitumor Responses[6]

Kefan Song, Dinh Chuong Nguyen*, Yonghui Wang, Simbarashe Jokonya, Omeed Yazdani, Drew L. Sellers, Patrick S. Stayton, and Suzie H. Pun*

ABSTRACT

Peptide therapeutic cancer vaccines are an attractive treatment modality for their safety and manufacturability, but have been hindered in clinical translation by low immunogenicity and insufficient $CD8^+$ T cell activation. We developed Virus Inspired Polymers for Endosomal Release (VIPER) to address systemic and intracellular delivery obstacles, but durable antitumor immunity remained elusive. Adjuvants stimulating innate immunity, such as Stimulator of Interferon Genes (STING) agonists, can enhance vaccine potency but risks systemic toxicity and improper immune activation. We developed STING "drugamers" with cathepsin-cleavable linkers and dendritic cell (DC)-targeting moieties for intracellular delivery of STING agonists to DCs. We explored two different STING drugamer structures: a hydrophilic statistical polymer "polySTING" and a diblock polymer "NPSTING" that forms into nanoparticles. PolySTING achieved higher systemic STING agonist delivery, whereas NPSTING is more efficient in delivering STING agonists into inguinal lymph nodes (LNs). Both drugamer platforms enhanced STING activation and DC maturation compared to the free drug. When combined with VIPER, NPSTING generated more antigen-presenting DCs in the LNs and more antigen-responsive $CD8^+$ T cells in the spleens, whereas polySTING generated more tumor-infiltrating $CD8^+$ T cells and $CD8^+$ DCs. Both VIPER-STING drugamer platforms demonstrated efficacy in a B16-OVA melanoma model and a MC38

[6] Chapter reproduced from: Song, K., Nguyen, DC. et al. Peptide Vaccine Formulations with Structurally Distinct STING Agonist Drugamers Induce Discrete, Efficacious Antitumor Responses. *PNAS* (2025). In press.

colon cancer model. Combination treatment with anti-PD-1 immune checkpoint inhibitor results in tumor remission and tumor immunity in a subset of mice. This study highlights how an endosomolytic peptide vaccine platform combined with two structurally different drugamers induce superior antitumor responses through distinctive mechanisms.

5.1 INTRODUCTION

Personalized therapeutic cancer vaccines hold great promise in cancer immunotherapy. Tumor cells can have somatic mutations that result in tumor-specific antigens called neoantigens that are not subject to central tolerance.[1] With recent advancements in bioinformatics and computational algorithms, neoantigens can be identified in a patient-specific manner to generate personalized cancer vaccines. Neoantigen vaccines have demonstrated promising results in clinical trials in patients with glioblastoma, melanoma and non-small cell lung cancer.[2–4] On their own, neoantigens generate suboptimal responses and need to be combined with adjuvants such as poly-ICLC[5] that boost the vaccine response. Clinically, these vaccines are compatible with and can benefit from combination therapy with immune checkpoint inhibitors,[6] chemotherapy,[7] and radiation therapy.[8]

Peptide-based cancer vaccines are attractive for their manufacturability and tolerability[9], but generate modest T cell responses[10]. Their low immunogenicity comes partly from multiscale drug delivery challenges: rapid systemic clearance or degradation, insufficient lymph node (LN) drainage, low dendritic cell (DC) uptake and inadequate intracellular access to the major histocompatibility class I (MHC-I) pathway for cross-presentation.[11–13] Altogether, these obstacles lead to poor $CD8^+$ T cell induction and suboptimal antitumor responses. We previously reported a mannosylated polymer-peptide conjugate that form 30-40 nm micelles that efficiently drain to LNs after vaccination and deliver peptide antigens to DCs through their mannose receptors.[14] We incorporated a membrane-lytic peptide D-melittin to make Virus-Inspired Polymers for Endosomal Release (VIPER). VIPER forms micelles at physiological pH but disassembles in the acidic endosomal environment to expose the lytic peptide D-melittin, which disrupts the endosomal membrane to facilitate cytosolic antigen release, cross-presentation, and $CD8^+$ T cell activation.[15]

VIPER generated more antigen-specific T cells than antigen-only polymers and showed moderate therapeutic efficacy in the B16-OVA melanoma model. As innate immune adjuvants can improve activity of vaccine formulations,[16,17] we hypothesize that the therapeutic efficacy of VIPER can be further improved by including a rising class of cancer vaccine adjuvant: Stimulator of Interferon Genes (STING) agonists[18].

STING agonism in dendritic cells provides the three signals for effective $CD8^+$ T cell activation: antigen cross-presentation, co-stimulatory molecule expression and inflammatory context in the form of type I interferons (IFNs).[19] STING promotes cross-presentation to facilitate antigen presentation by MHC Class I molecules.[20] In addition, STING activation induces DC maturation. The expression of higher levels of co-stimulatory molecules on mature DCs prevent T cell anergy upon antigen presentation.[21,22] Furthermore, STING activation leads to the production of proinflammatory cytokines like type I IFNs that are essential for the survival, memory and effector function of $CD8^+$ T cells.[19] However, outcomes from clinical testing of STING agonists in oncology have been disappointing, likely due to the poor pharmacokinetics properties and intracellular delivery barriers.[23] Uncontrolled and/or off-target STING activation also leads to toxicity.[24] STING activation in T cells induces ER stress and leads to T cell death.[25] While drug delivery platforms have previously been developed for STING-antigen dual-delivery in cancer vaccines to notable success,[26–30] differences in agonist selection, formulation method, administration route and dosing across heterogeneous vector designs complicates the derivation of general design principles for future cancer vaccine formulation development.

In this work, we adjuvant VIPER with two polymeric prodrugs of a synthetic STING agonist that provide both dendritic cell-targeted STING delivery and enzyme-triggered STING release, but differ in their structure and physicochemical properties to probe adjuvant structure effects on

STING pharmacokinetics, immunological outcome and vaccine efficacy. We utilized a commercial synthetic diamidobenzimidazole (diABZI) STING agonist that had both proven potent STING activation[31] and a hydroxyl group amenable to chemical conjugation. The diABZI STING agonist (hereafter referred simply as the STING agonist) is formulated into an enzyme-cleavable monomer through conjugation to a polymerizable methacrylate via a Cathepsin B-labile Val-Ala-PAB (VA) linker[32]. Analogous to its use in clinically-approved and efficacious antibody-drug conjugates (ADCs)[33,34], the VA-STING prodrug is relatively stable in circulation even under elevated protease conditions[35]. It is only labile upon receptor-mediated endocytosis through a co-polymerized internalizing ligand, as we have previously demonstrated[36]. We previously synthesized polySTING, a hydrophilic, water-soluble statistical copolymer with mannosylated monomers for targeting dendritic cells copolymerized with the STING prodrug monomer. PolySTING showed activity as an intravenous STING agonist cancer immunotherapy.[37] To evaluate the importance of STING-antigen co-delivery, we also synthesized a diblock polymer containing STING agonists in a pH-tunable hydrophobic block that self-assembles into nanoparticles at physiological pH. The drugamer 'NPSTING', named for its nanoparticle-assembling properties, can co-assemble with VIPER polymers to package antigen and STING within single particles. Both STING drugamers contain mannose to target mannose receptors expressed on DCs for optimal DC activation and T cell priming while minimizing off-target toxicity. The drugamers improved the pharmacokinetic properties of the STING agonist: both polySTING and NPSTING increased STING delivery to the lymph nodes, though polySTING also delivered STING to systemic circulation. STING drugamers also improved the level of STING activation compared to the free drug. Both STING drugamers demonstrated enhanced VIPER's DC maturation, while all VIPER-STING formulations enhanced T cell activation and tumoral T

cell infiltration. NPSTING's enhanced STING LN delivery compared to polySTING and free STING induced superior DC cross-presentation, while polySTING's systemic activity resulted in increased tumor infiltration of antigen-specific $CD8^+$ T cells and cross-presenting type 1 conventional DC (cDC1s) over all STING formulations. The VIPER-STING drugamer formulations slowed tumor progression and prolonged survival in the B16F10-OVA melanoma model in contrast to VIPER adjuvanted with free STING agonist. VIPER-STING drugamer is also efficacious in the MC38 colon cancer model as a neoantigen vaccine, and works in combination with the immune checkpoint inhibitor anti-PD-1 to induce partial tumor remission.

5.2 RESULTS

5.2.1 Synthesis and characterization of VIPER and STING drugamers

Co-delivery of antigen and STING agonists has been reported to be an important criterion for STING-adjuvanted vaccines[26]. Systemic administration of STING agonists can lead to broad STING activation and toxicity from resulting systemic cytokines[23]. The 'drugamer' platform utilizes enzyme-cleavable prodrug monomers for facile polymer functionalization with targeting and intracellular release properties, suitable for incorporating STING agonists into the polymeric VIPER platform[37,38]. We synthesized two STING agonist drugamers as adjuvants for our VIPER vaccine platform to make a DC-targeted adjuvanted vaccine that activates both the innate and adaptive immune response with enhanced $CD8^+$ T cell activation (**Fig. 5.1A**). We previously reported 'VIPER' (also known as 'Man-VIPER-NR'), a mannosylated DC-targeting intracellular peptide vaccine antigen delivery platform. The VIPER diblock polymer (21 kDa) used in this work consists of 42 mannose methacrylate (ManMA) units in the 1st hydrophilic block, 45 pH-responsive diisopropylamino ethyl methacrylate (DIPAMA) units and 2-3 peptide-conjugating units in the 2nd hydrophobic block that are conjugated to either a lytic D-melittin peptide (1-

2/polymer) or antigen peptides (2-3/polymer). VIPER self-assembles into 40-50 nm micelles that are loaded with both endosomal releasing D-melittin and peptide antigen[15]. Upon mannose-mediated internalization, VIPER disassembles in the acidic endosome, allowing D-melittin to lyse the endolysosomal membrane and releasing peptide antigens into the cytosolic MHC-I presentation pathway[15].

The first STING agonist drugamer, 'polySTING', is a linear, hydrophilic, statistical copolymer of ManMA and a cathepsin-cleavable STING prodrug monomer. PolySTING (12 kDa) has 35 ManMA units and 2 STING units (**Fig. 5.1B**). PolySTING is water-soluble and can be co-administered with VIPER, but is not expected to integrate into VIPER micelles. The second STING agonist drugamer, NPSTING, is a diblock copolymer constitutionally similar to the VIPER backbone that carries the STING prodrug monomer in the hydrophobic block. NPSTING (23 kDa) has 50 ManMA units in the 1st hydrophilic block, 33 pH-responsive DIPAMA units and 2 STING units in the hydrophobic 2nd block (**Fig. 5.1C**). NPSTING self-assembles into 30-40 nm micelles on its own or co-assembled with VIPER, similar to VIPER itself (**Fig. 5.1D-E, S5.2**). The compositional information of all polymers used are described in **Table S5.1.** Given the suboptimal response of VIPER, we sought to combine the two platforms to make an adjuvanted vaccine that activates both the innate and adaptive immune response with enhanced $CD8^+$ T cell activation (**Fig. 5.1A**). The two drugamer systems allow us to experimentally test the difference between simultaneous antigen and adjuvant delivery from the same nanoparticle (VIPER-co-NPSTING) and simple co-administration of the antigen delivery formulation (VIPER) with polymeric STING agonist (polySTING) that share a targeting moiety.

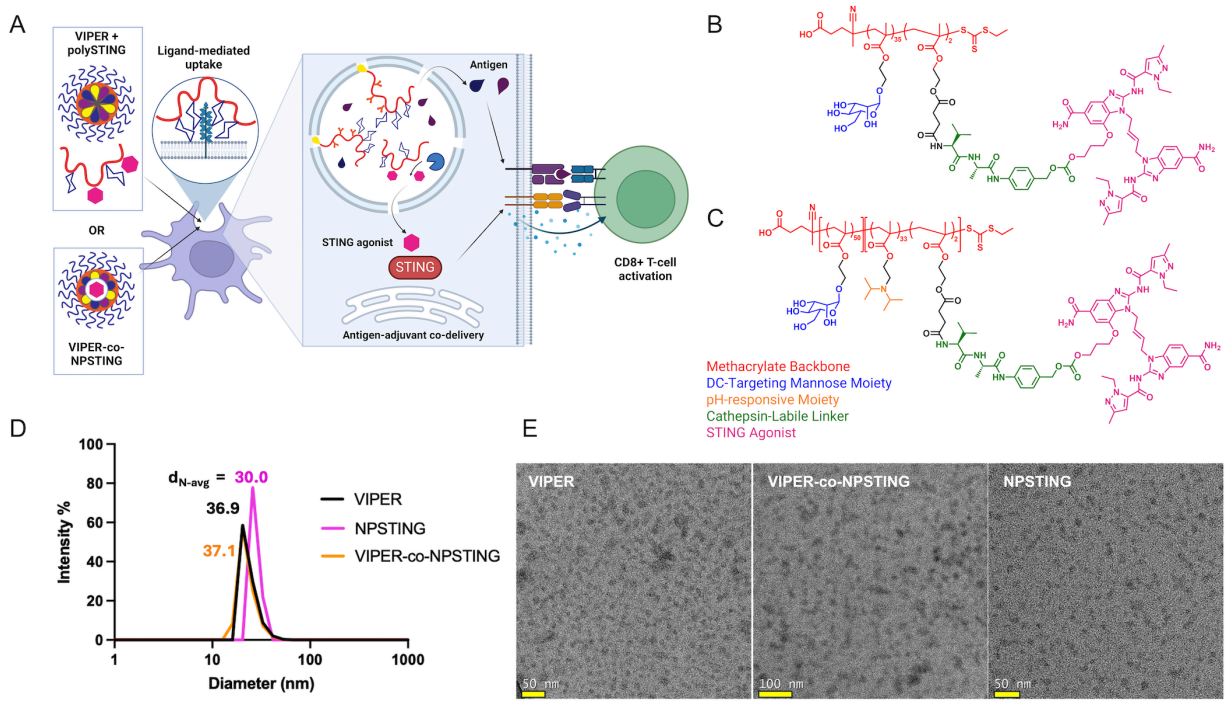

Figure 5.1 Design and characterization of VIPER and STING polymers.

(A) Schematic illustration of VIPER and STING polymers uptake by dendritic cells through receptor-mediated endocytosis, antigen cross-presentation, STING agonist release by cathepsin-cleavage and STING activation, which ultimately leads to enhanced $CD8^+$ T cell activation. (B-C) Chemical structures of polySTING and NPSTING with NMR-determined degree of polymerization indicated, respectively. (D) Size distribution of VIPER,, VIPER-co-NPSTING and NPSTING characterized by dynamic light scattering (d_{mean} = 36.9 nm, 37.1 nm and 30.0 nm respectively). (E) Transmission Electron Microscopy (TEM) of VIPER, VIPER-co-NPSTING and NPSTING micelles.

5.2.2 STING drugamers enhanced drug accumulation in lymph nodes and plasma in a structure-dependent manner

We first investigated how the different drugamer structures impact the pharmacokinetics of the released STING. We injected STING as free agonist, polySTING or NPSTING (10 μg of STING agonist) subcutaneously at the tail base of C57BL/6 mice and analyzed STING agonist concentrations in the plasma and inguinal lymph nodes (iLNs) by liquid chromatography/mass

spectrometry (LC/MS). The LC/MS method detects only released, free-agonist STING instead of the prodrug/polymer-bound drugamer form (**Fig. S5.3, S5.4**). STING signals were calibrated against naive matrices spiked with known agonist concentrations (**Fig. S5.5**). Free STING agonist treatment resulted in very low STING agonist concentrations detected at all timepoints, with only the plasma in two mice in the 1h group showing concentrations above the lower limit of quantification (LLOQ). An additional analysis for free agonist 30 minutes post-administration showed low but detectable STING concentrations in the plasma and spleen, suggesting rapid systemic clearance within minutes (**Table S5.2**). In contrast, drugamer treatments resulted in significantly higher drug concentrations in both plasma and iLNs. In the iLNs, within the duration of the study, polySTING- and NPSTING-treated mice reached maximal mean STING agonist concentrations of 2300 ng/g and 12000 ng/g respectively, both at 8h post-administration (**Fig. 5.2A**). Agonist concentration increased between 1h-8h for both drugamers, though NPSTING treatment resulted in a more drastic increase. NPSTING treatments also resulted in significantly higher STING agonist concentrations in the LNs at all timepoints. In the plasma, polySTING-treated mice had the highest systemically available STING agonist (58 ng/mL) at 1h that quickly decreased over time. NPSTING-treated mice had relatively lower systemic STING concentrations that peaked (20 ng/mL) at 4h.

5.2.3 STING drugamers activate STING and induces dendritic cell maturation

We next examined STING pathway activation after STING agonist administrations. Free STING, polySTING and NPSTING were administered subcutaneously at the tail base of C57BL/6 mice at 10 μg equivalent of STING agonist and iLNs were collected 24 h post-injection. The expression of STING-related cytokines (IFNB1) and chemokines (CXCL10) was quantified using RT-qPCR, normalized to the GAPDH housekeeping gene. Free STING, polySTING and NPSTING generated

a 2.2-, 4.5-, and 250-fold increase in IFNB1 expression, and a 8.1-, 28-, and 490-fold increase in CXCL10 expression compared to the vehicle control (**Fig. 5.2C-D**). The robust increases in STING-related gene expression after NPSTING administration are consistent with the PK data, which showed NPSTING has the highest accumulation in the iLNs.

PolySTING and NPSTING activate dendritic cells in a dose-dependent manner (**Fig. S5.6**). We injected three different dosages of NPSTING (containing 2, 5 or 10 μg of STING agonist) and polySTING (containing 10 μg, 30 μg and 50 μg of STING agonist) subcutaneously at the tail base and analyzed inguinal lymph nodes 24 h post-injection. NPSTING and polySTING both induced higher CD86 and CD80 expression in DCs at higher doses (**Fig. S5.6A,B**). The difference in CD40 expression was small (**Fig. S5.6C**). However, at higher dosages, both NPSTING and polySTING induced cell death in the lymph nodes (**Fig. S5.6D**) and higher dosage of NPSTING decreased the percentage of DCs in the LNs (**Fig. S5.6E**). This result is in line with STING's possible role in diverse cell death pathways.[39] At the same dosage, NPSTING generated a higher level of IFNB1 expression compared to polySTING (**Fig. S5.6F**), probably due to higher accumulation of the STING agonist in the LNs as shown in the PK data. We moved forward with using 2 μg of STING agonist as the preferred dose for NPSTING and 10 μg STING agonist as the preferred dosing for polySTING as these dosing levels induced a relatively high level of DC maturation without causing too much toxicity.

We next investigated how the STING drugamers affected DC maturation when combined with VIPER vaccines (gating scheme in **Fig. S5.7**). VIPER + polySTING and VIPER + NPSTING were formulated by making micellar VIPER containing peptide antigen separately and then admixing with soluble polySTING or NPSTING micelles. VIPER-co-NPSTING was formulated by dissolving both VIPER antigen polymers and NPSTING polymers in acidic solution and

increasing pH to induce micelle formulations containing both peptide antigen and STING agonists within the same micelle. As shown in **Fig. 5.1D-E and S5.2**, VIPER, NPSTING, VIPER + NPSTING and VIPER-co-NPSTING were all similar in size and morphology, ranging from 30-40 nm in diameter. Given similar physicochemical characteristics, we expect VIPER in all formulations to exhibit similar lymphatic drainage behavior[40]. The addition of polySTING and NPSTING to VIPER induced a much higher DC activation compared to VIPER alone in all three DC maturation markers (**Fig. 5.2E-G**). VIPER + polySTING induced a 10-, 26-, and 5-fold higher expression in CD86, CD80 and CD40 markers compared to VIPER. VIPER-co-NPSTING induced a 7-, 19-, and 5-fold higher expression in CD86, CD80 and CD40 markers compared to VIPER, whereas VIPER + free STING only induced 1.8-, 2.3- and 1.6-fold increase in the expression of DC maturation markers. The STING drugamers significantly increased DC maturation compared to free STING agonist. The results were in line with the PK data, which showed that free STING agonist is rapidly eliminated after administration. In addition, VIPER-co-NPSTING demonstrated higher DC activation compared to VIPER + NPSTING (**Fig. S5.8**), emphasizing the importance of co-delivery of antigens and adjuvants into the same DCs.

5.2.4 PolySTING induces systemic STING activation, while NPSTING increases antigen cross-presentation

When combined with the VIPER vaccine, STING drugamers generated a higher level of STING activation compared to free STING, while VIPER itself does not activate the STING pathway (**Fig. 5.2H**). VIPER + polySTING generated a higher level of IFNβ in plasma compared to VIPER + free STING and VIPER-co-NPSTING 4 h post injection (**Fig. 5.2H**), which is consistent with the PK data showing higher STING concentration in plasma after polySTING treatment at earlier time points. STING activation in the iLNs were low for VIPER-co-NPSTING 4 h post injection (**Fig.**

S5.9). This could be due to the fact that NPSTING was administered at a 5-fold lower concentration compared to free STING and polySTING, and the amount of STING agonist is still increasing at the 4 h timepoint for NPSTING (**Fig. 5.2A**).

STING activation is known to promote cross-presentation through the production of type I IFNs.[22,41] We next examined the level of antigen-presenting DCs in the inguinal LNs 24 h after vaccination (gating scheme in **Fig. S5.10**). Mice were vaccinated with VIPER containing OVA MHC I (SIINFEKL) and OVA MHC II (ISQAVHAAHAEINEAGR) epitopes and H-2Kb-SIINFEKL antibody was used to detect dendritic cells with SIINFEKL peptide bound to H-2Kb of MHC class I molecules. While STING-adjuvanted treatments trended toward higher numbers of antigen-presenting DCs compared to VIPER immunization alone, only VIPER-co-NPSTING generated a significantly higher level of antigen-presenting $CD11c^{+}$ DCs compared to VIPER alone (**Fig. 5.2I**).

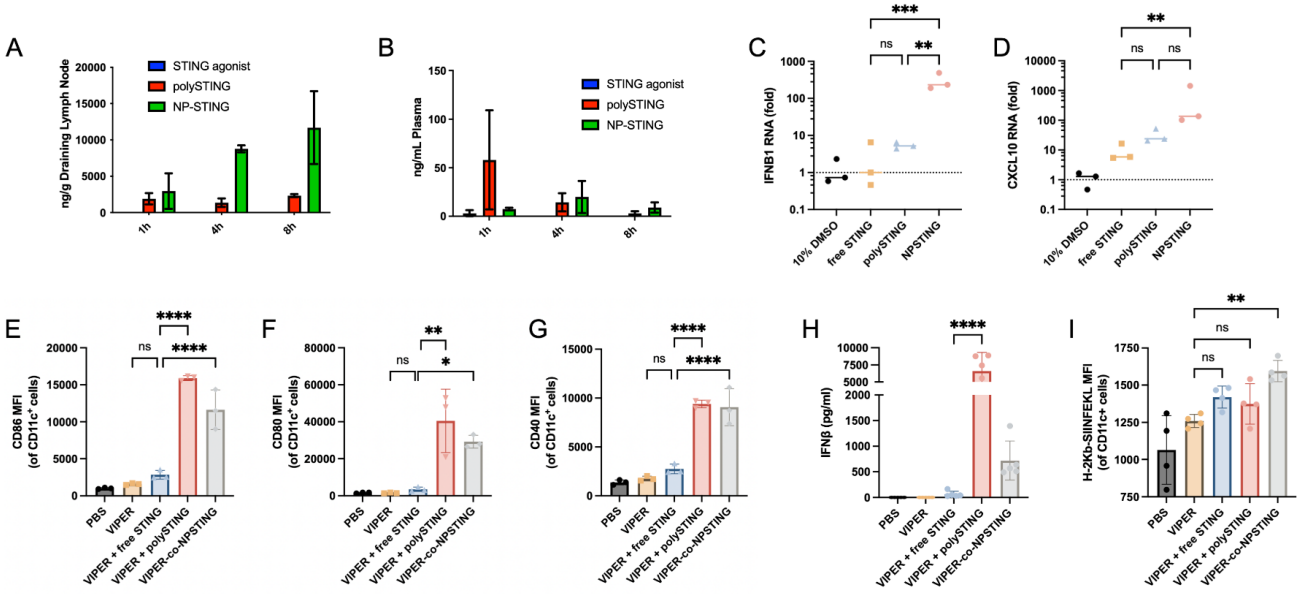

Figure 5.2 STING drugamers enhance pharmacokinetics and STING activation, promote DC activation and antigen cross-presentation.

(A-B) Quantification of STING agonists in iLNs (A) and plasma (B) 1 h, 4 h, and 8 h post injection (N=3). (C-D) IFNB1 and CXCL10 expression in iLNs 24 h post injection, normalized to GAPDH housekeeping gene (N=3). (E-G) Co-stimulatory molecule CD86, CD80 and CD40 expression on $CD11c^+$ cells in iLNs 24 h post injection (N=3). (H) Plasma IFNβ level 4 h post injection (N=5). Values below the detection limit were represented as 0. (I) Median fluorescence intensity (MFI) of H-2Kb-SIINFEKL on $CD11c^+$ cells in iLNs 24 h post injection (N=4). Data are represented as mean ± SD. Statistical analysis was performed using a one-way ANOVA with posthoc Tukey HSD test (*$p \leq 0.05$, **$p \leq 0.01$, ***$p \leq 0.001$, ****$p \leq 0.0001$, ns: not significant).

5.2.5 Co-delivery of STING agonists and antigens enhances T cell activation of VIPER vaccine

We next evaluated the adjuvanted VIPER formulations' capacity for T cell induction, a crucial step towards cytotoxic antitumor immunity (gating scheme in **Fig. S5.11**).[42] Mice were immunized with PBS, VIPER, or VIPER combined with free STING, polySTING or NPSTING on day 0 and day 14 and spleens were collected 7 days after the 2nd immunization for T cell analysis (**Fig. 5.3A**). All STING formulations induced more antigen-specific $CD8^+$ T cells in the spleen compared to VIPER (**Fig. 5.3B**), demonstrating the immunological boost of STING agonist adjuvants, though there were no significant differences between STING-adjuvanted formulations. Only VIPER-co-NPSTING generated a significantly higher amount of cytokine-producing $CD8^+$ T cells compared to VIPER when restimulated with the antigen *ex vivo* (**Fig. 5.3C**). Similarly, all STING formulations generated a higher amount of antigen-responsive $CD4^+$ T cells compared to VIPER, with VIPER + polySTING and VIPER-co-NPSTING generating slightly higher responses than VIPER + free STING (**Fig. 5.3D**). Co-stimulatory molecules on DCs lower the T cell activation threshold and make T cells more sensitive to antigen stimulation.[43] Additionally, STING activates the NF-kB pathway and induces the expression of pro-inflammatory cytokines such as TNF-α.[44] polySTING and NPSTING generated higher levels of co-stimulatory molecules expression on DCs and activated the STING pathway to a greater extent, and therefore could generate antigen-specific $CD8^+$ and $CD4^+$ T cells that are more responsive to antigens.

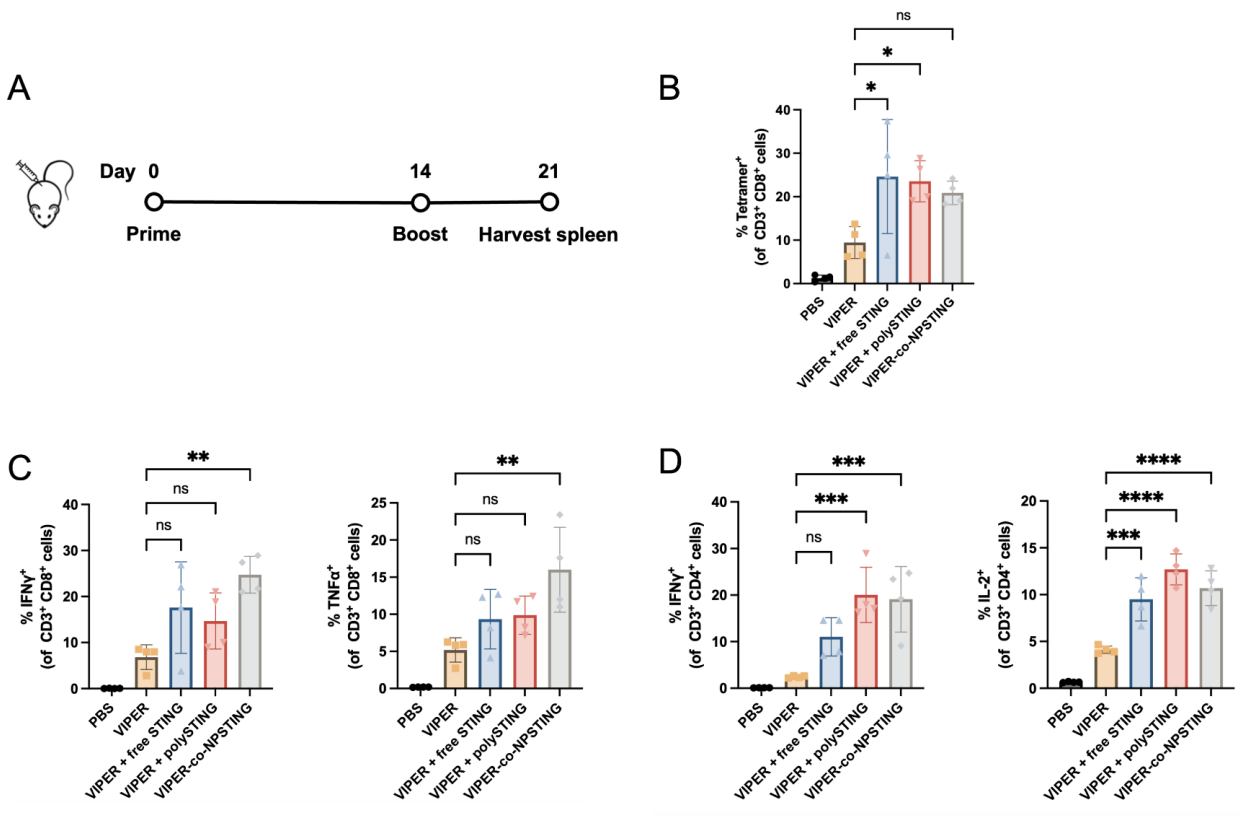

Figure 5.3 STING agonists improve antigen-specific T cell response *in vivo*.

(A) Study timeline. Mice were vaccinated on day 0 and day 14, and spleens were collected on day 21. (B) Percentage of antigen-specific $CD8^+$ T cells in the spleen. (C) Percentage of IFNγ- and TNFα-producing $CD8^+$ T cells in the spleen after restimulation with the antigen *ex vivo*. (D) Percentage of IFNγ- and IL-2--producing $CD4^+$ T cells in the spleen after restimulation with the antigen *ex vivo* (N=4). Data are represented as mean ± SD. Statistical analysis was performed using a one-way ANOVA with posthoc Tukey HSD test (*$p \leq 0.05$, **$p \leq 0.01$, ***$p \leq 0.001$, ****$p \leq 0.0001$, ns: not significant).

5.2.6 Co-delivery of STING agonists and antigens enhances antigen-specific T cell and cDC1 infiltration into the tumors

To investigate whether the activated immune cells infiltrate into tumors, we immunized B16F10-OVA-bearing mice subcutaneously at the tail base on days 5 and 12, and collected tumors on day 13 (gating scheme in **Fig. S5.12**). VIPER + polySTING induced significantly higher levels of tumor-infiltrating T cells and antigen-specific $CD8^+$ T cells compared to VIPER (**Fig. 5.4A-C**). VIPER + free STING and VIPER-co-NPSTING also induced higher levels of antigen-specific

$CD8^+$ T cell infiltration compared to VIPER, but were not statistically significant. The higher levels of T cell infiltration after VIPER + polySTING vaccination could be attributed to higher and more prolonged systemic distribution of STING agonist delivered from this formulation and its resultant IFNβ generation (**Fig. 5.2H**). Type I interferons such as IFNβ promote the production of chemokines like CXCL10,[45] which is critical for T cell infiltration into the tumor microenvironment.[46] We next investigated tumor-infiltrating dendritic cells as they are responsible for immune cell activation and recruitment.[47] All VIPER vaccine groups generated more tumor-infiltrating dendritic cells compared to the vehicle control (**Fig. 5.4D**). Additionally, VIPER + polySTING generated more tumor-infiltrating $CD8^+$ DCs than VIPER and VIPER-co-NPSTING generated more tumor-infiltrating $CD103^+$ DCs than VIPER (**Fig. 5.4E, F**). Both $CD8^+$ DCs and $CD103^+$ DCs belong to the conventional type 1 DCs (cDC1s) subset, which contributes to chemokine secretion, antigen cross-presentation and effector $CD8^+$ T cell recruitment in the tumor microenvironment, ultimately leading to antitumor immunity.[48] In summary, all STING-adjuvanted vaccine formulations increased cytotoxic T cell and dendritic cell recruitment into the tumor microenvironment. Of the three formulations, VIPER + polySTING provided the most robust increase in antigen-specific T cells in the tumor, while VIPER-co-NPSTING promoted the largest increase in cDC1s.

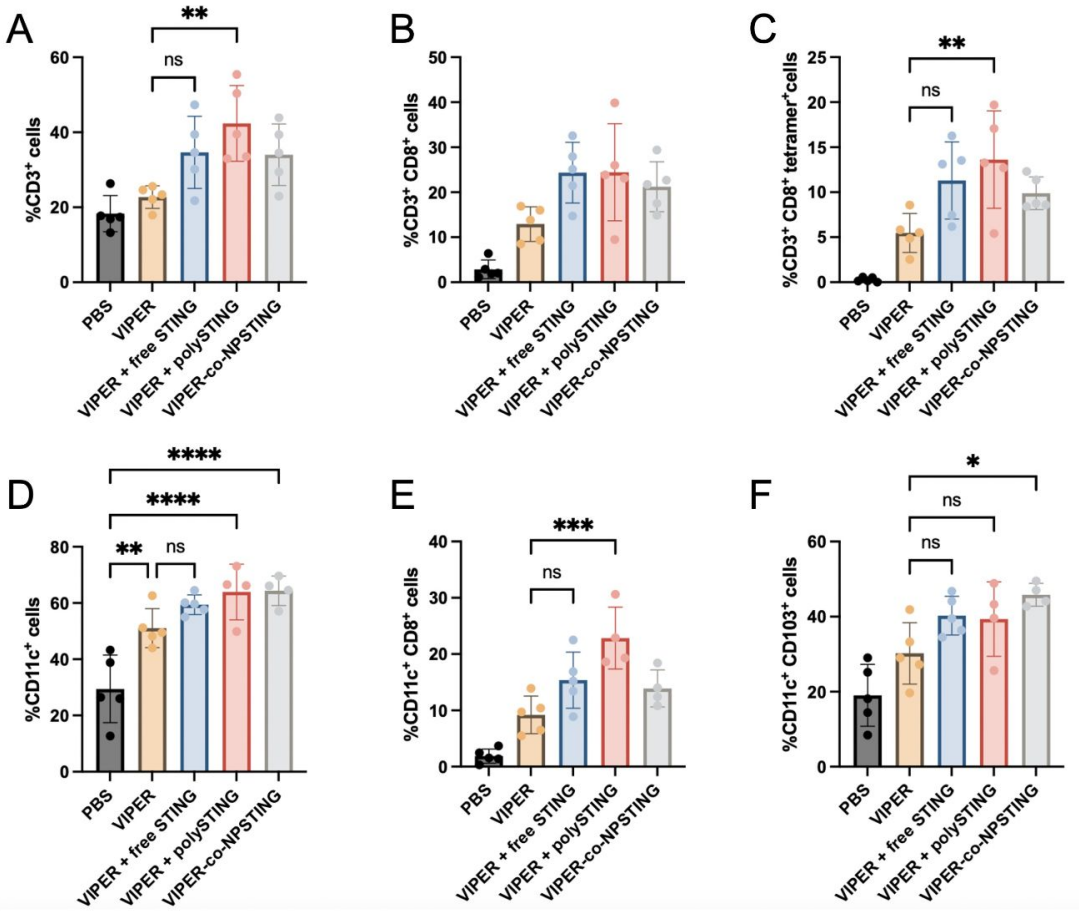

Figure 5.4 STING agonists induce T cell and cDC1 infiltration into the tumor.

(A-F) Frequency of tumor-infiltrating immune cells among all live cells in the tumor. (A) Percentage of T cells in the tumor. (B) Percentage of $CD8^+$ T cells in the tumor. (C) Percentage of antigen-specific $CD8^+$ T cells in the tumor. (D) Percentage of DCs in the tumor. (E) Percentage of $CD8^+$ DCs in the tumor. (F) Percentage of $CD103^+$ DCs in the tumor (N=4-5). Data are represented as mean ± SD. Statistical analysis was performed using a one-way ANOVA with post hoc Tukey HSD test (*$p \leq 0.05$, **$p \leq 0.01$, ***$p \leq 0.001$, ****$p \leq 0.0001$, ns: not significant).

5.2.7 Polymeric co-delivery of peptide antigens and STING agonists demonstrated therapeutic efficacy in murine melanoma and colon cancer models

Finally, we evaluated the efficacy of STING-adjuvanted VIPER formulations in murine tumor models. We first investigated efficacy in the B16-OVA model, an aggressive melanoma model engineered to express the model OVA antigen that we have previously tested with VIPER[15]. C57BL/6 mice were inoculated with B16-OVA cells subcutaneously at the right hind flank on day

0 and were vaccinated three times every 7 days starting on day 4 (**Fig. 5.5A**). Consistent with our previous results,[15] VIPER suppressed tumor growth and extended survival compared to vehicle-treated groups. This therapeutic effect was enhanced by both polySTING and NPSTING, but was not affected by free STING agonist (**Fig. 5.5B-C**). Free STING agonists generated a similar level of antigen-specific $CD8^+$ T cells as the STING drugamers (**Fig. 5.3B**), but the magnitude of antigen-specific T cell response is not the sole predictor of therapeutic cancer vaccine treatment outcome. While there were no differences in tumor growth rate and survival between polySTING and NPSTING, the manner of NPSTING incorporation into VIPER impacted therapeutic efficacy. Specifically, co-micellizing NPSTING with VIPER (VIPER-co-NPSTING) resulted in slightly stronger tumor growth suppression and longer survival than a separate micelle formulation (VIPER + NPSTING) (**Fig. S5.13**). All these factors highlight the importance of using a polymeric platform to co-deliver antigens and STING agonists to dendritic cells.

We next evaluated the therapeutic outcome of the lead formulations, VIPER + polySTING and VIPER-co-NPSTING, in a neoantigen MC38 colorectal carcinoma model in combination with immune checkpoint inhibitors. VIPER was used to deliver Adpgk, a MHC-I neoantigen peptide discovered previously (polymer composition information in **Table S5.1**).[49] Mice were vaccinated three times starting on day 8, when tumors were palpable, and anti-PD-1 immune checkpoint inhibitor was given every three to four days via intraperitoneal injections (**Fig. 5.5D**). Both VIPER + polySTING and VIPER-co-NPSTING suppressed MC38 tumor growth and prolonged survival compared to the vehicle control (**Fig. 5.5E-F, S5.14**). Anti-PD-1 alone has minimum tumor growth inhibition, but achieved complete remission in 1/8 mice. Anti-PD-1 treatment further improved outcome after vaccination. Addition of anti-PD-1 slightly slowed tumor growth (**Fig. 5.5E**) and prolonged survival (**Fig. 5.5F**), with 2/7 of VIPER + polySTING treated mice and 1/8 of VIPER-

co-NPSTING treated mice remaining tumor-free 150 days after tumor inoculation. All tumor-free mice demonstrated tumor rejection when rechallenged with MC38 tumor cells on the left hind flank on day 56, suggesting long-term tumor immunity.

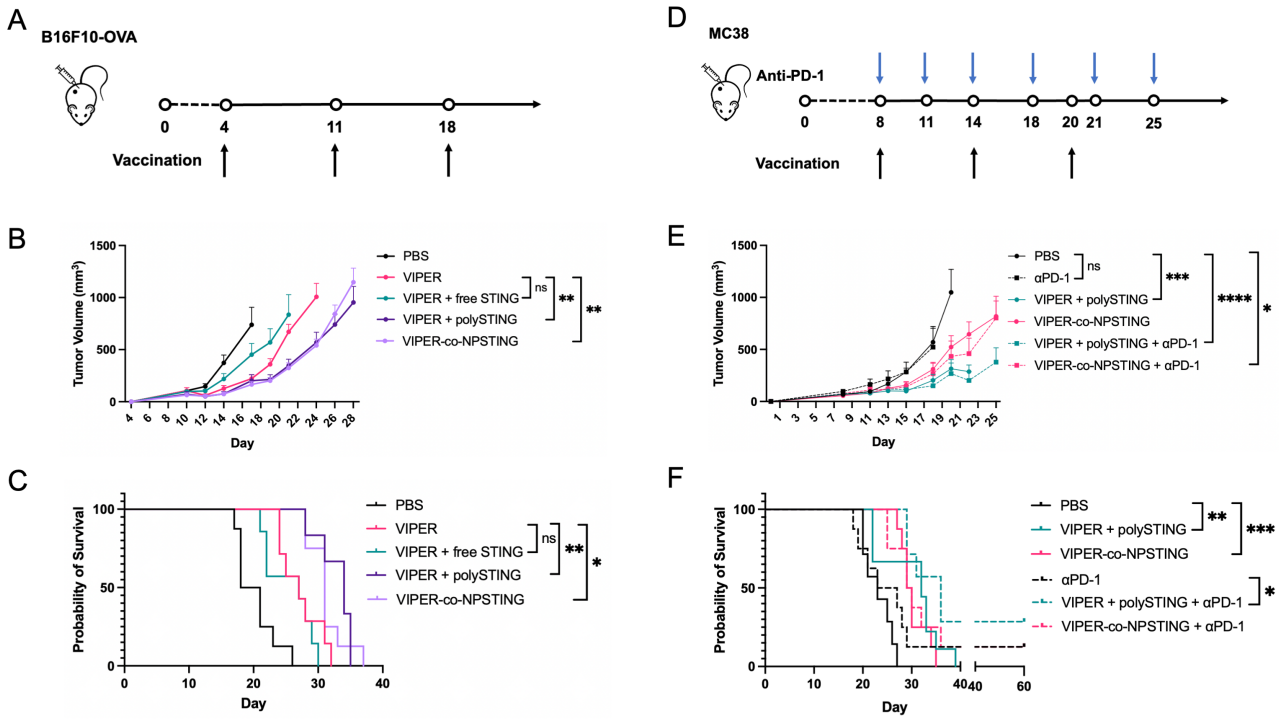

Figure 5.5 VIPER and the STING drugamer platform show antitumor effects in B16-OVA and MC38 tumor models.

(A) Study timeline of the B16-OVA tumor reduction study. Mice were inoculated with B16-OVA cells on day 0 and vaccinated on days 4, 11 and 18. (B) B16-OVA tumor growth curves. Data are represented as the mean ± SEM (N = 6-8). Statistical analysis was performed using two-way ANOVA with Tukey's multiple comparisons test (**p ≤ 0.01, ns: no significance). (C) Kaplan–Meier survival curve (N = 6-8). Survival analysis was performed using the log-rank test (*p ≤ 0.05, **p ≤ 0.01, ns, no significance). (D) Study timeline of the MC38 tumor reduction study. Mice were inoculated with MC38 cells on day 0 and vaccinated on days 8, 14 and 20. Anti-PD-1 was given on days 8, 11, 14, 18, 21 and 25. (E) MC38 tumor growth curves. Data are represented as the mean ± SEM (N = 7-9). Statistical analysis was performed using two-way ANOVA with Tukey's multiple comparisons test (*p ≤ 0.05, ***p ≤ 0.001, ****p ≤ 0.0001, ns: no significance). (F) Kaplan–Meier survival curve (N = 7-9). Survival analysis was performed using the log-rank test (*p ≤ 0.05, **p ≤ 0.01, ***p ≤ 0.001).

5.3 DISCUSSION

The expanding understanding of vaccinology and the STING pathway, as well as discoveries in novel STING agonists and nanotechnology delivery platforms, have resulted in an impressive number of preclinically efficacious cancer nano-vaccine candidates[26–30]. However, vast differences in agonist choice, route and timing of administration in combination with delivery vector heterogeneity[24] complicates direct comparison between reports, hampering generation of generalizable design rules. In this work, our drugamer platform permitted incorporation of a singular STING prodrug into distinct polymeric architectures that share common targeting and controlled-release properties. By combining these two drugamers with a singular antigen delivery platform, we are able to examine the effects of STING adjuvant structure on the resultant vaccine response.

The pharmacokinetics (PK) of STING agonist delivery to lymph nodes and plasma is improved by both polySTING and NPSTING compared to free STING agonist, resulting in elevated STING activation. Both drugamer treatments resulted in significantly elevated STING concentrations in the draining lymph nodes (LNs), consistent with our previous results utilizing mannnosylated polymers[14,37]. As a ~ 30-40 nm nanoparticle formulation, NPSTING offers the highest passive lymphatic drainage of all formulations[40] and showcases the pharmacological utility of dual active and passive targeting. LN STING concentrations from both drugamer treatments remained elevated during the course of the experiment, indicative of a continuous prodrug cleavage process[38]. Correspondingly, we observed elevated STING-related gene expression at post-acute phases (24h) for both drugamers compared to free drug, whose rapid clearance showed only an acute phase (4h) increase in STING-related gene expression. Prolonged immune activation has been reported with a nanoparticulate imidazoquinoline prodrug platform similar to the utilized

drugamers[50]. Jinming Gao's group have reported on the benefits of combining acute and post-acute STING activation utilizing encapsulated canonical STING agonists and polyvalent weak STING binders[51], and here we report similar results with a targeted polymeric prodrug of a strong synthetic STING agonist. This STING activation profile, unique to both drugamers, correlates with their later therapeutic efficacy over the free drug.

The elevated STING concentrations in the LNs resulting from NPSTING treatment posed an early dose-limiting toxicity through cell viability, consistent with STING's ability to induce apoptosis[52]. A reduced NPSTING dosage (5-fold lower) improved VIPER's DC maturation to the same extent as polySTING, which could reflect NPSTING's increased potency in the LNs. PolySTING may have benefited from systemic IFNβ release, as interferons alone can induce DC maturation[53]. NPSTING also increased antigen cross-presenting DCs compared to VIPER alone and other STING adjuvants, which may represent the benefit of antigen-adjuvant co-delivery on a cellular level. While STING agonism improves antigen cross-presentation, it can also induce DC maturation before antigen acquisition, which negatively impacts antigen uptake and presentation downstream[54]. NPSTING co-micellization with antigen polymers can deliver both STING agonist and antigen through every internalization event, minimizing the penalties of STING pre-activation. Free STING adjuvant conferred no meaningful improvement to VIPER's DC response despite some acute-phase STING gene expression in the LNs, likely due to inefficient DC STING delivery as a non-targeted formulation.

NPSTING generated slightly more antigen-responsive $CD8^+$ T cells, while polySTING generated more tumor-infiltrating tumor-specific $CD8^+$ T cells as well as cross-presenting $CD8^+$ DCs. The respective correlation with their therapeutic benefit as adjuvants is notable, but more so is their correlation with pharmacokinetic properties. The superior LN and DC STING delivery of

NPSTING likely resulted in superior T cell priming even at a 5-fold lower dose[55]. The systemic entry of polySTING may have allowed polySTING to act upon tumoral APCs, which can generate chemokines that promote tumor lymphocyte infiltration[37,56]. The induction of cross-presenting tumoral DCs, analogous to polySTING's activity as an intravenous immunotherapy, can also maintain intratumoral CTL activity[57–59]. PolySTING's multifactorial mechanism may underlie its arguably superior activity to NPSTING in the MC38 neoantigen model, though its severe systemic cytokine release may hint at potential toxicity mechanisms[60]. NPSTING exhibited comparable efficacy at a 5-fold lower dose, highlighting the utility of enhanced lymphatic targeting but also agreeing with reports on improved potency of nanoparticle-STING conjugates[61]. However, the improved potency accompanied the earlier-reported localized cytotoxicity, which should not be discounted. Nevertheless, the unique vaccine responses from both drugamers and their downsides, traceable to the drugamers' PK profiles, highlight the capacity of different polymeric adjuvant structures to induce meaningful therapeutic responses through distinct mechanisms between systemic and localized stimulation. Future work may either combine different adjuvant structures to achieve an optimal local-systemic STING response, or tailor STING vaccine formulations to be specific to patients' individual immune susceptibility in accordance with cancer nanomedicine paradigms[62]. The former approach is mirrored in a recent report on superior therapeutic efficacy in a subcutaneous prime-intravenous boost (i.e. local prime, systemic boost) vaccination strategy with a TLR7/8a-adjuvanted peptide nanoparticle vaccine platform[63]. Additionally, the MC38 colon tumor cells were implanted subcutaneously for more accessible and reliable tracking of tumor growth, but they are usually less immunosuppressive compared to orthotopic tumor models[64]. Future studies may be conducted in orthotopic models like the 4T1 breast cancer model by introducing cells into the mammary fat pad[65].

It is surprising that free STING adjuvant improved VIPER's T cell response to a similar extent as the drugamers despite the lack of enhanced DC maturation, yet failed to improve VIPER's therapeutic response in orthotopic tumor models. It is more surprising considering that diamidobenzimidazole (diABZI) STING agonists were efficacious as a systemic immunotherapy[31], compared to clinically-tested cyclic dinucleotide (CDN) STING agonists (e.g. 2'3-cGAMP, ADU-S100)[66], at lower doses than synthetic non-CDN agonists (e.g. SR-717, MSA-2…)[67,68]. It is possible that free STING agonist administration did not result in sufficient LN STING concentrations for DC maturation, but can induce sufficient splenic STING concentrations for splenic T cell expansion - consistent with PK data showing detectable splenic STING 30 minutes after free STING administration. STING agonism in T cells can induce strong cytokine signaling, which can also expand existing antigen-specific T cells. However, it also leads to terminal T cell differentiation and apoptosis, which negatively impacts antitumor CTL activity[69]. This may explain free STING's lack of therapeutic efficacy. It is also possible that this is a T cell-independent effect. Immature DCs can be reprogrammed by circulating tumor cells into immunosuppressive TGFβ-generating myeloid cells,[70,71] which is consistent with the relative lack of DC maturation in free STING-adjuvanted groups. Additionally, the lack of therapeutic efficacy of the free STING adjuvant could be attributed to insufficient STING activation and pro-inflammatory cytokine secretion. These results indicate that pharmacological STING activation in LNs, magnitudinally and temporally, and in DCs better correlates with adjuvanted vaccine antitumor responses than T cell responses. Single-dose pharmacological activation and DC maturation studies are less time-consuming than T cell response studies after prime-boost, and our results indicate that they may be better suited for screening adjuvanted vaccine candidates.

In conclusion, we developed and compared two structurally distinct STING drugamers as adjuvants to the VIPER peptide antigen delivery platform. Their unique pharmacokinetics profiles between the lymphatic and systemic compartments induced distinct vaccine response profiles that both resulted in superior antitumor efficacy over VIPER. The direct pharmacological-immunological comparison between the two drugamers provided insight into the benefits and drawbacks of targeted localized and systemic STING stimulation in cancer vaccination.

5.4 MATERIALS AND METHODS

5.4.1 Materials

Azobisisobutyronitrile (AIBN), 4,4'-azobis(4-cyanovaleric acid) (ABCVA), 2'-Azobis(4-methoxy-2,4-dimethylvaleronitrile) (V70) , cysteamine hydrochloride, piperidine, triisopropylsilane (TIPS) and ethanedithiol (EDT) were purchased from Sigma-Aldrich. Mannose ethyl methacrylate (ManEMA) and RAFT chain transfer agent 4-Cyano-4-[[(ethylthio)thioxomethyl]thio]pentanoic Acid (ECT) were purchased from Omm Scientific. Diisopropylcarbodiimide (DIC) and ethyl cyanohydroxyiminoacetate (Oxyma) were purchased from Chem-Impex. Dimethoxybenzene (DMB), trifluoroacetic acid (TFA), acetic acid (AcOH), acetonitrile (ACN) and Ellman's reagent were purchased from Fisher Scientific. Dithiothreitol (DTT) was purchased from Enzo Life Sciences. All were used as received. Diisopropyl ethyl methacrylate (DIPAMA) was purchased from Sigma-Aldrich. Pyridyl disulfide ethyl methacrylate (PDSEMA, also known as 2-(2-pyridinyldithio)ethyl methacrylate) and pentafluorobenzyl methacrylate (PFBzMA) was purchased from Tokyo Chemical Industries Ltd. These aforementioned monomers were purified by passing through a basic alumina column to remove any existing inhibitor prior to polymerization. Anhydrous N-methyl-2-pyrrolidone (NMP, 99.5%), and dimethylsulfoxide (DMSO, > 99%) were purchased from Sigma-Aldrich and stored with

activated molecular sieves. Protected amino acids were purchased from Novabiochem and used as received. Buffers were prepared in-house using endotoxin-free water and salts purchased from Fisher Scientific. The STING monomer (SMA-VA-STING) was synthesized as previously described[37].

5.4.2 Polymer synthesis

Polymer synthesis of Man-VIPER and polySTING, and peptide synthesis and conjugation of Man-VIPER was performed as previously described.[15,37]

For the synthesis of NPSTING, a modified synthesis protocol from the polymerization of Man-VIPER was used. ManEMA was combined with ECT, ABCVA (ECT:ManEMA = 1:44.4, ECT:ABCVA = 1:20) in dry DMSO (2.5 wt% monomer), purged with argon for 30 minutes, and reacted at 70°C for 4h with vigorous stirring. The mannose CTA (ManCTA) was purified by 3x precipitation in 1:1 (v/v) acetone and diethyl ether, dissolving in DMF in-between, and dried *in vacuo* for 2 days. To a 5 mL round-bottom flask with a stir bar was added ManCTA, SMA-VA-STING, DIPAMA and V70 (ManCTA:SVA-VA-STING:DIPAMA:V70 = 1:5:33:0.25) and anhydrous NMP as solvent (20 wt% monomer). The solution was stirred until all solids were fully dissolved. 8 µl of DMF was added (~1% v/v NMP) as an internal standard. A 20 µl aliquot of the reaction mixture was taken as a reference for conversion NMR. The flask was sealed with a septum and sparged with argon gas for 30 minutes. The mixture was then allowed to react with stirring at 40°C for 20 hours, before being quenched by introduction of air and chilling via an ice bath. The polymer was purified via dialysis in DMSO for 3 days (2 solvent changes each day), and in cold water for 4 days (2-3 solvent changes each day) before lyophilization to yield a fluffy white powder (150 mg, 90% conversion, 87% yield from purification).

5.4.3 Polymer and Micelle Characterization

All ^{1}H NMR spectra were recorded on a Bruker AV 300 (Bruker Corporation, Billerica, MA) nuclear magnetic resonance (NMR) instrument in deuterated DMSO (DMSO-d6). The size distribution profiles of micelles were recorded on a dynamic light scattering (DLS) system (DynaPro NanoStar, Wyatt technology) at a micelle concentration of 1 mg/mL diluted in the PBS.

5.4.4 Transmission electron microscopy (TEM)

Formulations were prepared freshly and diluted in Nanopure water to 1 mg/mL. The diluted formulations were adsorbed onto 200-mesh lacey carbon grids for 5 mins with the carbon film side facing down, with excess solution wicked away by filter paper. Afterwards, the grids were stained with NanoW (NanoProbes, Yaphank, NY) for 1 min, and blotted with a filter paper. Finally, the grids were dipped in Nanopure water for 30 s to wash away excess stain solution, and dried in a desiccator overnight. Grids were imaged with a Tecnai G2 F20 Supertwin TEM (FEI, Hillsboro, OR) at the Molecular Analysis Facility at University of Washington.

5.4.5 Vaccine formulation

We utilized our previously-described pH-switch method to formulate our micelles with slight modifications[15]. Briefly, individual VIPER polymer conjugates were dissolved in endotoxin-free water. The polymer solutions were combined at equal volumes. HCl (2.5% of 1 N solution) was added to the mixture until a clear solution was obtained. The solution was probe-sonicated for 30 seconds to ensure complete dissolution. 0.2 M pH 9.0 dibasic sodium phosphate was added to obtain the final pH around 7.0. The formulations were prepared at ambient conditions. All VIPER vaccines contain 15 μg of OVA MHC-I epitope, 15 μg of OVA MHC-II epitope and 143 μg of D-melittin. To form VIPER-STING vaccines, free STING and NPSTING were dissolved at 20x in DMSO, and polySTING was dissolved at 20x in PBS. VIPER was mixed with different STING formulations after micelle formation. For VIPER-co-NPSTING, NPSTING was added after HCl

addition, and then dibasic sodium phosphate was added to increase the pH to form micelles. Samples were filtered through a 0.22 μm filter before injections.

5.4.6 Cell lines and animals

The B16F10-OVA cell line (gift of Prof. Amanda Lund) and MC38 cell line (Sigma) were cultured in DMEM supplemented with 10% FBS and 1% P/S. Cells were incubated at 37°C and 5% CO_2. Female C57BL/6 mice aged 6 to 8 weeks were purchased from Charles River Laboratories. All animal studies were approved by the University of Washington Institutional Animal Care and Use Committee (IACUC).

5.4.7 Pharmacokinetics characterization

Female C57BL/6 mice were injected subcutaneously at the tail base with free STING agonist, polySTING or NPSTING at 10 μg/mice. 5 minutes before designated PK timepoints, mice were sacrificed with Avertin overdose (i.p.). The chest cavity was then opened to reveal the heart, and cardiac puncture was performed at the desired PK timepoint. Blood was collected into BP heparin tubes and centrifuged at 3000 RCF for 10 minutes at 4°C to isolate plasma. The inguinal lymph nodes (iLNs) and tail base (i.e. injection site) cutaneous fat were also collected and snap frozen on dry ice. To obtain organ homogenates, organs were mixed with molecular biology grade water (5 mL/g organ for iLNs, 2 mL/g for cutaneous fat, 1 mL/g for liver and spleen) and homogenized with a probe sonicator (iLNs and cutaneous fat) or mechanical disruption (Qiagen TissueLyzer II, Hilden, Germany). Upon analysis, plasma or tissue homogenate were mixed with a gembitabine internal standard solution (0.5 μg/mL in acetonitrile), 50% acetonitrile/water, and 100% acetonitrile in a 3:1:6:90 volumetric ratio. The solution was vortexed for 5 minutes, and centrifuged twice (removing supernatant in-between) to obtain solutions for LC-MS analysis.

Calibrators were prepared with naive plasma/homogenate spiked with known STING agonist concentrations in the 50% acetonitrile/water phase (1 μg/mL STING, 1:2 serial dilutions, representative calibration curves in **Fig. S5**). LC/MS was performed at the Mass Spectrometry Center in the University of Washington School of Pharmacy. For LC/MS (Xevo TQ-S, Waters Corporation, Milford, MA), the MS instrument was operated on a positive ion multiple-reaction monitoring (MRM) mode monitoring 136 m/z for the STING agonist and 112 m/z for the internal standard gemcitabine (LLOQ-ULOQ 8.2-2000 ng/mL plasma, 40-10000 ng/g lymph nodes, or 148-2000 ng/g cutaneous fat). The LC was performed with an InfinityLab Proshell 120 EC-C18 analytical (2.1x150mm) column (Agilent, Santa Clara, CA). The LC solvents were water supplemented with 0.1% (v/v) formic acid (solvent A), and acetonitrile supplemented with 0.1% (v/v) formic acid (solvent B). The linear gradient used was from 95:5 A:B to 0:100 A:B over 8 minutes at a 0.25 mL/min flow rate.

5.4.8 In vivo STING activation

Female C57BL/6 mice were injected subcutaneously at the tail base with free STING agonist, polySTING or NPSTING at 10 μg/mice and inguinal LNs were harvested 24 h post injection. In a separate study, female C57BL/6 mice were injected subcutaneously at the tail base with PBS, VIPER, VIPER + free STING, VIPER + polySTING or VIPER-co-NPSTING, with free STING and polySTING containing 10 μg of STING agonist and NPSTING containing 2 μg of STING agonist. Blood and inguinal LNs were harvested 4 h post injection. RT-qPCR was used to analyze interferon-stimulated gene expression as described previously.[37] Plasma IFNβ was analyzed using ELISA (Invivogen).

5.4.9 In vivo dendritic cell activation

Female C57BL/6 mice were injected subcutaneously at the tail base with indicated vaccine formulations. 24 h post immunization, inguinal lymph nodes were harvested, dissociated with pipette tips and digested in 50 U/mL type IV collagenase + 100 U/mL DNase I. Single-cell suspension was obtained by filtering cells through a 70 μm cell strainer. Cells were stained for viability with Zombie NIR viability kit, blocked with anti-CD16/32, and then stained with anti-CD86-BV510, anti-CD40-FITC, anti-CD11c-APC and anti-CD80-PE. In a separate study, cells were stained with anti-CD86-BV510, anti-CD8-FITC, anti-H-2Kb-SIINFEKL-PE and anti-CD11c-APC. An Attune NxT flow cytometer was used to analyze the data. Gating strategies are shown in **Fig. S5.7, S5.10**.

5.4.10 In vivo T cell responses

Female C57BL/6 mice were injected subcutaneously at the tail base with the indicated vaccine formulations on day 0 and day 14. Spleens were harvested on day 21. Tissues were passed through 70 μm cell strainers and treated with ACK lysis buffer. Splenocytes were resuspended in IMDM and plated in separate 96-well plates for tetramer staining and intracellular cytokine staining (ICCS). For the tetramer staining, splenocytes were stained with Zombie NIR for viability and then stained with PE-labeled H-2Kb/SIINFEKL tetramer (NIH Tetramer Core). Cells were blocked with anti-CD16/32 and stained with anti-CD3-eFluor450 and anti-CD8-FITC. For ICCS, splenocytes were either restimulated with 5 μg/ml SIINFEKL peptide or 5 mg/ml OVA protein. 3 hr later, Protein Transport Inhibitor Cocktail (PTIC) was added and cells were incubated for another 3 hr. After incubation, cells were stained with Zombie NIR for viability, blocked with anti-CD16/32 and stained with either anti-CD3-eFluor450 + anti-CD8-FITC for $CD8^+$ T cells or anti-CD3-eFluor450 + anti-CD4-FITC for $CD4^+$ T cells. Cells were then treated with the BD Cytofix/Cytoperm Fixation/Permeabilization Kit and stained with either anti-TNFα-PE and anti-

IFNγ-APC for $CD8^+$ T cells and anti-IL-2-PE and anti-IFNγ-APC for $CD4^+$ T cells. Data was collected using the Attune NxT flow cytometer and analyzed using Flowjo. Gating strategies are shown in **Fig. S5.11**.

5.4.11 Tumor-infiltrating lymphocytes

Female C57BL/6 mice were inoculated with 0.15 million B16-OVA cells on the right hind flank on day 0 and immunized subcutaneously at the tail base on day 5 and day 12. Tumors were collected 24 h post the 2nd injection, and digested with 20 U/mL type IV collagenase + 125 U/mL DNase I, and dissociated with the GentleMACS Dissociator. Tumors were then incubated on a rotating platform at 37 °C for 30 min. Single-cell suspensions were obtained by passing homogenate through a 70 μm cell strainer. Cells were treated with the ACK lysing buffer to remove red blood cells.

Tumor cells were stained for viability with Zombie NIR viability kit, blocked with Trustain anti-mouse CD16/32, and then stained in two plates for T cells (anti-CD3-eFluor450, anti-CD4-APC, anti-CD8-FITC, PE-labeled H-2Kb/SIINFEKL tetramer), and DCs (anti-CD11c-APC, anti-CD8-FITC, anti-CD103-PE, anti-CD86-BV510). Data was collected using the Attune NxT flow cytometer and analyzed using Flowjo. Gating strategies are shown in **Fig. S5.12**.

5.4.12 Tumor studies

Female C57BL/6 mice (N=6-8) were inoculated with 1.5×10^5 B16F10-OVA cells in the right-hind flank on day 0. On days 4, 11, and 18, mice were immunized with PBS, VIPER containing 15 μg CSSSIINFEKL, 15 μg CSSISQAVHAAHAEINEAGR antigen peptides and 143 μg D-Melittin peptide, VIPER with 10 μg free STING agonist-3, VIPER with NPSTING containing 2 μg STING agonist-3 in different micelles (VIPER+NPSTING), VIPER with NPSTING containing

2 μg STING agonist-3 in same micelles (VIPER-co-NPSTING) or VIPER with polySTING containing 10 μg STING agonist-3. Female C57BL/6 mice (N=7-9) were inoculated with 5×10^5 MC38 cells in the right-hind flank on day 0. On days 8, 14, and 20, mice were immunized with PBS, VIPER, VIPER + free STING, VIPER + polySTING or VIPER-co-NPSTING, with free STING and polySTING containing 10 μg of STING agonist and NPSTING containing 2 μg of STING agonist via subcutaneous injection at the tail base. On days 8, 11, 14, 18, 21 and 25, mice were injected with 150 μg of anti-PD-1 (Clone RMP1-14, BioXCell) via intraperitoneal injection. Tumor length and width were then measured three times a week using a vernier caliper, and volume was subsequently calculated using the formula: Volume = $(\text{Width}^2 \times \text{Length}) \div 2$. Weight was also measured three times a week. Mice were euthanized if total tumor volume exceeded 1500 mm^3, visible discharge was observed on ulcers of the tumors, or the body weight loss exceeded 20%.

5.4.13 Statistical analysis

Statistical analysis was performed using the Graphpad Prism software. One-way ANOVA with post-hoc Tukey HSD test was used to compare more than two groups. Log-rank test was used for survival analysis.

5.5 ACKNOWLEDGEMENTS

K.S. and D.C.N. contributed equally to this work. This work was supported by the U.S. National Institutes of Health, National Cancer Institute Grant R01CA257563 (S.H.P. and P.S.S.), and the U.S. National Institutes of Health National Institute of Allergy & Infectious Diseases Grant R01AI134729 (P.S.S.). NMR data from this work was also supported by the U.S. National Institutes of Health Grant S10 OD030224-01A1, which funded the NEO 500 instrument used. We

thank ABM Zakaria (University of Washington) for the initial development of the LC/MS method used in this study. We thank Prof. Amanda Lund for providing the B16F10-OVA cell line, and the NIH Tetramer Core Facility for providing the PE-labeled H-2Kb/SIINFEKL tetramer. We thank the Institute for Protein Design (IPD) at the University of Washington for the use of Dynamic Light Scattering and 384 real-time PCR system.

5.6 REFERENCES

1. Xie, N. *et al.* Neoantigens: promising targets for cancer therapy. *Signal Transduct. Target. Ther.* **8**, 1–38 (2023).
2. Keskin, D. B. *et al.* Neoantigen vaccine generates intratumoral T cell responses in phase Ib glioblastoma trial. *Nature* **565**, 234–239 (2019).
3. Ott, P. A. *et al.* A Phase Ib Trial of Personalized Neoantigen Therapy Plus Anti-PD-1 in Patients with Advanced Melanoma, Non-small Cell Lung Cancer, or Bladder Cancer. *Cell* **183**, 347-362.e24 (2020).
4. Hu, Z. *et al.* Personal neoantigen vaccines induce persistent memory T cell responses and epitope spreading in patients with melanoma. *Nat. Med.* **27**, 515–525 (2021).
5. Niemi, J. V. L., Sokolov, A. V. & Schiöth, H. B. Neoantigen Vaccines; Clinical Trials, Classes, Indications, Adjuvants and Combinatorial Treatments. *Cancers* **14**, 5163 (2022).
6. Batista-Duharte, A., Hassouneh, F., Alvarez-Heredia, P., Pera, A. & Solana, R. Immune Checkpoint Inhibitors for Vaccine Improvements: Current Status and New Approaches. *Pharmaceutics* **14**, 1721 (2022).
7. Kerr, M. D., McBride, D. A., Chumber, A. K. & Shah, N. J. Combining therapeutic vaccines with chemo- and immunotherapies in the treatment of cancer. *Expert Opin. Drug Discov.* **16**, 89–99 (2021).
8. Cadena, A. *et al.* Radiation and Anti-Cancer Vaccines: A Winning Combination. *Vaccines* **6**, 9 (2018).
9. Hu, Z., Ott, P. A. & Wu, C. J. Towards personalized, tumour-specific, therapeutic vaccines for cancer. *Nat. Rev. Immunol.* **18**, 168–182 (2018).
10. Liu, W. *et al.* Peptide-based therapeutic cancer vaccine: Current trends in clinical application. *Cell Prolif.* **54**, e13025 (2021).
11. Mempel, T. R., Henrickson, S. E. & von Andrian, U. H. T-cell priming by dendritic cells in lymph nodes occurs in three distinct phases. *Nature* **427**, 154–159 (2004).
12. Acar, H., M. Ting, J., Srivastava, S., L. LaBelle, J. & V. Tirrell, M. Molecular engineering solutions for therapeutic peptide delivery. *Chem. Soc. Rev.* **46**, 6553–6569 (2017).
13. Joffre, O. P., Segura, E., Savina, A. & Amigorena, S. Cross-presentation by dendritic cells. *Nat. Rev. Immunol.* **12**, 557–569 (2012).
14. Lv, S. *et al.* Well-Defined Mannosylated Polymer for Peptide Vaccine Delivery with Enhanced Antitumor Immunity. *Adv. Healthc. Mater.* **11**, 2101651 (2022).
15. Song, K. *et al.* A mannosylated polymer with endosomal release properties for peptide antigen delivery. *J. Controlled Release* **356**, 232–241 (2023).
16. Khong, H. & Overwijk, W. W. Adjuvants for peptide-based cancer vaccines. *J. Immunother. Cancer* **4**, 56 (2016).
17. Lynn, G. M. *et al.* Peptide–TLR-7/8a conjugate vaccines chemically programmed for nanoparticle self-assembly enhance CD8 T-cell immunity to tumor antigens. *Nat. Biotechnol.* **38**, 320–332 (2020).

18. Van Herck, S., Feng, B. & Tang, L. Delivery of STING agonists for adjuvanting subunit vaccines. *Adv. Drug Deliv. Rev.* **179**, 114020 (2021).
19. Curtsinger, J. M. & Mescher, M. F. Inflammatory cytokines as a third signal for T cell activation. *Curr. Opin. Immunol.* **22**, 333–340 (2010).
20. Li, G. *et al.* cGAS-STING pathway mediates activation of dendritic cell sensing of immunogenic tumors. *Cell. Mol. Life Sci.* **81**, 149 (2024).
21. Oh, Y. M. *et al.* Ndrg1 is a T-cell clonal anergy factor negatively regulated by CD28 costimulation and interleukin-2. *Nat. Commun.* **6**, 8698 (2015).
22. Vatner, R. E. & Janssen, E. M. STING, DCs and the link between innate and adaptive tumor immunity. *Mol. Immunol.* **110**, 13–23 (2019).
23. Motedayen Aval, L., Pease, J. E., Sharma, R. & Pinato, D. J. Challenges and Opportunities in the Clinical Development of STING Agonists for Cancer Immunotherapy. *J. Clin. Med.* **9**, 3323 (2020).
24. Garland, K. M., Sheehy, T. L. & Wilson, J. T. Chemical and Biomolecular Strategies for STING Pathway Activation in Cancer Immunotherapy. *Chem. Rev.* **122**, 5977–6039 (2022).
25. Larkin, B. *et al.* Cutting Edge: Activation of STING in T Cells Induces Type I IFN Responses and Cell Death. *J. Immunol.* **199**, 397–402 (2017).
26. Shae, D. *et al.* Co-delivery of Peptide Neoantigens and Stimulator of Interferon Genes Agonists Enhances Response to Cancer Vaccines. *ACS Nano* **14**, 9904–9916 (2020).
27. Luo, M. *et al.* A STING-activating nanovaccine for cancer immunotherapy. *Nat. Nanotechnol.* **12**, 648–654 (2017).
28. Baljon, J. J. *et al.* A Cancer Nanovaccine for Co-Delivery of Peptide Neoantigens and Optimized Combinations of STING and TLR4 Agonists. *ACS Nano* **18**, 6845–6862 (2024).
29. Sun, X. *et al.* Self-Assembled STING-Activating Coordination Nanoparticles for Cancer Immunotherapy and Vaccine Applications. *ACS Nano* **18**, 10439–10453 (2024).
30. Dane, E. L. *et al.* STING agonist delivery by tumour-penetrating PEG-lipid nanodiscs primes robust anticancer immunity. *Nat. Mater.* **21**, 710–720 (2022).
31. Ramanjulu, J. M. *et al.* Design of amidobenzimidazole STING receptor agonists with systemic activity. *Nature* **564**, 439–443 (2018).
32. Jeffrey, S. C. *et al.* Dipeptide-based highly potent doxorubicin antibody conjugates. *Bioorg. Med. Chem. Lett.* **16**, 358–362 (2006).
33. Shen, Y. & Li, X. Cathepsin B as a target in cancer therapy and imaging. *New J. Chem.* **46**, 19593–19611 (2022).
34. Dubowchik, G. M. *et al.* Cathepsin B-Labile Dipeptide Linkers for Lysosomal Release of Doxorubicin from Internalizing Immunoconjugates: Model Studies of Enzymatic Drug Release and Antigen-Specific In Vitro Anticancer Activity. *Bioconjug. Chem.* **13**, 855–869 (2002).
35. Salomon, P. L. *et al.* Optimizing Lysosomal Activation of Antibody–Drug Conjugates (ADCs) by Incorporation of Novel Cleavable Dipeptide Linkers. *Mol. Pharm.* **16**, 4817–4825 (2019).

36. Su, F.-Y. *et al.* Macrophage-targeted drugamers with enzyme-cleavable linkers deliver high intracellular drug dosing and sustained drug pharmacokinetics against alveolar pulmonary infections. *J. Controlled Release* **287**, 1–11 (2018).
37. Nguyen, D. C. *et al.* Mannosylated STING Agonist Drugamers for Dendritic Cell-Mediated Cancer Immunotherapy. *ACS Cent. Sci.* (2024) doi:10.1021/acscentsci.3c01310.
38. Chavas, T. E. J. *et al.* A macrophage-targeted platform for extending drug dosing with polymer prodrugs for pulmonary infection prophylaxis. *J. Controlled Release* **330**, 284–292 (2021).
39. Xu, Y., Chen, C., Liao, Z. & Xu, P. cGAS-STING signaling in cell death: Mechanisms of action and implications in pathologies. *Eur. J. Immunol.* **53**, 2350386 (2023).
40. Bachmann, M. F. & Jennings, G. T. Vaccine delivery: a matter of size, geometry, kinetics and molecular patterns. *Nat. Rev. Immunol.* **10**, 787–796 (2010).
41. Barber, G. N. STING: infection, inflammation and cancer. *Nat. Rev. Immunol.* **15**, 760–770 (2015).
42. Durgeau, A., Virk, Y., Corgnac, S. & Mami-Chouaib, F. Recent Advances in Targeting CD8 T-Cell Immunity for More Effective Cancer Immunotherapy. *Front. Immunol.* **9**, (2018).
43. Zumerle, S., Molon, B. & Viola, A. Membrane Rafts in T Cell Activation: A Spotlight on CD28 Costimulation. *Front. Immunol.* **8**, (2017).
44. Chen, Q., Sun, L. & Chen, Z. J. Regulation and function of the cGAS–STING pathway of cytosolic DNA sensing. *Nat. Immunol.* **17**, 1142–1149 (2016).
45. Makuch, E., Jasyk, I., Kula, A., Lipiński, T. & Siednienko, J. IFNβ-Induced CXCL10 Chemokine Expression Is Regulated by Pellino3 Ligase in Monocytes and Macrophages. *Int. J. Mol. Sci.* **23**, 14915 (2022).
46. Reschke, R. & Gajewski, T. F. CXCL9 and CXCL10 bring the heat to tumors. *Sci. Immunol.* **7**, eabq6509 (2022).
47. Janco, J. M. T., Lamichhane, P., Karyampudi, L. & Knutson, K. L. TUMOR-INFILTRATING DENDRITIC CELLS IN CANCER PATHOGENESIS1. *J. Immunol. Baltim. Md 1950* **194**, 2985–2991 (2015).
48. Böttcher, J. P. & Reis e Sousa, C. The Role of Type 1 Conventional Dendritic Cells in Cancer Immunity. *Trends Cancer* **4**, 784–792 (2018).
49. Yadav, M. *et al.* Predicting immunogenic tumour mutations by combining mass spectrometry and exome sequencing. *Nature* **515**, 572–576 (2014).
50. Wang, B. *et al.* Potent and Prolonged Innate Immune Activation by Enzyme-Responsive Imidazoquinoline TLR7/8 Agonist Prodrug Vesicles. *J. Am. Chem. Soc.* **142**, 12133–12139 (2020).
51. Li, S. *et al.* Prolonged activation of innate immune pathways by a polyvalent STING agonist. *Nat. Biomed. Eng.* **5**, 455–466 (2021).
52. Liu, S. & Guan, W. STING Signaling Promotes Apoptosis, Necrosis, and Cell Death: An Overview and Update. *Mediators Inflamm.* **2018**, 1202797 (2018).
53. Audsley, K. M. *et al.* IFNβ Is a Potent Adjuvant for Cancer Vaccination Strategies. *Front.*

Immunol. **12**, (2021).
54. Wilson, N. S. *et al.* Systemic activation of dendritic cells by Toll-like receptor ligands or malaria infection impairs cross-presentation and antiviral immunity. *Nat. Immunol.* **7**, 165–172 (2006).
55. Jneid, B. *et al.* Selective STING stimulation in dendritic cells primes antitumor T cell responses. *Sci. Immunol.* **8**, eabn6612 (2023).
56. Woo, S.-R., Corrales, L. & Gajewski, T. F. The STING pathway and the T cell-inflamed tumor microenvironment. *Trends Immunol.* **36**, 250–256 (2015).
57. Hildner, K. *et al.* Batf3 Deficiency Reveals a Critical Role for CD8α+ Dendritic Cells in Cytotoxic T Cell Immunity. *Science* **322**, 1097–1100 (2008).
58. den Haan, J. M. M., Lehar, S. M. & Bevan, M. J. Cd8+ but Not Cd8− Dendritic Cells Cross-Prime Cytotoxic T Cells in Vivo. *J. Exp. Med.* **192**, 1685–1696 (2000).
59. Mellman, I., Chen, D. S., Powles, T. & Turley, S. J. The cancer-immunity cycle: Indication, genotype, and immunotype. *Immunity* **56**, 2188–2205 (2023).
60. Kitamura, H. *et al.* Long Peptide Vaccination Can Lead to Lethality through CD4+ T Cell-Mediated Cytokine Storm. *J. Immunol.* **185**, 892–901 (2010).
61. Dosta, P. *et al.* Investigation of the enhanced antitumour potency of STING agonist after conjugation to polymer nanoparticles. *Nat. Nanotechnol.* 1–13 (2023) doi:10.1038/s41565-023-01447-7.
62. van der Meel, R. *et al.* Smart cancer nanomedicine. *Nat. Nanotechnol.* **14**, 1007–1017 (2019).
63. Baharom, F. *et al.* Intravenous nanoparticle vaccination generates stem-like TCF1+ neoantigen-specific CD8+ T cells. *Nat. Immunol.* **22**, 41–52 (2021).
64. Guerin, M. V., Finisguerra, V., Van den Eynde, B. J., Bercovici, N. & Trautmann, A. Preclinical murine tumor models: A structural and functional perspective. *eLife* **9**, e50740.
65. Pillar, N., Polsky, A. L., Weissglas-Volkov, D. & Shomron, N. Comparison of breast cancer metastasis models reveals a possible mechanism of tumor aggressiveness. *Cell Death Dis.* **9**, 1–11 (2018).
66. Wehbe, M. *et al.* Nanoparticle delivery improves the pharmacokinetic properties of cyclic dinucleotide STING agonists to open a therapeutic window for intravenous administration. *J. Controlled Release* **330**, 1118–1129 (2021).
67. Chin, E. N. *et al.* Antitumor activity of a systemic STING-activating non-nucleotide cGAMP mimetic. *Science* **369**, 993–999 (2020).
68. Pan, B.-S. *et al.* An orally available non-nucleotide STING agonist with antitumor activity. *Science* **369**, (2020).
69. Larkin, B. *et al.* Cutting Edge: Activation of STING in T Cells Induces Type I IFN Responses and Cell Death. *J. Immunol.* **199**, 397–402 (2017).
70. Ghiringhelli, F. *et al.* Tumor cells convert immature myeloid dendritic cells into TGF-β–secreting cells inducing CD4+CD25+ regulatory T cell proliferation. *J. Exp. Med.* **202**, 919–929 (2005).

71. Kim, R., Emi, M. & Tanabe, K. Functional roles of immature dendritic cells in impaired immunity of solid tumour and their targeted strategies for provoking tumour immunity. *Clin. Exp. Immunol.* **146**, 189–196 (2006).

5.7 SUPPORTING INFORMATION

Table S 5.1 Compositional information for polymers used.

Name	Description	Mn (kDa)	# Mannose per polymer	# peptides or STING per polymer	Wt% peptide or STING
OVA1	Ovalbumin MHC1 epitope polymer conjugate	24.5	42	1.7 peptides/polymer	8.8%
OVA2	Ovalbumin MHC2 epitope polymer conjugate	29.4	42	3.4 peptides/polymer	23.7%
VIPER-NR	Endosomolytic D-melittin polymer conjugate	25.2	42	1.4 peptides/polymer	12.5%
polySTING	Soluble STING drugamer	12	35	2.4 STING/polymer	9.8%
NP-STING	Self-assembling STING drugamer	24.1	50	1.8 STING/polymer	6.9%
Adgpk	MC38 neoantigen polymer conjugate	28.1	42	4.2 peptides/polymer	20.1%

Mouse	1	2	3
ng/mL plasma	2.38	3.28	< LLOQ
ng/g lymph nodes	<LLOQ	<LLOQ	<LLOQ
ng/g spleen	3.77	2.87	3.34
ng/g liver	5.08	<LLOQ	<LLOQ

Table S 5.2 Pharmacokinetics characterization of free STING agonist at 30 minutes post-administration

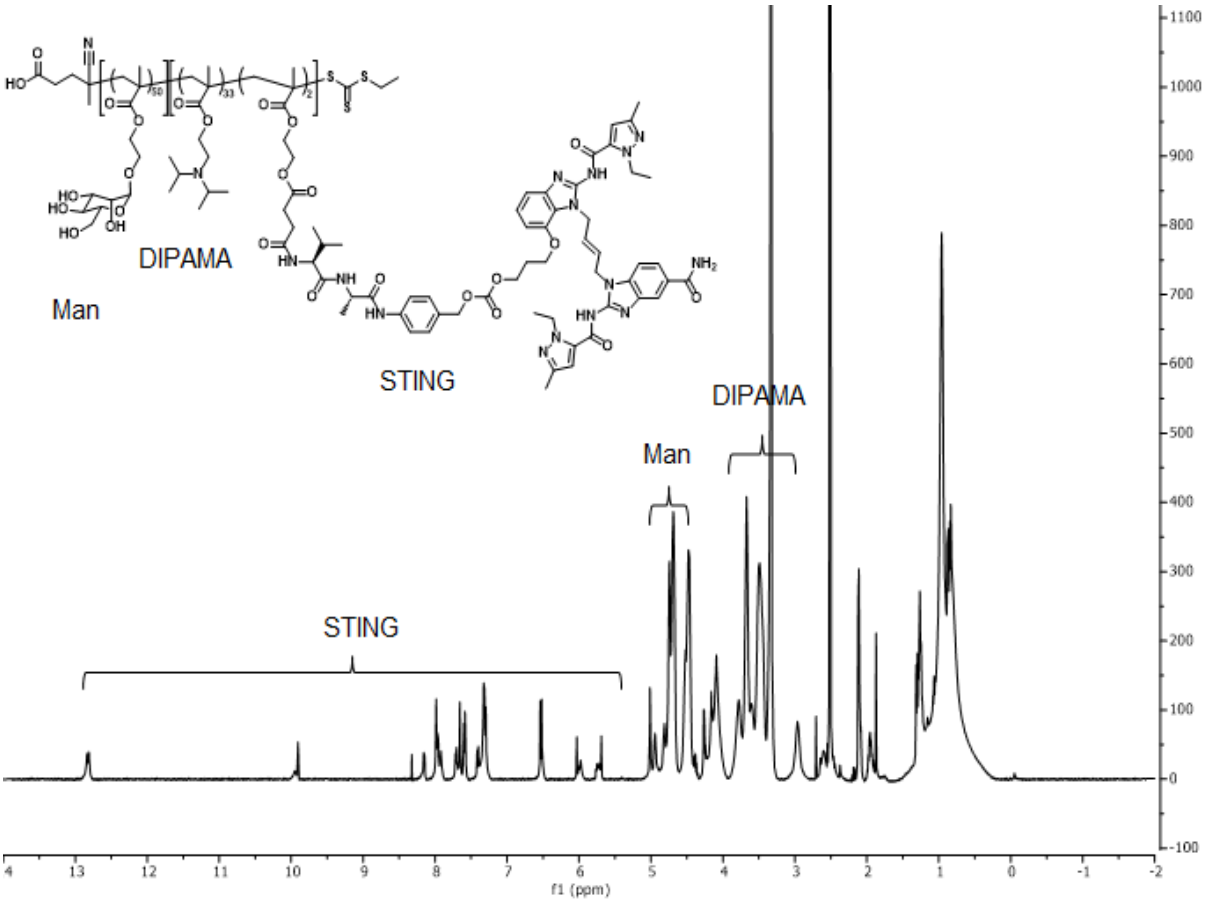

Figure S 5.1 ^{1}H-NMR spectrum of NP-STING.

NMR spectra of VIPER polymers and polySTING have been previously reported[1,2].

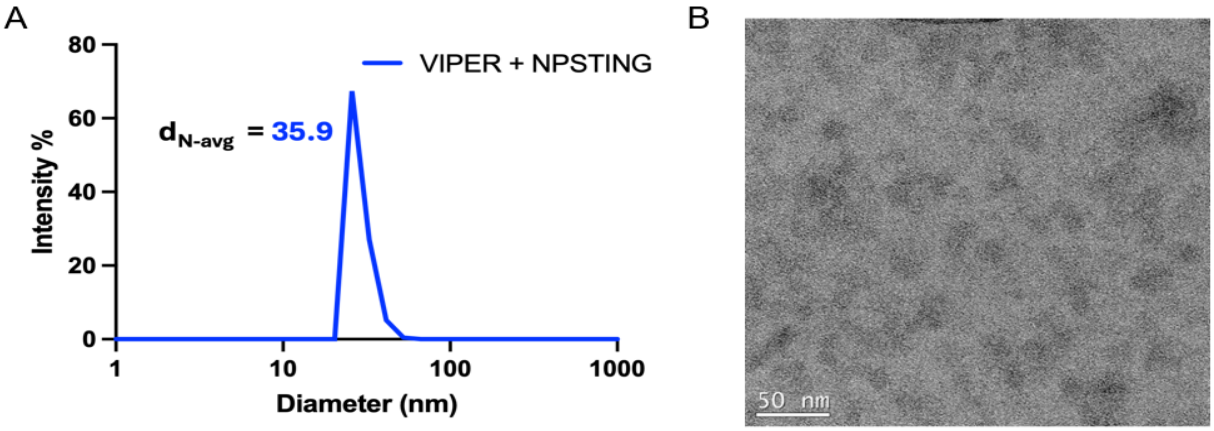

Figure S 5.2Characterization of VIPER micelles admixed with NPSTING micelles

(A) DLS characterization of VIPER + NPSTING (B) TEM micrograph of VIPER + NPSTING

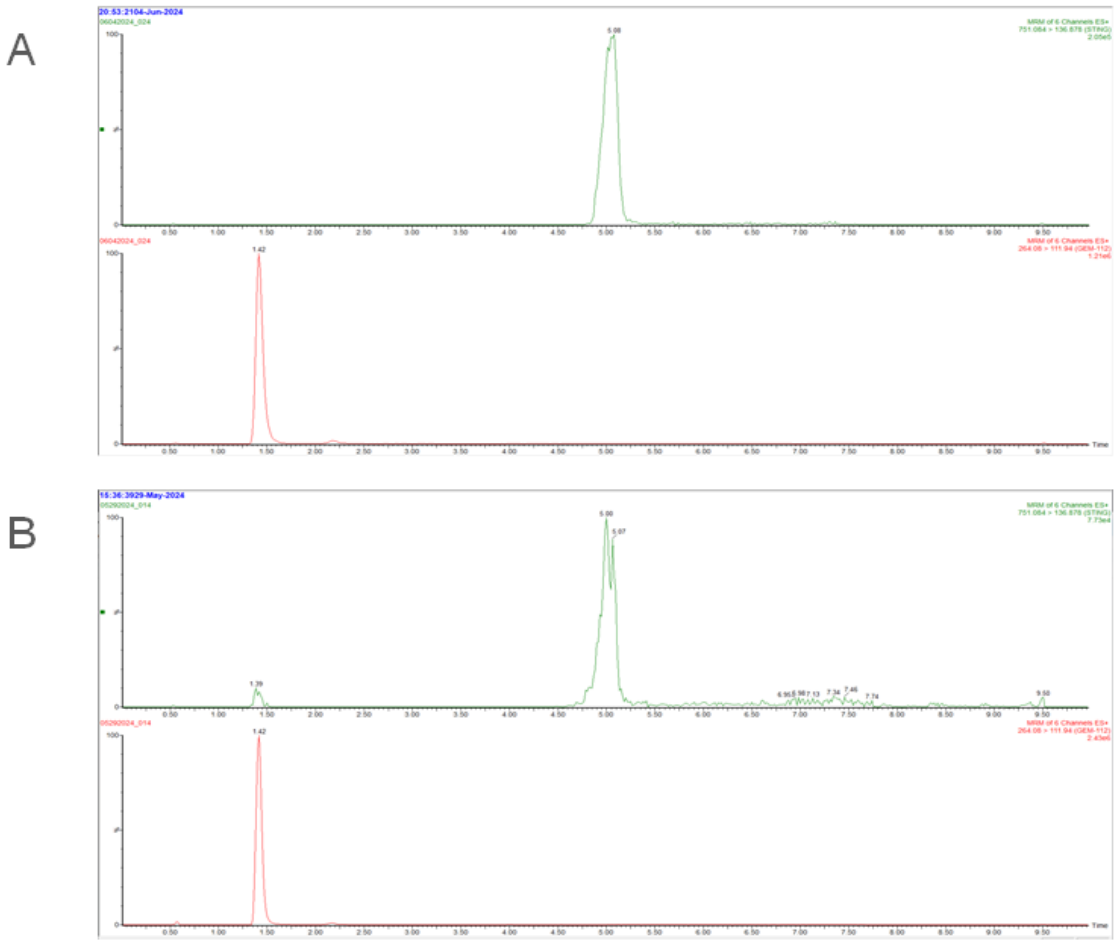

Figure S 5.3 Sample LC/MS chromatograms

Green trace: STING-137 daughter ion for STING quantification. Red trace: Gemcitabine-112 daughter ion for internal standard quantification. (A) Representative LC/MS chromatogram of a calibrator (4000 ng/g lymph node shown). (B) Representative LC/MS chromatogram of a study sample (polySTING lymph node, 1h).

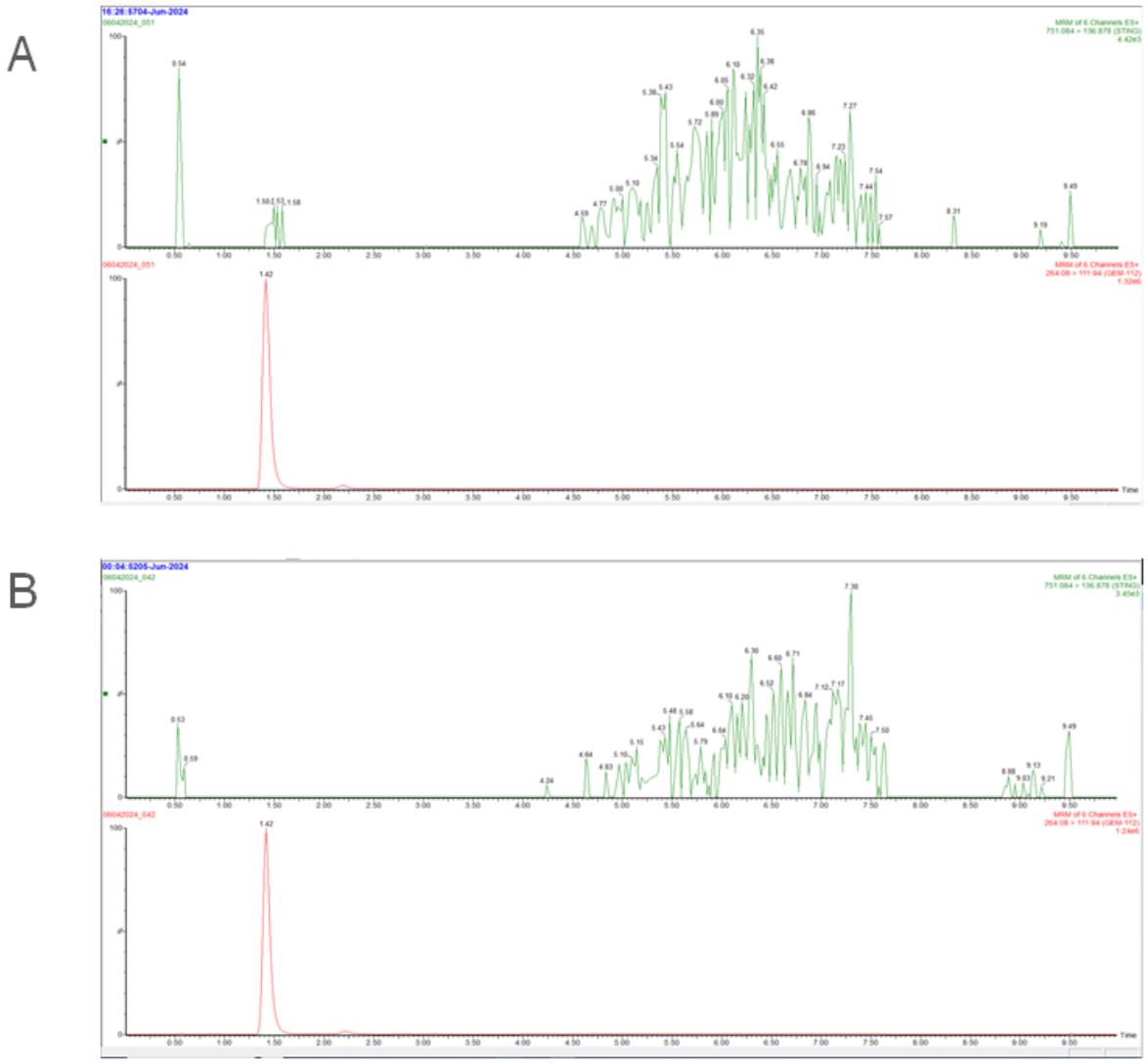

Figure S 5.4 LC/MS method does not detect STING in polymeric prodrug form.

Green trace: STING-137 daughter ion for STING quantification. Red trace: Gemcitabine-112 daughter ion for internal standard quantification. (A) Chromatogram of blank plasma with internal standard. (B) Chromatogram of plasma spiked with polySTING at 1000 ng STING/mL plasma, with internal standard. Identical results were obtained with NPSTING.

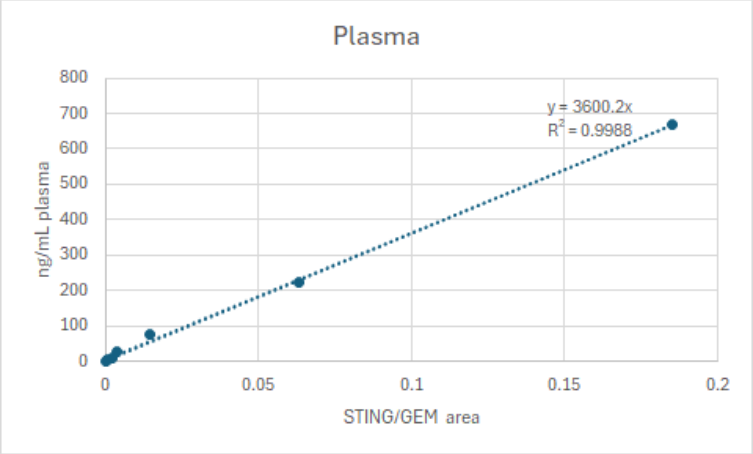
Plasma
y = 3600.2x
R² = 0.9988
ng/mL plasma
STING/GEM area
800
700
600
500
400
300
200
100
0
0
0.05
0.1
0.15
0.2

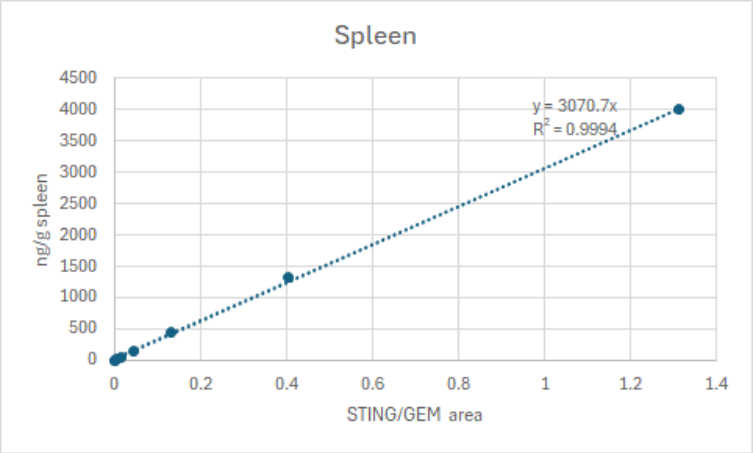
Spleen
y = 3070.7x
R² = 0.9994
ng/g spleen
STING/GEM area
4500
4000
3500
3000
2500
2000
1500
1000
500
0
0
0.2
0.4
0.6
0.8
1
1.2
1.4

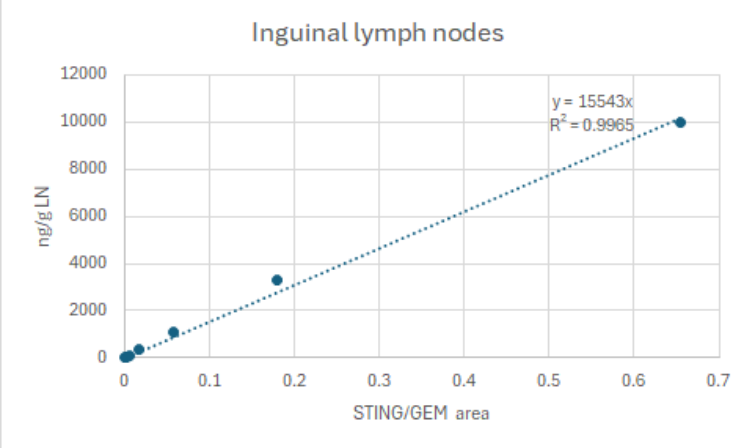
Inguinal lymph nodes
y = 15543x
R² = 0.9965
ng/g LN
STING/GEM area
12000
10000
8000
6000
4000
2000
0
0
0.1
0.2
0.3
0.4
0.5
0.6
0.7

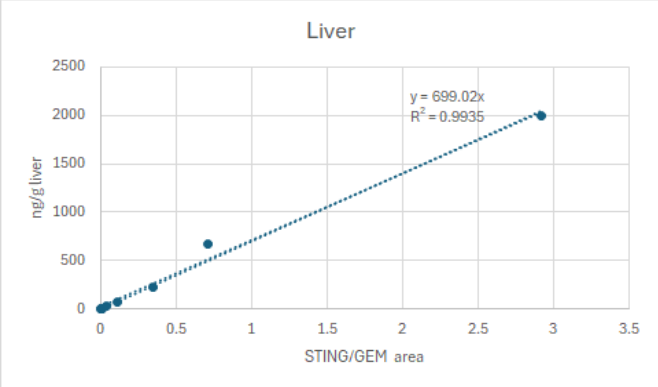

Figure S 5.5 Representative LC/MS calibration curves for the pharmacokinetics study

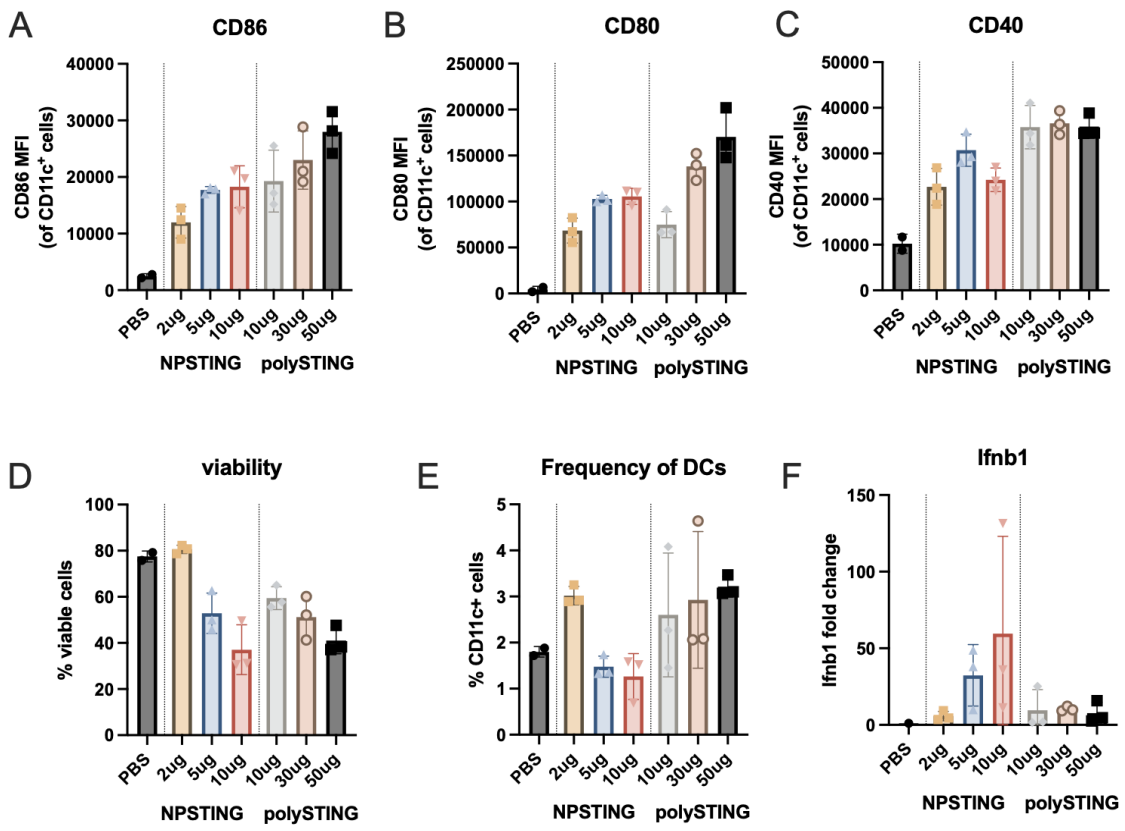

Figure S 5.6 NPSTING and polySTING dose response.

(A-C) Costimulatory molecule CD86, CD80 and CD40 expression in $CD11c^+$ cells in inguinal lymph nodes 24 h after vaccination. (D) Percentage of live cells in the inguinal lymph nodes determined by flow cytometry. (E) Percentage of $CD11c^+$ cells in the inguinal lymph nodes. (F) IFNB1 expression normalized to GAPDH housekeeping gene in inguinal lymph nodes by RT-qPCR. Data are represented as the mean ± SD.

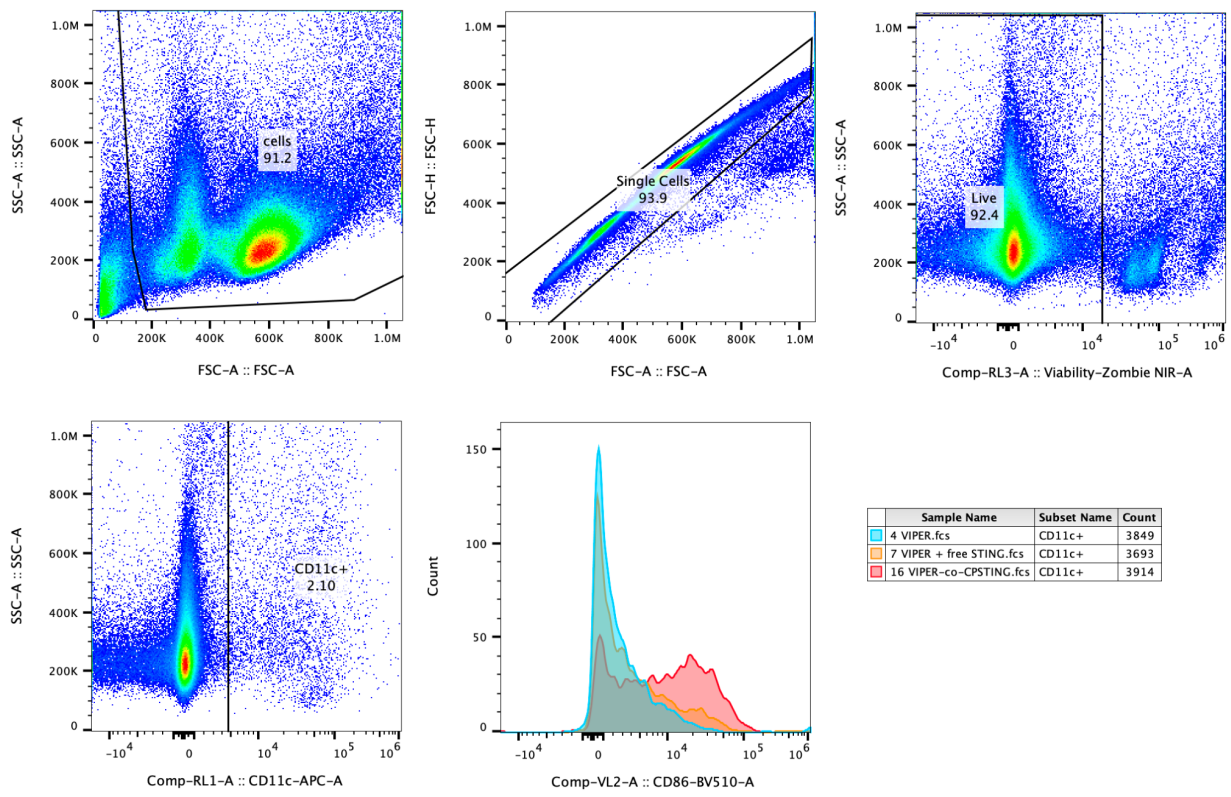

Figure S 5.7 Flow cytometry gating for in vivo dendritic cell maturation study.

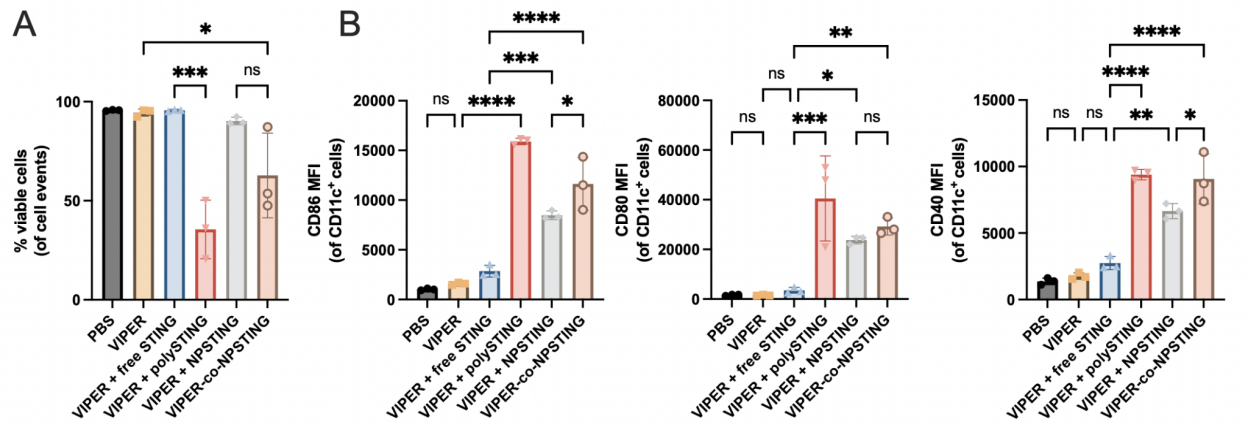

Figure S 5.8 *In vivo* dendritic cell activation

(A) Percentage of live cells in the iLNs 24 h after treatment. (B-D) Costimulatory molecule CD86, CD80 and CD40 expression in $CD11c^+$ cells in iLNs 24 h after vaccination (N=3). Data are represented as mean ± SD. Statistical analysis was performed using a one-way ANOVA with posthoc Tukey HSD test (*$p \leq 0.05$, **$p \leq 0.01$, ***$p \leq 0.001$, ****$p \leq 0.0001$ ns: not significant).

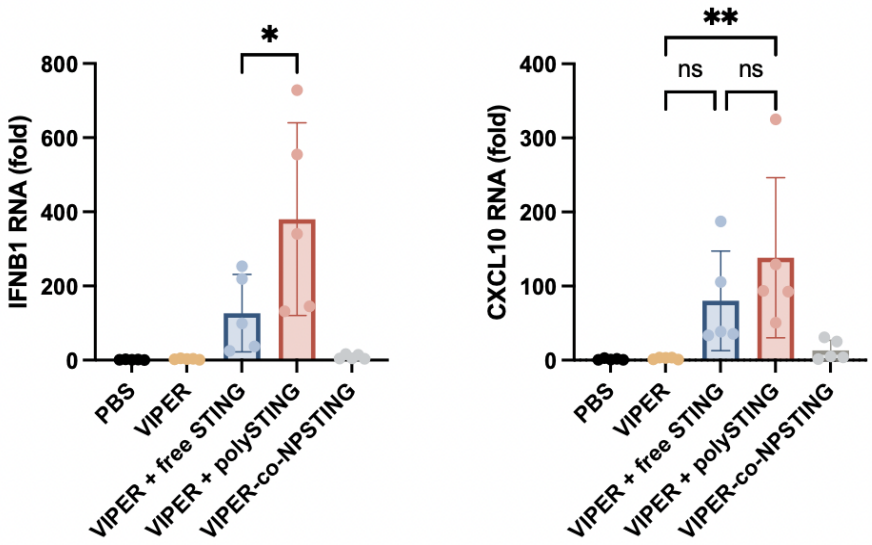

Figure S 5.9 Interferon-stimulated gene expression in iLNs 4 h after vaccination

iLNs were collected 4 h after vaccination. IFNB1 and CXCL10 expression were quantified using RT-qPCR and normalized to the GAPDH housekeeping gene (N=5). Data are represented as mean ± SD. Statistical analysis was performed using a one-way ANOVA with posthoc Tukey HSD test (*p ≤ 0.05, **p ≤ 0.01, ns: not significant).

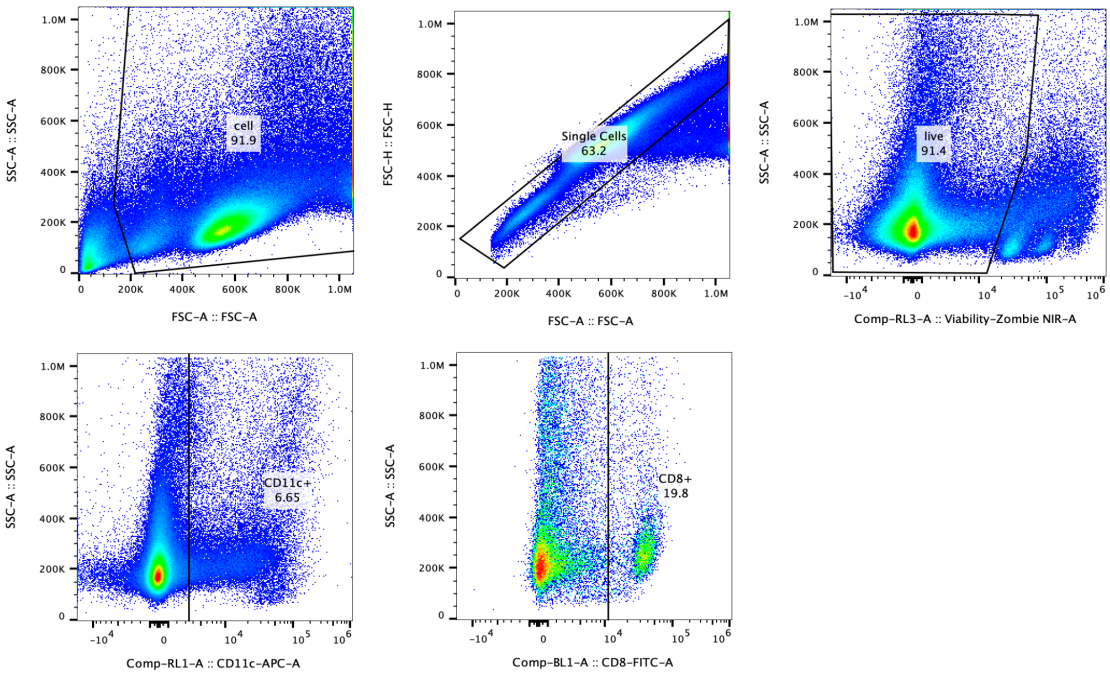

Figure S 5.10 Flow cytometry gating for in vivo cross-presenting dendritic cell study.

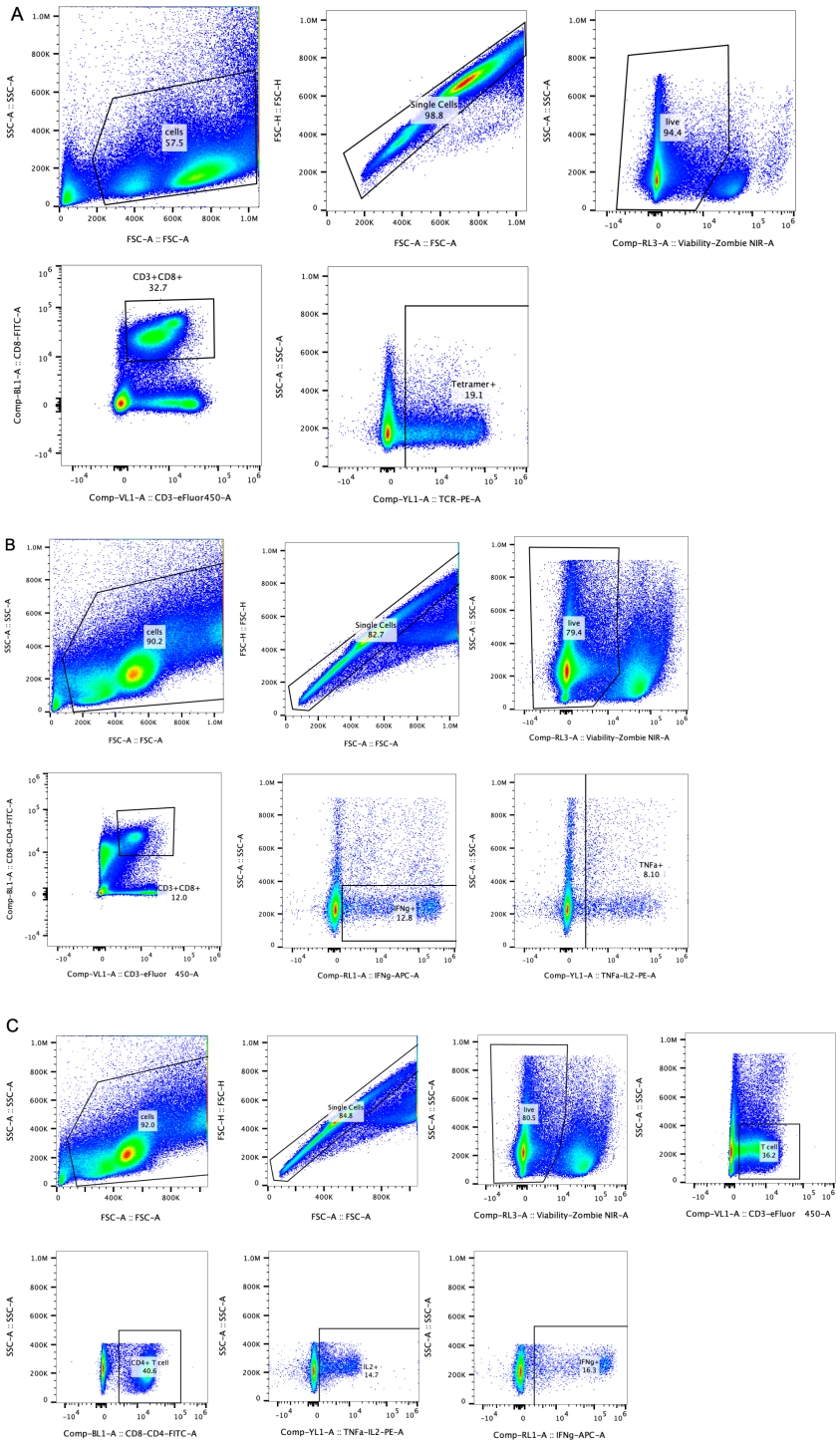

Figure S 5.11 Flow cytometry gating for in vivo T cell activation study.

(A) Flow cytometry gating for antigen-specific $CD8^+$ T cells. (B) Flow cytometry gating for cytokine-producing $CD8^+$ T cells after antigen restimulation analyzed with intracellular cytokine staining. (C) Flow cytometry gating for cytokine-producing $CD4^+$ T cells after antigen restimulation analyzed with intracellular cytokine staining.

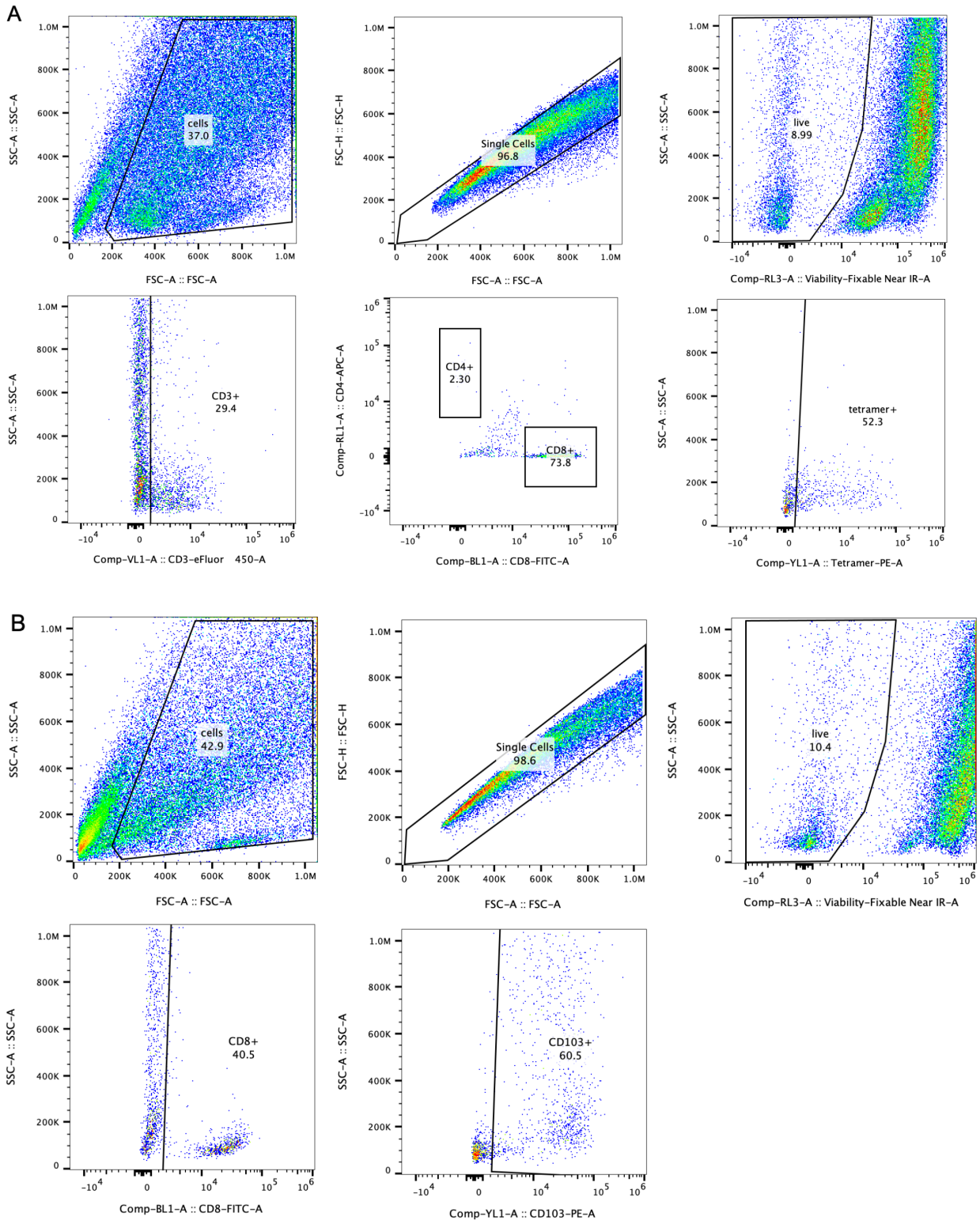

Figure S 5.12 Flow cytometry gating for tumor-infiltrating lymphocytes.

(A) Flow cytometry gating for antigen-specific $CD8^+$ T cells. (B) Flow cytometry gating for $CD8^+$ DCs and $CD103^+$ DCs.

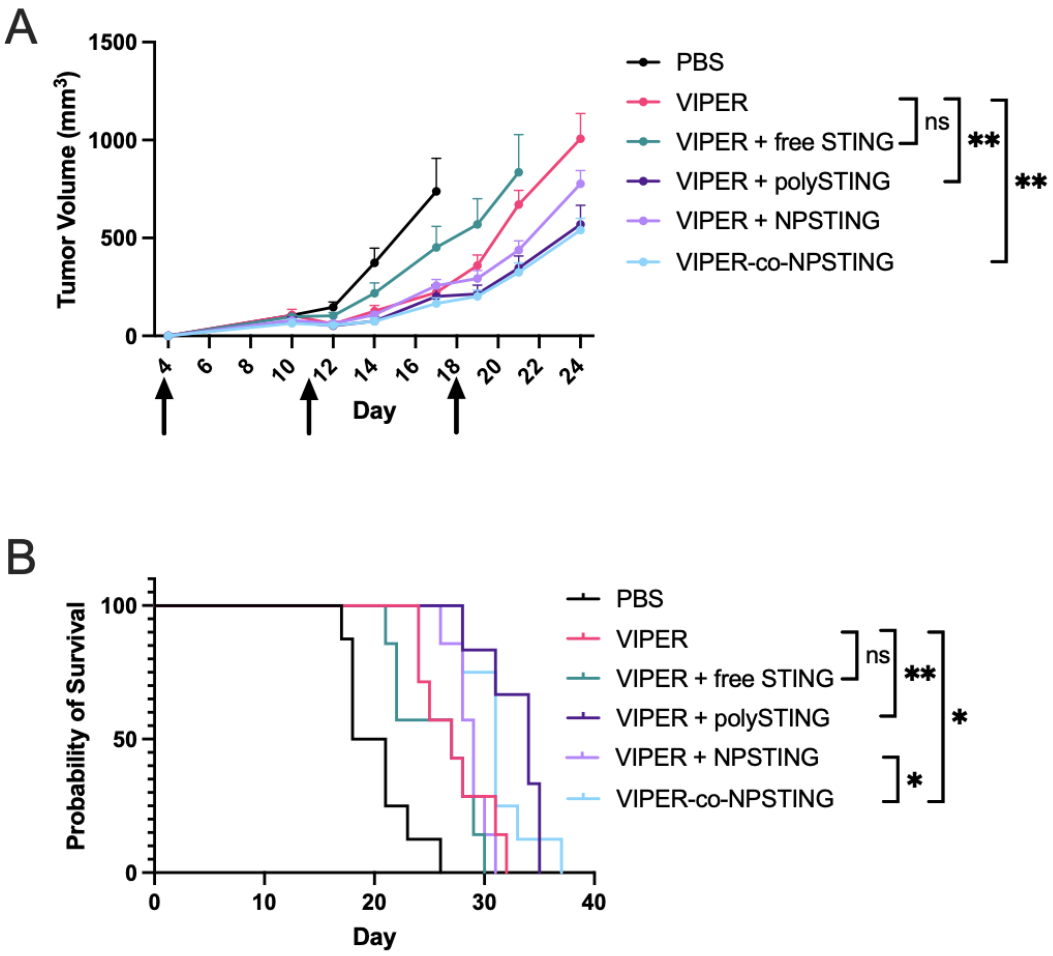

Figure S 5.13 B16-OVA tumor reduction study with admixed and co-micellized NP-STING

(A) Tumor growth curve. Mice were inoculated with B16-OVA cells on day 0 and immunized on days 4, 11 and 18. Statistical analysis was performed using two-way ANOVA with Tukey's multiple comparisons test (**p ≤ 0.01, ns: not significant). (B) Kaplan–Meier survival curve (N = 6-8). Survival analysis was performed using the log-rank test (*p ≤ 0.05, **p ≤ 0.01, ns: not significant).

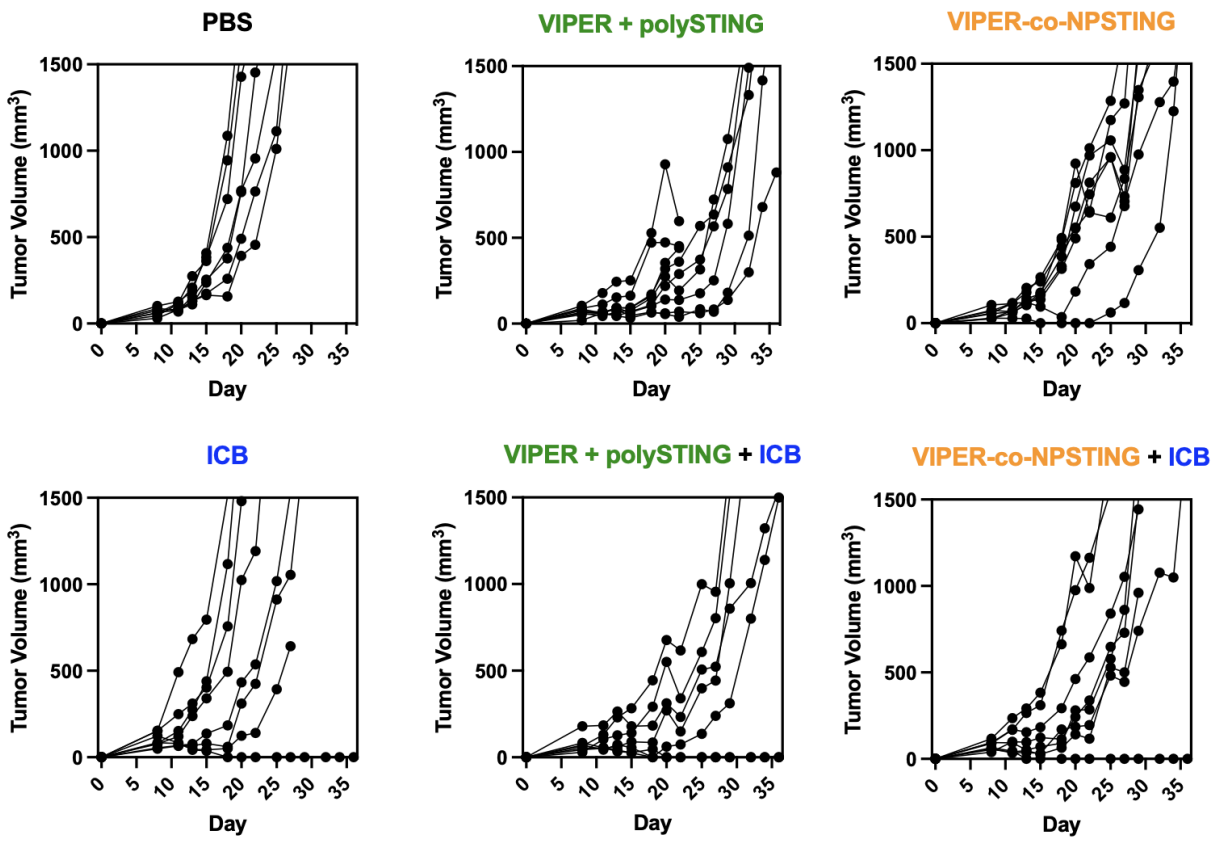

Figure S 5.14 Individual MC38 tumor growth curves

References

(1) Song, K.; Nguyen, D. C.; Luu, T.; Yazdani, O.; Roy, D.; Stayton, P. S.; Pun, S. H. A Mannosylated Polymer with Endosomal Release Properties for Peptide Antigen Delivery. *J. Controlled Release* **2023**, *356*, 232–241. https://doi.org/10.1016/j.jconrel.2023.03.004.

(2) Nguyen, D. C.; Song, K.; Jokonya, S.; Yazdani, O.; Sellers, D. L.; Wang, Y.; Zakaria, A.; Pun, S. H.; Stayton, P. S. Mannosylated STING Agonist Drugamers for Dendritic Cell-Mediated Cancer Immunotherapy. *ACS Cent. Sci.* **2024**. https://doi.org/10.1021/acscentsci.3c01310.

Chapter 6 : Developing Tumor Extracellular Matrix (ECM)-Targeted Drug Depots to Modulate Tumor Microenvironment

Kefan Song, Kairui Jiang, Yonghui Wang and Suzie H. Pun

ABSTRACT

Our previous work demonstrates that the VIPER cancer vaccine platform combined with the STING drugamer platform generates high levels of antigen-specific $CD8^+$ T cells in the spleen. However, complete tumor remission in the aggressive B16F10 melanoma tumor model has not been achieved. The suboptimal efficacy could be due to the immunosuppressive tumor microenvironment and insufficient T cell recruitment. In this chapter, we propose using fibronectin and tenascin C-binding peptides that bind to the tumor extracellular matrix (ECM) for tumor delivery of drugs that increase T cell recruitment to the tumor microenvironment.

6.1 INTRODUCTION

Cancer immunotherapy such as chimeric antigen receptor (CAR) T cell therapy and immune checkpoint inhibitors has demonstrated great potential in clinical studies.[1,2] However, these therapies are often limited to specific cancer subtypes and face challenges in treating a broad range of solid tumors.[3] This limitation is largely due to the immunosuppressive tumor microenvironment (TME), which contains regulatory T cells (Tregs), myeloid-derive suppressor cells (MDSCs) and cytokines like TGF-β and IL-10, which causes immune resistance.[4] In addition, tumors have dysregulated chemokine signaling, which hinders T cells trafficking into the tumors.[5]

To address these challenges, one approach involves normalizing chemokine signaling by delivering chemokine receptor agonists or drugs that stimulate the production of specific chemokines in tumors. CXCR3, a chemokine receptor expressed on activated $CD8^+$ T cells, memory T cells, natural killer cells, but not on regulatory T cells, is a promising target.[6] CXCR3 agonists such as VUF10611 have been shown to stimulate effector and memory T cell chemotaxis.[7,8] Another way to induce T cell infiltration into tumors is to deliver drugs that can stimulate the production of CXCL9/10, ligands of CXCR3.[9] Adjuvants such as STING agonists, TLR9 agonists like CpG ODN and TLR7/8 agonists like resiquimod have been reported to enhance the CXCR3-CXCL9/10 axis to recruit immune cells into the tumor.[10–13]

To overcome the immunosuppressive TME, researchers have used cytokines such as IL-2,[14] IL-12,[15] IL-21,[16] interferons,[17] and adjuvants such as STING agonists,[18] TLR agonists[19] to remodel the tumor microenvironment. However, cytokines and immunomodulators can cause cytokine release syndrome (CRS) and neurotoxicity when delivered systemically.[20] Researchers have

delivered cytokines locally to the tumors via intratumoral injections to elicit antitumor immunity without causing toxicity.[21,22]

Both the cytokine- and chemokine-based treatment can benefit from tumor-targeted delivery strategies. Cytokines require targeted action to reduce off-target toxicity, while chemokines need to be delivered to the tumors to create a gradient that can induce immune cell migration. Tumor-specific characteristics, such as the overexpression of fibronectin in the extracellular matrix (ECM), provide an opportunity for selective targeting.[23] Arnoldini et al. discovered a peptide that binds to relaxed fibronectin fibers and showed the fibronectin-binding peptide had higher accumulation in prostate tumor xenografts compared to the scrambled control after intravenous administration.[24]

Here, we present some preliminary results on the development of a tumor ECM targeting platform and evaluate the potential of a chemokine receptor agonist in promoting T cell infiltration into tumors. Additionally, we outline future directions for optimizing this strategy to enhance antitumor immunity.

6.2 PRELIMINARY DATA

6.2.1 PolyFN binds to fibronectin

We synthesized the fibronectin-binding peptide (CGGGQVTTESNLVEFDEESTKGIVTGAVSDHTTVEDTK) as previously reported.[24] The peptide was modified with biotin on the N-terminus. Peptide binding to fibronectin was confirmed by biolayer interferometry (BLI) (**Fig. 6.1A**). The fibronectin-binding peptide binds to fibronectin at a high affinity, with a K_D of 26.0 nM. There was no binding of a control peptide to

fibronectin or fibronectin-binding peptide to collagen. After confirming peptide binding to fibronectin, we conjugated the fibronectin-binding peptide and the scrambled peptide (CGSEQEDLTGTKVDFGETIVVNEATETVTSGSTHGTKV) to a hydrophilic polymer with rhodamine poly(GmMA-PFB-Rho) to make polyFN, which contains the fibronectin-binding peptide and polySCRM, which contains the scrambled peptide. We added polyFN and polySCRM to untreated plate or fibronectin-coated plate and binding was only observed in polyFN on fibronectin-coated plate, indicating polyFN binds to fibronectin (**Fig. 6.1B**).

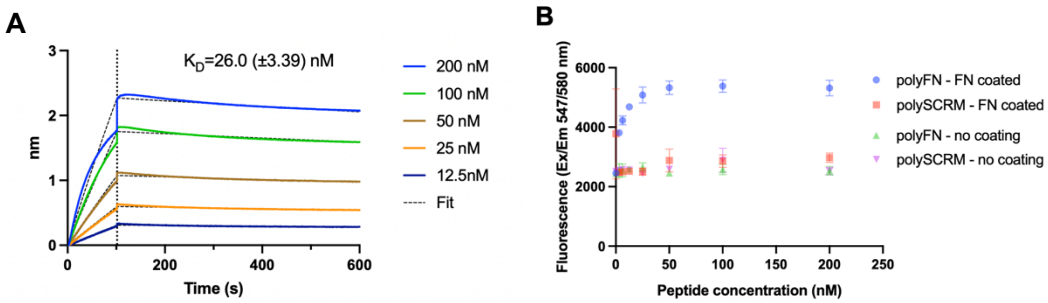

Figure 6.1 Fibronectin-binding peptide and polyFN binds to fibronectin.

(A) Biolayer interferometry (BLI) of fibronectin-binding peptide and control peptide binding to fibronectin at various concentrations and collagen at 200 nM. (B) Binding of polyFN or polySCRM to untreated and fibronectin-coated plate (N=3).

6.2.2 Biodistribution of polyFN and polySCRM

We next evaluated whether polyFN and polySCRM accumulate into tumors after intravenous injection. The pilot study showed that both polyFN and polySCRM accumulated mostly in the liver and kidney 4 h post tail vein injections (**Fig. 6.2A-B**). Only polyFN 4 h post injection showed signal in the tumors above the detection limit, but the amount of polymers that accumulated in the tumor was relatively low at 1.5% injected dose per gram of tumor (**Fig. 6.2B**).

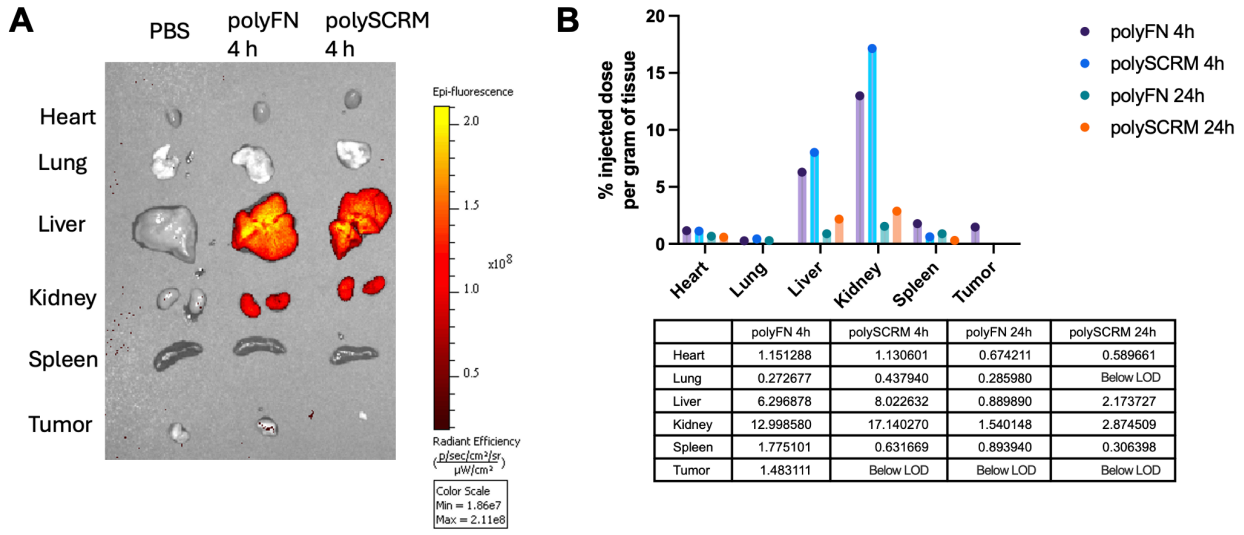

	polyFN 4h	polySCRM 4h	polyFN 24h	polySCRM 24h
Heart	1.151288	1.130601	0.674211	0.589661
Lung	0.272677	0.437940	0.285980	Below LOD
Liver	6.296878	8.022632	0.889890	2.173727
Kidney	12.998580	17.140270	1.540148	2.874509
Spleen	1.775101	0.631669	0.893940	0.306398
Tumor	1.483111	Below LOD	Below LOD	Below LOD

Figure 6.2 Biodistribution of polyFN and polySCRM.

PolyFN and polySCRM were injected via tail vein injections and tissues were collected 4 h or 24 h post injection. (A) IVIS imaging. (B) Quantification of polymer accumulation in different tissues.

Given that only a small amount of the polymers got into the tumor after intravenous administration, we next did a pilot study to evaluate whether polyFN would display increased retention in tumors after intratumoral injection compared to control polymers synthesized with scrambled peptide sequences. Both polymers showed high tumor accumulation around 3.5 h and 5 h post injections, and the signal went down after 24 h (**Fig. 6.3A-B**). Surprisingly, both polyFN and polySCRM showed detectable signals in some mice 96 h post injections, which could be useful as a drug depot. However, there was no difference in tumor retention between the two polymers (**Fig. 6.3B**).

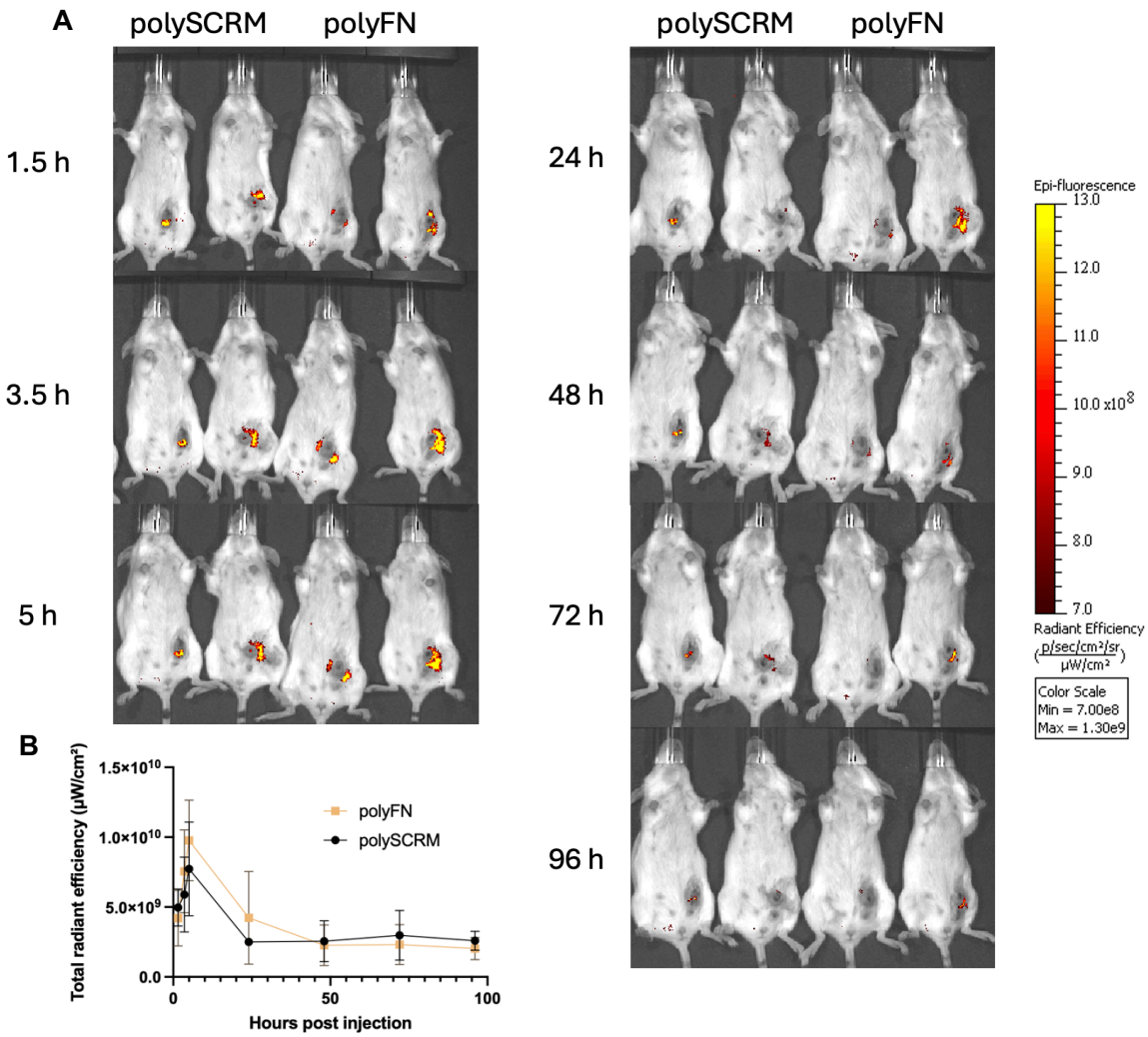

Figure 6.3 IVIS imaging of mice treated with polyFN and polySCRM.

Mice bearing 4T1 tumors were injected with rhodamine labeled-polySCRM or polyFN intratumorally and fluorescence images were taken at various time points post injections. (A) IVIS imaging. (B) Total radiant efficiency at the tumor site.

6.2.3 Tumor-ECM targeted polymers increase retention in the tumor compared to free peptides

We further tested alternative tumor ECM-targeting peptides PL1 and PL3, which bind to tenascin-C (TNC-C), a protein also upregulated in the tumor ECM.[25,26] The PL1 and PL3 peptides were modified with CGGG at the N-terminus for conjugation to the poly(GmMA-PFB-Rho) polymer, resulgint in polyPL1 and polyPL3. FNpep, a fibronectin-binding peptide

conjugated with rhodamine b, was used as a control. All four polymers exhibited higher tumor retention compared to the peptide control at all time points, whereas FNpep has no detectable signal at the same color scale (**Fig. 6.4A-B**).

At 24 hours post intratumoral injection, tumors were harvested, and the percentage of the injected dose was quantified in both the tumor and the liver. All polymers demonstrated higher tumor retention, with the percentage of injected dose ranging between 6% and 9%. In contrast, FNpep retained only 2% in the tumor 24 h post injection (**Fig. 6.4C**). The percentage of the injected dose of the polymers in the liver ranged from 1% to 6%. Given that the liver is approximately five times larger than the tumor, it's clear that the polymers achieved significantly higher tumor accumulation compared to liver accumulation.

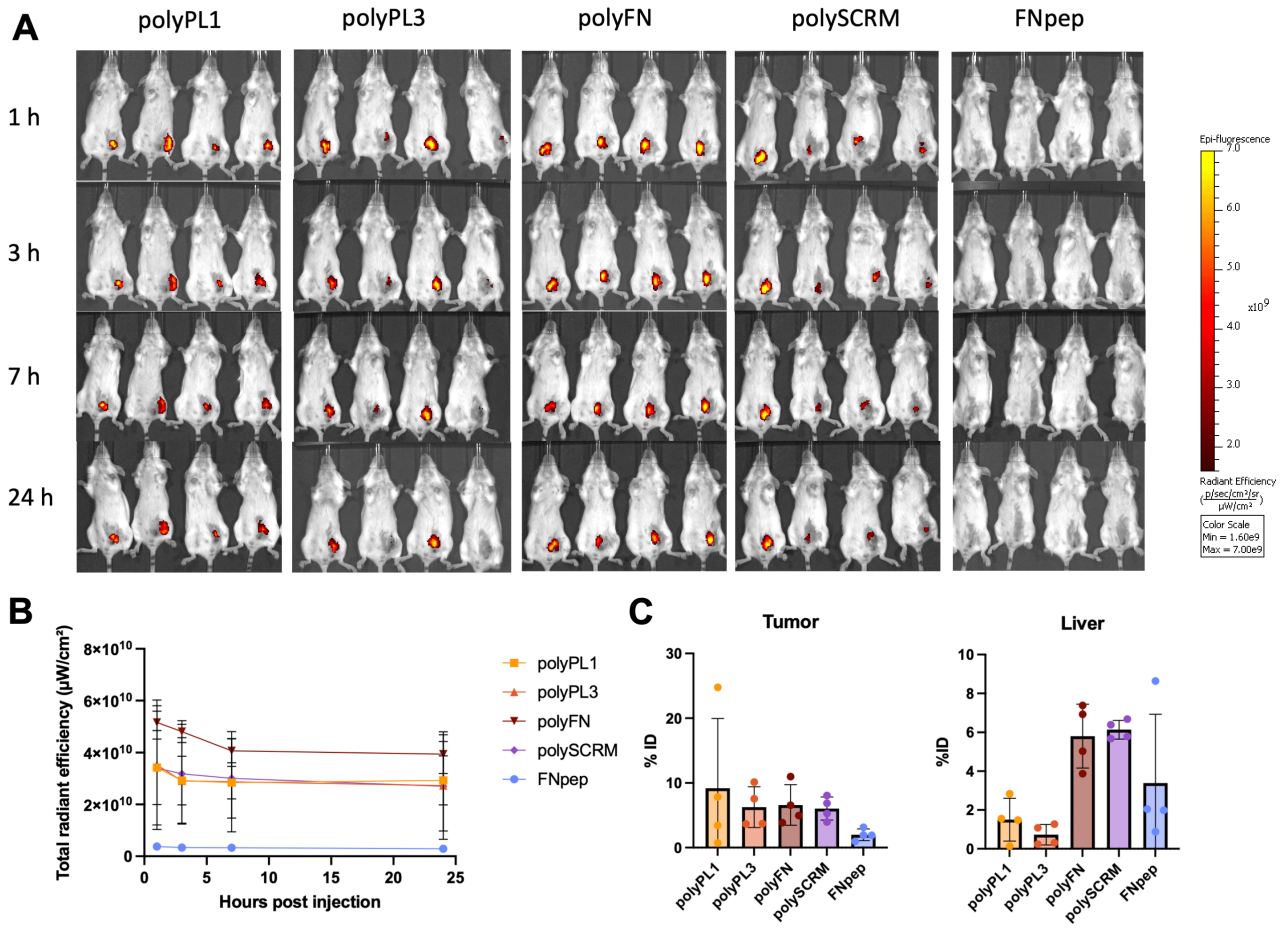

Figure 6.4 ECM-targeted polymers increase retention in the tumor compared to free peptides.

Mice bearing 4T1 tumors were injected with polyPL1, polyPL3, polyFN, polySCRM or FNpep intratumorally. (A) IVIS imaging at different time points. (B) Total radiant efficiency at the tumor site. (C) Percentage of the injected dose in the tumor and in the liver 24 h post-injection.

6.2.4 Intratumorally injected VUF10661 changes the T cell population in the tumor

VUF10661 has been shown to promote T cell migration after topical application at the mouse ears.[8] However, its role hasn't been explored in cancer applications. We hypothesized that VUF10611 delivered to the tumors could enhance activated $CD8^+$ T cell migration, but not Tregs, as VUF10611 is a CXCR3 agonist. We treated 4T1-tumor bearing mice with PBS, VUF10611 at a low dose (VUF LD, 1 μg) and VUF10611 at a high dose (VUF HD, 10 μg) via intratumoral injection, and collected tumors to analyze tumor-infiltrating T cells 48 h post injection. Both VUF LD and VUF HD treated mice, but not the PBS treated mice, generated high variance within the group, which could probably be due to unsuccessful intratumoral injection given the small sample size (**Fig. 6.5A-D**). PBS-treated mice all had low levels of $CD8^+$ T cells and $CD4^+$ T cells in the tumors (**Fig. 6.5A-C**). There was no difference in the average number of tumor-infiltrating T cells across the groups. However, both the VUF LD group and the VUF HD group had an outlier that demonstrated higher level of T cell infiltration into the tumor (**Fig. 6.5A-C**). This study should be repeated with a larger sample size to confirm whether VUF10611 could attract T cells into the tumors.

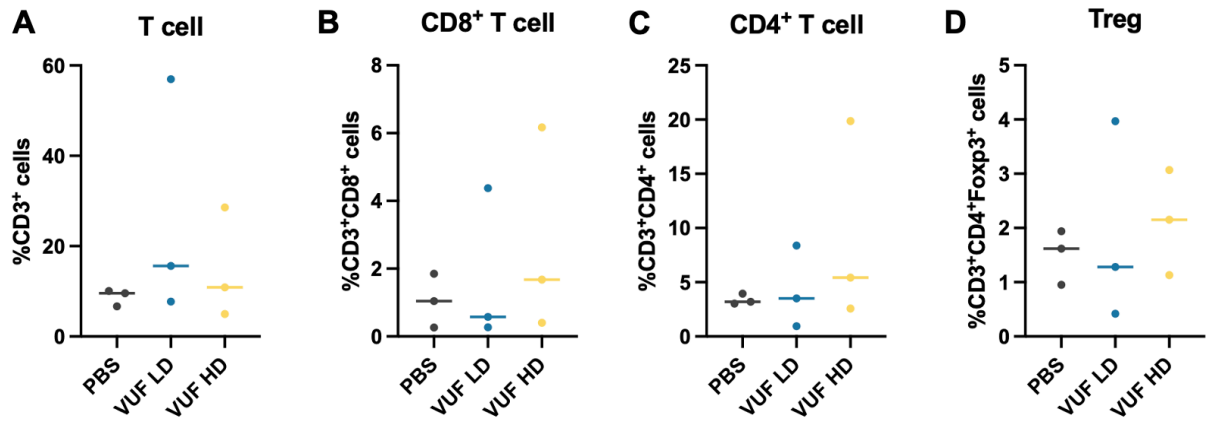

Figure 6.5 Tumor-infiltrating T cells.

Mice bearing 4T1 tumors were injected with PBS, 1 μg VUF10661 (VUF LD) or 10 μg VUF10661 (VUF HD) intratumorally. Tumors were harvested 48 h post injection. (A) Percentage of T cells in the tumor. (B) Percentage of $CD8^+$ T cells in the tumor. (C) Percentage of $CD4^+$ T cells in the tumor. (D) Percentage of regulatory T cells in the tumor (N=3).

6.3 PROPOSED FUTURE WORK

6.3.1 Alternative tumor-targeting strategies

We tested the FnBPA5 peptide as a candidate for tumor-targeted delivery. However, the amount of drug reaching the tumor after systemic administration was relatively low, possibly due to the binding target (relaxed fibronectin) or to low extravasation in this tumor model. Testing other fibronectin-binding peptides, reducing the polymer molecular weight or evaluating different tumor model could address this limitation.[27,28] Additionally, tumor cell markers such as HER2, EGFR, folate receptors could also serve as potential targets for tumor-targeted drug delivery.[29]

6.3.2 Alternative drug candidates

We performed a pilot study on tumor-infiltrating T cells after intratumoral injection of VUF10661. However, the sample size was small, and no convincing conclusion could be drawn.

This study could be repeated with a larger sample size and an optimized dosing schedule. Additionally, other drugs such as STING agonists and TLR agonists that stimulate the production of CXCL9 and CXCL10 could also be tested. The Baker lab developed an IL-21 mimic that induced cytotoxic T cells, reduced Tregs in the TME and demonstrated potent antitumor activity.[30] However, the drug needs to be administered daily, and there's toxicity associated with the systemic delivery of the drug. We are collaborating with the Baker lab to conjugate the IL-21 mimic to our tumor ECM-targeted polymer, which has the potential to reduce dosing frequency and minimize toxicity.

6.3.3 Optimization of the drug release profile

The tumor-targeted delivery platform can be used in two different ways. First, through intravenous injection, which has a broader application but faces challenges such as insufficient tumor delivery and off-target toxicity. Second, through intratumoral injection, which can form a drug depot in the tumor, but is limited to accessible tumors.

For intravenous applications, the major challenge is reducing off-target toxicity, as only a small portion of drug reaches the tumor. Linkers that respond to the tumor microenvironment (TME) could address this issue. The TME is characterized by acidic, hypoxic and reducing conditions.[31] Therefore, pH-responsive, hypoxia-responsive and redox-responsive linkers could be utilized to enable drug release specifically within the TME and reduce off-target effects. In addition, tumors overexpress enzymes like matrix metalloproteinases (MMPs) and cathepsins, which could guide the development of MMP- and cathepsin-cleavable linkers.[32]

For intratumoral applications, it is important to prolong the retention of drugs like chemokines in the tumor to create a continuous chemokine gradient for T cell migration and to reduce dosage

frequency. Our preliminary study showed that a fibronectin-binding peptide-conjugated polymer was detectable in the tumor 96 h after intratumoral injection. It would be interesting to test whether conjugating chemokine receptor agonists to the polymer would increase T cell infiltration compared to the unconjugated drug.

6.3.4 Combination with cancer vaccines

The aforementioned approaches addressed two major challenges faced by therapeutic vaccines: insufficient T cell infiltration into tumors and immunosuppressive TME. Exploring the combination of these strategies could provide synergistic effects and further enhance the antitumor immunity elicited by cancer vaccines.

6.4 MATERIALS AND METHODS

6.4.1 Polymer synthesis

pGmMA-co-PFBzMA-co-RhMA was synthesized via reversible addition-fragmentation chain transfer (RAFT) polymerization. 0.025 g PFBzMA, 0.0096 g RhMA and 0.35 g GmMA were combined with 0.0033 g CCC and 0.00018 g AIBN in dimethylacetamide. The mixture was purged with Argon for 15 min and reacted for 19 hr at 70°C. The reaction was endcapped with 20x molar excess of AIBN at 70°C overnight. Polymer was purified by dialysis.

6.4.2 Peptide synthesis and conjugation

Fibronectin-binding peptide (CGGGQVTTESNLVEFDEESTKGIVTGAVSDHTTVEDTK), scrambled fibronectin peptide (CGSEQEDLTGTKVDFGETIVVNEATETVTSGSTHGTKV), biotinylated fibronectin peptide (biotin-

CGGGQVTTESNLVEFDEESTKGIVTGAVSDHTTVEDTK), PL1 peptide (CGGG PPRRGLIKLKTS) and PL3 peptide (CGGG AGRGRLVR) were synthesized using a Liberty Blue microwave peptide synthesizer on Rink Amide resin. Peptides were purified with reverse phase HPLC. Peptides were conjugated to pGmMA-co-PFBzMA-co-RhMA via a PFB-thiol reaction as described previously.[33] Briefly, peptide and PFB were dissolved at 40 mM and DBU was added at 20x excess. The reaction was proceeded overnight at room temperature and dialyzed for purification. ^{19}F-NMR was used to quantify peptide weight percentage. For the fibronectin-binding peptide and rhodamine b coupling, peptide was synthesized with final deprotection and reacted with rhodamine b in the presence of Oxyma, DIPEA and DIC at 80°C for 10 min and transferred to a rotating platform overnight. The process was repeated and peptide was cleaved and purified with HPLC.

6.4.3 Cell lines and animals

4T1 cells were cultured in RPMI supplemented with 10% FBS and 1% P/S. Cells were incubated at 37°C and 5% CO_2. Female BALB/c mice aged 6 to 8 weeks were purchased from Jackson Laboratories. All animal studies were approved by the University of Washington Institutional Animal Care and Use Committee (IACUC).

6.4.4 Biolayer interferometry (BLI)

BLI was performed on an Octet RED96 instrument as previously described.[32] Briefly, biotinylated peptides were dissolved at 250 nM in PBS supplemented with 1% BSA and 0.01% Tween-20. Peptides were loaded onto streptavidin biosensors and associated with fibronectin at various concentrations ranged from 0 to 200 nM. Collagen at 200 nM was used as a control. Kinetic constant was calculated using a global fit.

6.4.5 ELISA

Black 96-well TC-treated plate were coated with fibronectin at 20 μg/ml in PBS at 4C overnight. Plate was washed twice with PBS containing 0.05% Tween-20 and then blocked with PBS containing 3% BSA and 0.05% Tween-20 for 1.5 h at room temperature. PolyFN and polySCRM at different concentrations were added to the wells and incubated for 1 h at room temperature with gentle shaking. The plate was washed 5 times with PBS containing 0.05% Tween-20 and then run on a plate reader (Ex. 547 nm, Em. 580 nm).

6.4.6 Biodistribution study

BALB/c mice were inoculated with 0.5 million 4T1 cells in the mammary fat pad on day 0. On day 10, when tumors were around 100 to 200 mm^3, 0.2 mg of polyFN or polySCRM dissolved in 100 μl PBS were injected through the tail vein. 4 h or 24 h post injection, mice were euthanized and perfused with PBS. Tissues were collected and imaged on IVIS Xenogen (Ex. 535 nm, Em. 580 nm). Tissues were homogenized with a handheld homogenizer and supernatant was collected to analyze fluorescence using a plate reader (Ex. 547 nm, Em. 580 nm). Fluorescence was converted to polymer mass using a standard curve with different concentrations of rhodamine-labeled polymer.

6.4.7 Tumor retention study

BALB/c mice were inoculated with 4T1 cells and allowed to grow until 100 to 200 mm^3 as previously described. 0.2 mg of polyFN or polySCRM dissolved in 20 μl PBS were injected intratumorally. Mice were imaged using IVIS Xenogen (Ex. 547 nm, Em. 580 nm) at various timepoints. Region of Interest (ROI) tool was used to select the tumor region to quantify total radiant efficiency. Tumors and livers were harvested 24 h post-injection and homogenized in

RIPA buffer. The percentage of the injected dose was quantified using a standard curve correlating fluorescence with polymer concentration.

6.4.8 Tumor-infiltrating T cell analysis

BALB/c mice with 4T1 tumors around 100 to 200 mm^3 were injected with PBS, 1 μg of VUF10661 or 10 μg VUF10661. VUF10661 was dissolved in PBS with 10% DMSO. All intratumoral injections have injection volume of 20 μl. 48 h post injection, tumors were collected and dissociated with 20 U/μl DNase and 2 U/μl Col IV at 37C for 30 min. A gentleMACS dissociator was used to break up the tumor pieces. Tumor cells were filtered through a 70 μm filter and treated with ACK lysing buffer to lyse red blood cells. Cells were stained with Zombie NIR for viability, blocked with CD16/CD32 and stained with surface markers (anti-CD3-eFluor450, anti-CD4-APC and anti-CD8-FITC). Cells were permeabilized and fixed with the eBioscience Foxp3/Transcription Factor Staining Buffer Set and then stained with anti-Foxp3-PE. Data was collected using the Attune NxT flow cytometer and analyzed using Flowjo.

6.5 REFERENCES

1. Wang, V., Gauthier, M., Decot, V., Reppel, L. & Bensoussan, D. Systematic Review on CAR-T Cell Clinical Trials Up to 2022: Academic Center Input. *Cancers* **15**, 1003 (2023).
2. Alturki, N. A. Review of the Immune Checkpoint Inhibitors in the Context of Cancer Treatment. *J. Clin. Med.* **12**, 4301 (2023).
3. Sun, Q. *et al.* Immune checkpoint therapy for solid tumours: clinical dilemmas and future trends. *Signal Transduct. Target. Ther.* **8**, 1–26 (2023).
4. Tie, Y., Tang, F., Wei, Y. & Wei, X. Immunosuppressive cells in cancer: mechanisms and potential therapeutic targets. *J. Hematol. Oncol.J Hematol Oncol* **15**, 61 (2022).
5. Kohli, K., Pillarisetty, V. G. & Kim, T. S. Key chemokines direct migration of immune cells in solid tumors. *Cancer Gene Ther.* **29**, 10–21 (2022).
6. Hughes, C. E. & Nibbs, R. J. B. A guide to chemokines and their receptors. *Febs J.* **285**, 2944 (2018).
7. Scholten, D. J. *et al.* Pharmacological characterization of a small-molecule agonist for the chemokine receptor CXCR3. *Br. J. Pharmacol.* **166**, 898 (2012).
8. Smith, J. S. *et al.* Biased agonists of the chemokine receptor CXCR3 differentially control chemotaxis and inflammation. *Sci. Signal.* (2018) doi:10.1126/scisignal.aaq1075.
9. Hoch, T. *et al.* Multiplexed imaging mass cytometry of the chemokine milieus in melanoma characterizes features of the response to immunotherapy. *Sci. Immunol.* **7**, eabk1692 (2022).
10. Corrales, L. *et al.* Direct Activation of STING in the Tumor Microenvironment Leads to Potent and Systemic Tumor Regression and Immunity. *Cell Rep.* **11**, 1018–1030 (2015).
11. Vonderhaar, E. P. *et al.* STING Activated Tumor-Intrinsic Type I Interferon Signaling Promotes CXCR3 Dependent Antitumor Immunity in Pancreatic Cancer. *Cell. Mol. Gastroenterol. Hepatol.* **12**, 41 (2021).
12. Majumder, S., Bhattacharjee, A., Chowdhury, B. P., Majumdar, S. B. & Majumdar, S. Antigen-Pulsed CpG-ODN-Activated Dendritic Cells Induce Host-Protective Immune Response by Regulating the T Regulatory Cell Functioning in Leishmania donovani-Infected Mice: Critical Role of CXCL10. *Front. Immunol.* **5**, 261 (2014).
13. Jensen, S. B. *et al.* An in situ depot for the sustained release of a TLR7/8 agonist in combination with a TGFβ inhibitor promotes anti-tumor immune responses. *Nat. Commun.* **15**, 7687 (2024).
14. Brog, R. A. *et al.* Superkine IL-2 and IL-33 Armored CAR T Cells Reshape the Tumor Microenvironment and Reduce Growth of Multiple Solid Tumors. *Cancer Immunol. Res.* **10**, 962–977 (2022).
15. Kaczanowska, S. *et al.* Genetically engineered myeloid cells rebalance the core immune suppression program in metastasis. *Cell* **184**, 2033-2052.e21 (2021).
16. Li, Y. *et al.* Targeting IL-21 to tumor-reactive T cells enhances memory T cell responses and anti-PD-1 antibody therapy. *Nat. Commun.* **12**, 951 (2021).
17. Müller, E. *et al.* Both Type I and Type II Interferons Can Activate Antitumor M1 Macrophages When Combined With TLR Stimulation. *Front. Immunol.* **9**, (2018).
18. Nguyen, D. C. *et al.* Mannosylated STING Agonist Drugamers for Dendritic Cell-Mediated Cancer Immunotherapy. *ACS Cent. Sci.* **10**, 666–675 (2024).
19. Michaelis, K. A. *et al.* The TLR7/8 agonist R848 remodels tumor and host responses to promote survival in pancreatic cancer. *Nat. Commun.* **10**, 4682 (2019).

20. Morris, E. C., Neelapu, S. S., Giavridis, T. & Sadelain, M. Cytokine release syndrome and associated neurotoxicity in cancer immunotherapy. *Nat. Rev. Immunol.* **22**, 85–96 (2022).
21. Hotz, C. *et al.* Local delivery of mRNA-encoded cytokines promotes antitumor immunity and tumor eradication across multiple preclinical tumor models. *Sci. Transl. Med.* **13**, eabc7804 (2021).
22. Santollani, L. *et al.* Local delivery of cell surface-targeted immunocytokines programs systemic antitumor immunity. *Nat. Immunol.* **25**, 1820–1829 (2024).
23. Wang, J. P. & Hielscher, A. Fibronectin: How Its Aberrant Expression in Tumors May Improve Therapeutic Targeting. *J. Cancer* **8**, 674 (2017).
24. Arnoldini, S. *et al.* Novel peptide probes to assess the tensional state of fibronectin fibers in cancer. *Nat. Commun.* **8**, 1793 (2017).
25. Lingasamy, P. *et al.* Bi-specific tenascin-C and fibronectin targeted peptide for solid tumor delivery. *Biomaterials* **219**, 119373 (2019).
26. Lingasamy, P. *et al.* Tumor-penetrating peptide for systemic targeting of Tenascin-C. *Sci. Rep.* **10**, 5809 (2020).
27. Signäs, C. *et al.* Nucleotide sequence of the gene for a fibronectin-binding protein from Staphylococcus aureus: use of this peptide sequence in the synthesis of biologically active peptides. *Proc. Natl. Acad. Sci.* **86**, 699–703 (1989).
28. Liu, Y. *et al.* Identification and Characterization of Fibronectin-Binding Peptides in Gelatin. *Polymers* **14**, 3757 (2022).
29. Zhou, Y. *et al.* Tumor biomarkers for diagnosis, prognosis and targeted therapy. *Signal Transduct. Target. Ther.* **9**, 1–86 (2024).
30. Chun, J.-H. *et al.* Potent antitumor activity of a designed interleukin-21 mimic. 2024.12.06.626481 Preprint at https://doi.org/10.1101/2024.12.06.626481 (2024).
31. Boedtkjer, E. & Pedersen, S. F. The Acidic Tumor Microenvironment as a Driver of Cancer. *Annu. Rev. Physiol.* **82**, 103–126 (2020).
32. Emmert-Buck, M. R. *et al.* Increased gelatinase A (MMP-2) and cathepsin B activity in invasive tumor regions of human colon cancer samples. *Am. J. Pathol.* **145**, 1285 (1994).
33. Song, K. *et al.* A mannosylated polymer with endosomal release properties for peptide antigen delivery. *J. Controlled Release* **356**, 232–241 (2023).
34. Cheng, E. L. *et al.* Discovery of a Transferrin Receptor 1-Binding Aptamer and Its Application in Cancer Cell Depletion for Adoptive T-Cell Therapy Manufacturing. *J. Am. Chem. Soc.* **144**, 13851–13864 (2022).